Atmospheric Stationary Wave Modelling

TAO–YONG PENG

Ph.D. Thesis

1992

Department of Meteorology,

University of Edinburgh,

The King's Buildings,

Edinburgh,

EH9 3JZ

ACKNOWLEDGMENTS

Dr. C. N. Duncan, as my supervisor, contributed continuing support and guidance in various dimensions thoroughout this study. I wish to also express my gratitudes to the departmental teaching staff for their annual discussions with me for my work, from which I benefited considerably. In addition, Dr. K. J. Weston, also my supervisor, gave me invaluable assitance in language for the final completion of the thesis. I am also grateful for the help directly or indirectly from other members in the department, in particular, Mr. B. Cameron and Mrs. L. Gormley.

This study also benefited from the generosity of the Department of Meteorology, Reading University, for providing the heating data. Without these data, an important part of my thesis would not be possible.

I was financially supported by the Chinese State Education Commission and the British Council's "Technical Coorporation Training" programme. Special thanks should also be given to the Nanjing Institute of Meteorology and in particular Prof. Du–Ming Weng for sending me to study in Britian.

Finally I wish to thank my wife and my parents for their encouragement and support during my stay here.

ABSTRACT

Stationary waves are vitally important in the general circulation of the atmosphere. These planetary scale waves are generally attributed to large scale orography and diabatic heating. The purpose of the present study is to investigate stationary waves as a linear response to the large scale orography and steady–state diabatic heating by developing a linear steady–state spectral model with the primitive equations in the global domain, in which Rayleigh friction and Newtonian cooling as well as biharmonic horizontal diffusion are included. We use pertubation theory to linearize the nonlinear system of primitive equations with respect to the zonally symmetric component of the dependent variables. The structure of the dependent variables is described by truncated series of spherical harmonics in the horizontal and orthogonal functions in the vertical. The model solution is obtained by way of linear superimposition of zonal waves calculated in the spectral domain for each zonal wave.

The three dimensional wave activity flux, which was derived by Plumb (1985) for linear quasi–geostrophic stationary waves on a zonal mean flow, as well as the EP flux are used as a diagnostic method for studying the three dimensional structure of wave propagation. The Plumb flux is a conservable measure of the wave activity flux which reduces to EP flux in the zonal mean, and is non–divergent for steady, conservative, linear waves.

The results of this thesis may present new insights into forcing mechanisms of

the stationary waves. The numerical experiments for the response to idealised orography in northern middle latitudes and actual global orography show that the northern middle latitude orographic forcing, in particular the Tibetan Plateau, plays the most important role in the maintenance of the orographically forced stationary waves in the middle and upper troposphere as well as lower stratosphere, while forcing by the orographic effect of the Antarctic plateau is also very important, but restricted only to the lower troposphere of the southern high latitudes. It is also shown that middle latitude orographic forcing can play an important role in the maintenance of the planetary scale motion in the subtropics and tropics. The stationary waves induced by the climatological thermal forcing have a comparable amplitude with those forced by orographic forcing except in the lower troposphere of the Antarctic area. It might be considered that between these two categories of forcing, the orographic forcing was more important in the lower troposphere, particularly in high latitudes of the southern hemisphere, but having a lesser role in the upper troposphere and lower stratosphere in the northern hemisphere, for the maintenance of the planetary stationary waves in northern winter. This was also supported by the longitude–pressure cross–sections of geopotential height, from which it might be concluded that the thermal and orographic forcing were comparably important in the middle latitudes of the northern hemisphere, while the circulation in the high latitudes of the southern hemisphere is primarily orographic. However, due to the simplicity of the model, the results presented in the thesis must be treated with caution.

Contents

List of Figures

Chapter 1

Introduction

§1.1 Introduction

Atmospheric phenomena may be divided into quasi-steady and time-dependent categories (White, 1990). The quasi-steady category may include climatological averages, climate anomalies, blocking and other weather anomalies lasting up to several weeks. An important and challenging area of research in the time–averaged circulation of the atmosphere is the attempt to thoroughly understand the structure and maintenance of planetary scale waves which remain stationary with respect to the earth, in the troposphere and lower stratosphere. This climatological circulation of stationary waves has been identified as resulting primarily from the asymmetrical distribution of the Earth's orography and thermal forcing, particularly that connected with sea surface temperatures (**SST**), and also to transient eddies (Wallace, 1983).

The variation of stationary waves is closely connected with low frequency variability

and climate change. Observational evidence has shown that, superimposed on the climatological distribution of the **SST**, there exist persistent and large scale temperature anomalies. The **SST** anomalies play a significant role in producing deviations from the long–term climatology and appear as the most easily monitored potential perturbers of the climate system (see Webster, 1982).

A numerical model able to faithfully reproduce some essential features of these long term circulation systems, to interpret the results clearly in terms of basic dynamical principles, and to understand the long–term atmospheric response to the imposition of **SST** anomalies, would be suitable for use as a test–bed for the validity and physically consistent understanding of the dynamical principles and parameterization used in numerical weather prediction and climate modelling models, and thus have a clear relevance and conjunction with the improvements of these models for understanding and perhaps to some extent forecasting climate variability.

Given the desire to understand the long–term atmospheric response to these steady forcings, considerable effort has been made for the past decade. For instance, general circulation models (GCMs) have been very successful in simulating many aspects of the observed structure of stationary waves (e.g. Laursen and Eliasen, 1989; Xu et al., 1990; Schneider, 1990; Ting, 1991). However, the interpretation of the fundamental dynamics of **GCM** results has proven to be more difficult than expected, and remains a challenging problem. Therefore we seek here to develop a simplified linear steady–state model to investigate the stationary waves in response to large scale orography and diabatic heating forcing as well as its anomaly.

Since simplified atmospheric numerical models are developed on the basis of ob-

servational experience and dynamical principles of atmospheric systems, and thus can be considered very fundamental to the understanding of the behaviour of the atmosphere, they are suitable for our understanding of this behaviour under some predefined conditions. The importance of simplified models and their relationship with observation and other numerical experimental results has been widely recognized in recent years (e.g. White, 1990; Robertson et al, 1990; Eliasen et al., 1990) for their ability to present useful insights into the long–term–averaged atmospheric general circulation and other atmospheric phenomena in the quasi–steady–state group.

The rest of this chapter will describe a historical review of stationary wave studies and outline the thesis.

§1.2 Review

Since the pioneering work by Charney and Eliassen (1949) who used a simple linear stationary wave model to show convincingly that the maintenance of stationary waves by orographic forcing is necessary for accurate short term numerical weather prediction, a lot of more complex and computationally demanding linear stationary wave models have been solved in the effort to better understand the processes which maintain atmospheric stationary waves. However, the problem of explaining the planetary-scale stationary waves still remains one of the most important subjects in the area of general circulation research.

There is evidence showing that there is a fairly close correspondence between the

structure of the wavetrain between 120W and 60W and the linear waves forced by the Rockies, and similarly for the high–low couplet in the Eastern Pacific and the linear response to the Tibetan plateau (e.g. Horel and Wallace, 1981). These teleconnection patterns described, for example, by Wallace and Gutzler (1981) and Horel and Wallace (1981) show that the stationary wavetrains are a dominant response to a localized source. Furthermore there is substantial evidence to suggest the existence of other teleconnection chains between the tropics and higher latitudes. Bjerknes (1966, 1969), Namias (1976), Horel and Wallace (1981, 1983), Shukla (1986), Branstator (1990) and many others have shown that variations in the stationary features of the tropical atmosphere, forced by large–scale forcing anomalies (e.g. SST), may be one of the primary causes of interannual variability in the climate of the higher latitudes. These observations have been simulated by using general circulation models (e.g. Rowntree, 1972, 1976; Shukla, 1986; Da Silva and Lindzen, 1987; Navarra, 1990; Robertson, et al., 1990; and Weber, 1990) to correlate the El Niño–like events of the Pacific Ocean with the anomalous location of the higher latitude long waves. Theoretical explanations of these teleconnections have been provided by a number of studies (e.g. Opsteegh and van den Dool, 1980; Webster, 1981, 1982; and Hoskins and Karoly, 1981; Simmons, 1982; Robertson et al., 1990).

Hoskins and Karoly (1981) used a linearized steady–state, five–layer baroclinic model to study the response of the tropospheric atmosphere to thermal and orographic forcing. They found that both thermal and orographic forcing were important in determining the stationary wave structure in the troposphere and the circulation patterns generated by forcing in a global atmosphere are generally in agreement with those results from observational studies and, to some extent, GCM

integrations, and confirmed the importance for middle latitudes of subtropical forcing, shown by others (e.g. Webster, 1981; et al.) Their results also showed that in the upper troposphere the thermal and orographic sources generate wavetrains similar to those given by barotropic models. They also claimed that the orographic forcing played a more important role than thermal forcing in the maintenance of the stationary waves in the troposphere.

Then Otto–Bliesner et al. (1982) developed a global, spectral, primitive equation model to study the seasonal climatology of the large–scale features of the atmosphere. The model reasonably reproduces the general features of the observed atmospheric circulation, seasonal cycles, interannual variations and hemispheric differences. The success of this low–resolution model in simulating the large–scale features of the atmospheric seasonal cycle illustrates the usefulness of such models for climate studies in conjunction with high–resolution general circulation model simulations.

Subsequently, Simmons (1982) used a high resolution, steady, linear, primitive equation model to examine both the extratropical and the tropical response to isolated regions of forcing in the tropics. The results are largely in agreement with those obtained using lower resolution models by a number of authors (Hoskins and Karoly 1981; Webster 1981). These results suggested that an isolated tropical region of heating may excite a wavetrain with a substantial poleward direction of propagation. The tropical response is largely in agreement with that obtained by a much simpler model proposed by Gill (1980).

Karoly and Hoskins (1983) investigated the stationary planetary wave response of the stratosphere to thermal and orographic forcing in the troposphere, using a

linearized, steady–state, 15–level numerical model which was an updated version of their 5–level model (Hoskins and Karoly, 1981). Together with Eliassen–Palm cross–sections, and the new model, they carried out some experiments on the effect of the inclusion of a realistic stratospheric structure on the tropospheric solutions, studied the propogation of planetary waves from the troposphere into the stratosphere and tested the sensitivity of the wave structure to variations of the forcing, basic state and dissipation. They found that in wintertime the stratospheric solutions for both orographic and thermal forcing are very similar. These model results suggest that the response in the stratosphere is determined by propagation from the perturbation in the troposphere and is independent of the forcing mechanism.

Lindzen (1986) suggested that anomalies of planetary waves are not, for the most part, unusually persistent, though some interannual variability exists. He argued that there is neither an observational nor physical basis for current models of multiple equilibria. He showed that realistic anomalies in tropical heating produced only modest anomalies in midlatitude stationary waves and that the distribution of these wave anomalies depended strongly on the zonal wind distribution. It was noted that observed free Rossby waves contribute significantly to the large, transient planetary–waves anomalies, but by no means totally account for them.

Shukla (1986) presented a summary of supposed important physical concepts that had, over a long time, appeared in connection with the problem of the influence of SST anomalies on extratropical circulation anomalies. He proposed two approaches to study the influence of tropical heating on midlatitude circulation, i.e. past atmospheric observations and models of varying degrees of complexity ranging from

linear and simple nonlinear models to global general circulation models. He stated that the most significant difference between the simple models and the GCMs lies on the treatment of the heating anomaly ∂Q which is explicitly calculated by ∂T in GCMs from their model physics and dynamics, but is prescribed in the simple models. Moreover the simple models also prescribe the large scale mean flow. However, despite the above restrictions of the simple models, they are very useful tools for carrying out a large number of experiments and for helping to understand the mechanisms for the remote response to tropical heating anomalies.

Laursen and Eliasen (1989) investigated the effects of the damping mechanisms using a version of ECMWF's first spectral model (T21) with a comprehensive physical parameterization package for long term integrations in perpetual January. They found that the effect of the damping parameters on the simulated mean fields was of considerable magnitude, and in particular, the inclusion of gravity wave drag had a substantial impact on the simulations and horizontal diffusion is necessary in order to represent the effect of the unresolved scales on the explicitly predicted scales. In spite of the fact that the introduction of the damping parameterization cannot prevent the model from significant climate drift such as too little kinetic energy and too small variability, they insisted that GCMs like the one they used can generally be considered as useful tools for studies of principal climatic features related to the general circulation of the atmosphere such as the atmospheric response to external changes.

Nigam and Lindzen (1989) used a linear, primitive equation stationary model having high vertical and meridional resolution to examine the sensitivity of orographically forced (primarily by Himalayas) stationary waves at middle and high

latitudes to variations in the basic state zonal wind distribution. They found that stationary waves at middle and high latitudes are sensitive to modest changes in the subtropical jet, and fluctuations well within the range of observed variability in the jet could lead to large variations in the stationary waves of the high latitude stratosphere, and to large changes even in tropospheric stationary waves. It was shown that these sensitivities would be sufficient to implicate variations in subtropical winds in both the generation of persistent large–scale anomalies in the extratropical troposphere, and in the initiation of sudden warming.

Lindzen and Fox–Rabinovitz (1989) developed a simple physical criterion for examining the consistancy of vertical resolution with horizontal resolution in both models and observing systems. With that criterion, they found that virtually all large scale models and observing systems have inadequate vertical resolution, and that the excessive horizontal resolution in models can lead to increased model "noise" rather than improved accuracy. However, they identified three possibilities which made the existing models work, i.e. data initialization, use of smoothing and damping (especially diffusive damping), and the nonlinear processes included in the GCM models.

Zimmerman et al. (1989) investigated the sensitivity of a weak winter extratropical cyclone to latent heat release (LHR). They found that the presence and intensity of the latent heat release is of critical importance to that cyclone's intensification. They also concluded that, using height tendency diagnoses, in the lower troposphere the dominant latent heat release influence is direct through explicit diabatic heating forcing in the height tendency equation while in the middle and upper troposphere this direct LHR role is no longer dominant, but rather shares

its importance with the indirect effect which is represented by the influnce of LHR on the dynamical forcing mechanisms.

O'Brien and Branscome (1989) investigated the ability of low–order, two–layer models to reproduce the essential elements of the mid–latitude general circulation. They examined in detail the changes in model behaviour with increased spectral resolution. They showed that many fundamental processes and structures of the mid–latitude circulation are successfully reproduced if the model resolution exceeds a critical truncation level, and the model is more responsive to changes in external parameters than to changes in resolution above this truncation level. They suggested that a horizontal resolution of three wavenumbers in the zonal and meridional direction is sufficient to capture several essential features of the extratropical circulation and remove certain distortions caused by more severe horizontal truncation.

Schneider (1990) used a linear stationary wave model to diagnose the causes of stationary waves in integrations of a GCM and to indicate the reasons for differences between the stationary waves produced by separate integarations and those of two consecutive months of a GCM integration. He found that the transient forcing is the major cause for the differences according to the linear model. He argued that the success of the diagnosis of the linear stationary wave model might have been due to the predominance of the transient forcing in the inter–monthly variations of the GCM stationary waves. He also commented that the linear model showed positive skill in diagnosing the differences.

Xu et al. (1990) described several models' ability to reproduce the Southern Hemisphere circulation, and compared these models' results with observations, using

four GCMs. They found that both the winter double jet and the semiannual variation of sea level pressure were reflected in the meridional gradient of the tropospheric temperature which is associated with differences in the seasonal heating and cooling of land, ocean and ice. They suggested that the GCMs' inability to simulate the winter double jet and semiannual variation might be indicative of an inadequate thermal coupling between the surface and the troposphere in the four models, and that the models' deficiencies were mostly due to insufficient parameterizations of subgridscale physical processes.

Kang (1990) investigated the influence of change in the zonal mean flow on stationary wave fluctuations by examining the extent to which the change of the stationary waves is simulated by a simple linear model with different states of zonal mean flow. He showed that the response of the forced Rossby waves depends strongly on the structure of the zonal mean flow, and in particular, that the precise location of the turning latitude plays an important role in determining the pattern and amplitude of remote response to a fixed forcing in a barotropic model. It is indicated that the correct prediction and simulation of the stationary waves require precise information on the zonal mean state. However, the causes of zonal mean flow fluctuations remain unrevealed in that study. Therefore, he suggested that further research related to this topic should be pursued to improve the long–range prediction of regional atmospheric circulation.

Navarra (1990) also tried to ascertain the steady linear response of the atmosphere to diabatic heating which is prescribed in equatorial and midlatitude regions , using an anomaly model which is linearized around the observed winter climatology. It was shown that the simulated features of the model response are consistent with

those of models linearized about zonally symmetric states. However, it was also pointed out that neglecting the stationary waves in the basic state can lead to substantial underestimation of the midlatitude response for some locations of the heating.

Eliasen and Laursen (1990) considered the possibility of reducing systematic errors (climatic drift) by investigating the effect of horizontal resolution and diffusion in a two–layer general circulation model with a simple zonally symmetric forcing. They found that an increase in the horizontal resolution of the model can significantly influence the zonal as well as the meridional mean flows. They demonstrated that the response of the model to an increase in the horizontal resolution can be obtained to a considerable extent by using a suitable, strongly scale–dependent, linear diffusion in the model, and that the eddy activity is strongly dependent on the horizontal resolution. They further demonstrated that with the use of the strongly scale–selective horizontal diffusion in the model with medium resolution, it is quite possible to obtain an increase in the eddy activity very similar to that obtained by the high resolution version of the model.

Robertson and Frankignoul (1990) used a linear steady–state multi–layer primitive equations model which is forced thermally in an attempt to reproduce two general–circulation–model–produced February climatologies in the tropics. They employed a hyphothesis–testing strategy to quantify the simulations of the target climatologies by the simple model taking into account the natural variability of the GCM fields. They found that the linear model is generally consistent with the two GCMs used at a high level of statistical significance when the zonal mean flow and the diabatic heating field are prescribed from the GCMs. They also found

that the strong dissipation imposed to regions of the critical lines, as suggested by Simmons (1982), can worsen the simulation significantly, underlining the need for high uniform dissipation rates in the tropics in linear models. The linear model is found to have an ability to reproduce to a large extent the GCMs' results.

Hurrell and Vincent (1990) investigated the short–term relationship between the upper level outflow from a tropical heat source and the subtropical westerly maximum in the southern hemisphere during summer. They found that the episodes of strong outflow measured by upper tropospheric velocity potential were well correlated with the enhancement and propagation of subtropical westerly maxima located at certain longitudes. They also found that latitudinal distance between the maximum tropical outflow regions and the subtropical westerly flows was, in the mean, about 16^0. This strong correlation shows that there is close connection between the tropical heating source and the subtropical westerly flow in the southern hemisphere.

Recently, Ting et al. (1990) used an idealized GCM to predict the atmospheric response to a tropical SST anomaly. Their results are similar to those on the climatological wintertime stationary waves by Nigam et al. (1986, 1988), and the response to El Niño SSTs by Held et al. (1989). They found that the response of the time–mean flow to the heating field is very linear, both in the tropics and the extratropics; and that the linear steady state model is quite successful in simulating these stationary wave patterns induced by the heating field. Ting (1991) also examined the atmospheric stationary wave response to a midlatitude **SST** anomaly by using the same model as Ting (1990), as well as a steady–linear model. It was found with the GCM that the stationary wave response is roughly linear

in the sign of the SST anomaly, despite evidence of strong nonlinearity shown by precipitation. The linear model response reproduced the GCM's stationary waves excellently. Furthermore, Ting simplified the design of the idealized GCM experiments to relate the midlatitude heat source directly with the SST anomaly. He also suggested that the relationship between the atmospheric heating and SST anomaly is still complex even in this relatively simple case. The relevance of his model's response to a realistic GCM case and to the real atmosphere is however still very obscure.

Ruosteenoja (1991) used a linear two–layer stationary wave model to examine the roles of the reflection coefficients for the critical latitude (CL) for the model's total response to all the forcing functions (mountains, diabatic heating, nonlinear eddy fluxes). It was found that the best simulations were obtained with low CL reflectivities. However, the author indicated that the two–layer linear model was inadequate for quantitative simulation of stationary waves in the real atmosphere, even if the reflection by the CL is parameterized by modifying the basic state.

§1.3 Present Study

In order to reproduce the essential features of the real atmosphere one might expect to use a general circulation model. Nonetheless, a limiting factor in the use of high–resolution GCMs, with their detailed physical parameterizations, for the study of climate, is the large amount of computing resources required. The large number of simulations required to study the sensitivity of seasonal change to various physical processes and parameterizations simply cannot be performed with such expensive

models.

Rather than utilize a sophisticated and expensive model, we will use a much simpler model yet strive to maintain compatibility with observational evidence and the results obtained from GCMs. In fact, we use a linear, steady–state, baroclinic primitive equation model in spherical geometry. This three dimensional spectral model in the global domain is developed, by using linearized primitive equations, in which the vertical as well as the horizontal structure is described by truncated series of orthogonal functions.

In Chapter 2, the framework of the model is described in detail. The governing equations of the model are introduced as well as Rayleigh friction, the effect of Newtonian cooling and scale selective horizontal smoothing. The physical forcing included in the model is also briefly described.

The algorithms used to obtain model solution are presented in Chapter 3. The structure of the model in three dimensions is represented by truncated series of orthogonal functions, i.e. the vertical structure is described in terms of normalized Legendre polynomials and the horizontal structure of each vertical mode is represented in terms of spherical harmonics. Moreover, the truncation relations, required for equivalence between velocity components and streamfunction are derived.

In addition to the Eliassen–Palm (EP) cross–section, the wave activity flux which constitutes a useful diagnostic of the three–dimensional propagation of stationary wave activity for the model solution is described. The flux appears in a locally applicable (non–zonally averaged) conservtion relation which was derived by Plumb

(1985) for quasi-geostrophic stationary waves on a zonal flow. It is a generalization of the Eliassen-Palm relation. The basic definitions, evaluation procedures relevant to the three dimensional wave activity and the EP cross-section and the graphic conventions used are outlined in Chapter 4.

A number of experiments to validate the model are carried out in Chapter 5. These experiments are designed for comparative convenience on the basis of work already done by others (e.g. Gill, 1980; Simmons, 1982; Lei, 1986; Robertson et al., 1990) to examine the model response to external forcing. They give us both confidence in the correctness of the model code and an initial understanding of the linear response of the model atmosphere to forcing by idealized large scale orography and diabatic heating. The sensitivity of the model solution to different dissipation conditions and the longitudinally averaged basic state is also shown in this Chapter for cases where the only forcing is either large scale orography in middle latitude or large scale diabatic heating in middle and low latitudes.

In order to understand the relative importance and impact of orography and diabatic forcing on stationary waves several experiments have been caried out. It is of interest to understand the essence and possible mechanism of the stationary wave behaviour in response to the above two physical processes in the time-averaged atmospheric system. We will present these experiments and their diagnostic results in Chapter 6.

Finally in Chapter 7, the conclusions of the studies are drawn up, and possible future development on this study is suggested.

Chapter 2

Model Configuration

§2.1 Introduction

The primitive equations governing the atmospheric motion are following those by Machenhauer and Daley (1972). In this Chapter, a steady state, linearized primitive equation system is formulated. This system is obtained by utilizing perturbation theory (e.g. Holton, 1979) to simplify the corresponding set of nonlinear primitive equations. The model equations are derived in §2.2. The perturbation method is described in §2.3. And the linearized steady state primitive equations are obtained in §2.4. Some aspects related to the configuration of the model are described briefly in the remaining Sections.

§2.2 Continuous Governing Equations

A vertical coordinate is same as that proposed by Machenhauer and Daley (1972), which may be defined as

$$\sigma = 2\frac{P}{P_s} - 1 \tag{2.1}$$

where P is pressure at any level, while P_s is the surface pressure. It might be noted that

$$\begin{cases} \sigma = 1 & \text{at } P = P_s \\ \sigma = -1 & \text{at } P = 0 \end{cases} \tag{2.2}$$

The primitive equations in spherical coordinates using this vertical coordinate may be written as

Momentum equations:

$$\begin{aligned} \frac{\partial u}{\partial t} = & -u\frac{1}{a\cos\varphi}\frac{\partial u}{\partial \lambda} - v\frac{1}{a}\frac{\partial u}{\partial \varphi} + uv\frac{\tan\varphi}{a} - \dot{\sigma}\frac{\partial u}{\partial \sigma} \\ & + fv - \frac{1}{a\cos\varphi}\frac{\partial \phi}{\partial \lambda} - \frac{RT}{P_s}\frac{1}{a\cos\varphi}\frac{\partial P_s}{\partial \lambda} + F_\lambda \end{aligned} \tag{2.3}$$

$$\begin{aligned} \frac{\partial v}{\partial t} = & -u\frac{1}{a\cos\varphi}\frac{\partial v}{\partial \lambda} - v\frac{1}{a}\frac{\partial v}{\partial \varphi} + u^2\frac{\tan\varphi}{a} - \dot{\sigma}\frac{\partial v}{\partial \sigma} \\ & - fu - \frac{1}{a}\frac{\partial \phi}{\partial \varphi} - \frac{RT}{P_s}\frac{1}{a}\frac{\partial P_s}{\partial \varphi} + F_\varphi \end{aligned} \tag{2.4}$$

Thermodynamic equation:

$$\frac{\partial T}{\partial t} = -u\frac{1}{a\cos\varphi}\frac{\partial T}{\partial \lambda} - v\frac{1}{a}\frac{\partial T}{\partial \varphi} - \dot{\sigma}\left[\frac{\partial T}{\partial \sigma} - \frac{R}{C_p}\frac{T}{1+\sigma}\right] \frac{RT}{C_p}\left[\frac{1}{a\cos\varphi}\frac{\partial u}{\partial \lambda} + \frac{1}{a}\frac{\partial v}{\partial \varphi} - v\frac{\tan\varphi}{a} + \frac{\partial \dot{\sigma}}{\partial \sigma}\right] + \frac{Q}{C_p} \tag{2.5}$$

Surface pressure tendency equation:

$$\frac{1}{P_s}\frac{\partial P_s}{\partial t} = -\frac{1}{2}\int_{-1}^{1}\left[\frac{1}{a\cos\varphi}\frac{\partial u}{\partial \lambda} + \frac{1}{a}\frac{\partial v}{\partial \varphi} - v\frac{\tan\varphi}{a} + \frac{u}{P_s}\frac{1}{a\cos\varphi}\frac{\partial P_s}{\partial \lambda} + \frac{v}{P_s}\frac{1}{a}\frac{\partial P_s}{\partial \varphi}\right] d\sigma \tag{2.6}$$

Vertical velocity equation:

$$\dot{\sigma} = -\int_{1}^{\sigma}\left[\frac{1}{a\cos\varphi}\frac{\partial u}{\partial \lambda} + \frac{1}{a}\frac{\partial v}{\partial \varphi} - v\frac{\tan\varphi}{a} + \frac{u}{P_s}\frac{1}{a\cos\varphi}\frac{\partial P_s}{\partial \lambda} + \frac{v}{P_s}\frac{1}{a}\frac{\partial P_s}{\partial \varphi}\right] d\sigma + \frac{1-\sigma}{P_s}\frac{\partial Ps}{\partial t} \tag{2.7}$$

Hydrostatic equation:

$$(1+\sigma)\frac{\partial \phi}{\partial \sigma} = -RT \tag{2.8}$$

with the following notation

φ latitude,

λ longitude,

a radius of the earth,

t time,

u zonal component of velocity,

v meridional component of velocity,

$\dot{\sigma}$ $= \frac{d\sigma}{dt}$, individual time derivative of σ,

T temperature (in K),

ϕ geopotential,

F_λ zonal component of friction force per unit mass,

F_φ meridional component of friction force per unit mass,

Q diabatic heating per unit mass per unit time,

f $= 2\Omega \sin\varphi$, the Coriolis parameter,

Ω being angular velocity of the earth,

R the gas constant for dry air,

C_p specific heat at constant pressure for dry air.

The tendency equation (2.6) and the vertical velocity equation (2.7) are derived from continuity equation by vertical integration using the boundary condition

$$\dot{\sigma} = 0 \qquad \text{at } \sigma = 1 \text{ and } \sigma = -1 \tag{2.9}$$

It may be noted that the solution of the hydrostatic equation (2.8) should satisfy the boundary condition

$$\phi \mid_{\sigma=1} = \phi_s \tag{2.10}$$

where ϕ_s is the surface geopotential.

For numerical convenience, the following variables are introduced

$$\begin{cases} U = u\cos\varphi \\ V = v\cos\varphi \\ q = \ln P_s \\ S = \frac{a}{1-\sigma^2}\dot{\sigma} \end{cases} \tag{2.11}$$

The model equations (2.3) - (2.8) are well established system describing atmospheric motions, thus could be used for prediction, or time-related diagnosis. However, since the purpose of the present study is to set up a set of time-independent

equations such that investigation of steady–state atmospheric phenomena in response to large scale diabatic and orographic forcing is possible, all the partial derivatives with respect to time in the model equations are henceforth assumed to be zero. The following model equations with the variable transformation of (2.11) are thus obtained, and used as the basic equations of the model developed for this study.

$$\frac{1}{1-\mu^2}\left(-UU^{(\lambda)}+VU^{(\mu)}\right)+SU^{(\sigma)}+2\Omega a\mu V - \phi^{(\lambda)}-RTq^{(\lambda)}-a\left(R_f+\alpha\nabla^4\right)U = 0 \tag{2.12}$$

$$\frac{1}{1-\mu^2}\left(-UV^{(\lambda)}+VV^{(\mu)}\right)+SV^{(\sigma)}-\frac{\mu\left(U^2+V^2\right)}{1-\mu^2} - 2\Omega a\mu U+\phi^{(\mu)}+RTq^{(\mu)}-a\left(R_f+\alpha\nabla^4\right)V = 0 \tag{2.13}$$

$$\frac{1}{1-\mu^2}\left(-UT^{(\lambda)}+VT^{(\mu)}-\kappa T\left(U^{(\lambda)}-V^{(\mu)}\right)\right)+\kappa TS^{(\sigma)} + S\left(T^{(\sigma)}+\kappa\left(1+\sigma\right)T\right)+\frac{aQ}{C_p}-a\left(K_t+\nu\nabla^4\right)T = 0 \tag{2.14}$$

$$\int_{-1}^{1}\left(U^{(\lambda)}-V^{(\mu)}+Uq^{(\lambda)}-Vq^{(\mu)}\right)d\sigma = 0 \tag{2.15}$$

$$S = -\frac{1}{\left(1-\mu^2\right)\left(1-\sigma^2\right)}\int_1^{\sigma}\left(U^{(\lambda)}-V^{(\mu)}+Uq^{(\lambda)}-Vq^{(\mu)}\right)d\sigma \tag{2.16}$$

$$\left(1+\sigma\right)\frac{\partial\phi}{\partial\sigma} = -RT \tag{2.17}$$

where the following notations are used:

$$\begin{cases} \mu & = \sin\varphi \\ \kappa & = \dfrac{R}{C_p} \\ A^{(\lambda)} & = \dfrac{\partial A}{\partial \lambda} \\ A^{(\mu)} & = (\mu^2 - 1)\dfrac{\partial A}{\partial \mu} \\ A^{(\sigma)} & = (\sigma^2 - 1)\dfrac{\partial A}{\partial \sigma} \end{cases} \tag{2.18}$$

where A stands for any of the variables. In addition, included are the Rayleigh friction R_f and Newtonian cooling K_t, and the scale–selective horizontal diffusion terms $\alpha\nabla^4$ and $\nu\nabla^4$. Equations (2.12) – (2.17) are clearly the steady state non–linear primitive equations. Linearization of this set of model equations is therefore necessary, and described in the following section.

§2.3 Linearization of the Model

In order to linearize the nonlinear system of equations (2.12) – (2.17), the perturbation method is used. According to the perturbation method, all field variables are divided into two parts, a basic state portion which is presumed to be independent of longitude (and probably time in dealing with some time dependent problems), and a perturbation part which is a local deviation of the field variable from its basic state portion. Suppose $[u]$, for instance, represents a longitudinally averaged

zonal component of velocity, and u^* is its departure from the average, the complete zonal component of velocity field can be hereby expressed as

$$u\,(\lambda,\mu,\sigma) \;=\; [u]\,(\mu,\sigma) + u^*\,(\lambda,\mu,\sigma) \tag{2.19}$$

where the square brackets denote zonal average of the variable, and superscript $*$ indicates its pertubation.

The advection term in the momentum equation, as an example, $\frac{u}{a\cos\varphi}\frac{\partial u}{\partial\lambda}$ can be written as

$$\begin{aligned} u\,\frac{\partial u}{a\cos\varphi\;\partial\lambda} &= \{[u]+u^*\}\;\frac{\partial\,\{[u]+u^*\}}{a\cos\varphi\;\partial\lambda} \\ &= [u]\,\frac{\partial u^*}{a\cos\varphi\;\partial\lambda} + u^*\,\frac{\partial u^*}{a\cos\varphi\,\partial\lambda} \end{aligned} \tag{2.20}$$

Following the perturbation theory, we assume that the second term on the right side of (2.20) is at least one order smaller than the first term, and therefore can be neglected.

By neglecting all the terms of second order, i.e. nonlinear in perturbation quantities which are though important in the real atmospheric processes, the non–linear primitive equations can be reduced to linear differential equations with perturbation variables as dependent variables.

§2.4 Linear Primitive Equations

After considerable mathematical manipulation, the linearized primitive equations, corresponding to (2.12) - (2.17) may be writen as

$$\frac{1}{1-\mu^2}\left\{-[U]\,U^{*(\lambda)}+V^*\,[U]^{(\mu)}\right\}+S^*\,[U]^{(\sigma)}+2\Omega a\mu\,V^* - \phi^{*(\lambda)}-R[T]q^{*(\lambda)}-a\left(R_f+\alpha\,\nabla^4\right)\,U^* \;=\; 0 \tag{2.21}$$

$$\frac{1}{1-\mu^2}\left\{-[U]\,V^{*(\lambda)}-2\mu\,[U]\,U^*\right\}-2\Omega a\mu\,U^*+\phi^{*(\mu)} + R[T]q^{*(\mu)}+RT^*\,[q]^{(\mu)}-a\left(R_f+\alpha\,\nabla^4\right)\,V^* \;=\; 0 \tag{2.22}$$

$$\frac{1}{1-\mu^2}\left\{-[U]\,T^{*(\lambda)}+V^*\,[T]^{(\mu)}-\kappa\,[T]\,\left\{U^{*(\lambda)}-V^{*(\mu)}\right\}\right\} + S^*\,\left\{\,[T]^{(\sigma)}+\kappa(1+\sigma)\,[T]\,\right\}+\kappa\,[T]\,S^{*(\sigma)} + \frac{a\,Q}{C_p}-a\left(K_t+\nu\,\nabla^4\right)\,T^* \;=\; 0 \tag{2.23}$$

$$\int_{-1}^{1}\left\{\,U^{*(\lambda)}-V^{*(\mu)}+[U]\,q^{*(\lambda)}-V^*\,[q]^{(\mu)}\,\right\}\,d\sigma \;=\; 0 \tag{2.24}$$

$$S^* \;=\; -\frac{1}{(1-\mu^2)\,(1-\sigma^2)}\int_1^{\sigma}\left\{U^{*(\lambda)}-V^{*(\mu)}+[U]\,q^{*(\lambda)}-V^*\,[q]^{(\mu)}\right\}d\sigma \tag{2.25}$$

$$(1+\sigma)\frac{\partial\phi^*}{\partial\sigma} \;=\; -\,R\,T^* \tag{2.26}$$

It should be particularly noted here that a pair of square brackets in the linearized equations indicates the longitudinal average, whereas a superscript asterisk denotes the local deviation from the zonal average.

This set of linear differential equations (2.21) - (2.26) constitutes a conceptual model for this study, governing the large scale atmospheric dynamics. The model

can be solved by numerical techniques one of which is the spectral method which is adopted in this investigation. The algorithm used and some related numerical techniques are fully described in Chapter 3.

§2.5 Forcing by Orography and Diabatic Heatings

In this model, the only physical forcings are mechanical forcing by orography and diabatic heating. Surface orography is coupled into the model by term ϕ_s in the boundary condition for (2.26). Both idealized and realistic forcing functions are used in this study. The idealized forcings are described where they are used. The topographic data used in this study were obtained from **ECMWF** at 1.875×1.875 degree resolution. The orography is smoothed in spectral space by mutiplying a smoothing function same as that introduced by Hoskins (1980). The diabatic heating, apart from Newtonian cooling, is collectively incorporated into the model via term aQ/C_p in (2.23). The "observed" diabatic heating used in this study is provided by the Department of Meteorology, Reading University (Hoskins, et el, 1989). Corrections in the lower levels of the observed heating data are described in Chapter 5 (Hoskins et al , personal communication).

§2.6 Parametrization of Dissipation

The parametrization of dissipation varies from model to model and is used to tune a specific model to be well behaved (see, e.g. Laursen et. el, 1989) . In the model of this study, Rayleigh friction, and Newtonian cooling R_f and K_t respectively with spatially-varying decay rates are included. A scale-selective horizontal smoothing is included by bi-Laplacian diffusion terms $\alpha\nabla^4$ and $\nu\nabla^4$. The dissipation coefficients R_f , K_t , α and ν are specified in Chapter 5 after various sensitivity experiments.

§2.7 Zonal Mean State

The zonal mean state has an essential influence on the model result (Nigam, et el, 1989; Kang, 1990). As we here investigate sattionary waves in northern–hemisphere winter, we have chosen to use the monthly mean of the **FGGE** data in January, 1979. The zonal mean state is incorporated into the model by interpolating it into σ levels both with and without inclusion of zonal mean orography. Both of the two kind of zonal mean states are used in the validation experiments in Chapter 5 although only the one with inclusion of zonal mean orography, which is considered more consistent, is used in Chapter 6.

Chapter 3

Numerical Algorithms

§3.1 Introduction

For the purpose of numerical integration, the field variables of meteorological parameters can be represented in different ways such as by values at a number of grid points or by the coefficients of a truncated expansion in orthogonal functions in the horizontal or vertical. In the present study, we choose numerical algorithms such that the dependent variables U, V, T, q of the linear primitive equations derived in Chapter 2 could be represented by truncated series of orthogonal functions, more specifically the normalized Legendre polynomials in the vertical and surface spherical harmonics in the horizontal, known as a three dimensional spectral representation. Since the model is linear, all the model operations are performed in spectral space. The solution of the model may be obtained via linear superimposition of different zonal wavenumbers.

The numerical algorithms used in the study follow those of Lei (1986) for his

hemispheric model with extension to global domain for this investigation. In this Chapter, we will describe the spectral method in detail, including the calculation of related terms in solving the model equations such as vertical velocity and geopotential height. Finally a method for obtaining the solution of the model is described.

§3.2 Three Dimensional Spectral Representation

Each of the dependent variables is now represented by truncated series of orthogonal spectral functions. For the vertical representation, the normalized Legendre polynomials with σ as argument are chosen, while the surface spherical harmonics are used as a basis function for the horizontal representation. Their characteristics and their evaluation are described below.

§3.2.1 Normalized Legendre Polynomials

The normalized Legendre polynomials, used for vertical representation, are defined as

$$P_k(\sigma) = \frac{(2k+1)^{1/2}}{2^k(k!)} \frac{d^k}{d\sigma^k} \left(\sigma^2 - 1\right)^k \tag{3.1}$$

They are orthogonal over the range of $-1 \leq \sigma \leq +1$:

$$\frac{1}{2}\int_{-1}^{1} P_k(\sigma)\, P_l(\sigma) d\sigma \;=\; \begin{cases} 1 & \text{for } k = l \\ 0 & \text{for } k \neq l \end{cases} \tag{3.2}$$

The horizontal representation of the dependent variables for each vertical mode is based on the surface spherical harmonics defined as

$$Y_{m,n}\,(\lambda,\mu) \;=\; P_{m,n}\,(\mu)\, e^{im\lambda} \tag{3.3}$$

where the normalized and associated Legendre functions $P_{m,n}\,(\mu)$ with μ as argument are defined as

$$P_{m,n}\,(\mu) \;=\; \left[(2n+1)\frac{(n-|m|)!}{(n+|m|)!}\right]^{1/2} \frac{(1-\mu^2)^{|m|/2}}{2^n n!} \frac{d^{n+|m|}}{d\mu^{n+|m|}} \left(\mu^2-1\right)^n \tag{3.4}$$

and are orthogonal over the range of $-1 \leq \mu \leq +1$:

$$\frac{1}{2}\int_{-1}^{1} P_{m,n}\,(\mu)\, P_{m',n'}\,(\mu) d\mu \;=\; \begin{cases} 1 & \text{for } m = m' \text{ and } n = n' \\ 0 & \text{otherwise} \end{cases} \tag{3.5}$$

Figs. 3.1 and 3.2 illustrates normalized Legendre functions with m and n annotated on each curve. Here $|m|$ is the zonal wavenumber, and $n - |m|$ is the number of

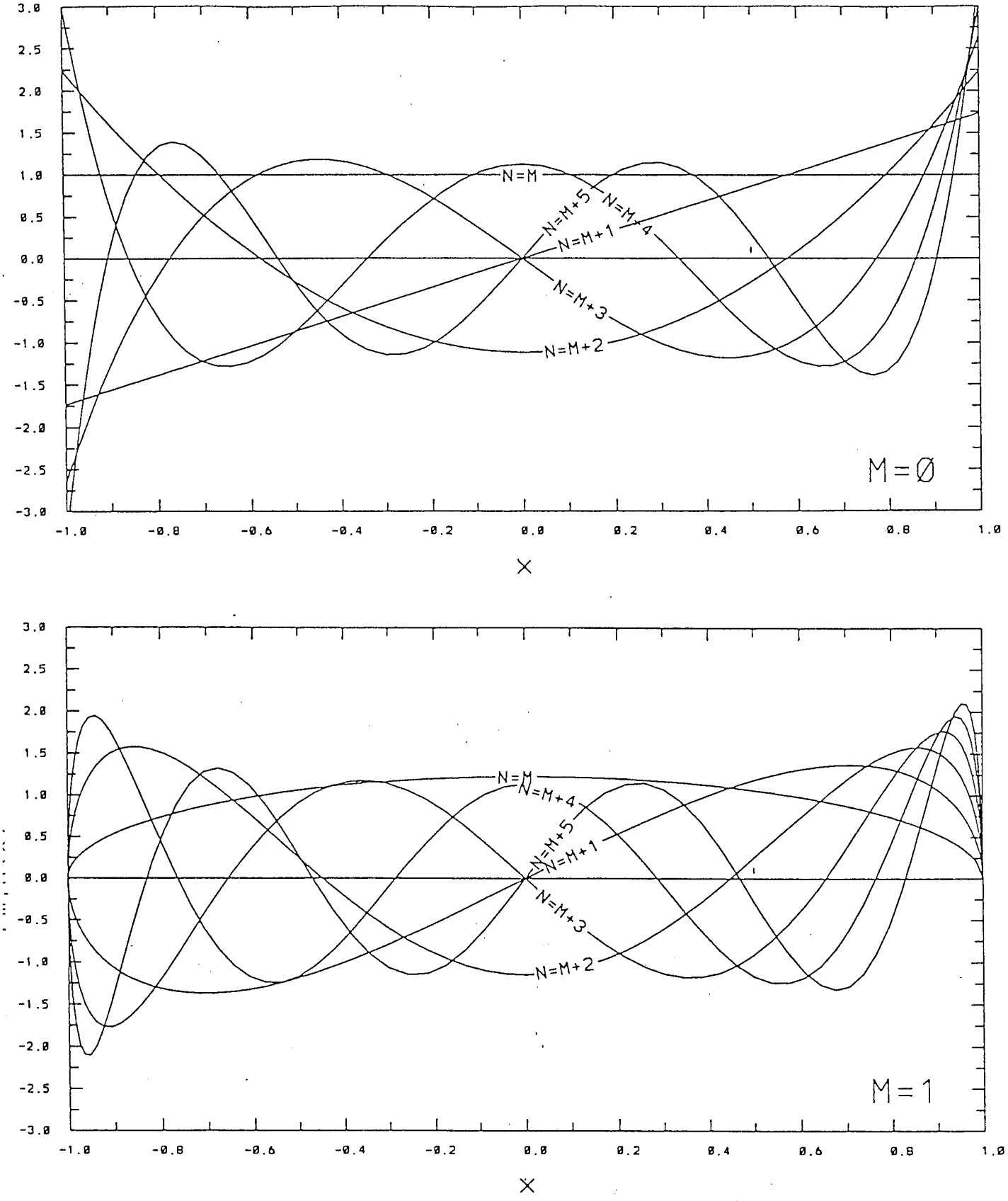

Figure 3.1: Legendre Function for M at lower-right corner of each figure, and N labeled on each curve.

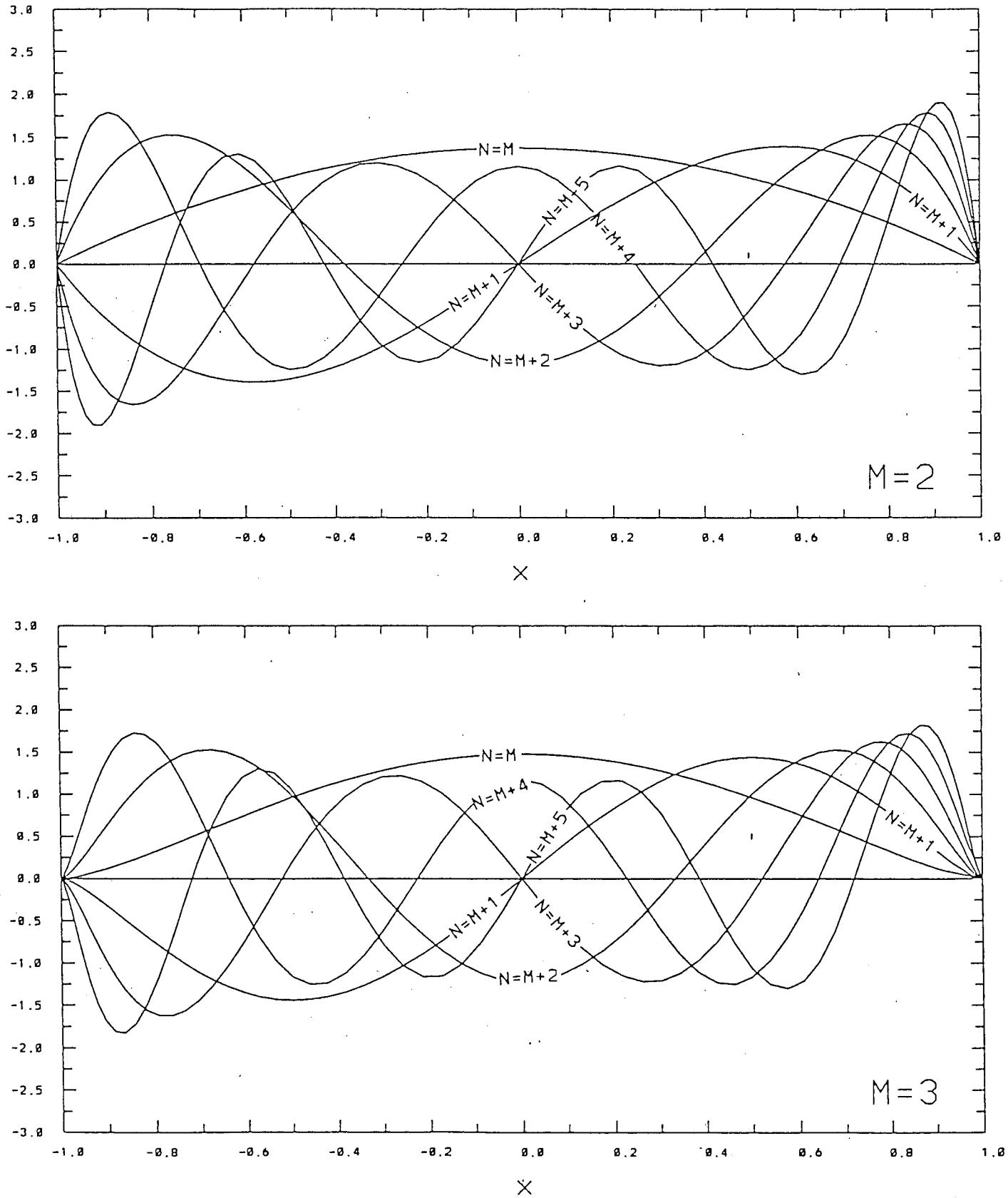

Figure 3.2: Figure 3.1 continued.

zeros for the Legendre functions between two poles.

For computational practicality, the following properties are used to compute the normalized and associated Legendre functions $P_{m,n}(\mu)$, namely,

$$\begin{cases} P_{m,n}(\mu) = 0 \qquad \text{when } n < m \\ P_{-m,n}(\mu) = P_{m,n}(\mu) \end{cases} \tag{3.6}$$

Together with the following recursion relationships:

$$P_{m,m+1}(\mu) = (2m+3)^{1/2}\mu P_{m,m}(\mu) \tag{3.7}$$

$$P_{m+1,m+1}(\mu) = \left[\frac{2m+3}{2m+2}\left(1-\mu^2\right)\right]^{1/2} P_{m,m}(\mu) \tag{3.8}$$

$$D_{m,n+1}P_{m,n+1}(\mu) = \mu P_{m,n}(\mu) - D_{m,n}P_{m,n-1}(\mu) \tag{3.9}$$

where

$$D_{m,n} = \left[\frac{n^2-m^2}{4n^2-1}\right]^{1/2} \tag{3.10}$$

Clearly, the associated Legendre functions $P_{m,n}(\mu)$ can be easily calculated at a specific coordinate point μ. For the Legendre polynomials $P_k(\sigma)$, they are just a subset of $P_{m,k}(\sigma)$ for $m = 0$. Therefore they are evaluated similarly with σ as the independent variable.

§3.2.2 Derivatives of the Normalized Legendre Polynomial

Using spectral representation in the present spectral model, the spatial partial derivatives of dependent variables with respect to μ and σ are easily computed in terms of the derivatives of normalized Legendre polynomials, $H_{m,n}(\mu)$ and $H_k(\sigma)$, respectively, which are expressed as

$$\begin{aligned} H_{m,n}(\mu) &= \left(\mu^2 - 1\right) \frac{dP_{m,n}(\mu)}{d\mu} \\ &= nD_{m,n+1} P_{m,n+1}(\mu) - (n+1) D_{m,n} P_{m,n-1}(\mu) \end{aligned} \tag{3.11}$$

$$\begin{aligned} H_k(\sigma) &= \left(\sigma^2 - 1\right) \frac{dP_k(\sigma)}{d\sigma} \\ &= kD_{0,k+1} P_{k+1}(\sigma) - (k+1) D_{0,k} P_{k-1}(\sigma) \end{aligned} \tag{3.12}$$

where $D_{m,n}$ has the same meaning as (3.10).

As shown in (3.11) and (3.12), the evaluation of $H_{m,n}(\mu)$ and $H_k(\sigma)$ is mainly dependent on the values of Legendre functions $P_{m,n}(\mu)$ and $P_k(\sigma)$ respectively. Since the $P_{m,n}(\mu)$ and $P_k(\sigma)$ are already available, the derivatives of the nomalized associated Legendre polynomials can be calculated easily.

§3.2.3 Spherical Harmonics

With the definition of spherical harmonics in (3.3), it can be seen that the functions $e^{im\lambda}$ are normalized, and exhibit the following orthogonality conditions,

$$\frac{1}{2\pi}\int_0^{2\pi} e^{im\lambda}\left(e^{im'\lambda}\right)^* d\lambda \;=\; \begin{cases} 1 \quad \text{for } m = m' \\ \\ 0 \quad \text{for } m \neq m' \end{cases} \tag{3.13}$$

From (3.5) and (3.13) , the spherical harmonics $Y_{m,n}(\mu,\,\lambda)$ have the following orthogonality relationship

$$\frac{1}{4\pi}\int_0^{2\pi}\int_{-1}^{1} Y_{m,n}\,(\mu,\lambda)\; Y^*_{m',n'}\,(\mu,\lambda)\,d\mu\,d\lambda \;=\; \begin{cases} 1 \quad \text{for } (m,n) = (m',n') \\ \\ 0 \quad \text{for } (m,n) \neq (m',n') \end{cases} \tag{3.14}$$

where the asterisk $*$ denotes the complex conjugate, i.e. $(e^{im'\lambda})^*$ and $e^{im'\lambda}$ are mutual complex conjugates, as are the $Y^*_{m',n'}\,(\mu,\lambda)$ and $Y_{m,n}\,(\mu,\lambda)$.

Furthermore, it is well known that the spherical harmonics $Y_{m,n}$ are *eigenfunctions* of the equation

$$\nabla^2\, Y + b\, Y \;=\; 0 \tag{3.15}$$

where ∇^2 is the two dimensional *Laplacian* operator on the sphere, i.e.

$$\nabla^2 \;\equiv\; \frac{1}{a^2}\left\{\frac{1}{1-\mu^2}\frac{\partial^2}{\partial\lambda^2} + \frac{\partial}{\partial\mu}\left[\left(1-\mu^2\right)\frac{\partial}{\partial\mu}\right]\right\} \tag{3.16}$$

and the *eigenvalues* b are given by

$$b = \frac{n(n+1)}{a^2} \tag{3.17}$$

With this characteristic of the spherical harmonics, diffusion terms of the form $\alpha\nabla^4$ are conveniently incorporated into the model, the details of which will be described in a later section.

§3.2.4 3–D Spectral Representation

From the orthogonality conditions of (3.2), (3.5) (3.13), we can now combine them to form three dimensional spectral functions as

$$X_{k,m,n}(\lambda,\mu,\sigma) = P_k(\sigma)\, P_{m,n}(\mu)\, e^{im\lambda} \tag{3.18}$$

and its orthogonality property

$$\frac{1}{8\pi}\int_0^{2\pi}\int_{-1}^{1}\int_{-1}^{1} X_{k,m,n}\, X^*_{k',m',n'}\, d\sigma\, d\mu\, d\lambda = \begin{cases} 1 & \text{for } (k,m,n) = (k',m',n') \\ 0 & \text{for } (k,m,n) \neq (k',m',n') \end{cases} \tag{3.19}$$

The functions expressed in (3.18) are now the basis functions for three dimensional spectral representation. For explicit expressions, we will later use the right hand side of (3.18) instead of $X_{k,m,n}(\lambda,\mu,\sigma)$ itself.

By using these basis functions, the dependent variables and the constant surface geopotential height described by surface orography are simply represented by the following truncated series

$$U(\lambda,\mu,\sigma) = \sum_{k=0}^{L}\sum_{m=-M}^{M}\sum_{n=|m|}^{N} U_{k,m,n}P_k(\sigma)e^{im\lambda}P_{m,n}(\mu) \tag{3.20}$$

$$V(\lambda,\mu,\sigma) = \sum_{k=0}^{L}\sum_{m=-M}^{M}\sum_{n=|m|}^{N} V_{k,m,n}P_k(\sigma)e^{im\lambda}P_{m,n}(\mu) \tag{3.21}$$

$$T(\lambda,\mu,\sigma) = \sum_{k=0}^{L}\sum_{m=-M}^{M}\sum_{n=|m|}^{N} V_{k,m,n}P_k(\sigma)e^{im\lambda}P_{m,n}(\mu) \tag{3.22}$$

$$q(\lambda,\,\mu) = \sum_{m=-M}^{M}\sum_{n=|m|}^{N} q_{m,n}e^{im\lambda}P_{m,n}(\mu) \tag{3.23}$$

$$\phi_s\,(\lambda,\,\mu) = \sum_{m=-M}^{M}\sum_{n=|m|}^{N} \phi_{s\;m,n}e^{im\lambda}P_{m,n}(\mu) \tag{3.24}$$

Each of these series may be split up as shown below for U as an example

$$\begin{cases} U\,(\lambda,\mu,\sigma) = \sum\limits_{k=0}^{L} U_k\,(\lambda,\mu)\;P_k\,(\sigma) \\ U_k\,(\lambda,\mu) = \sum\limits_{m=-M}^{M} U_{k,m}\,(\mu)\;e^{im\lambda} \\ U_{k,m}\,(\mu) = \sum\limits_{n=|m|}^{M} U_{k,m,n}\;P_{mn}\,(\mu) \end{cases} \tag{3.25}$$

The longitudinally averaged zonal component of velocity $[U]_{k,n}$ can be hereby represented as a subset of $U_{k,m,n}$ for $m = 0$, and its deviation from the zonal mean U^* for $m \neq 0$.

In view of the orthogonality property of the spherical harmonics and Legendre polynomials, the expansion coefficients on the right hand of (3.20) – (3.24) are conveniently evaluated if the spatial distributation of the relevant variables is known. For example, the coefficients $U_{k,m,n}$ can be thought of as the orthogonal projection of $U_{\lambda,\mu,\sigma}$ onto the spectral space generated by $P_k\ (\sigma)\ e^{im\,\lambda}\ P_{m,n}\ (\mu)$, namely

$$U_{k,m,n} = \frac{1}{8\pi}\int_{-1}^{1}\int_{-1}^{1}\int_{0}^{2\pi} U(\lambda,\mu,\sigma)\ P_k(\sigma)\ e^{im\lambda}\ P_{m,n}(\mu)\ d\lambda\, d\mu\, d\sigma \qquad (3.26)$$

The expressions for $V_{k,m,n}$, $T_{k,m,n}$, $q_{m,n}$, *and* $\phi_{s\,m,n}$ may be expressed in an analogous fashion.

§3.2.5 Calculation of Spectral Coefficients of Dependent Variables and Their Derivatives

The spectral coefficients, $U_{k,m,n}$, for instance, in (3.26) can be calculated by numerical integration. It is triple integration but may be split up into three single integrals, i.e.

$$U_{k,m,n} = \frac{1}{2}\int_{-1}^{1} U_{m,n}\ (\sigma)\ P_k(\sigma)\ d\sigma \qquad (3.27)$$

$$U_{m,n}(\sigma) = \frac{1}{2}\int_{-1}^{1} U_m(\mu,\sigma)\, P_{m',n}(\mu)d\mu \tag{3.28}$$

$$U_m(\mu,\sigma) = \frac{1}{2\pi}\int_0^{2\pi} U(\lambda,\mu,\sigma)\, e^{-im\lambda}d\lambda \tag{3.29}$$

Commonly the integral in (3.29) could be calculated efficiently by using the Fast Fourier Transform (FFT) method in numerical weather prediction models and general circulation models, in which the prognostic variables are represented by spherical harmonics and there are nonlinear problems involved. In this model, however, the trapezodial quadrature formula is chosen for computing the integration in (3.29) along with the Gauss–Legendre quadrature formula for (3.27) and (3.28). Both of the quadrature formulae are described briefly below.

Trapezoidal Quadrature For any function $f(x)$ which is a truncated trigonometric series, the integral $\frac{1}{2\pi}\int_0^{2\pi} f(x)\,dx$ can be evaluated by trapezodial quadrature on equally spaced abscissae with the following expression

$$\frac{1}{2\pi}\int_0^{2\pi} f(x)\,dx \approx \frac{1}{N}\sum_{i=1}^{N} f\left[\frac{2\pi}{N}i\right] \tag{3.30}$$

It is exact in the truncated area with maximum wavenumber smaller than or equal to $N-1$ (e.g. Krylov (1962)). With this formula, (3.29) could be calculated for a particular μ and σ by the expression below

$$U_m(\mu,\sigma) = \frac{1}{N}\sum_{j=1}^{N} U(\lambda_j,\mu,\sigma)\, e^{-im\lambda_j} \tag{3.31}$$

Gauss–Legendre Quadrature The idea of *Gaussian Quadrature* is to choose both weighting coefficients and the location of the abscissae–Gaussian grid points at which the function is to be evaluated. The Gaussian grid points are not equally spaced. Using Gaussian quadrature, a satisfactory accuracy can be achieved. Furthermore, the weights and abscissae can be arranged for the Gaussian quadrature formulae to make the integral exact for (3.27) and (3.28). Given the number of Gaussian grid points between poles N, a set of weights w_i and Gaussian grid points μ_i could be found such that the approximation for any polynomial of degree smaller than or equal to $2N-1$ may be obtained by the expression

$$\int_{-1}^{1} f(\mu)\, d\mu \approx \sum_{i=1}^{N} w_i\, f(\mu_i) \tag{3.32}$$

where the Gaussian grid points μ_i's are given by the roots of the *Legendre Polynomial* $P_N(\mu)$, and the corresponding weighting coefficients are given by

$$w_i = \frac{2\,(1-\mu_i^2)}{(N\, P_{N-1}(\mu_i))^2} \tag{3.33}$$

The weights themselves satisfy

$$\sum_{i=1}^{N} w_i = 2.0 \tag{3.34}$$

Then the abcsissa μ_i's are obtained by using **Newtonian iteration** to solve the following nonlinear equation

$$P_N(\mu_i) = 0 \tag{3.35}$$

With Newtonian iteration, the iteration procedure can be described as below

$$\mu_i^{(k+1)} = \mu_i^{(k)} - \frac{P_N(\mu_i^{(k)})}{P'_N(\mu_i^{(k)})} \tag{3.36}$$

where the derivative $P'_N(\mu_i^{(k)})$ may be computed by the recurrence formula

$$P'_N(\mu) = \frac{N\left(P_{N-1}(\mu) - \mu P_N(\mu)\right)}{1-\mu^2} \tag{3.37}$$

and the initial guess $x_i^{(0)}$ can be taken as

$$\mu_i^{(0)} = \sin\left[\frac{\pi(i-0.5)}{N} - \frac{\pi}{2}\right] \tag{3.38}$$

Using the *Gaussian quadrature* formula, the integrals (3.27) and (3.28) may be evaluated respectively as follows

$$U_{k,m,n} = \frac{1}{2}\sum_{i=1}^{N3} U_{m,n}(\sigma_i)\, P_k(\sigma_i)\, w(\sigma_i) \tag{3.39}$$

$$U_{m,n}(\sigma) = \frac{1}{2}\sum_{j=1}^{N2} U_m(\mu_j, \sigma)\, P_{m,n}(\mu_j)\, w(\mu_j) \tag{3.40}$$

where N_2 and N_3 are the numbers of the Gaussian grid points for variables μ and σ respectively, and will be described in detail later.

Derivatives of field variables Since the truncated series used in the spectral model to represent the dependent variables have prescribed spatial structures, the spatial partial derivatives of the dependent variables can be easily expressed in spectral form, which is shown below, taking an example for U :

$$U^{(\lambda)} = \sum_{k=0}^{L} \sum_{m=-M}^{M} \sum_{n=|m|}^{N+1} imU_{k,m,n} P_k(\sigma) e^{im\lambda} P_{m,n}(\mu) \tag{3.41}$$

$$U^{(\mu)} = \sum_{k=0}^{L} \sum_{m=-M}^{M} \sum_{n=|m|}^{N+1} U_{k,m,n} P_k(\sigma) e^{im\lambda} H_{m,n}(\mu) \tag{3.42}$$

$$U^{(\sigma)} = \sum_{k=0}^{L} \sum_{m=-M}^{M} \sum_{n=|m|}^{N+1} imU_{k,m,n} H_k(\sigma) e^{im\lambda} P_{m,n}(\mu) \tag{3.43}$$

where $H_{m,n}(\mu)$ and $H_k(\sigma)$ are defined in (3.11) and (3.12) respectively. It can be seen that the spatial partial derivatives of the dependent variable U in physical space can be easily evaluated as long as the spectral coefficients $U_{k,m,n}$ are known.

Computational Grid In order to make numerical integration by trapezoidal quadrature and Gauss–Legendre quadrature exact within the truncated area, there should be a sufficient number of grid points. The algebra involved in numbering computational grid points for a variety of trunctions has been presented in several publications (Daley et el., 1978; Bourke, 1972, 1974; Bourke et el., 1977; Machenhauer, 1979; Williamson et el., 1987). If the triangular type of truncation ($N = M$) is used for all variables, with satisfactory accuracy of integration

for quadratic terms, the number of grid points for equally spaced longitudes, N_1, Gaussian latitudes, N_2, and Gaussian levels, N_3 must satisfy respectively

$$\begin{cases} N_1 \geq 3M+1 \\ N_2 \geq \frac{3M+1}{2} \\ N_3 \geq \frac{3L+1}{2} \end{cases} \tag{3.44}$$

§3.3 Streamfunction and Velocity Potential

As shown by Eliasen et al. (1970) and Machenhauer (1979), the representation of the velocity field U, V is equivalent to the representation of a velocity field by the truncated series of the streamfunction ψ and velocity potential χ, expressed as

$$\begin{cases} \psi = \sum_{m=-M}^{M} \sum_{n=|m|}^{N} \psi_{m,n}(\sigma)\, Y_{m,n}(\lambda,\mu) \\ \chi = \sum_{m=-M}^{M} \sum_{n=|m|}^{N} \chi_{m,n}(\sigma)\, Y_{m,n}(\lambda,\mu) \end{cases} \tag{3.45}$$

with the definitions between U, V, and χ, ψ as follows :

$$\begin{cases} U &= \frac{1}{a}\left(\chi^{(\lambda)} + \psi^{(\mu)}\right) \\ V &= \frac{1}{a}\left(\psi^{(\lambda)} - \chi^{(\mu)}\right) \end{cases} \tag{3.46}$$

then the ψ and χ may be diagnosed by using U, V from the following explicit expression

$$\begin{cases} \nabla^2 \psi &= \frac{1}{a}\left(U^{(\mu)} + V^{(\lambda)}\right) / (1-\mu^2) \\ \nabla^2 \chi &= \frac{1}{a}\left(U^{(\lambda)} - V^{(\mu)}\right) / (1-\mu^2) \end{cases} \tag{3.47}$$

If we substitute the truncated series of (3.45) into equation (3.46), then we obtain

$$\begin{cases} U &= \sum_{m=-M}^{M} \sum_{n=|m|}^{N+1} U_{m,n}(\sigma)\, Y_{m,n}(\lambda,\mu) \\ V &= \sum_{m=-M}^{M} \sum_{n=|m|}^{N+1} V_{m,n}(\sigma)\, Y_{m,n}(\lambda,\mu) \end{cases} \tag{3.48}$$

where the coefficients $U_{m,n}$ and $V_{m,n}$ are, by making use of relations (3.11) and (3.9), determined from the coefficients $\psi_{m,n}$ and $\chi_{m,n}$ by the relations

$$U_{m,n} = \frac{1}{a}\left[(n-1)D_{m,n}\,\psi_{m,n-1} + im\chi_{m,n} - (n+2)D_{m,n+1}\,\psi_{m,n+1}\right] \tag{3.49}$$

$$V_{m,n} = \frac{1}{a}\left[(n-1)D_{m,n}\,\chi_{m,n-1} + im\psi_{m,n} + (n+2)D_{m,n+1}\,\chi_{m,n+1}\right] \quad (3.50)$$

where

$$D_{m,n} = \left[\frac{n^2-m^2}{4n^2-1}\right]^{1/2}$$

From (3.49)and (3.50), it is obvious that there must exist certain relationships between $U_{m,n}$ and $V_{m,n}$ as the number of those coefficients is one degree larger than that of the coefficients $\psi_{m,n}$ and $\chi_{m,n}$. These relations can be derived and have the following expression (see Machenhauer, 1979)

$$\sum_{n=|m|}^{N+1}\left(\delta_A^{(n-m)}\,U_{m,n} + \delta_S^{(n-m)}\,i\,V_{m,n}\right)\,C_{m,n} = 0 \quad (3.51)$$

$$\sum_{n=|m|}^{N+1}\left(\delta_S^{(n-m)}\,U_{m,n} + \delta_A^{(n-m)}\,i\,V_{m,n}\right)\,C_{m,n} = 0 \quad (3.52)$$

where

$$\delta_A^{(n-m)} = \begin{cases} 1 & \text{for } n-m \text{ odd} \\ 0 & \text{for } n-m \text{ even} \end{cases}$$

and

$$\delta_S^{(n-m)} = \begin{cases} 1 & \text{for } n-m \text{ even} \\ 0 & \text{for } n-m \text{ odd} \end{cases}$$

The values of $C_{m,n}$ for $n \leq N$ are given by

$$C_{m,n} = -\left[\frac{2n+1}{2n+3}\frac{(n-m+1)}{(n+m+1)}\frac{(n-m)}{(n+m)}\frac{(n-m-1)}{(n+m-1)}\frac{\ldots(n-m+1)}{\ldots((n+m+1)}\right]^{1/2}$$

providing the values $C_{m,N+1}$ are chosen to be

$$C_{m,N+1} = -1$$

From equations (3.51)–(3.52), the coefficients of $U_{m,N+1}$ and $V_{m,N+1}$ are described separately with their symmetricity and antisymmetricity (that is, U symmetric and V antisymmetric with respect to the Equator). In another words, the symmetric part of the coefficients $U_{m,N+1}$ and antisymmetric part of $V_{m,N+1}$ can only be evaluated by the symmetric part of coefficients $U_{m,n}$ and the antisymmetric part of $V_{m,n}$ for particular m, where $0 \leq m \leq n \leq N$.

In the special case $m = 0$, the relations above become

$$\sum_{0}^{N+1} \delta_A^{(n-m)} C_{0,n} U_{0,n} = 0 \qquad (3.53)$$

$$\sum_{0}^{N+1} \delta_S^{(n-m)} C_{0,n} V_{0,n} = 0 \tag{3.54}$$

$$\sum_{0}^{N+1} \delta_S^{(n-m)} C_{0,n} U_{0,n} = 0 \tag{3.55}$$

$$\sum_{0}^{N+1} \delta_A^{(n-m)} C_{0,n} V_{0,n} = 0 \tag{3.56}$$

The equations (3.51) – (3.56) are referred to as "truncation relations" with which the extra degree of coefficients for U and V are calculated.

§3.4 Vertical Velocity

The vertical velocity S as well as its partial derivative with respect to σ $S^{(\sigma)}$ can be evaluated in terms of the spectral coefficients of U, V, and q. The calculation of S and $S^{(\sigma)}$ involves the vertical integration of the continuity equation. S may be calculated from (2.16). Substituting the vertical expansions of U and V, integrating the finite series term by term and using (2.15), then we have

$$S = \frac{1}{1-\mu^2} \sum_{k=1}^{L} \left(U_k^{(\lambda)} - V_k^{(\mu)} + U_k q^{(\lambda)} - V_k q^{(\mu)} \right) K_k(\sigma) \tag{3.57}$$

where

$$K_k(\sigma) = \frac{1}{\sigma^2 - 1} \int_1^{\sigma} P_k(\sigma)\, d\sigma \tag{3.58}$$

$K_k(\sigma)$ are found to be polynomials of degree $k-1$ with σ as their argument.

In order to calculate the vertical velocity, the intergrals (3.58) must be evaluated first. A substitution of independent variable needs to be made such that the integral intervals are transformed into the interval from -1 to 1 inclusive. For example, the integral (3.58) can be transformed into

$$K_l(\sigma) = \frac{1}{2(\sigma+1)} \int_{-1}^{1} P_l \left[\frac{\sigma+1}{2} + \frac{\sigma-1}{2} t \right] dt \tag{3.59}$$

Using the Gauss-Legendre quadrature formula, (3.32), for the above integral at each Gaussian level σ_k , we have

$$K_l(\sigma_k) = \frac{1}{2(\sigma_k+1)} \sum_{i=1}^{n} w_i P_l(x_i) \tag{3.60}$$

where x_i is in a form as

$$x_i = \frac{\sigma_k+1}{2} + \frac{\sigma_k-1}{2} t_i \tag{3.61}$$

and the t_i are the zero points of the Legendre polynomial $P_N(t)$, i.e.

$$P_N(t_i) = 0 \tag{3.62}$$

The partial derivative of vertical velocity with respect to σ, i.e. $S^{(\sigma)}$ may be evaluated according to a formula derived directly from (3.57), in an expression as

$$S^{(\sigma)} = \frac{1}{1-\mu^2}\sum_{k=2}^{L}\left(U_k^{(\lambda)} - V_k^{(\mu)} + U_k q^{(\lambda)} - V_k q^{(\mu)}\right) G_k(\sigma) \tag{3.63}$$

where $G_k(\sigma)$ bear the expression below

$$\begin{aligned} G_k(\sigma) &= \left(\sigma^2 - 1\right)\frac{dK_k(\sigma)}{d\sigma} \\ &= P_k(\sigma) - \frac{2\sigma}{\sigma^2 - 1}\int_1^\sigma P_k(\sigma)\, d\sigma \end{aligned} \tag{3.64}$$

It can be seen that $G_k(\sigma)$ are easily calculated with the values of $K_k(\sigma)$ which are evaluated previously. It may also be seen that $G_k(\sigma)$ are polynomials in σ of degree k, and the lower index in (3.63) is 2 because $G_1(\sigma) \equiv 0$ (see, e.g. Lei, 1986).

§3.5 Geopotential Height

The geopotential height ϕ can be diagnosed from temperature field by integrating the hydrostatic equation (2.26) with the lower boundary condition (2.10), i.e.

$$\phi = \phi_s - R\int_1^\sigma \frac{T}{1+\sigma}\, d\sigma \tag{3.65}$$

Substituting the vertical expansion of T in (3.22) into (3.65) and integrating term by term, we have the following expression as

$$\phi = \phi_s - R\sum_{k=0}^{L} T_k\, I_k(\sigma) \tag{3.66}$$

where

$$I_k(\sigma) = \int_1^{\sigma} \frac{P_k(\sigma)}{1+\sigma}\, d\sigma \tag{3.67}$$

The $I_k(\sigma)$ is found not to be a polynomial in σ as the result of the integration with respect to σ, rather it may be calculated approximately by numerical integration for each vertical level σ_k ($\sigma_k \neq 0$). The Gauss–Legendre quadrature described in the previous section is employed to evaluate $I_k(\sigma)$, i.e. in the same manner as $K_k(\sigma)$.

For evaluation of geopotential height, a temperature correction procedure has been suggested by Machenhaure and Daley (1972) in their forecasting model, which leads to another scheme to evaluate the geopotential and ensure that there are no spurious energy sources introduced during the time integration. It is not necessary in the present formulation of the steady–state model since there is no time integration involved.

§3.6 Calculation of Horizontal Diffusion

The horizontal diffusion term $\alpha\nabla^4$, mentioned in a previous section, is easily represented by the following expression

$$\alpha \nabla^4 U = \frac{\alpha}{a^4} \sum_{k=0}^{L} \sum_{m=-M}^{M} \sum_{n=|m|}^{M} n^2(n+1)^2 U_{k,m,n} P_k(\sigma) e^{im\lambda} P_{m,n}(\mu) \quad (3.68)$$

§3.7 Method for the Solution of the Model

With the algorithms described above for computing the relevant terms of the model, the model solution could be achieved in spectral space for zonal wavenumber one by one. The method for the solution of the model follows much the same approach as Lei (1986). For the completeness of the thesis, the procedure is outlined in this section.

In order to obtain a linear algebraic equation system, i.e. a matrix, the following procedures are taken:

- add the diagnostic equations for vertical velocity and geopotential to equations (2.21) - (2.24) to yield a complete system for the unknown variables U^*, V^*, T^*, q^* and diagnostic variables ϕ^* and S^*;
- insert the spectral expressions of the unknown variable fields into those equations;
- make an orthogonal projection on the sub-spectral space generated by $P_l(\sigma)\, e^{im\lambda}\, P_{m,j}(\mu)$ with respect to various combinations of index values of k and n.

After laborious manipulation, the linear equation for each zonal wavenumber m may be written in the form

$$\begin{bmatrix} \mathbf{X1} & \mathbf{X2} & \mathbf{X3} & \mathbf{X4} \\ \mathbf{Y1} & \mathbf{Y2} & \mathbf{Y3} & \mathbf{Y4} \\ \mathbf{T1} & \mathbf{T2} & \mathbf{T3} & \mathbf{T4} \\ \mathbf{C1} & \mathbf{C2} & \mathbf{C3} & \mathbf{C4} \end{bmatrix} \begin{bmatrix} \mathbf{U} \\ \mathbf{V} \\ \mathbf{T} \\ \mathbf{Q} \end{bmatrix} = \begin{bmatrix} \mathbf{F1} \\ \mathbf{F2} \\ \mathbf{F3} \\ \mathbf{0} \end{bmatrix} \tag{3.69}$$

where $\mathbf{U}$ is the column vector with the element $U_{k,m,n}$ $(k = 0, 1, \ldots, L; n = m, m+1, \ldots, N.)$ and $\mathbf{V}$, $\mathbf{T}$, $\mathbf{Q}$ are similar column vectors. $\mathbf{0}$ is a zero column vector. The elements of the coefficient matrix and the other column vectors in the right hand side of the (3.69) could be expressed as follows

$$\begin{aligned} X1_{l,n;k,j} &= -\frac{1}{4}\int_{-1}^{1}\int_{-1}^{1}\left\{\frac{im}{1-\mu^2}[U] + aR_f + \frac{\alpha j^2(j+1)^2}{a^3}\right\} \\ &\qquad P_{m,j}P_kP_{m,n}P_l \; d\mu d\sigma \\ &\quad + \delta'_{k,0} im \frac{1}{4}\int_{-1}^{1}\int_{-1}^{1}\frac{1}{1-\mu^2}[U]^{(\sigma)}P_{m,j}K_kP_{m,n}P_l d\mu d\sigma \end{aligned} \tag{3.70}$$

$$\begin{aligned} X2_{l,n;k,j} &= \frac{1}{4}\int_{-1}^{1}\int_{-1}^{1}\frac{1}{1-\mu^2}[U]^{(\mu)}P_{m,j}P_kP_{m,n}P_l \; d\mu d\sigma \\ &\quad - \delta'_{k,0}\frac{1}{4}\int_{-1}^{1}\int_{-1}^{1}\frac{1}{1-\mu^2}[U]^{(\sigma)}H_{m,j}K_kP_{m,n}P_l \; d\mu a\sigma \\ &\quad - \delta'_{k,0}\frac{1}{4}\int_{-1}^{1}\int_{-1}^{1}\frac{1}{1-\mu^2}[U]^{(\sigma)}[q]^{(\sigma)}P_{m,j}K_kP_{m,n}P_l \; d\mu d\sigma \\ &\quad + \delta_{k,l}\Omega a\int_{-1}^{1}\mu P_{m,j}P_{m,n} \; d\mu \end{aligned} \tag{3.71}$$

$$X3_{l,n;k,j} = \varepsilon_{k,l}\,\delta_{j,n}\,imR \tag{3.72}$$

$$X4_{l,n;j} = \frac{im}{4}\int_{-1}^{1}\int_{-1}^{1}\left\{\frac{1}{1-\mu^2}[U]^{(\sigma)}\overline{U}^* - R[T]\right\}P_{m,j}P_{m,n}P_l\,d\mu d\sigma \tag{3.73}$$

$$\begin{aligned} Y1_{l,n;k,j} &= -\frac{1}{2}\int_{-1}^{1}\int_{-1}^{1}\frac{1}{1-\mu^2}\mu[U]P_{m,j}P_kP_{m,n}P_l\,d\mu d\sigma \\ &\quad - \delta_{k,l}\Omega a\int_{-1}^{1}\mu P_{m,j}P_{m,n}\,a\mu \end{aligned} \tag{3.74}$$

$$\begin{aligned} Y2_{l,n;k,j} &= -\frac{1}{4}\int_{-1}^{1}\int_{-1}^{1}\left\{\frac{im}{1-\mu^2}[U] + aR_f + \frac{\alpha j^2(j+1)^2}{a^3}\right\} \\ &\qquad P_{m,j}P_kP_{m,n}P_l\,d\mu d\sigma \end{aligned} \tag{3.75}$$

$$\begin{aligned} Y3_{l,n;k,j} &= \delta_{k,l}R\frac{1}{2}\int_{-1}^{1}[q]^{(\mu)}P_{m,j}P_{m,n} \\ &\quad + \varepsilon_{k,l}\left\{-\delta_{j,n-1}(n-1)RD_{m,n} - \delta_{j,n+1}(n+2)RD_{m,n+1}\right\} \end{aligned} \tag{3.76}$$

$$Y4_{l,n;j} = \frac{R}{4}\int_{-1}^{1}\int_{-1}^{1}[T]H_{m,j}P_{m,n}P_l\,d\mu d\sigma \tag{3.77}$$

$$\begin{aligned} T1_{l,n;k,j} &= -\frac{im\kappa}{4}\int_{-1}^{1}\int_{-1}^{1}\frac{1-\mu^2}{[}T]P_{m,j}P_kP_{m,n}P_l\,d\mu d\sigma \\ &\quad + \delta'_{k,0}\frac{im}{4}\int_{-1}^{1}\int_{-1}^{1}\frac{1}{1-\mu^2}\left\{[T]^{(\sigma)} + \kappa(1+\sigma)[T]\right\} \\ &\qquad P_{m,j}K_kP_{m,n}P_l\,d\mu d\sigma \\ &\quad + \delta'_{k,0}\delta'_{k,1}\frac{im\kappa}{4}\int_{-1}^{1}\int_{-1}^{1}\frac{1}{1-\mu^2}[T]P_{m,j}G_kP_{m,n}P_l\,d\mu d\sigma \end{aligned} \tag{3.78}$$

$$\begin{aligned} T2_{l,n;k,j} &= \frac{1}{4}\int_{-1}^{1}\int_{-1}^{1}\frac{1}{1-\mu^2}[T]^{(\mu)}P_{m,j}P_kP_{m,n}P_l\,d\mu d\sigma \\ &\quad + \frac{\kappa}{4}\int_{-1}^{1}\int_{-1}^{1}\frac{1}{1-\mu^2}[T]H_{m,j}P_kP_{m,n}P_l\,d\mu d\sigma \\ &\quad - \delta'_{k,0}\frac{1}{4}\int_{-1}^{1}\int_{-1}^{1}\frac{1}{1-\mu^2}\left\{[T]^{(\sigma)} + \kappa(1+\sigma)[T]\right\} \\ &\qquad H_{m,j}K_kP_{m,n}P_l\,d\mu d\sigma \\ &\quad - \delta'_{k,0}\frac{1}{4}\int^{1} -1\int_{-1}^{1}\frac{1}{1-\mu^2}\left\{[T]^{(\sigma)} + \kappa(1+\sigma)[T]\right\} \\ &\qquad [q]^{(\mu)}P_{m,j}K_kP_{m,n}P_l\,d\mu d\sigma \\ &\quad - \delta'_{k,0}\delta'_{k,1}\frac{\kappa}{4}\int_{-1}^{1}\int_{-1}^{1}\frac{1}{1-\mu^2}[T]H_{m,j}G_kP_{m,n}P_l\,d\mu d\sigma \\ &\quad - \delta'_{k,0}\delta'_{k,1}\frac{\kappa}{4}\int_{-1}^{1}\int_{-1}^{1}\frac{1}{1-\mu^2}[T][q]^{(\mu)} \\ &\qquad H_{m,j}G_kP_{m,n}P_l\,d\mu d\sigma \end{aligned} \tag{3.79}$$

$$T3_{l,n;k,j} = -\frac{1}{4}\int_{-1}^{1}\int_{-1}^{1}\left\{\frac{im}{1-\mu^2}[U] + aK_t + \frac{\nu j^2(j+1)^2}{a^3}\right\} P_{m,j}P_kP_{m,n}P_l\,d\mu d\sigma \tag{3.80}$$

$$T4_{l,n;j} = \frac{im}{4}\int_{-1}^{1}\int_{-1}^{1}\frac{1}{1-\mu^2}\left\{[T]^{(\sigma)} + \kappa(1+\sigma)[T]\right\} \overline{U}^{*}P_{m,j}P_{m,n}P_l\,d\mu d\sigma + \frac{im\kappa}{4}\int_{-1}^{1}\int_{-1}^{1}\frac{1}{1-\mu^2}[T]\overline{U}^{**}P_{m,j}P_{m,n}P_l\,d\mu d\sigma \tag{3.81}$$

$$C1_{n;k,j} = \delta_{k,0}\,\delta_{j,n}\,im \tag{3.82}$$

$$C2_{n;k,j} = -\delta_{k,0}\frac{1}{2}\int_{-1}^{1}[q]^{(\mu)}P_{m,j}\,P_{m,n}\,d\mu - \delta_{k,0}\left\{\delta_{j,n-1}(n-1)D_{m,n} - \delta_{j,n+1}(n+2)D_{m,n+1}\right\} \tag{3.83}$$

$$C3_{n;k,j} = 0 \tag{3.84}$$

$$C4_{n;j} = \frac{im}{2}\int_{-1}^{1}U_{0,0}P_{m,j}P_{m,n}\,d\mu \tag{3.85}$$

$$F1_{l,n} = \delta_{l,0}\,im\,\phi_{s\,m,n} \tag{3.86}$$

$$F2_{l,n} = -\delta_{l,0}\left\{(n-1)D_{m,n}\phi_{s\,m,n-1} - (n+2)D_{m,n+1}\phi_{s\,m,n+1}\right\} \tag{3.87}$$

$$F3_{l,n} = -\frac{a\,Q_{l,m,n}}{C_p} \tag{3.88}$$

where

$$\overline{U}^{*} = \sum_{k=1}^{L}U_{k,0}\,K_k\,(\sigma) \tag{3.89}$$

$$\overline{U}^{**} = \sum_{k=2}^{L}U_{k,0}\,G_k\,(\sigma) \tag{3.90}$$

$$U_{0,0} = \frac{1}{2}\int_{-1}^{1}[U]\,d\sigma \tag{3.91}$$

$$\varepsilon_{k,l} = \frac{1}{2}\int_{-1}^{1}I_k\,(\sigma)\,P_l\,(\sigma)\,d\sigma \tag{3.92}$$

$$\delta_{l,k} = \begin{cases} 1 \quad \text{when} \quad l = k \\ 0 \quad \text{otherwise} \end{cases}$$

$$\delta'_{l,k} = \begin{cases} 0 \quad \text{when} \quad l = k \\ 1 \quad \text{otherwise} \end{cases}$$

$$\begin{cases} l,\ k = 0, 1, 2, \ldots, L \\ j,\ n = m, m+1, \ldots, N \end{cases}$$

It may be seen from the above expressions that the calculation of the elements of the coefficient matrice are mainly involved in evaluating the integrals with respect to μ and σ. If the basic zonal mean state is represented by truncated series, those integrals can be calculated exactly in terms of the Gauss–Legendre quadrature formula described in §3.2.5.

The set of equations (3.69) being a linear system could be solved by usual way of matrix conversion, e.g. Gauss elimination. The solution for several wavenumbers is just a linear superimposition of solutions for every individual wavenumber.

§3.8 Transformation from Spectral to Grid Space

The transformation from spectral to grid space needs to be performed in the present study for evaluating spatial partial derivatives and post-processing of the model product. For variable U, for instance, at certain isobaric surface, the horizontal transformation is given by

$$U(\lambda, \mu) = \sum_{m=-M}^{M} \left[\sum_{n=|m|}^{N+1} U_{m,n} P_{m,n}(\mu) \right] e^{im\lambda} \tag{3.93}$$

The inner sum is performed essentially as a vector product over n. The outer sum could be performed again by an **FFT** subroutine in most forecasting spectral models and general circulation spectral models. However, due to simplicity in configuration as well as in computation of the model, we perform the outer summation directly from the procedure below.

Since the $U(\lambda, \mu)$ should be real, the calculation of (3.93) need be made only over $m \geq 0$ because the $U_{m,n}$ for $m < 0$ are the complex conjugate of $U_{m,n}$ for $m > 0$. Therefore equation (3.93) can be rewritten as

$$\begin{aligned} U(\lambda, \mu) = & \sum_{n=0}^{N+1} U_{0,n} P_{0,n}(\mu) \\ & + \sum_{m=1}^{M} \sum_{n=m}^{N+1} 2 \left(U^r_{m,n} \cos(m\lambda) - U^i_{m,n} \sin(m\lambda) \right) P_{m,n}(\mu) \end{aligned} \tag{3.94}$$

where the superscripts "r" and "i" represent the real and imaginary parts, respectively, of the spectral coefficients $U_{m,n}$.

Chapter 4

Methods for Diagnostic Analysis and Graphic Conventions

§4.1 Introduction

In this study, we have chosen to use Eliassen–Palm (EP) cross–section and three dimensional wave activity flux (Plumb, 1985) as diagnostic tools. Most of this chapter is concerned with details of these two fluxes in two aspects, their properties, and their evaluation.

The EP cross–sections are meridional cross–sections showing the EP flux **E** by arrows and its divergence by contours. The exceptional success in the use of EP cross-sections, the theory of which was originally presented by Andrews and McIntyre (1976), as a diagnostic for both wave propagation and wave, mean–flow interaction has been described by a number of authors (see, e.g. Dunkerton et al., 1981; Edmon et al., 1980; Palmer, 1981; Karoly, et al., 1982; Hoskins, 1983; Holopainen, 1983; Held, et al. 1985; Hartmann, 1985). The use of the EP flux is so successful

in identifying and interpreting some important atmospheric processes, such as stratospheric warming (see, e.g. McIntyre, 1982; Andrews, 1985), that there is broad enthusiasm for the wide application of the EP flux in the meteorological community.

However, the EP flux is a zonally averaged quantity and therefore it can provide insights only into zonally averaged latitudinal and vertical wave propagation characteristics. Thus the limitations of EP flux become apparent. Plumb (1985) derived a three dimensional wave activity flux (thus named Plumb flux), a generalization of the Eliassen–Palm relation, for linear, quasi-geostrophic stationary waves on a zonal flow. Lei (1986) used the Plumb flux along with the EP flux to identify the relative importance of stationary wave forcings. Kang (1990) applied the Plumb flux to show how the wave propagation characteristics are significantly modified under the influence of zonal mean flow change on stationary wave fluctuation. The Plumb flux can provide an insight into the three dimensional structure of wave propagation characteristics. Therefore, it obviously has some fundamental advantages over the EP flux, and can be recognized as a equally useful diagnostic as the EP flux for the three-dimensional Rossby–like propagation of stationary waves (Plumb, 1985).

The rest of the Chapter will describe the Plumb flux and the EP flux in detail. A discussion of graphic convention concludes the Chapter.

§4.2 Stationary Wave Activity Flux – Plumb Flux

In this section, the details of the three–dimensional wave activity flux will be fully described. They include the basic definition, properties, and the evaluation procedure of the Plumb flux.

§4.2.1 Definitions

The Plumb flux is defined in the vertical coordinate which may be called "pressure height" in plots shown herein. This "pressure–height" coordinate may be defined as follows

$$z = -H \ln \frac{P}{P_0} \tag{4.1}$$

where H is a normal constant scale height and set to be 8 km, and P_0 is the standard constant reference surface pressure which is assumed to be 1000 mb and P is a local pressure. In an isothermal atmosphere, in which the temperature is equal to $\frac{gH}{R}$, where g is gravitational acceleration rate, and R the gas constant for dry air, z will be exactly equal to geometric height everywhere, measured from the level $P = P_0$. With the coordinate defined in (4.1), the quasi-geostrophic approximation to the wave activity flux in spherical geometry for linear, stationary waves on the zonal flow (Plumb, 1985) may be written as (see, e.g. Lei, 1986)

$$
\mathbf{F} = \begin{bmatrix} F_\lambda \\ F_\varphi \\ F_z \end{bmatrix}
$$

$$
= \frac{P}{P_0}\cos\varphi \begin{bmatrix} \frac{1}{2a^2\cos^2\varphi}\left\{\frac{\partial\psi^*}{\partial\lambda}\frac{\partial\psi^*}{\partial\lambda} - \psi^*\frac{\partial^2\psi^*}{\partial\lambda^2}\right\} \\ \frac{1}{2a^2\cos\varphi}\left\{\frac{\partial\psi^*}{\partial\lambda}\frac{\partial\psi^*}{\partial\varphi} - \psi^*\frac{\partial^2\psi^*}{\partial\lambda\partial\varphi}\right\} \\ \frac{2\Omega^2\sin^2\varphi}{N^2 a\cos\varphi}\left\{\frac{\partial\psi^*}{\partial\lambda}\frac{\partial\psi^*}{\partial z} - \psi^*\frac{\partial^2\psi^*}{\partial\lambda\partial z}\right\} \end{bmatrix} \tag{4.2}
$$

where ψ represents the streamfunction of the nondivergent geostrophic flow, an asterisk $*$ indicates deviation from zonal mean, Ω is the angular velocity of the Earth, and N is the buoyancy frequency. All other symbols bear their usual meaning.

§4.2.2 Properties of Plumb Flux

As mentioned previously, the three dimensional wave activity flux **F** has some fundamental advantages over the EP flux. Plumb (1985) showed that the **F** in general exhibits all the properties of the EP flux as an indicator of the propagation of the wave activity. He summarized the properties of the Flux **F** as:

- **F** is a conservable measure of the flux of wave activity. In another word, **F** is non-divergent for steady, conservative linear waves.

- In westerly flows, the convergence of **F** indicates the piling-up (generation) of the wave activity, while the divergence of **F** indicates its export (dissipation).

- In the limit of almost-plane waves, **F** is a phase–independent quantity and in the direction parallel to the group velocity.

- If zonal averages are taken, **F** reduces to the EP flux, except for the addition of the zonal component which is of no particular consequence for the zonally-averaged case.

- It is noted that the divergence of **F**, and therefore the generation or dissipation of wave activity, is directly related to non-conservative effects or nonlinearity. In addition, the boundaries may also be the sources or sinks of the flux. This indicates that the orography may also be a source of stationary wave activity.

Attention is particularly drawn to the fact that the locally applicable measure of flux of wave activity, **F**, is conservative under the non-acceleration condition for stationary waves on a steady zonal flow. However, we may use it to diagnose where and how the conservation relation is violated under some non–conservative effects of large scale external forcings, like orography and diabatic heatings, such that we can interprete the possible mechanism of stationary wave response to the forcings, which is a main motivation of this study.

§4.2.3 The Evaluation Procedure

The wave activity flux **F** can be evaluated by using the (4.2) of which all the derivatives are taken on pressure–height surfaces, i.e. isobaric surfaces. For graphical convenience, a computational grid of equal interval pressure levels at 800, 725, 650, 575, 500, 425, 350, 275, 200, 125 and 50 mb, is chosen for evaluating the flux. On each level, the horizontal computational grid consists of the intersections of 28 equally spaced meridians and 36 Gaussian latitudes, which satisfy the requirement of gridpoints under the truncation limit used in this study, therefore the horizontal derivatives may be evaluated by a spectral method similar to that described in §3.2.5. The evaluation procedure may be outlined as follows:

1. Compute the velocity components U and V at grid points at isobaric surfaces from model output by using (3.20) and (3.21) where σ is not only a function of P but also a function of λ and μ.

2. Calculate the streamfunction ψ on presure–height surfaces, which is expressed by

$$\psi = \sum_{m=-M}^{M} \sum_{n=|m|}^{M} \psi_{m,n}\, e^{im\lambda}\, P_{m,n}\,(\mu) \tag{4.3}$$

where the spectral coefficients

$$\psi_{m,n} = -\frac{a}{n\,(n+1)} \frac{1}{4\pi} \int_{-1}^{1} \int_{0}^{2\pi} \frac{1}{1-\mu^2} \left[U^{(\mu)} + V^{(\lambda)}\right] e^{-im\lambda}\, P_{m,n}\,(\mu)\, d\lambda\, d\mu \tag{4.4}$$

It is worth noting that some grid points at the lowest one or two levels may be located under the ground if orography is inserted into the model. In such

cases, an approximation approach is made for easiness and simplicity, namely, if the value of the integrand in (4.4) at a grid point is unknown, it will be simply dropped out from the summation of the Fourier transformation and then the total number of grid points along that latitude circle, by which the summation is divided (see e.g. (3.30)), is, accordingly, decremented by one. This artificial treatment to the grid points laid below the surface may raise problem if the divergence of the flux is calculated.

3. Calculate the wave activity flux by using (4.2)

   This stage finalises the evaluation of the Plumb flux **F**. The vertical derivative in (4.2) is calculated differently from horizontal derivatives. It is calculated using centred finite differences except at the boundaries of the above–specified levels, where one–sided finite differences are used.

§4.3 Eliassen–Palm Flux

This section describes the Eliassen–Palm (EP) flux in full detail. It includes the definition of EP flux and its relation with Plumb flux. The evaluation procedure and properties of the EP flux are also described.

§4.3.1 Definition

With the pressure height, z, as vertical coordinate, the Eliassen-Palm (**EP**) flux under the quasi-geostrophic approximation could be defined as

$$\mathbf{E} = \begin{bmatrix} E_\varphi \\ \\ E_z \end{bmatrix} \tag{4.5}$$

where

$$E_\varphi = \varrho_0 \exp(-\frac{z}{H})\, a^{-1} \left[\frac{\partial \psi^*}{\partial \lambda} \frac{\partial \psi^*}{\partial \varphi}\right] \tag{4.6}$$

$$E_z = \varrho_0 \exp(-\frac{z}{H})\, 4\,\Omega^2 \sin^2 \varphi\, N^{-2} \left[\frac{\partial \psi^*}{\partial \lambda} \frac{\partial \psi^*}{\partial z}\right] \tag{4.7}$$

Here the square brackets denote the zonal mean and

$$\varrho_0 = \frac{P_0}{g\,H} \tag{4.8}$$

is the standard density. Under this definition, the EP flux vector is parallel to the group velocity for the quasi–geostrophic conservative waves on the steady, zonal mean flow, so that the EP flux is a good measure of wave propagation (see, e.g. Edmon et al., 1980).

§4.3.2 Relation with Plumb Flux

As mentioned in §4.2.2, if zonal averages are taken, F_φ and F_z are reduced to be E_φ and E_z respectively. Comparing (4.5) with (4.2), the following relations are

obvious

$$\begin{cases} E_\varphi &= \varrho_0\, a\, [F_\varphi] \\ \\ E_z &= \varrho_0\, a\, [F_z] \end{cases} \tag{4.9}$$

where the square brackets denote zonal mean, and the factor $\varrho_0\, a$ is simply a constant with a representing the radius of the earth. 4.9 explicitly indicates that the quantity of the EP flux can be simply replaced by the longitudinally averaged quantity of the Plumb flux multiplied by a constant factor. Therefore, in actual calculation of the EP flux, we simply use the zonally averaged quantity of the Plumb flux rather than calculate the EP flux itself using (4.6) and (4.7).

§4.3.3 Property and Evaluation of EP Flux

The EP flux has the fundamental advantage that its divergence

$$\nabla \bullet \mathbf{E} = \frac{1}{a \cos \varphi} \frac{\partial}{\partial \varphi} (E_\varphi \cos \varphi) + \frac{\partial}{\partial z} (E_z) \tag{4.10}$$

is zero under "nonacceleration conditions" (for steady, conservative linear waves on a zonal mean flow) (see, e.g. Andrews, 1985). Furthermore, the EP flux divergence is equal to the meridional flux of quasi-geostrophic potential vorticity (see, e.g. Holopainen, 1983; Karoly, 1982). Therefore the EP cross-section, in which as

mentioned at the beginning of the chapter the vector $\mathbf{E}$ is represented by arrows and its divergence $\nabla \bullet \mathbf{E}$ by contours, is a convenient way to visualize information not only on the net transfer of planetary wave activity from one latitude and height to another, but also as an indicator on where and how the zonally averged time–mean flow experiences the net local effect of departure from the non-acceleration conditions.

The evaluation procedure and graphical conventions virtually follow those of Lei (1986) with extension to southern hemisphere in this study, which are equivalent to those of Dunkerton, et al (1981). The volume element for integration of (4.10) over a zonally symmetric portion of the atmosphere may be written as

$$dv = 2\pi a^2 \cos\varphi \, d\varphi \, dz \tag{4.11}$$

From (4.10) and (4.11), we have

$$\int \nabla \bullet \mathbf{E} \, dv = \int \Delta \, d\varphi \, dz \tag{4.12}$$

where

$$\Delta = \frac{\partial}{\partial \varphi} \{2\pi a \cos\varphi \, E_\varphi\} + \frac{\partial}{\partial z} \left\{2\pi a^2 \cos\varphi \, E_z\right\} \tag{4.13}$$

Here the Δ is a natural form of the divergence of $\mathbf{E}$ for contouring in the $(\varphi,\ z)$ plane. The arrows of $\mathbf{E}$ will be drawn with horizontal and vertical components proportional to the quantities within the curly brackets in (4.13), namely

$$\begin{aligned} \left\{\hat{E}_\varphi\ ,\ \hat{E}_z\right\} &= 2\pi a^2\ \cos\varphi\ \left\{a^{-1}\ E_\varphi\ ,\ E_z\right\} \\ &= 2\pi a^3\ \varrho_0\ \cos\varphi\ \left\{a^{-1}\ [F_\varphi]\ ,\ [F_z]\right\} \end{aligned} \tag{4.14}$$

Thus for the calculation of the horizontal and vertical arrow components as measured on the plotting diagram, the $[F_\varphi]$ and $[F_z]$ are first evaluated in $m^2\ s^{-2}$, and then multiplied by $d_1\ a^{-1}\ \cos\varphi$ and $d_2\ \cos\varphi$ respectively, where d_1 and d_2 are scale factors proportional to the distances occupied on the diagram by 1 radians or 57.3^0 of latitude, and one metre of pressure height. From that evaluation, it can be seen that the (4.12) implies that the pattern of arrows will look nondivergent in the $(\varphi,\ z)$ plane if and only if the $\nabla \bullet \mathbf{E}$ is equal to zero.

§4.4 Graphic Conventions

The designation of graphics for model outputs is based on the consideration of visualising the three dimensional structure of the results. Therefore a variety of plots from various angles are plotted. In order to reduce the number of diagrams, each isobaric surface plot is plotted in an equi–distance cylindrical projection. For simplicity, each of the field variables and diagnostics for both hemispheres is plotted in the same viewport. The following diagrams have been plotted for each experiment, but not all of them are shown in this thesis:

- Contour maps for orography height and horizontal distribution of vertically integrated climatological diabatic heating in northern wintertime;
- Contour maps for streamfunction, which represents the rotational components of stream field, superimposed with isobaric velocity fields, and geopotential height respectively at 700, 500, 200, and 100 mb levels.
- Vector maps for isobaric streamline corresponding to the velocity fields at the levels same as for streamfunction.
- Maps of wave activity flux at 800, 500, and 200 mb, in which arrows represent horizontal components and contours vertical component.
- EP cross–section.
- The longitude–pressure cross-section for the departure from the zonal mean of geopotential height and vertical velocity in the pressure system which is calculated by

$$\begin{aligned} \omega &\equiv \frac{dP}{dt} \\ &= \frac{u}{a\cos\varphi}\left[\frac{\partial P}{\partial \lambda}\right]_\sigma + \frac{v}{a}\left[\frac{\partial P}{\partial \varphi}\right]_\sigma + \dot{\sigma}\frac{\partial P}{\partial \sigma} \\ &= \frac{\sigma+1}{2}\left\{\frac{u}{\cos\varphi}\frac{\partial P_s}{\partial \lambda} + \frac{v}{a}\frac{\partial P_s}{\partial \varphi}\right\} + \frac{\dot{\sigma} P_s}{2} \end{aligned} \tag{4.15}$$

It can be written alternatively as follows if the notations introduced in Chapter 2 are used.

$$\omega = \frac{\exp(q)}{2a}\left\{\frac{1+\sigma}{1-\mu^2}\left(U q^{(\lambda)} - V q^{(\mu)}\right) + (1-\sigma^2) S\right\} \tag{4.16}$$

Chapter 5

Model Validation and Sensitivity Test

Before using the model to investigate atmospheric behaviour in response to global orography and "climatological" diabatic heating in winter, we first verify the model itself, by comparing our model results with those obtained by others (e.g. Gill, 1980; Simmons, 1982, Lei, 1986; et al). We focus primarily on idealized orography in middle latitudes, and idealized diabatic heating centred at various latitudes. These experimental results not only display the appropriateness and validity of the model, but also give us some initial insights into the behaviour of stationary waves in response to external forcing in the model atmosphere.

In this Chapter, we start by describing dissipation parameters as well as the symmetric component of the time-averaged basic state $[U]$ and $[T]$. Then we consider a case in which only idealized large scale orography is involved and no steady–state heating source exists. Subsequently three cases in which stationary heating is the only forcing are included. The heating is centred in midlatitudes, subtropical latitudes and over the equator respectively for different experiments. Finally some sensitivity tests of the model results to changes in dissipation parameters and the

basic state climatology are performed and discussed.

§5.1 Model Parameters

The model parameters used in the sensitivity tests are Rayleigh friction, Newtonian cooling, coefficients of bi–harmonic horizontal diffusion, and zonal mean basic state. After these sensitivity tests, they are fixed for all model experiments.

§5.1.1 Dissipation Parameters

In order to ensure that a steady–state model is well behaved, it is necessary to include dissipation which is parameterized in this model by means of Newtonian damping and Rayleigh friction with spatially varying decay rates. The coefficients for vertical distribution of Rayleigh friction, R_f, and Newtonian cooling, K_t, are taken to be similar to those of Simmons (1982) and Nigam et al (1986), and identical to those of Lei (1986). R_f is set to be $(20\ day)^{-1}$ above $\sigma = 0.6$ and increased below this level linearly with pressure to approach the value of $(2\ day)^{-1}$ at the surface where $\sigma = 1.0$ such that the effect of boundary layer drag is expected to be parameterized in the model. K_t is initially set to $(20\ day)^{-1}$ below 200 mb ($\sigma = -0.6$) and increased above this level linearly with the logarithm of pressure to reach the value $(4.25\ day)^{-1}$ at the highest model level ($\sigma = -0.97391$). This is intended to represent radiative damping (Fig. 5.1). Both the Newtonian cooling and Rayleigh friction are enhanced in polar regions by multiplying the forementioned coefficients by the factor $\left(\frac{\cos\varphi_0}{\cos\varphi}\right)^{4.5}$ when $|\varphi| \geq \varphi_0$, where φ_0 is set to be

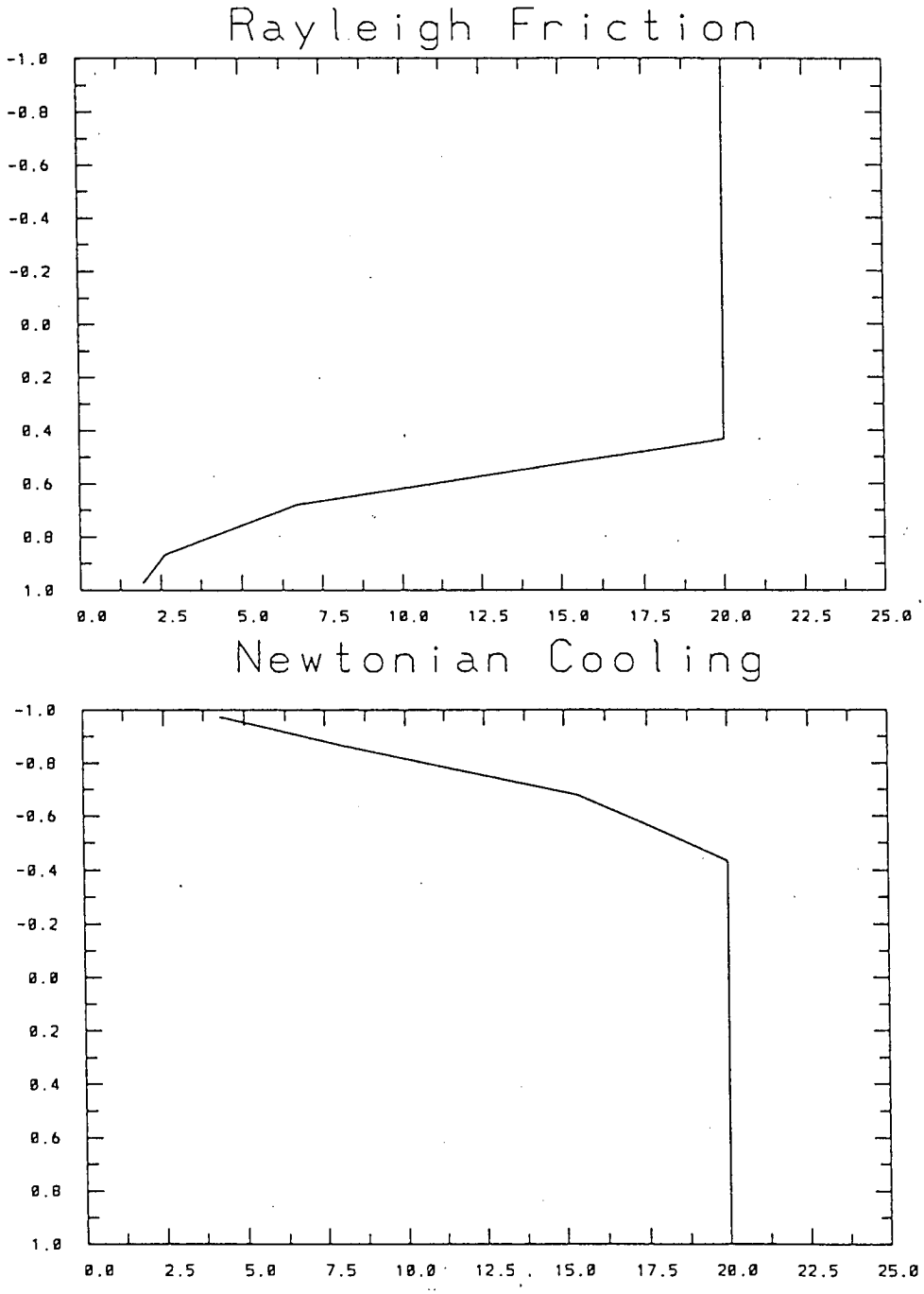

Figure 5.1: Vertical distribution of Rayleigh friction and Newtonian cooling. Horizontal coordinate is damping rate R_f, K_t $(day)^{-1}$, while the vertical coordinate is σ levels.

60^0. This enhancement is intended to remove the resonance which is possible in the polar region. In tropical areas, both coefficients are increased by the factor $\left(\frac{\sin\varphi_0}{\sin\varphi}\right)^{3.0}$, when $|\varphi| \leq \varphi_0$, where φ_0 is set to be 30^0 such that the waves reaching the area of tropical easterly are substantially damped. Some results which will be shown later suggest that the proper imposition of the dissipative elements is essential for simulating the best possible stationary wave response to steady–state forcing.

In the vicinity of critical latitudes, where the symmetric component of zonal velocity vanishes, the dissipative coefficients are increased by dividing the decay rates in Figure 5.1 by $\{[U]^2 d\}^{-1}$, where $[U]$ is the zonal mean flow in ms^{-1} and treated as a non–dimensional quantity, whenever they fall below the specified value.

Both the coefficients of the bi–harmonic horizontal diffusion are taken to be $1.169\times 10^{17}\ m^4\, s^{-1}$, which is identical to that of Lei (1986). The value of the two coefficients are justified not only on the basis of e-folding time as discussed by Lei (1986), but also various model results as compared with those results obtained by others (e.g. Lei, 1986; Nigam et al., 1989; Schneider, 1990; et. al).

§5.1.2 Zonal Mean State

As described in Chapter 2, the monthly–averaged symmetric component of zonal velocity $[U]$ and temperature $[T]$, used in this model as basic state, are derived from the monthly mean climatology in January 1979. No attempt is made to adjust the basic state $[U]$ and $[T]$ into geostrophic balance, or a balance state as done for instance by Lei (1986). It is very difficult, between $[U]$ and $[T]$, to choose one

field variable as being more realistic and deriving the other as, e.g., suggested by Watterson et al. (1987). Instead, several sensitivity tests of model results to the basic state were conducted with the above-described $[U]$ and $[T]$ interpolated into σ levels with and without insertion of orography. Figure 5.2 displays the $[U]$ and $[T]$ interpolated into σ levels assuming that the Earth surface is flat. Figure 5.3 is equivalent to Figure 5.2 but with surface geopotential (i.e. orography) included. Comparing Figure 5.2 with Figure 5.3, it can be seen that there is very small difference for zonal mean $[U]$ except for the lower troposphere of the southern polar region. However, there do exist distinct differences for zonal mean $[T]$ in all levels of the southern high latitudes. The experimental results will show that the two different basic states do not have significant influence on the model results except for the response to an idealized mid-latitude orography. However, the difference by the different zonal mean states for orographic forcing is still deemed to be little and reasonably acceptable. Furthermore, using the basic states described in either Figure 5.2 or Figure 5.3 for experiments in this chapter gives visually very similar results which are in overall consistancy with atmospheric dynamics and similar work done by others. But the basic state described in Figure 5.3 more "truely" represents the atmosphere. Therefore, the zonal mean state in Figure 5.2 will be used as basic state for the numerical experiments in this chapter except those for sensitivity tests, but that in Figure 5.3 will be used in Chapter 6.

The model coding was tested by two simple experiments, one for reproducing Gill's (1980) analytical solution using our model, the other for investigating response of the isothermal atmosphere in superrotation to the spherical harmonic boundary. It is shown from the physics and dynamics of the atmosphere that there does not exist errors in the model programing. The results are shown in Appendix A.

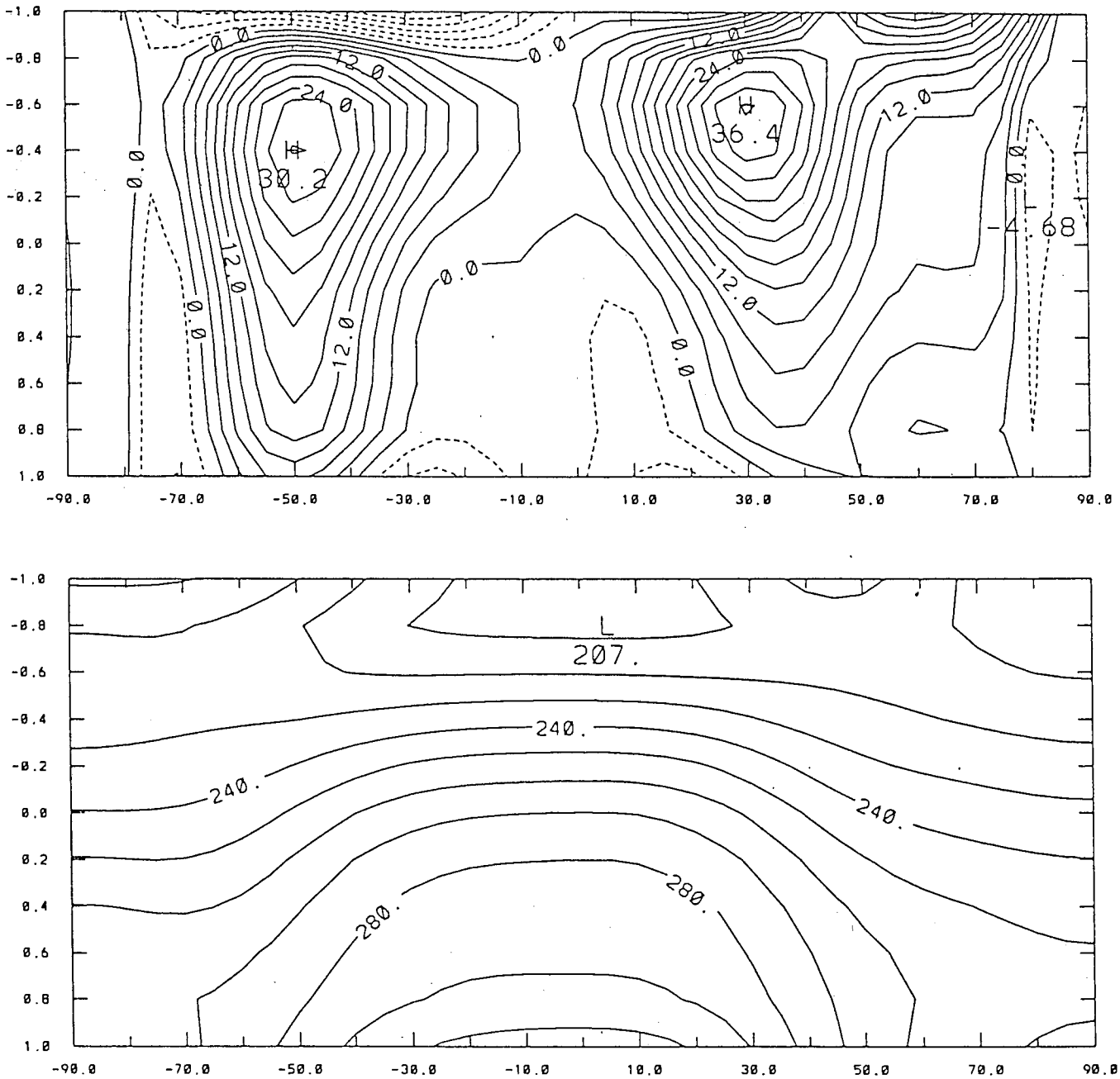

Figure 5.2: Zonal mean state $[U]$ (upper) and $[T]$ (lower), derived from FGGE formated climatology in January 1979, interpolated into Gaussian latitudes and Gaussian levels without inserting orography. It is plotted through transformation from spectral coefficients.

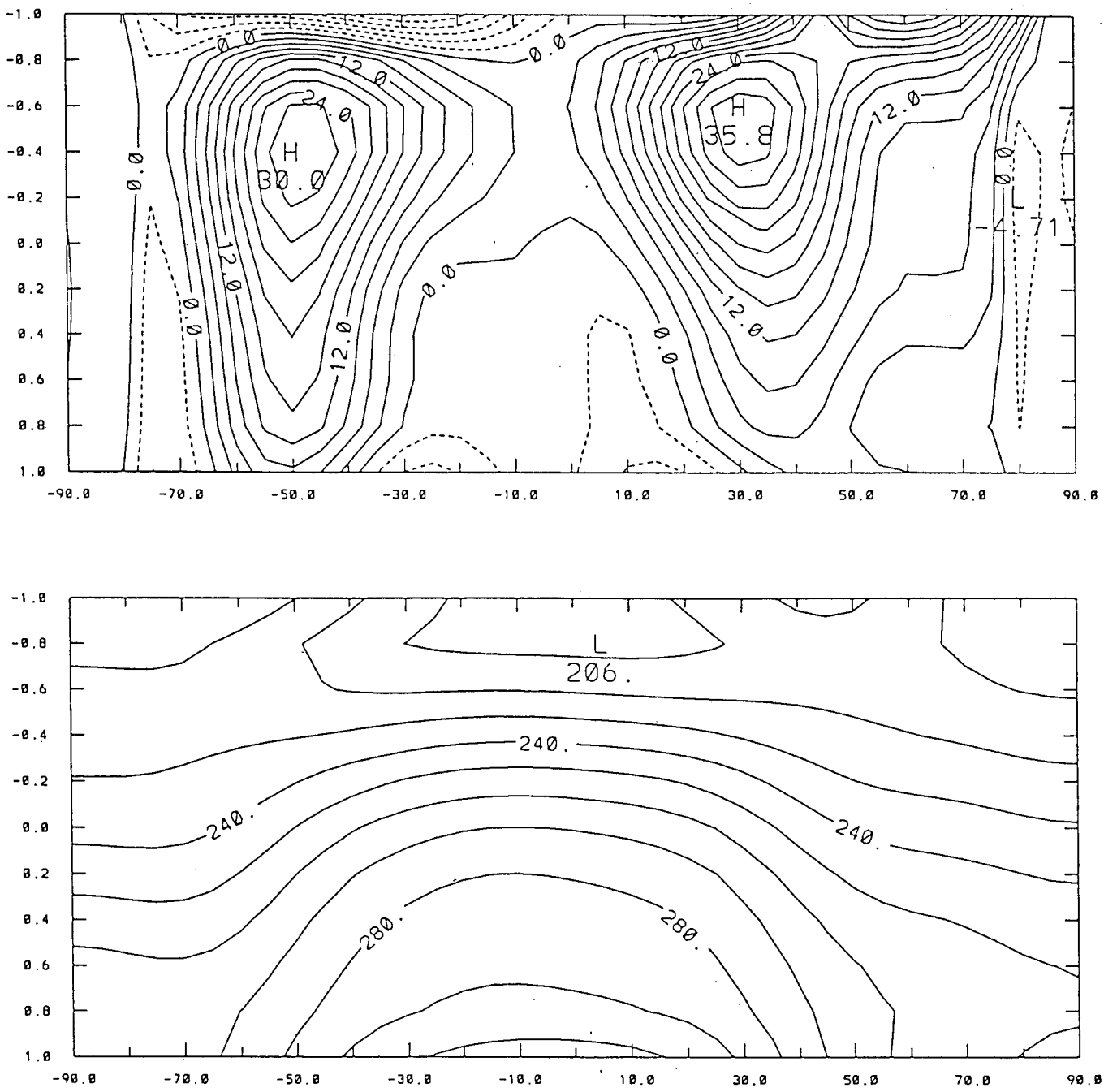

Figure 5.3: As in Figure 5.2, but with insertion of global orography.

§5.2 Model Response to Mid–latitude Large Scale Orography

This experiment is intended to simulate to a certain extent the possible role which the Tibetan Plateau may play in the real atmosphere. Attention must be drawn to the fact that we are by no means attempting to simulate the observed climatology of stationary waves. Our emphasis is focused on the investigation of stationary waves in response to large–scale idealized steady–state forcing.

§5.2.1 Description of Orography

In this calculation, we assume that there are no external heating sources, and the only external forcing involved in exciting stationary waves is an idealized large scale orography in middle latitudes. The surface geopotential is specified as

$$\phi_s = \begin{cases} g_0 A \left[\sin\dfrac{\pi(\lambda-\lambda_1)}{(\lambda_2-\lambda_1)}\ \sin\dfrac{\pi(\varphi-\varphi_1)}{(\varphi_2-\varphi_1)}\right]^2, & \lambda_1 \le \lambda \le \lambda_2, \\ & \varphi_1 \le \varphi \le \varphi_2. \\ 0 \qquad\qquad \text{Otherwise.} \end{cases} \tag{5.1}$$

where g_0 is the globally averaged gravitational acceleration at mean sea level, taken to be 9.807 $m\,s^{-2}$. For comparative convenience, without loss of good approximation to the Tibetan plateau, the value for A is taken to be 2500 m. The values for φ_1, φ_2, λ_1, λ_2 are set to be 20^0, 50^0, 30^0, 150^0 respectively. The orography is incorporated into the model by spectral coefficients transformed from values

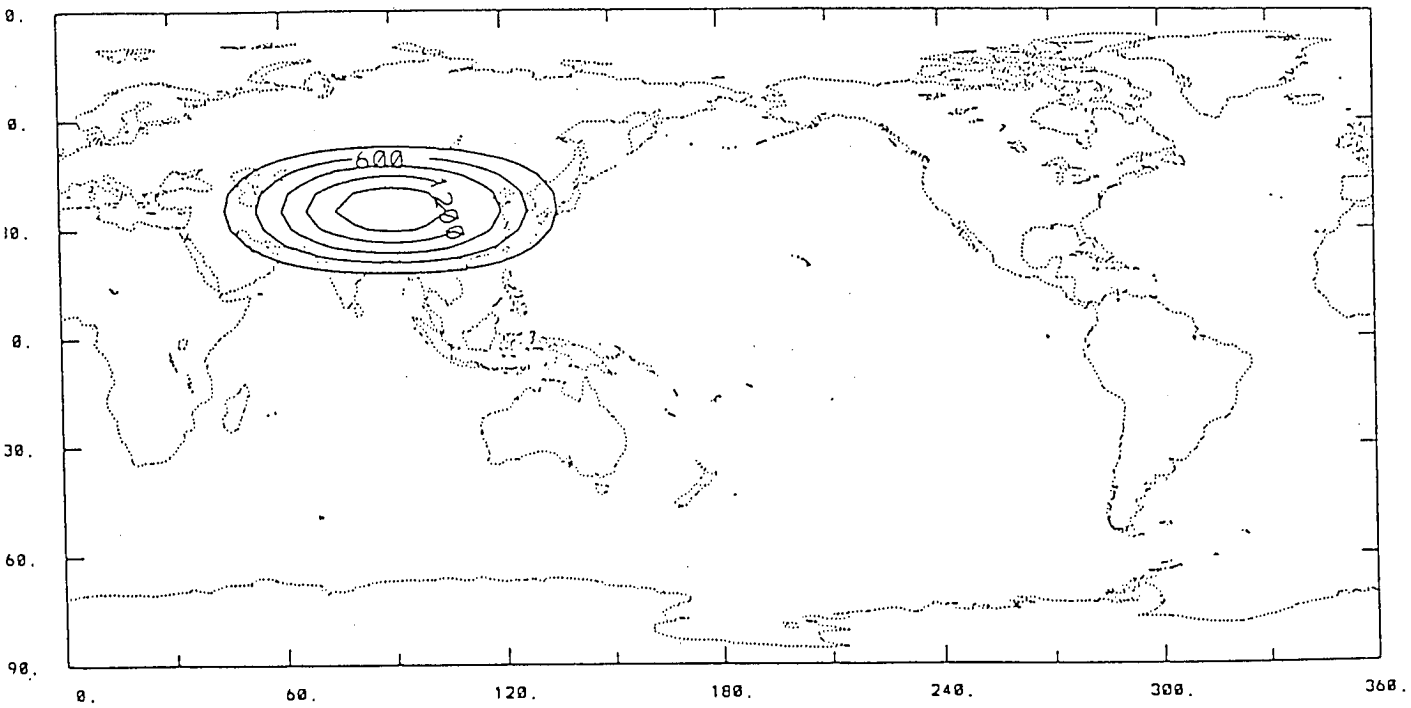

Figure 5.4: Horizontal distribution of surface geopotential height, expressed by truncated series of spherical harmonics, for an idealized mountain in mid-latitudes. Contours represent the geopotential height. Contour interval is 300 (m). The zero contour is excluded for clarity.

which are initially evaluated on grid-points. It is well represented by the spectral expansion described in Chapter 3, and can be seen in Figure 5.4.

§5.2.2 Experimental Results

The model response to the above-specified large scale orography in mid-latitudes (Figure 5.4) is shown by perturbation streamfunction superimposed with the horizontal velocity field on isobaric surfaces, at 700 mb (Figure 5.5) and 200 mb (Figure 5.6), respectively.

At 700 mb, an anti-cyclonic circulation is found to the west, and on the upslope

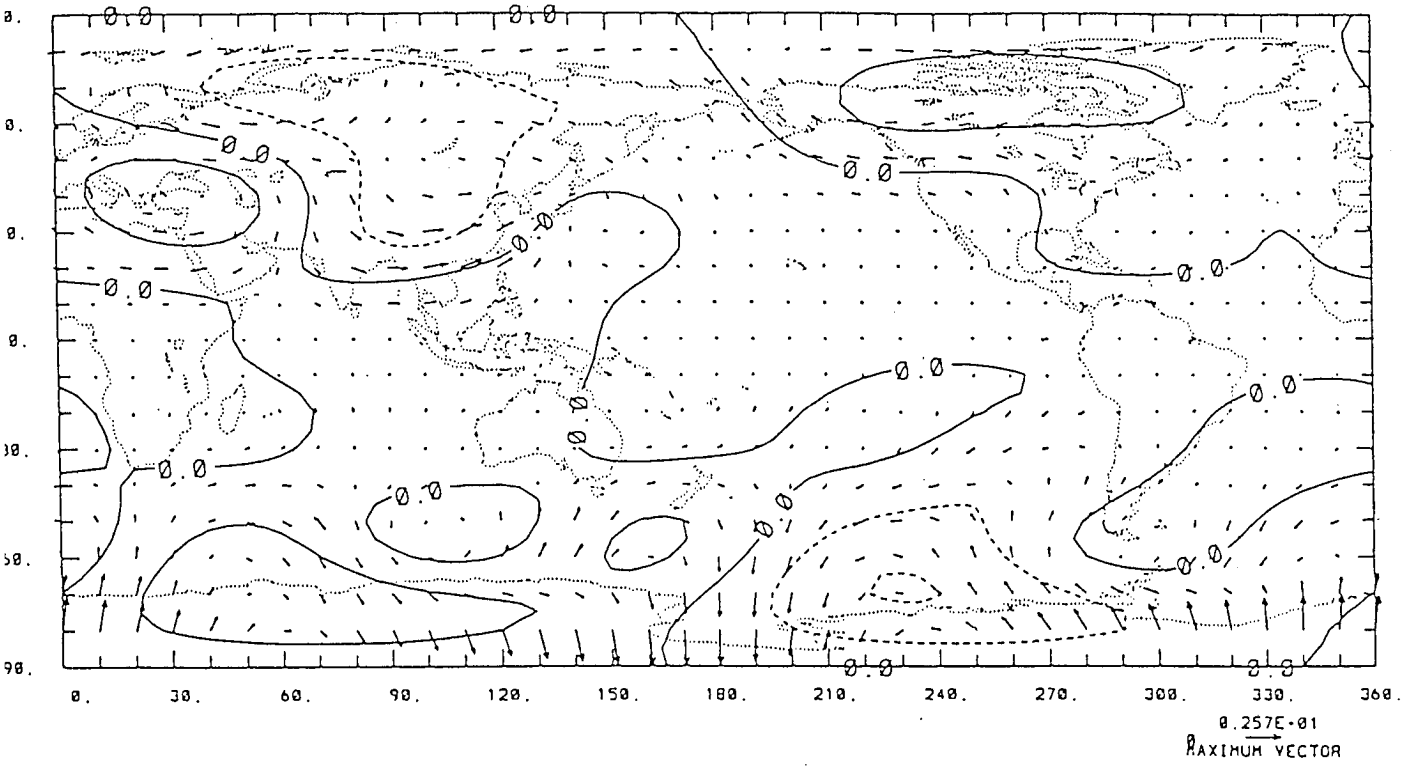

Figure 5.5: 700 mb perturbation stream field for the model response to an idealized orography in mid-latitudes. Contours are the perturbation streamfunction ($\times 10^5\ m^2 s^{-1}$), with an interval of 10 units. The negative contours are dashed. Vectors denote the horizontal velocity on isobaric surface, and an arrow scale in units of ms^{-1} is indicated at the bottom right of the picture.

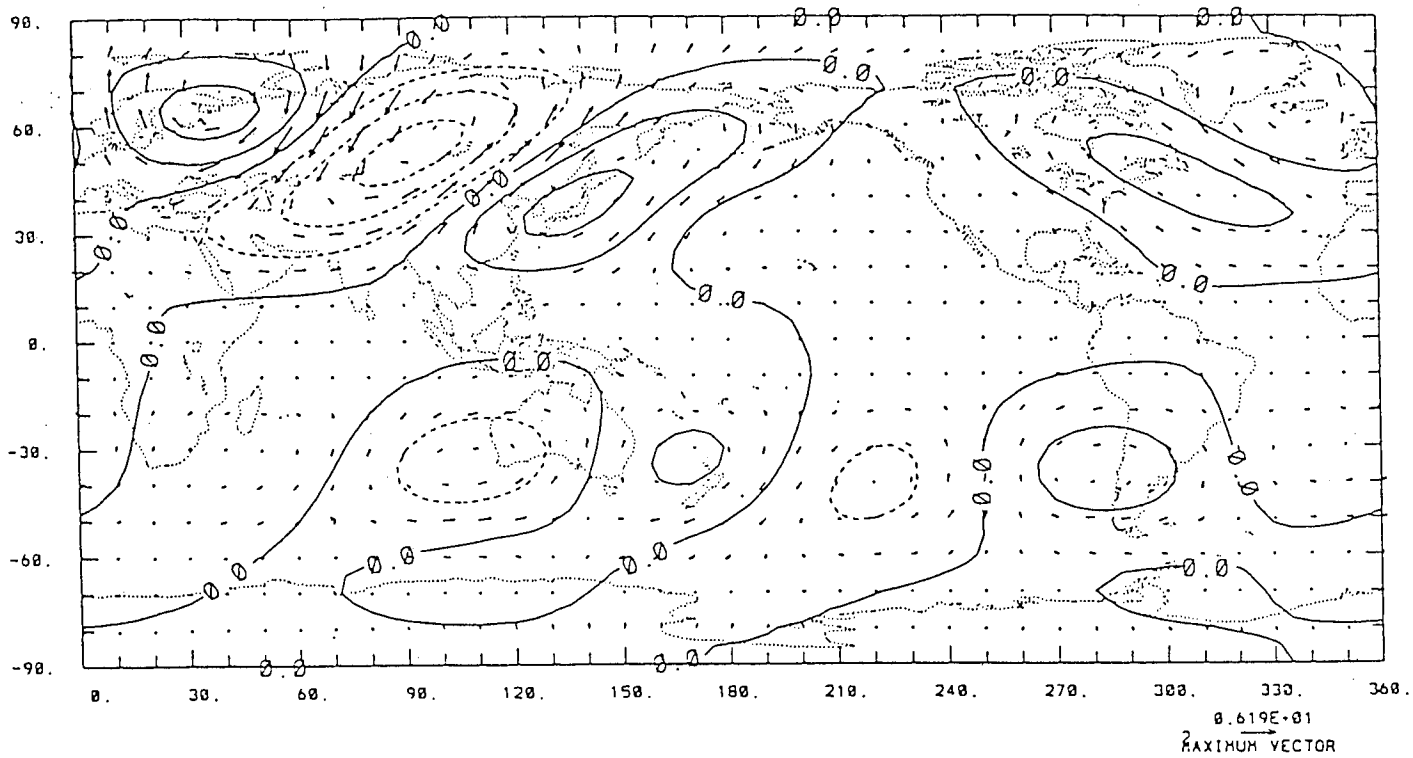

Figure 5.6: As in Figure 5.5, but for 200 mb, with contour interval of 20 units.

region of the mountain, while a cyclonic circulation exists to the north and north-east side of the orography, and is stretched over the mountain top. Most of the mountain is covered by the cyclonic circulation. This result is consistent with the result obtained by Hoskins and Karoly (1981) for the β–plane channel barotropic theory. Furthermore, far down–stream of the mountain, another anti–cyclonic circulation exists over northern America, and it extends to high latitudes. It is worth noting that the velocity field has an obvious splitting tendency over the north edge of the mountain.

It is of interest to see the "remote response" around the Antarctic region while no significant response can be found in mid–latitudes of the southern hemisphere . To the west of the date–line, an anti–cyclonic circulation dominates stretching to the southwest of New Zealand. In contrast, there is a cyclonic circulation to the east of the dateline. The magnitude of the remote response in the southern hemisphere

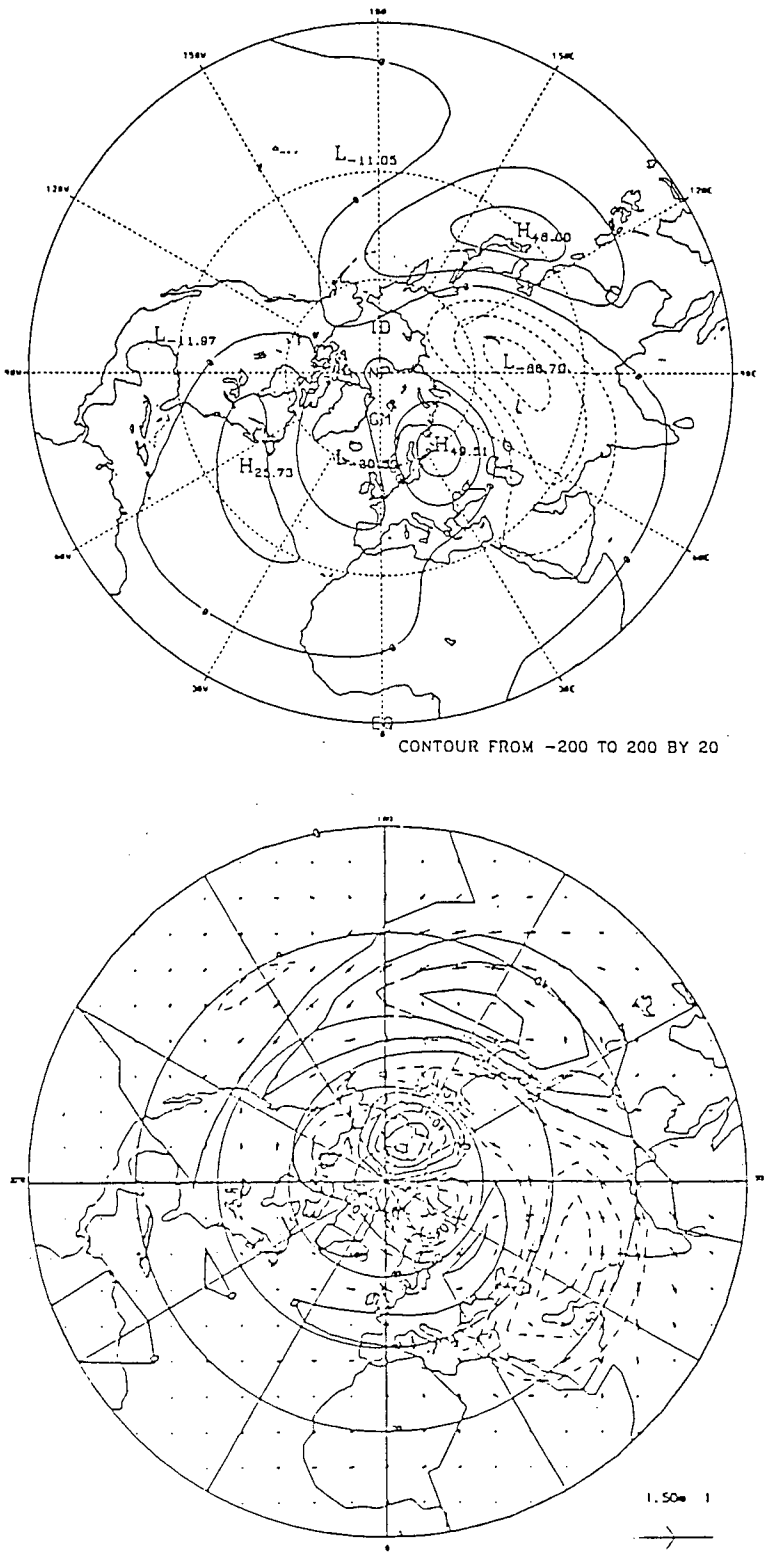

Figure 5.6b: The 200mb streamfunction for the response to the mid-latitude orography in the northern hemisphere. Upper — the result of this model; lower — result of Lei's hemispheric model, copied from his thesis (1986). The contour interval for both diagrams is 20 units.

is comparable to the response near the forcing source.

At 200 mb, the model response in subtropical areas of the both hemispheres is much stronger than that at the lower level. In the northern hemisphere, an anti–cyclonic circulation is situated about 50^0 east of the mountain peak, while a cyclonic circulation covers most of the mountain and is centred at 15^0 north of the mountain top. To the northwest of the mountain, there is a relatively small (in extent) anti–cyclonic circulation. Furthermore, there is another subtropical anti–cyclonic circulation further down–stream of the orography, covering most of the eastern part of north America and the north Atlantic.

In the southern hemisphere, however, the 200 mb response in subtropical regions is relatively small in extent and weak in magnitude, compared with that in the northern hemisphere, but stronger than that at lower level. The subtropical response in the southern hemisphere is dominated by wavenumber 2. Unlike the 700 mb response, the "remote response" at 200 mb around Antarctic is negligible.

The result of this experiment in the northern hemisphere is in qualitative agreement with that of Lei (1986) using a hemispheric model. In addition, this model produced a remote response around the Antarctic region at lower levels and in the southern subtropical area at upper levels. This result implies that the zonally asymmetric distribution of large scale orography in the northern hemisphere has an effect not only around the mountain itself, but also in remote areas including the southern hemisphere.

Figures 5.7 and 5.8 illustrate the Plumb (1985) flux which is represented by vectors in the horizontal, and contours in the vertical, at 800 mb and 500 mb respectively.

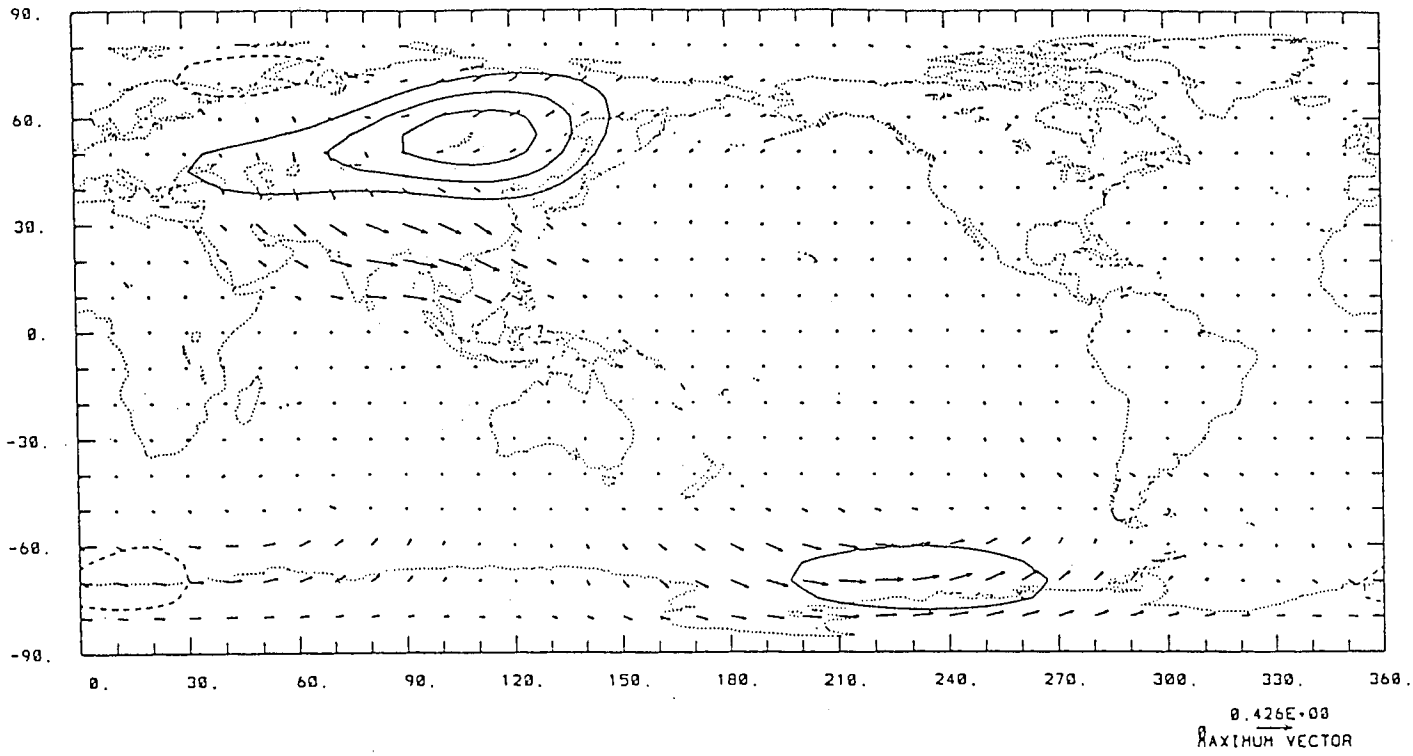

Figure 5.7: Wave activity flux **F** at 800 mb for the model response to idealized orography in mid-latitudes. Contours are the vertical component F_z ($10^{-3}\ m^2 s^{-2}$) with an interval of 10 units (positive upward). The zero contour is excluded. An arrow with scale on at the bottom right represents the horizontal components (in units: $m^2 s^{-2}$).

At 800 mb, the wave activity propagates upward (positive) just north of the mountain crest, and splits horizontally into two branches the northerly of which propagates polarward while the southerly propagates equatorward. This feature seems in good agreement with the dynamics of the atmosphere in response to the Tibetan Plateau. In the southern hemisphere, the wave activity flux features mainly in two regions in high latitudes propagating upward east of the dateline and downward east of the Greenwich meridian. In the horizontal, however, it propagates eastward and then equatorward in both regions.

At 500 mb, the Plumb flux shows propagation upward over the mountain ridge and

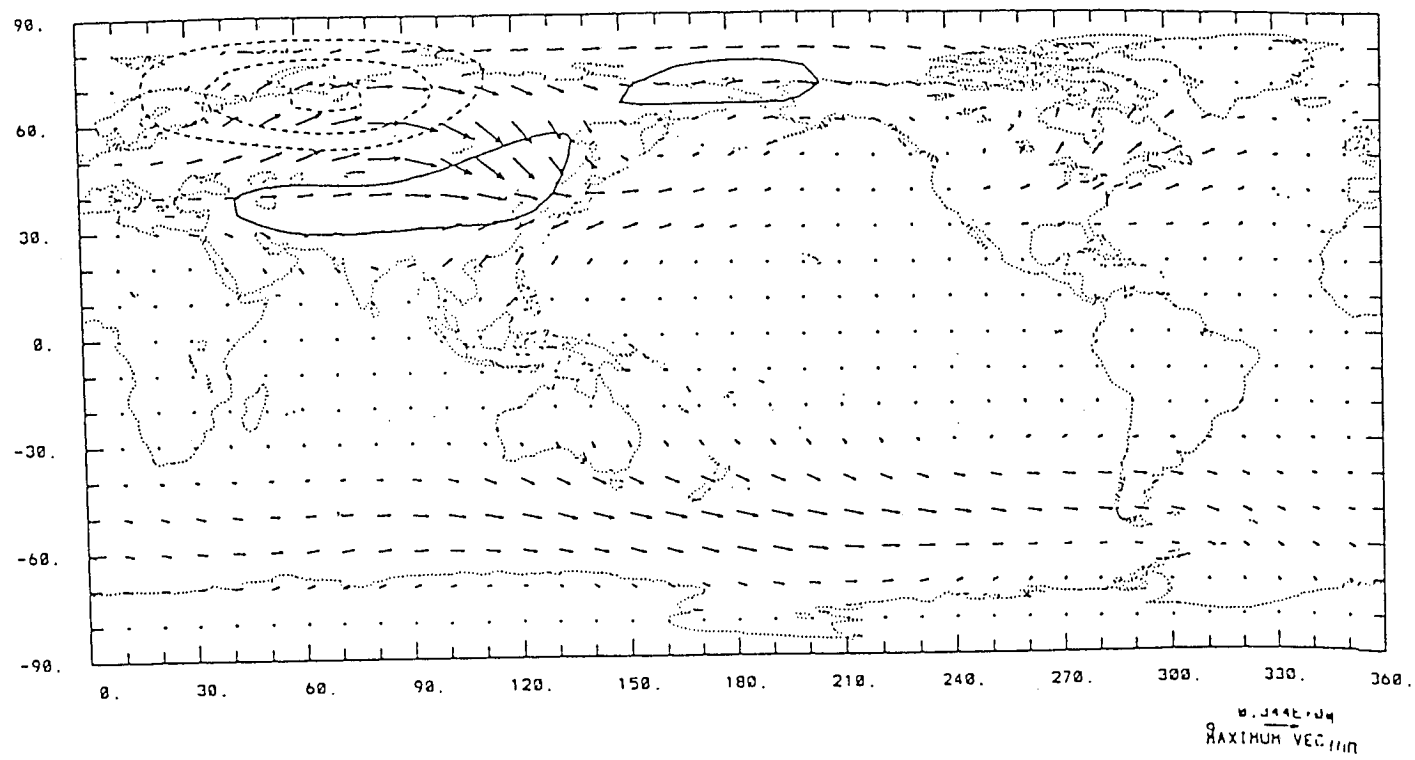

Figure 5.8: Same as Figure 5.7, but for 500 mb. The contour interval is 10 units.

near the Bering Sea, but downward to the northwest of the orography, whereas in the horizontal it propagates alongside the north edge of the mountain and breaks down into two branches, of which one is spreading eastward, while the other is turning southeastward and finally merging with those propagating eastward over the mountain ridge near Japan. In the southern hemisphere, however, no pronounced vertical propagation of wave activity is found, but its horizontal propagation is significant and almost uniformly eastward in the subtropics.

The meridional and vertical components of the Plumb flux reduce to the EP flux if the longitudinal average is taken. Figure 5.9 shows that the strongest EP flux is located at the lower levels over the mountain. The largest convergence of the EP flux is in the same place. Beside the convergence maximum, there is also quite strong divergence of the EP flux at subtropical lower levels.

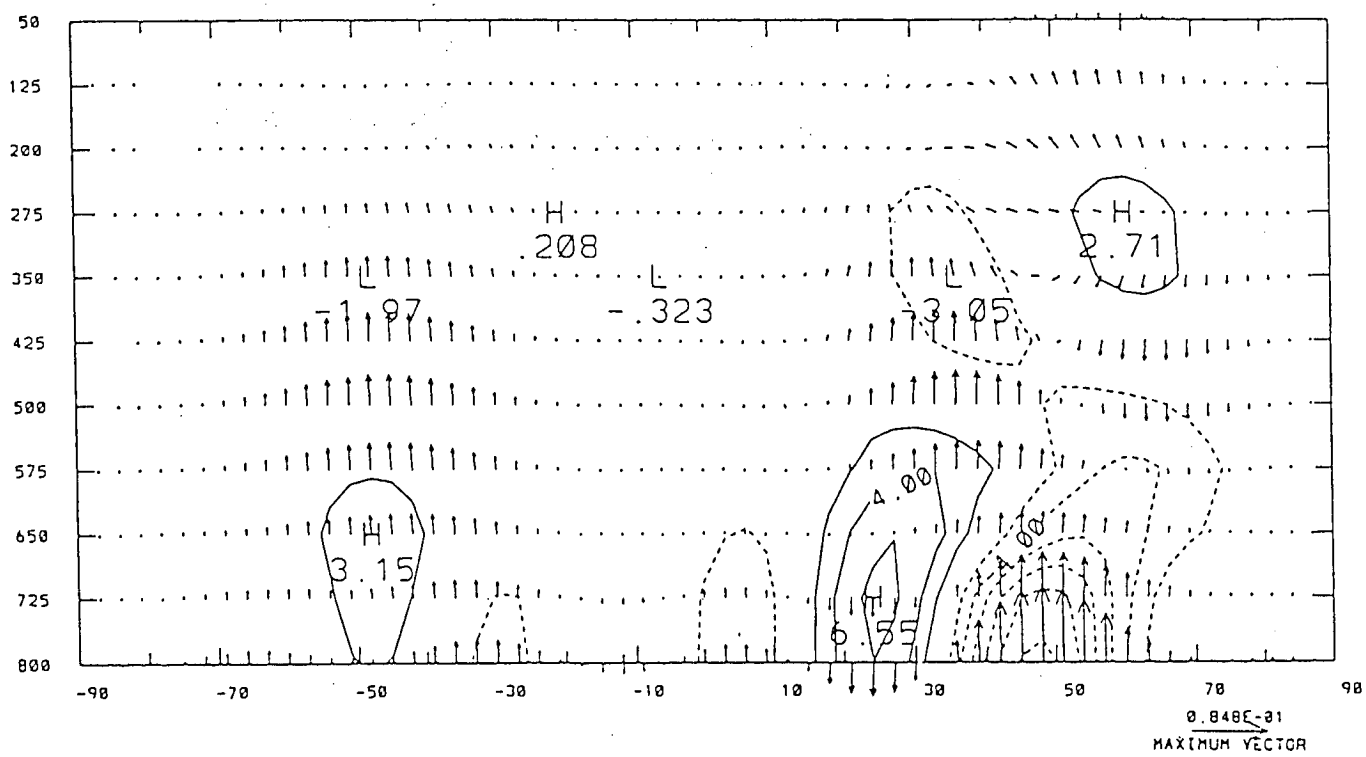

Figure 5.9: EP cross-section for the model response to an idealized orography in mid-latitudes. An arrow scale is plotted at bottom right. The numerical value marked is to be multiplied by $2\pi a^2 \rho_0 \ m^2 s^{-2}$ for $\hat{E}_\varphi$ and $2\pi a^3 \rho_0 \ m^2 s^{-2}$ for $\hat{E}_z$ respectively. The contours represent the quantity Δ defined by expression (4.13); the numerical values marked on the contours to be multiplied by $2\pi a^3 \rho_0 \times 10^{-7} m \ s^{-2}$. The contour interval is 10 units. The zero contour is excluded.

§5.3 Response to an isolated Mid–Latitude Heating

Assuming that no orography exists at the Earth surface, an experiment is conducted for the model response to an idealized diabatic heating in mid–latitudes, which is the only external forcing to induce the stationary waves. The horizontal distribution of the heating may be specified as

$$\frac{Q}{C_p} = \begin{cases} A\left[\sin\frac{\pi(\lambda-\lambda_1)}{(\lambda_2-\lambda_1)}\ \sin\frac{\pi(\varphi-\varphi_1)}{(\varphi_2-\varphi_1)}\right]^2, & \lambda_1 \le \lambda \le \lambda_2, \\ & \varphi_1 \le \varphi \le \varphi_2. \\ 0 \qquad \text{Otherwise.} \end{cases} \tag{5.2}$$

This isolated heating is illustrated in Figure 5.10 for the values $\varphi_1 = 30^0N$, $\varphi_2 = 60^0N$, $\lambda_1 = 90^0$, $\lambda_2 = 180^0$, with the maximum amplitude $A_{max} = 5\ K\ d^{-1}$ (A is dependent of σ) which could imply a precipitation rate of the order of 10 $mm\ d^{-1}$, a value appropriate for the wettest regions in the tropics (Simmons, 1982; Robertson et al, 1990). The vertical distribution of the heating is profiled by the function in formula (5.3) to parameterize the net effect of localized regions of intense mean latent heating peaked in the middle to upper troposphere (e.g. Hartmann et al, 1984)

$$\frac{A(\sigma)}{A_{max}} = \begin{cases} \left[\sin\frac{\pi(\sigma-\sigma_1)}{(\sigma_2-\sigma_1)}\right]^2, & \sigma_1 < \sigma < \sigma_2; \\ 0 \qquad \text{Otherwise.} \end{cases} \tag{5.3}$$

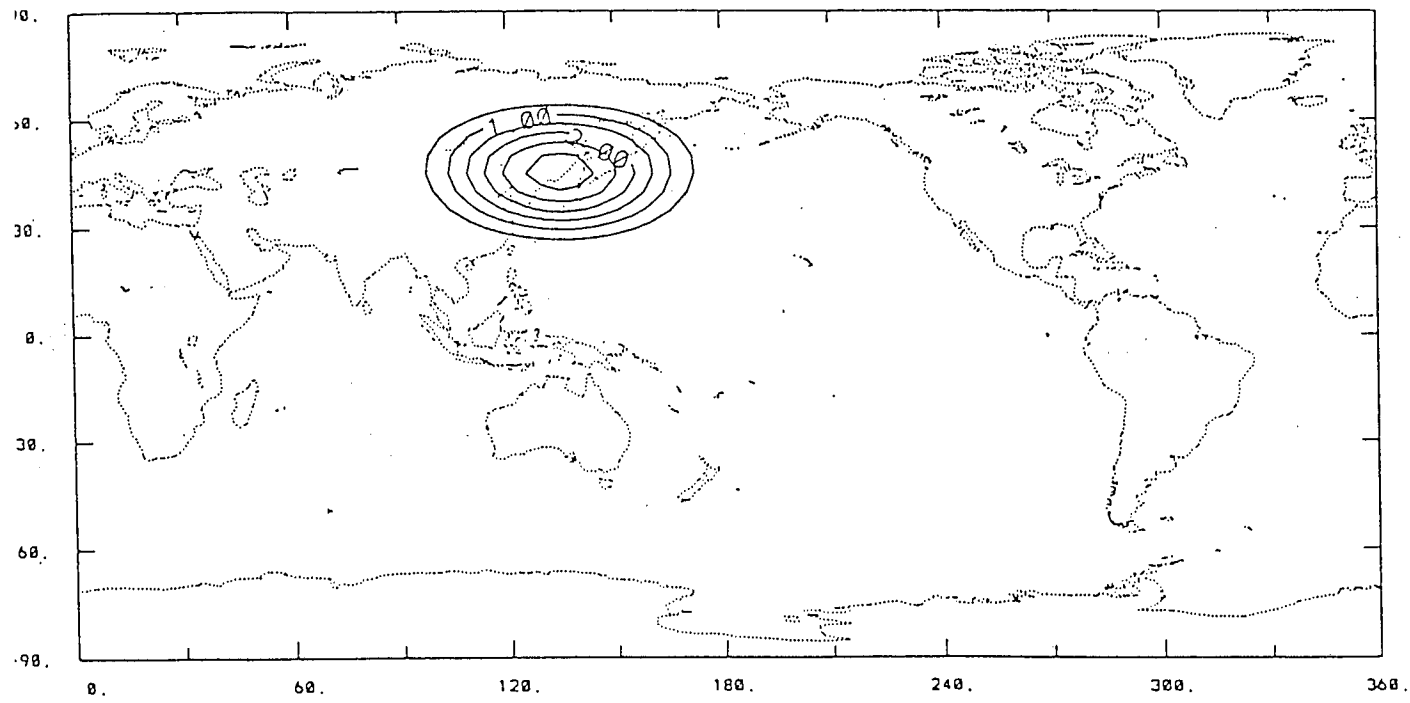

Figure 5.10: Idealized diabatic heating in mid-latitude, centred at $45^0N, 135^0E$. The contour interval is 0.5 Kd^{-1}. The zero contour is supressed.

where $\sigma_1 = -0.86$, $\sigma_2 = 1.0$ for this experiment and later calculations.

The perturbation streamfunction fields of the response to the isolated heating in mid-latitudes are illustrated in Figure 5.11 and 5.12 at 700 mb and 200 mb respectively.

The overall patterns of circulation at both levels is relatively simple and constrained in mid-latitudes of the northern hemisphere. At 700 mb, a cyclonic circulation is located to the east of the heating centre with an anti-cyclonic circulation in the west. At 200 mb, however, the circulation patterns are roughly reversed, with an anti-cyclonic circulation in the east of the heating centre and a cyclonic circulation in the west. The baroclinity of the response is very obvious in northern mid-latitude belt. The result fully agrees with those obtained by others (e.g. Simmons, 1982; Lei, 1986) in mid-latitudes, but differs significantly in polar regions and the

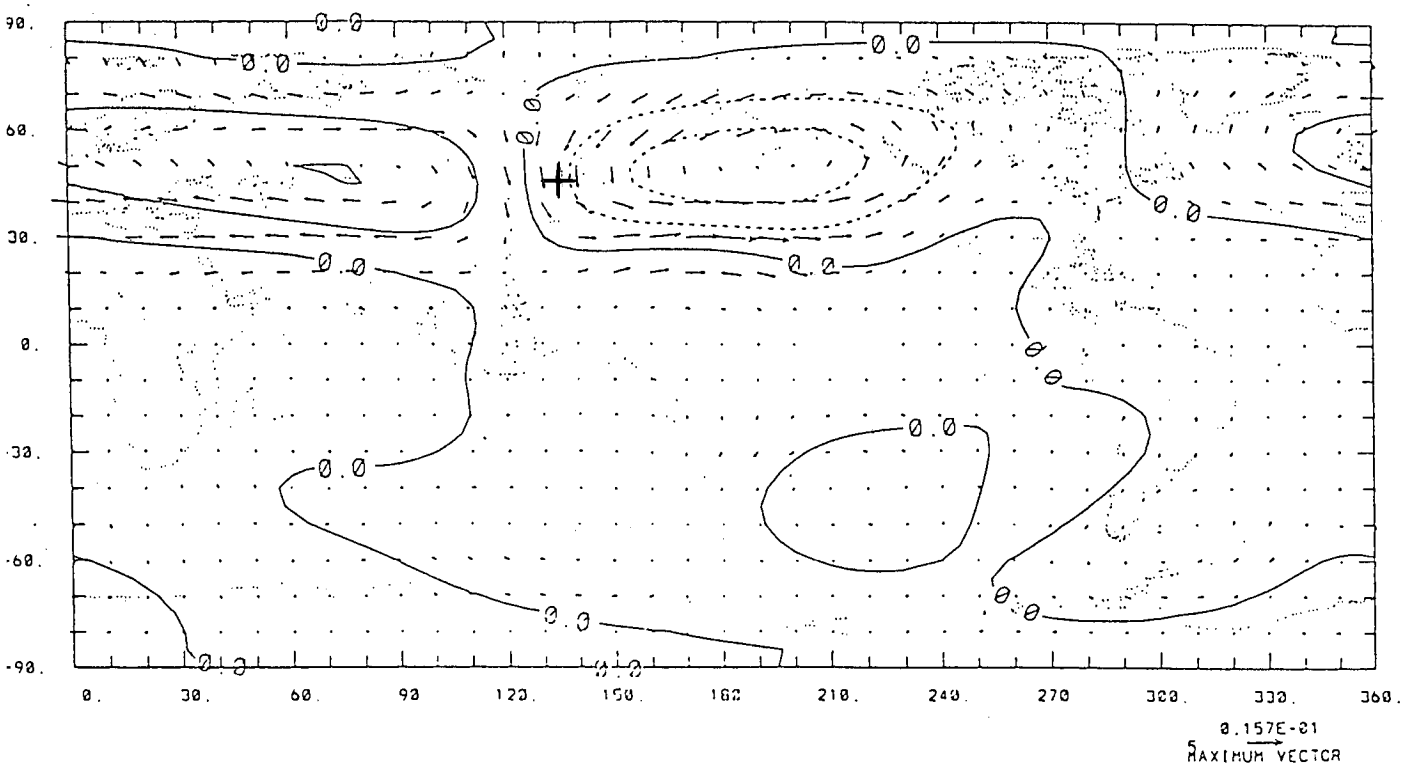

Figure 5.11: 700 mb as in Figure 5.5 but for the model response to an isolated heating in middle latitudes. Contour interval is 10 units. The thickened symbol + marks the centre of the heating source.

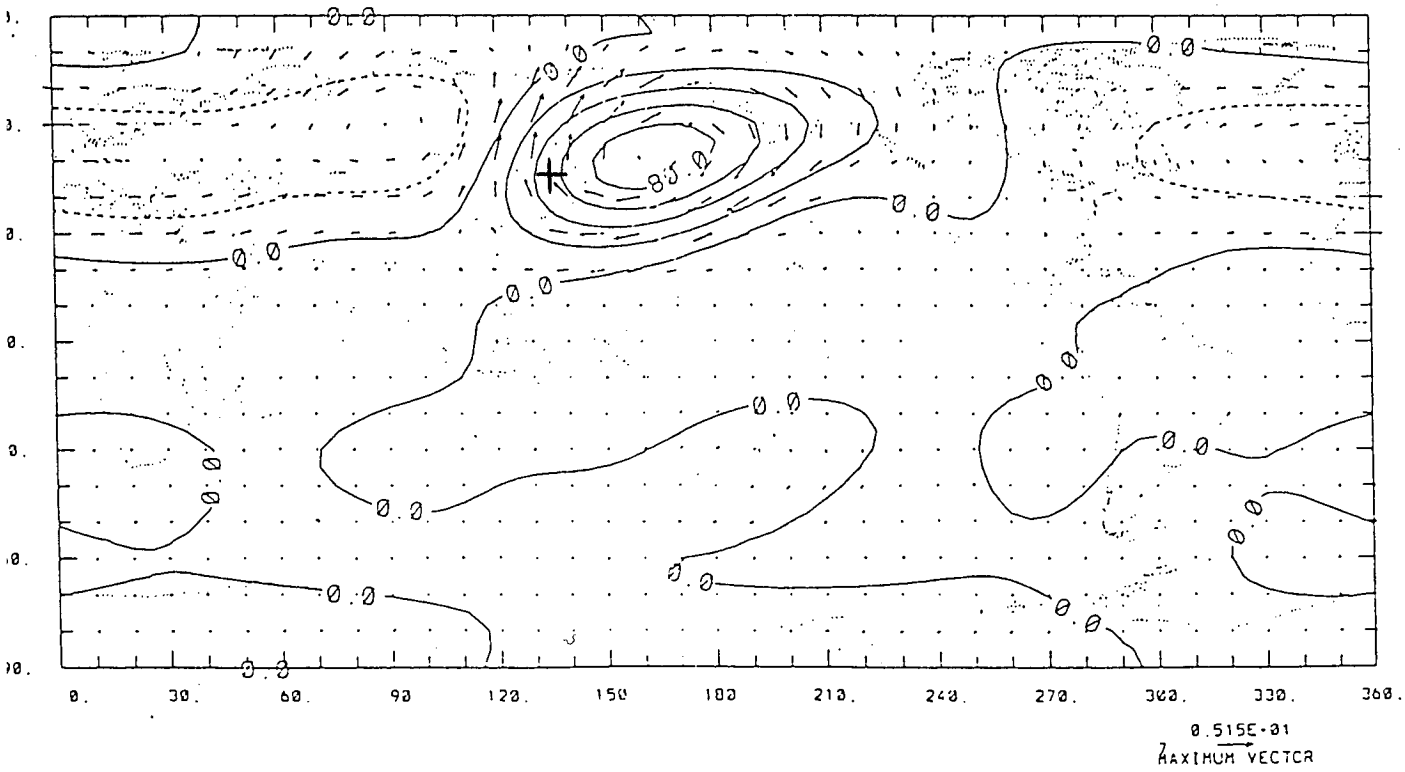

Figure 5.12: Same as Figure 5.11, but for 200 mb. Contour interval is 20 units.

tropical areas, due to different imposition of damping rates enhancement. It is also of interest to point out that there is no pronounced response in the southern hemisphere to the heating centred in northern mid–latitudes.

The Plumb flux at both 800 mb (Figure 5.13) and 500 mb (Figure 5.14) highlights that the wave activity propagates predominantly eastward over, and downward downstream of the heating centre. At 200 mb (not shown), however, it propagates eastward then turning to southeastward over the heating source, and upward to the east of the heating centre. Furthermore, from the EP cross–section (Figure 5.15), it clearly denotes that the wave activity propagates both downward, and upward to the stratosphere, with the maximum divergence of the EP flux situated at about 400 mb, the location of the maximum of the vertical distribution of diabatic heating. Also, both Plumb flux and EP cross-section illustrate that the isolated diabatic heating in northern middle latitudes has little effect in the southern hemisphere, and a very restricted effect in the northern hemisphere itself.

§5.4 Response to Tropical Heating

This experiment is virtually the same as the previous one, but with the heating shifted to low latitudes centred at $15^0N, 135^0E$ with the change of values to $\varphi_1 = 0^0$, $\varphi_2 = 30^0N$ of function (5.2). The streamfunction and velocity field in response to this tropical heating are displayed in Figure 5.16 and 5.17 at 700 mb and 200 mb respectively. In low latitudes, there is a cyclonic circulation at lower levels, with an anti–cyclonic circulation at upper levels, centred to the northeast of the heating centre. Due to the imposition of a high damping rate in low latitudes, the tropical

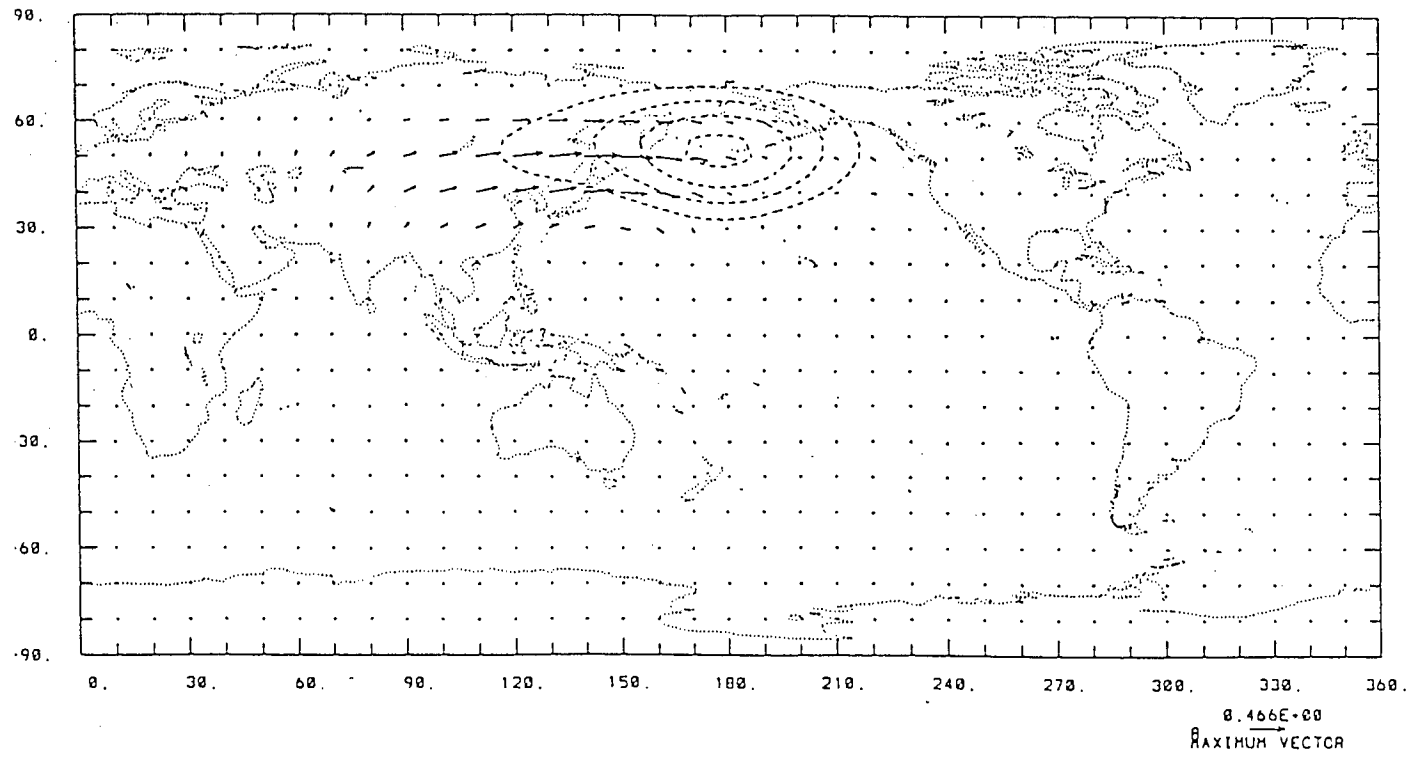

Figure 5.13: Plumb flux: as in Figure 5.7, but for the model response to an isolated diabatic heating in northern middle latitudes. Contour interval is 5 units. The thickened symbol + marks the centre of the heating source.

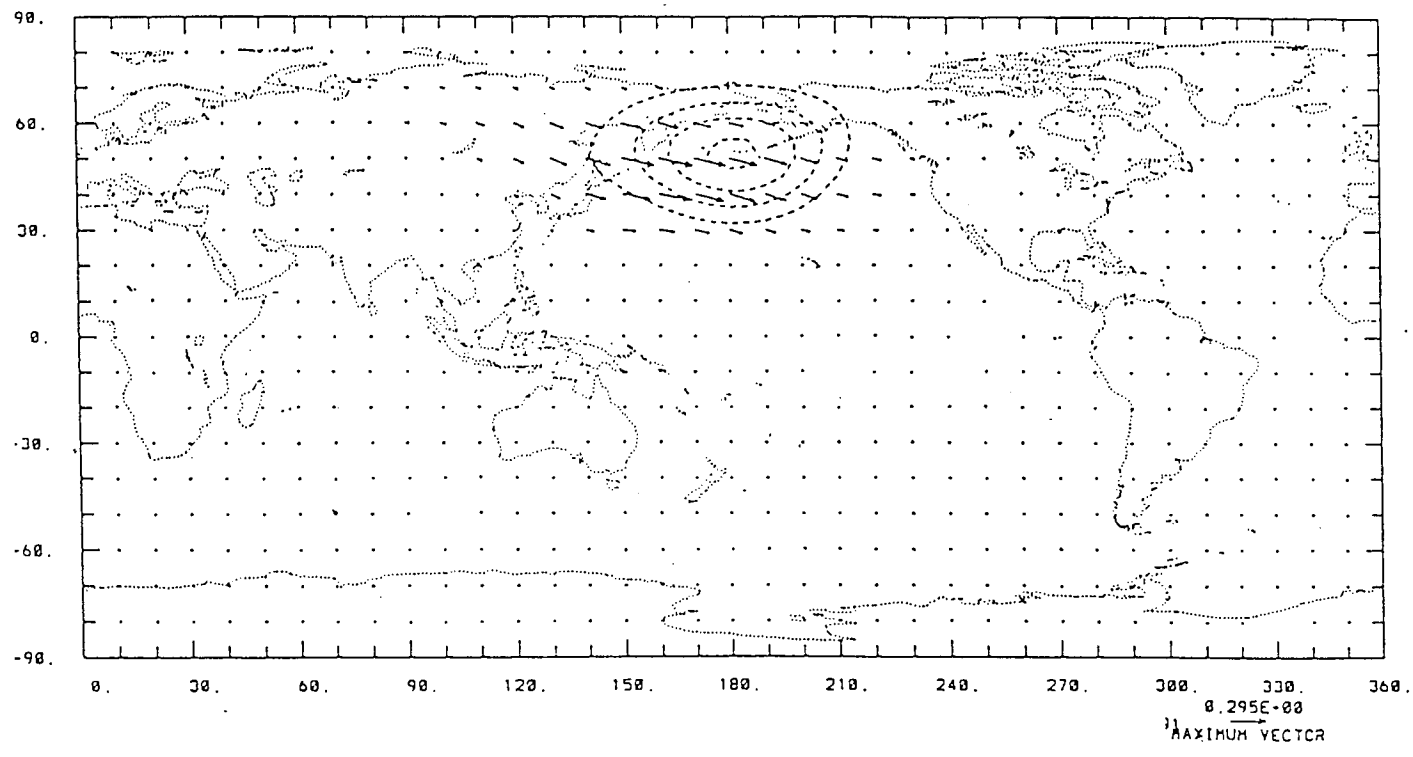

Figure 5.14: Same as Figure 5.13, but for 500 mb. Contour interval is 5 units.

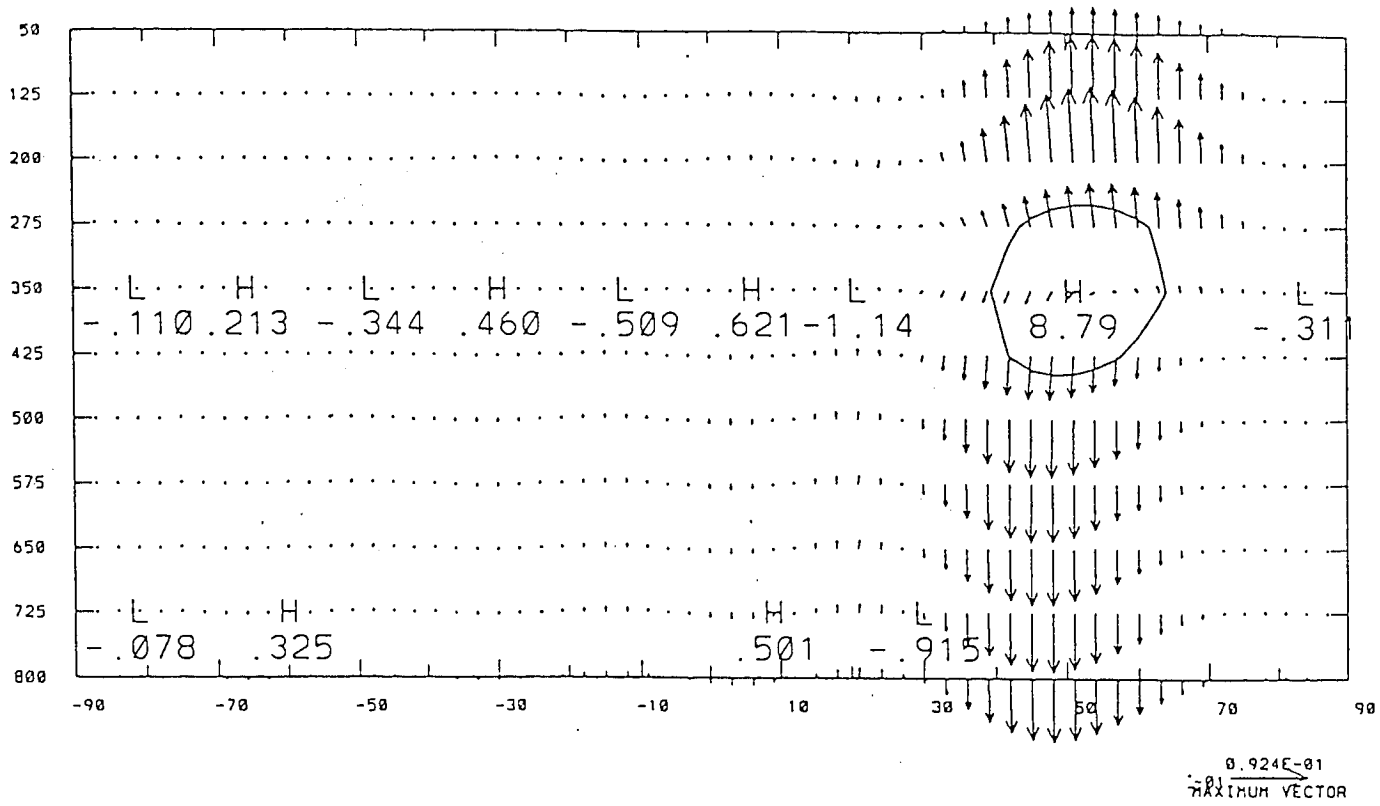

Figure 5.15: EP cross-section: As in Figure 5.9, but for the model response to an isolated diabatic heating in northern mid-latitudes. Contour interval is 5 units.

response away from the heating source at both levels is very weak. A weak cyclonic circulation at upper levels and an anti-cyclonic circulation at lower levels can be visualized from the velocity field far downstream of the heating centre.

In addition, there is clear evidence that the northern tropical diabatic heating has a strong impact on mid-latitudes of both hemispheres. In northern mid-latitudes, a cyclonic circulation northeast of Japan and an anti-cyclonic circulation over north America can be found at 200 mb, but only a relatively weak response can be seen at lower level. In southern mid-latitudes, a cyclonic system, though small, exists. However the model response in both of the polar regions and southern tropics is hardly seen.

Figures 5.18 and 5.19 highlights the wave activity flux at 800 mb and 500 mb respectively. At 800 mb, the wave activity propagates predominately upward and

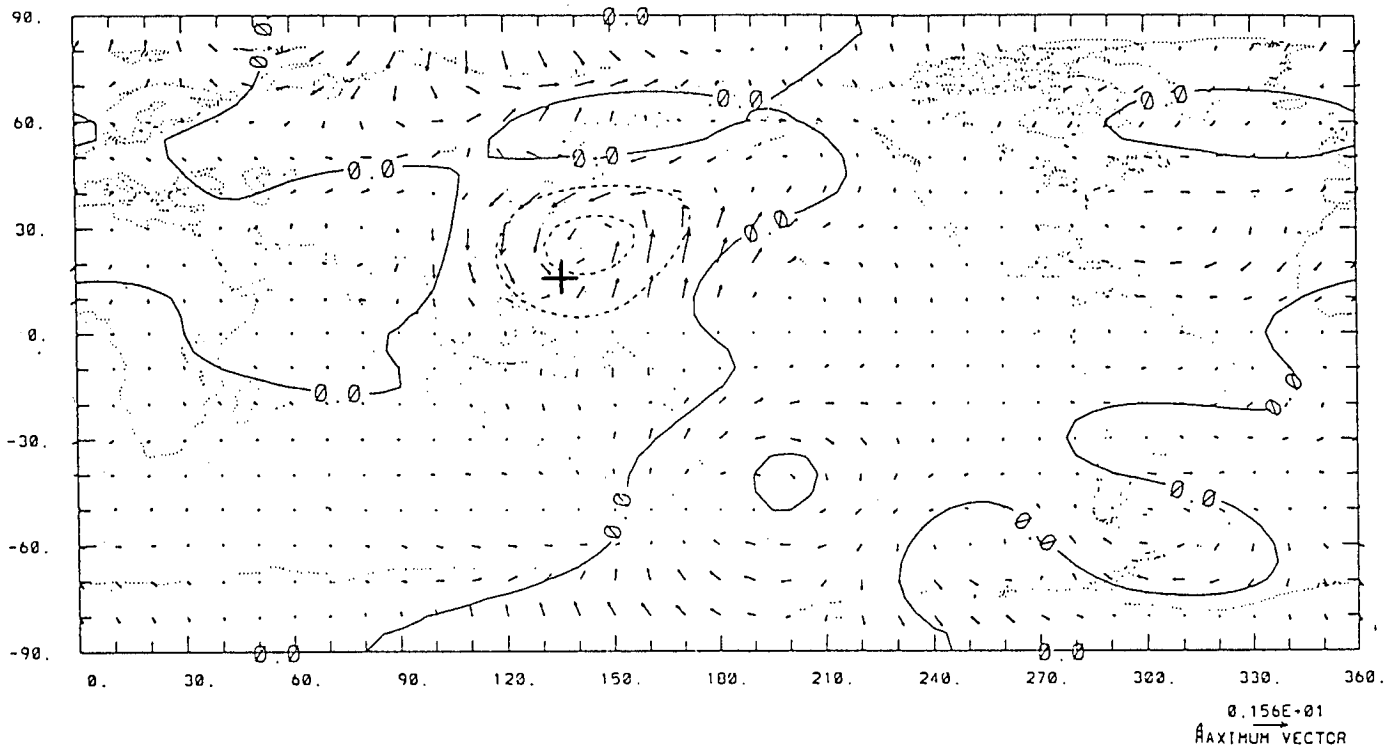

Figure 5.16: 700 mb as in Figure 5.5 but for the model response to an isolated heating in northern tropics. Contour interval is 10 units.

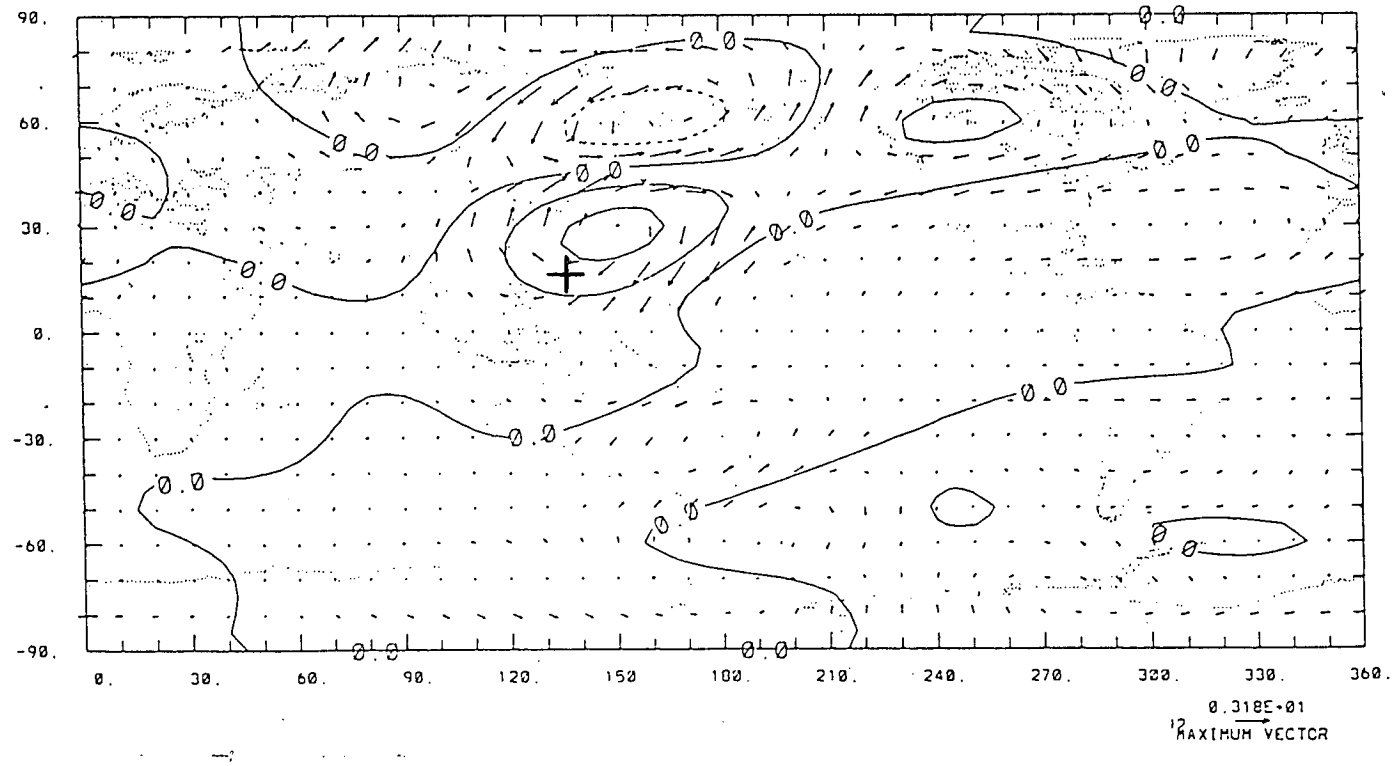

Figure 5.17: Same as Figure 5.16, but for 200 mb. Contour interval is 20 units.

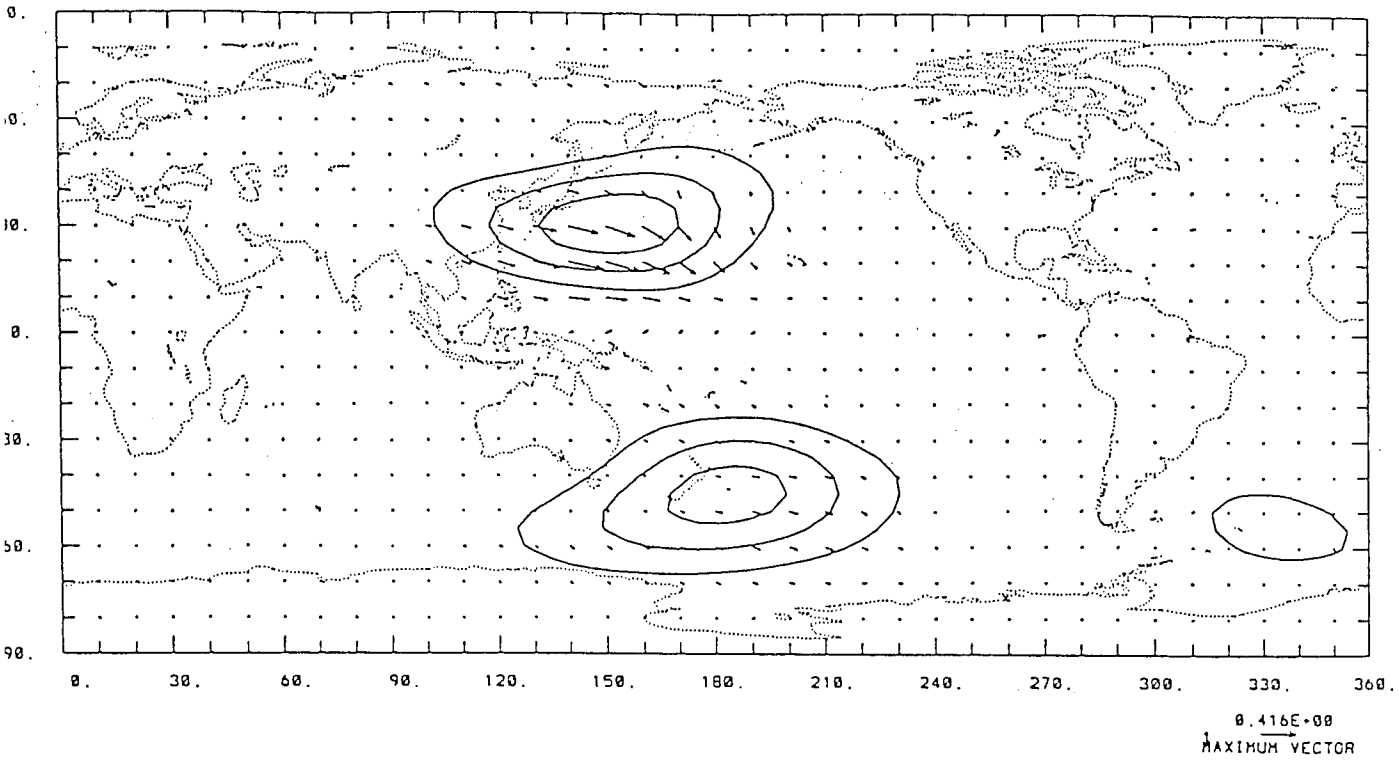

Figure 5.18: Plumb flux: As in Figure 5.7, but for model response to an isolated diabatic heating in northern tropics. The contour interval is 1 unit.

east–to–southeastward to the north of the heating centre. It is of interest to note that the upward propagation of wave activity in southern mid–latitudes is quantitavely significant, while its horizontal propagation is negligible.

At 500 mb, the main feature of the wave activity propagation in the northern hemisphere is an increased southeastward component to the north of the heating centre, extending to high latitudes. The upward propagation to the north of the heating centre is comparable to that at 800 mb. In the southern hemisphere, however, the wave activity propagation is much weaker in the vertical, while stronger and more predominantly eastward in the horizontal, than that at 800 mb. At further higher level (200 mb, not shown here), the Plumb flux is much reduced in the vertical, but enhanced significantly in southeastward direction. This vertical structure of the wave activity flux implies that the wave activity flux over the heating source

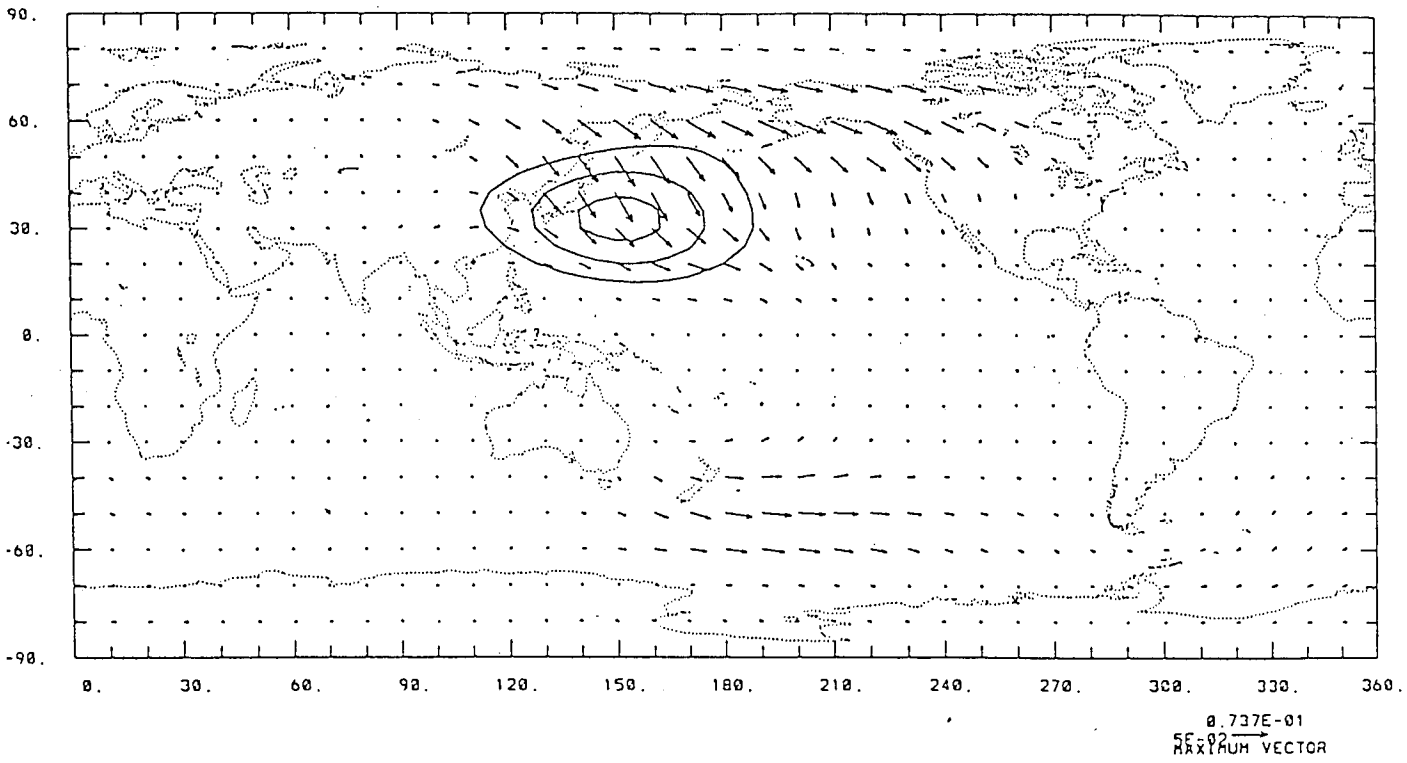

Figure 5.19: As in Figure 5.18, but for 500 mb. The contour interval is 1 unit.

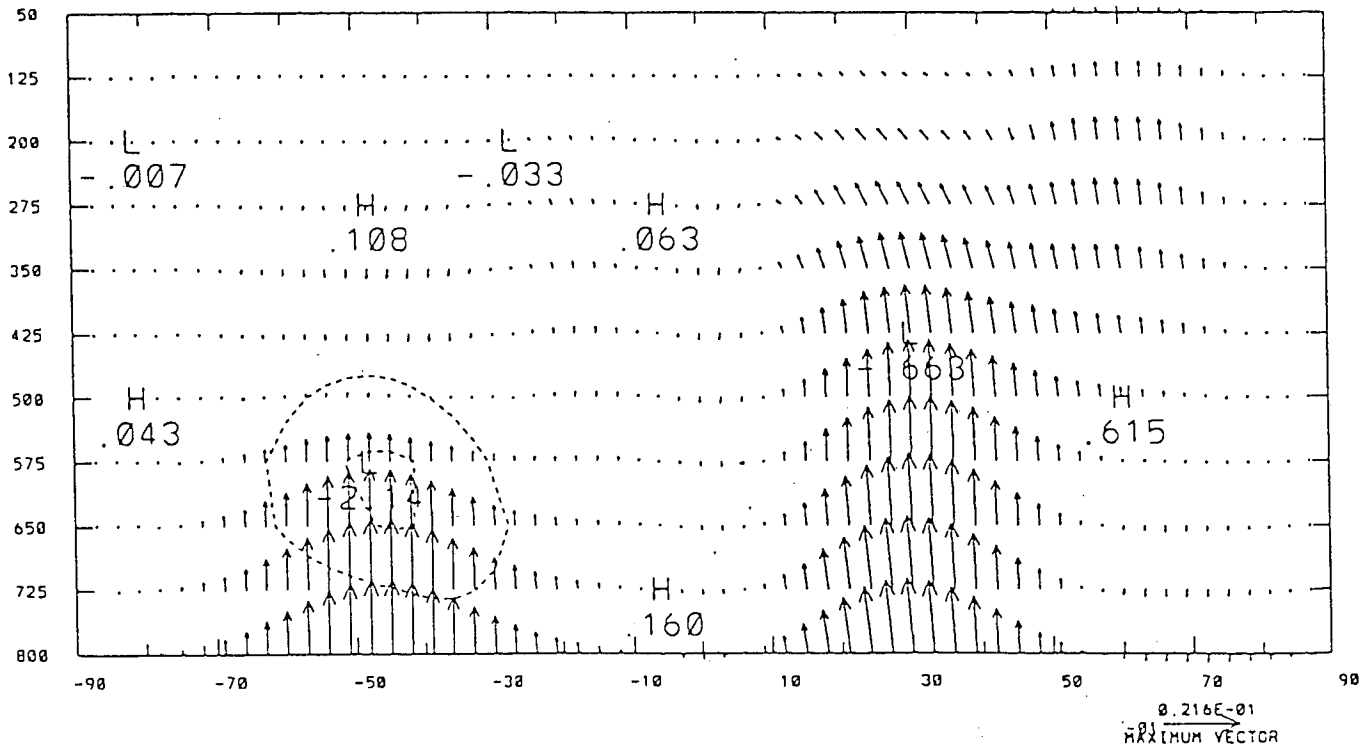

Figure 5.20: EP cross-section: As in Figure 5.9, but for model response to an isolated diabatic heating in northern tropics. The contour interval is 1 unit.

will be refracted towards the tropics in upper troposphere. This feature can be further illustrated by the EP cross–section in Figure 5.20, which also shows that the strongest EP flux is located at lower levels over the north side of the heating centre. Moreover, the EP cross–section denotes the significant effect of northern tropical heating on mid–latitude low–levels of the southern hemisphere.

§5.5 Response to Equatorial Heating

To further reinforce the validity of the model, one more calculation is carried out for tropical and ex–tropical response to the diabatic heating centred at equator. Gill (1980) obtained an analytical solution for this response by establishing a simple analytical model for an atmosphere on an equatorial β–plane, with zero zonal–mean wind and a very simple vertical structure. His result is in good qualitative agreement with observation, with inflows to the heating region, and cyclonic circulation in the north– and southwest of the heating maximum at lower levels, with reversed flow pattern and circulation at upper level. Simmons (1982) and many others carried out similar experiments employing a more sophisticated model and found similar results.

Experiments were conducted using our model for the diabatic heating specified by expression (5.2) for the values $\varphi_1 = 15^0S$, $\varphi_2 = 15^0N$, $\lambda_1 = 90^0$, $\lambda_2 = 180^0$, with damping rates of both Newtonian cooling and Rayleigh friction being relaxed to constant coefficients of $(7\ d)^{-1}$ at tropics wherever φ falls into interval $-30^0 \leq \varphi \leq 30^0$. The zonal mean state is the same as that used in the previous experiments of the Chapter.

The perturbation velocity field and its streamline are illustrated in Figure 5.21 and 5.22 at 700 mb and 200 mb respectively. The response is generally in good agreement with that of Simmons. It differs slightly from Gill's results in the symmetricity of the flow pattern, but the overall visual perception agrees qualitatively.

If the foregoing experiment is repeated with the zonal mean velocity $[U]$ set to zero everywhere , but the zonal mean temperature remaining as climatology, the model response is almost identical to Gill's results. The results of this experiment are revealed in Figure 5.23 and 5.24 for perturbation velocity at 700 mb and 200 mb respectively.

Furthermore, the difference between the above two experiments may be interpreted as showing the influence of the zonal mean velocity $[U]$.

Figure 5.25 and 5.26 show the wave activity flux at 800 mb and 500 mb respectively for the case with the zonal mean velocity $[U]$. At 800 mb, the upward and eastward propagation of the wave activity dominate north- and southeast of the heating centre. It is very interesting to see that the wave activity flux is stronger on the southern flank of the heating than on the northern. However, the wave activity is relatively weak in the heating centre and in high latitudes of both hemispheres. At 500 mb, the strongest vertical component of the Plumb flux is to the southeast of the heating centre with eastward propagation in the horizontal. To the north of the heating centre, the wave activity in the horizontal tends to propagate northeastward then turn around towards the southeast, with small vertical propagation. Attention might also be paid to the fact that the wave activity flux is stronger in the southern hemisphere than in northern at both of the levels. This result can further be illustrated by the EP cross-section (Figure 5.27) from which

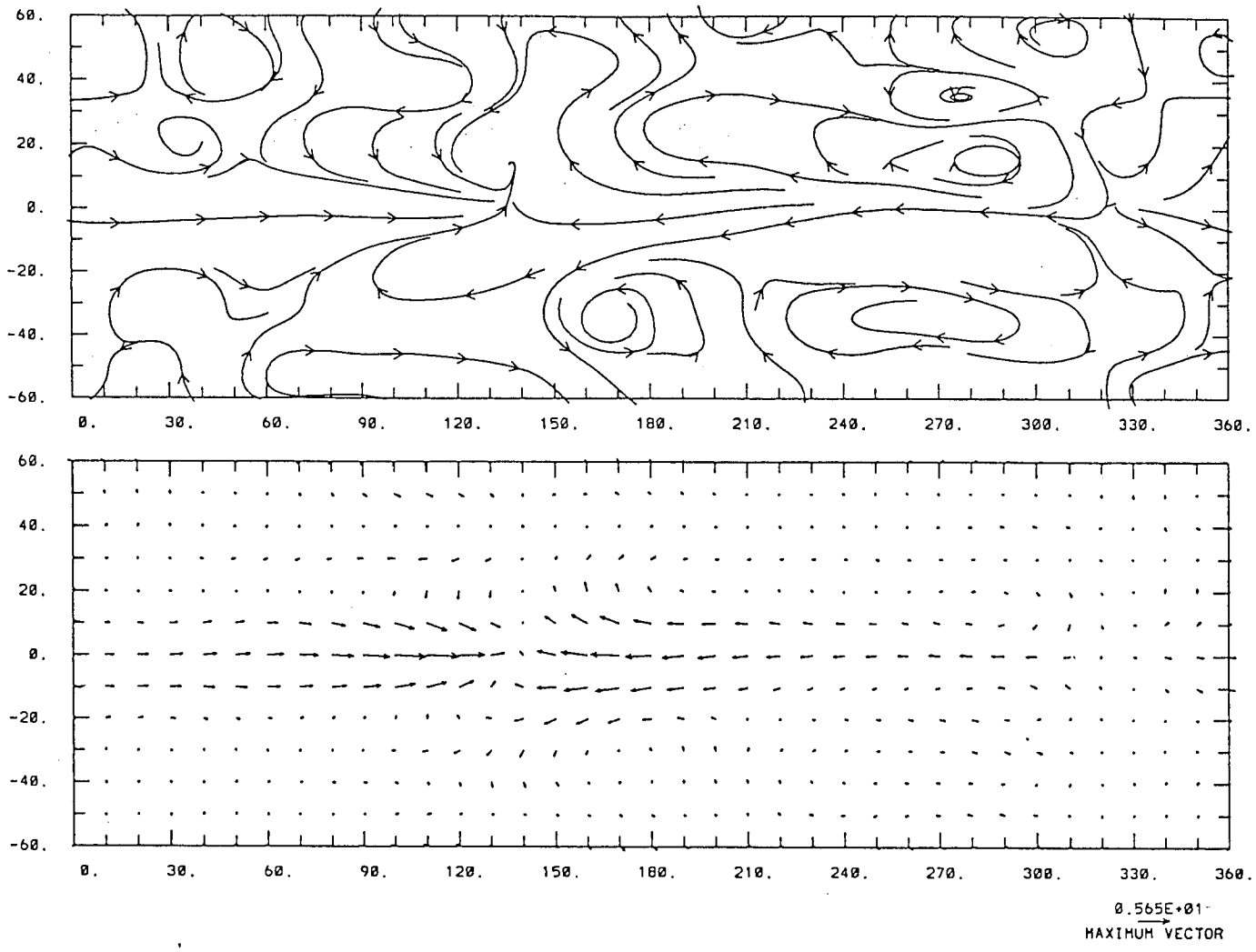

Figure 5.21: 700 mb perturbation velocity field (lower) and its streamline (upper) for the model response to an isolated heating at the equator.

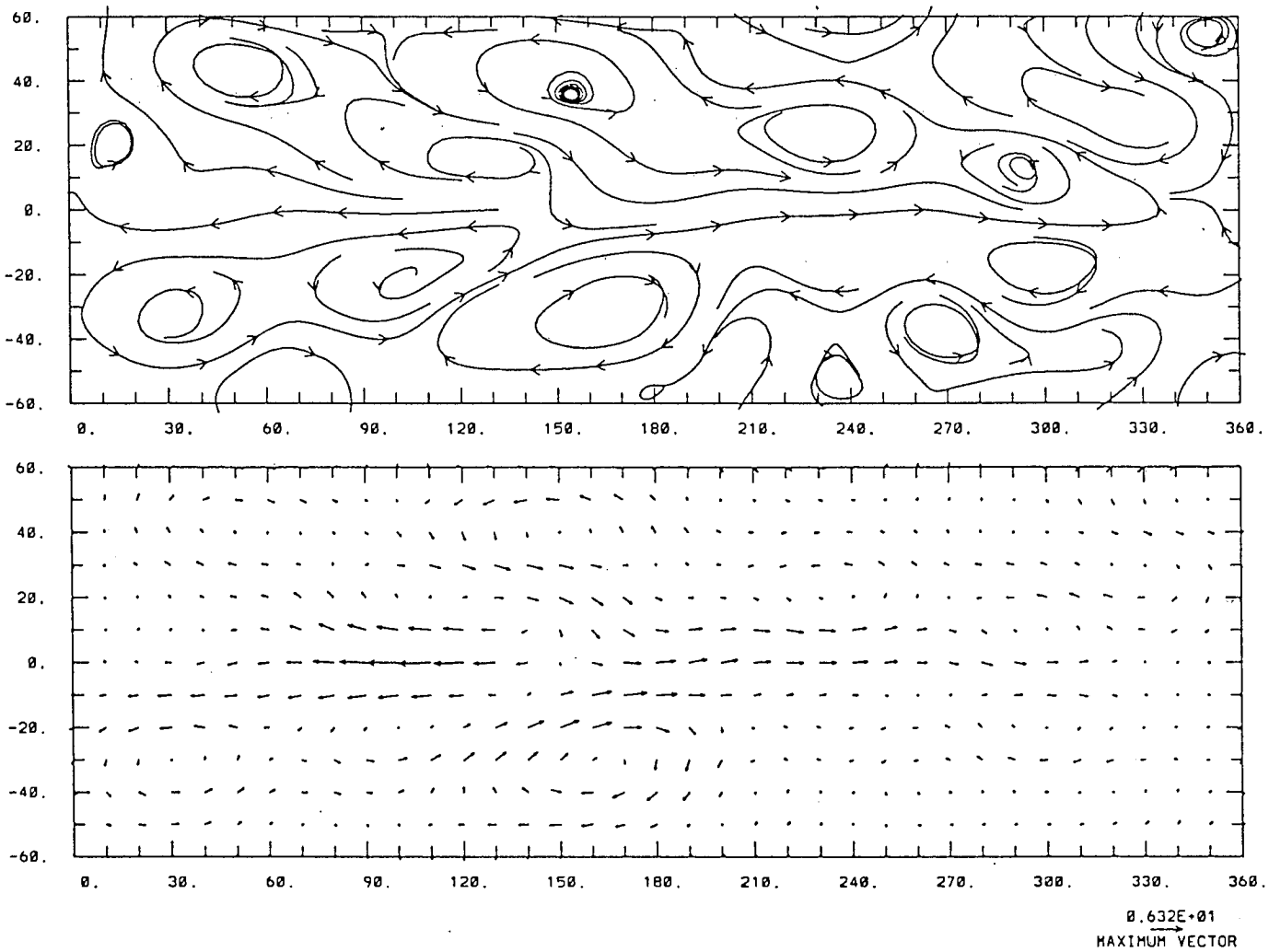

Figure 5.22: Same as Figure 5.21, but for 200 mb.

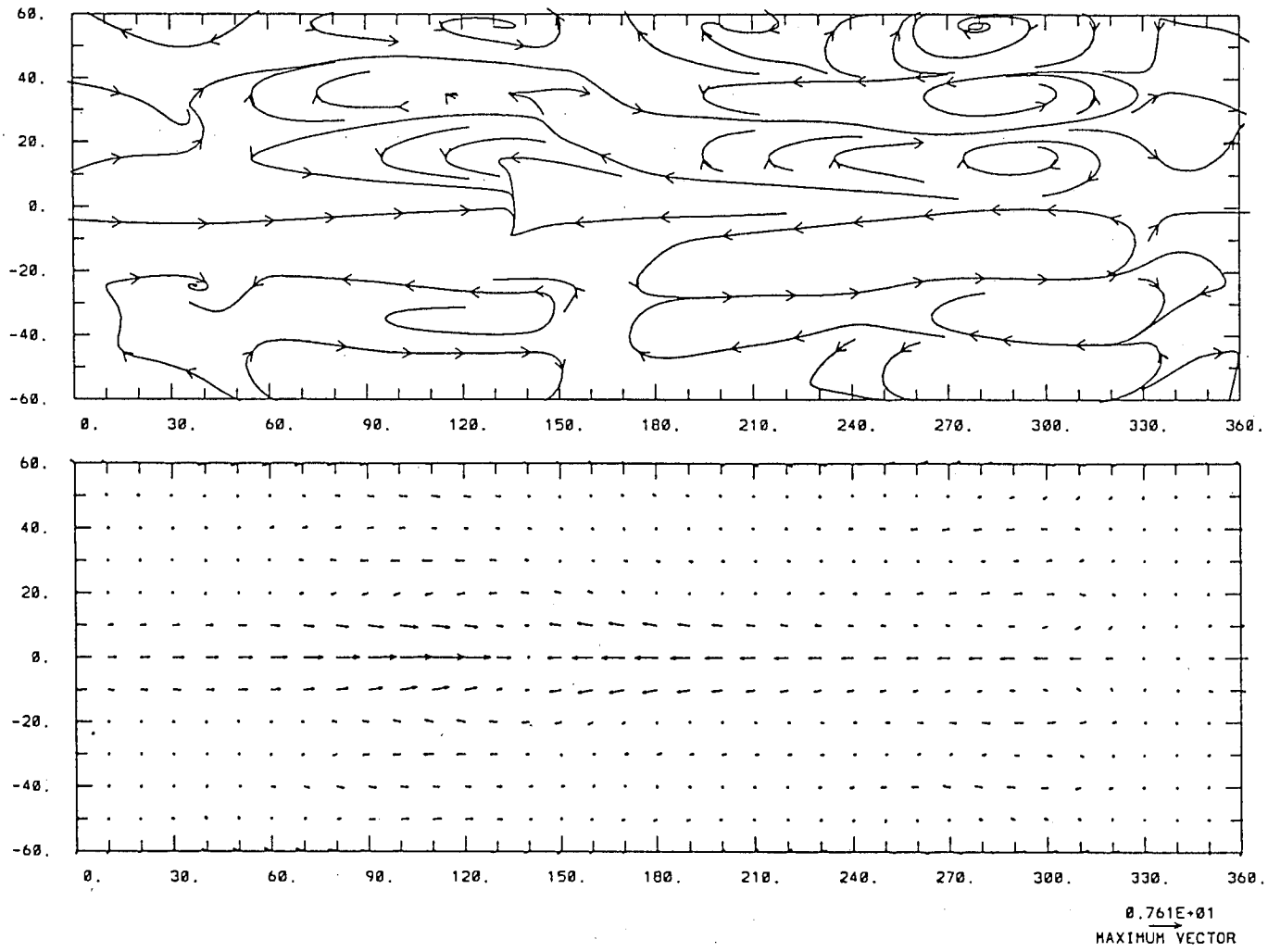

Figure 5.23: Same as Figure 5.21, but for zonal mean velocity $[U]$ set to be zero everywhere.

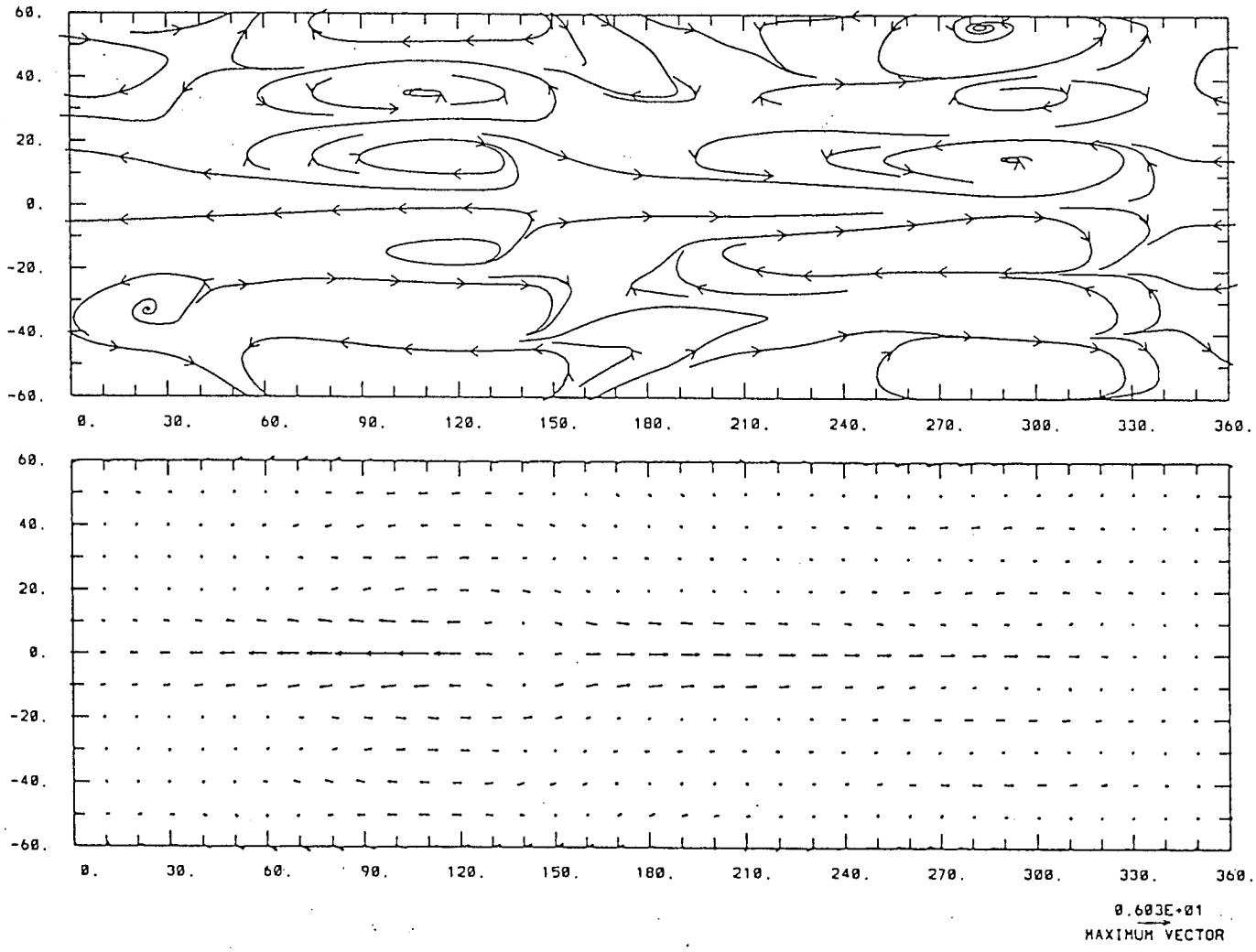

Figure 5.24: Same as Figure 5.23, but for 200 mb.

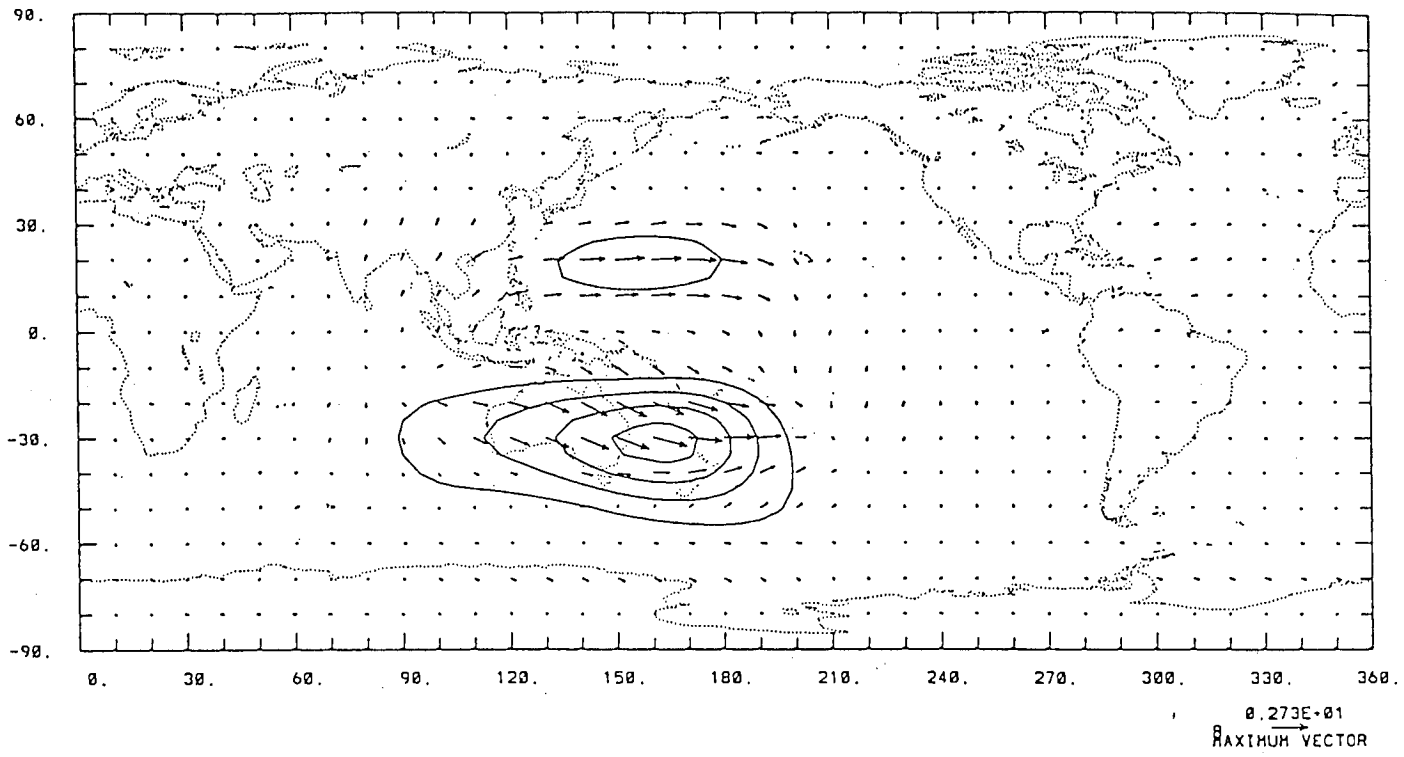

Figure 5.25: Plumb Flux: as in Figure 5.7, but for model response to an isolated diabatic heating in equator. The contour interval is 10 unit.

the maximum EP flux and its convergence can be found in the southern side of the heating.

§5.6 Sensitivity Experiments

Since the model in the previous experiments has demonstrated ability in producing the essential features of the response to various idealized forcing, it might be used as a diagnostic method and a basic tool for the study of stationary waves. Prior to that we proceed to investigate sensitivity to model parameters mentioned at the beginning of this Chapter. For convenience, but without loss of generality, only some selected experimental results with idealized forcing used in the previous sections are illustrated here. It may be worth noting that the results of the sensitivity

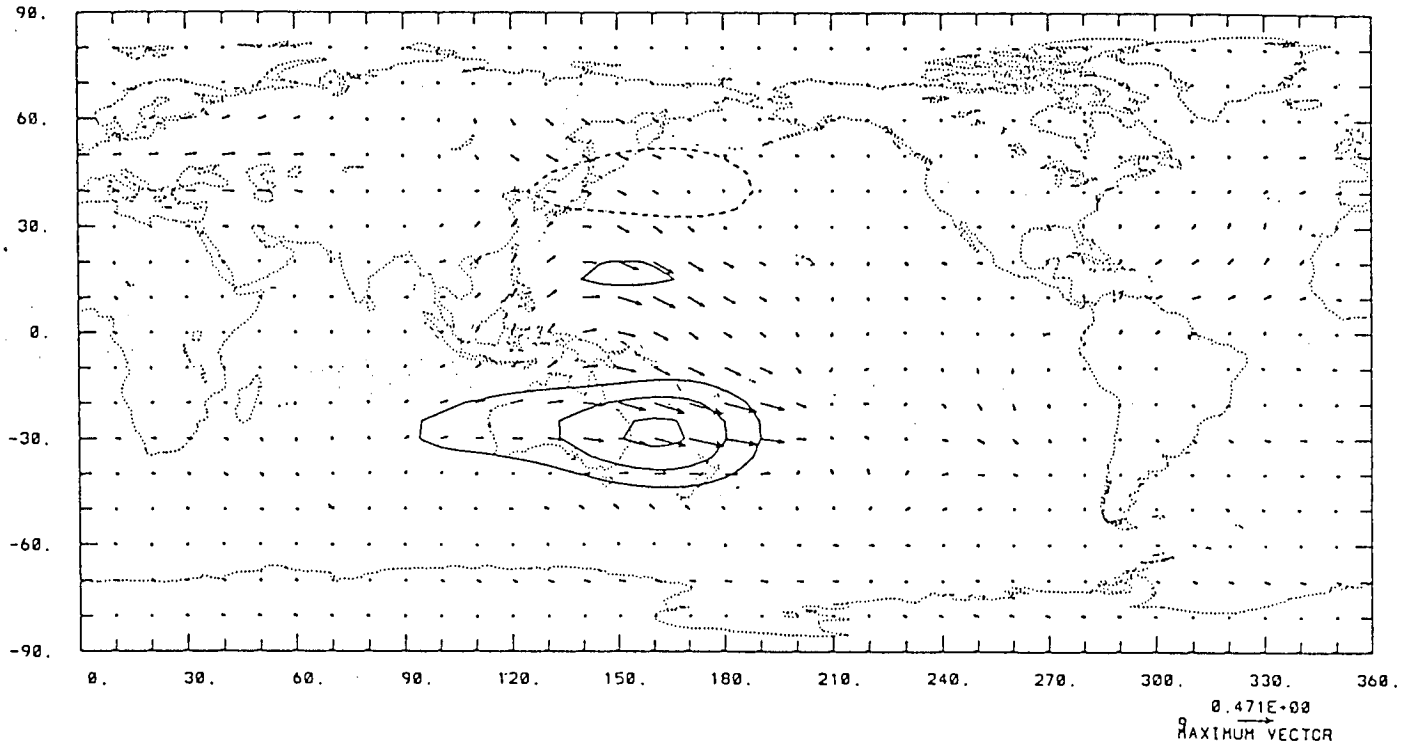

Figure 5.26: As in Figure 5.25, but for 500 mb. The contour interval is 5 unit.

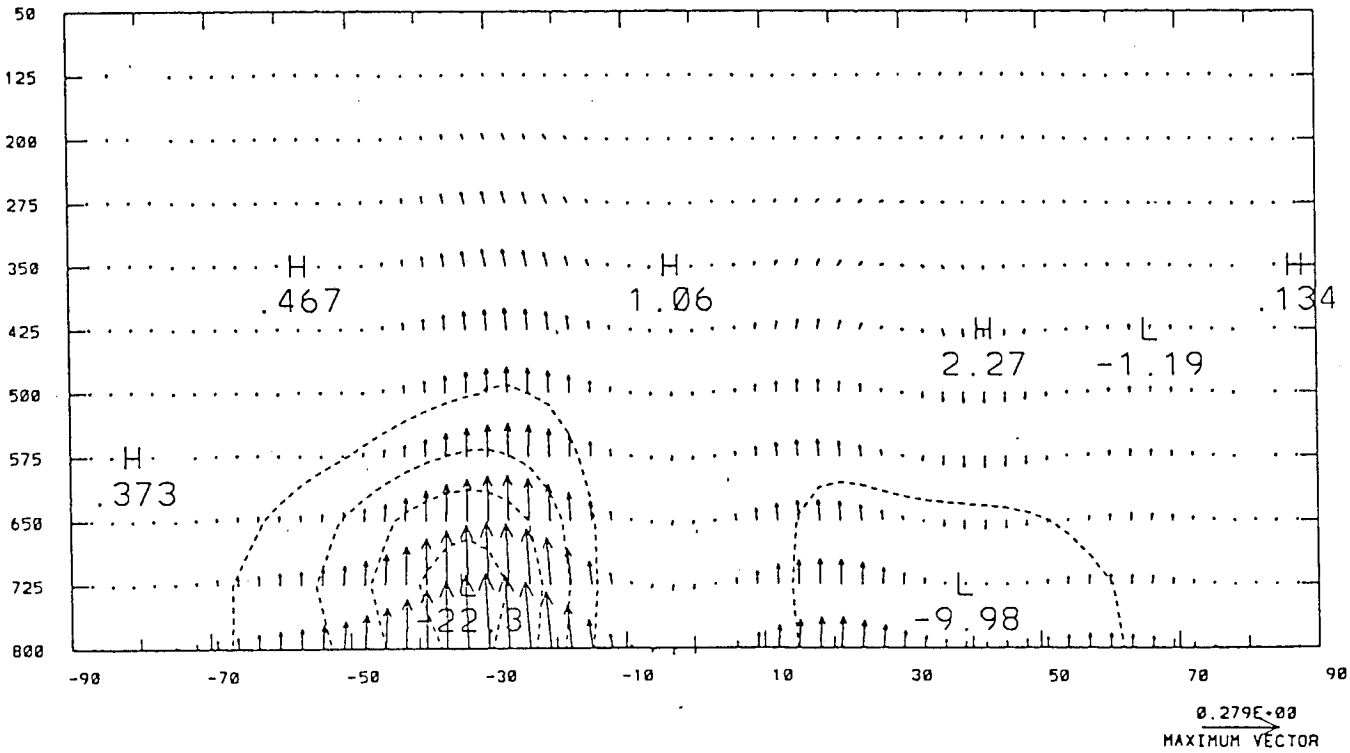

Figure 5.27: EP cross-section: As in Figure 5.9, but for model response to an isolated diabatic heating in equator. The contour interval is 5 unit.

tests may be valid only for the model used here.

§5.6.1 Sensitivity to the Zonal Mean State

The model sensitivity to the zonal mean state could be tested by re–running the previous four experiments but replacing the basic state $[U]$ and $[T]$ represented in Figure 5.2 with Figure 5.3, while all other model parameters are unmodified. The experimental results are compared with their respective counterpart in the foregoing sections. No pronounced difference could be visually perceived for the model response to the three cases of idealized diabatic heating (thus not shown here). However, the model response to idealised middle latitudes orography differs significantly in amplitude to that in §5.2 (see Figure 5.28 and 5.29). It may be seen from Figure 5.28, comparing with Figure 5.5, that the cyclonic system at 700 mb to the north of the idealized mountain is much stronger, and northerly shifted, and the other systems elsewhere at the lower levels are similar except that the anti-cyclonic system to the west of the mountain is much weakened. At the higher level 200 mb (5.29), in contrast to Figure 5.6, the patterns and the locations of the circulation systems are similar. However, in spite of the fact that the amplitude of the circulations is weaker in the east northern hemisphere, but stronger in the north America and the northern Atlantic, it is nonetheless comparable. From the above comparasion, though the sensitivity to the zonal mean states using idealized orography is perceivable, the results for both sets of the zonal mean states are comparable and reasonably acceptable.

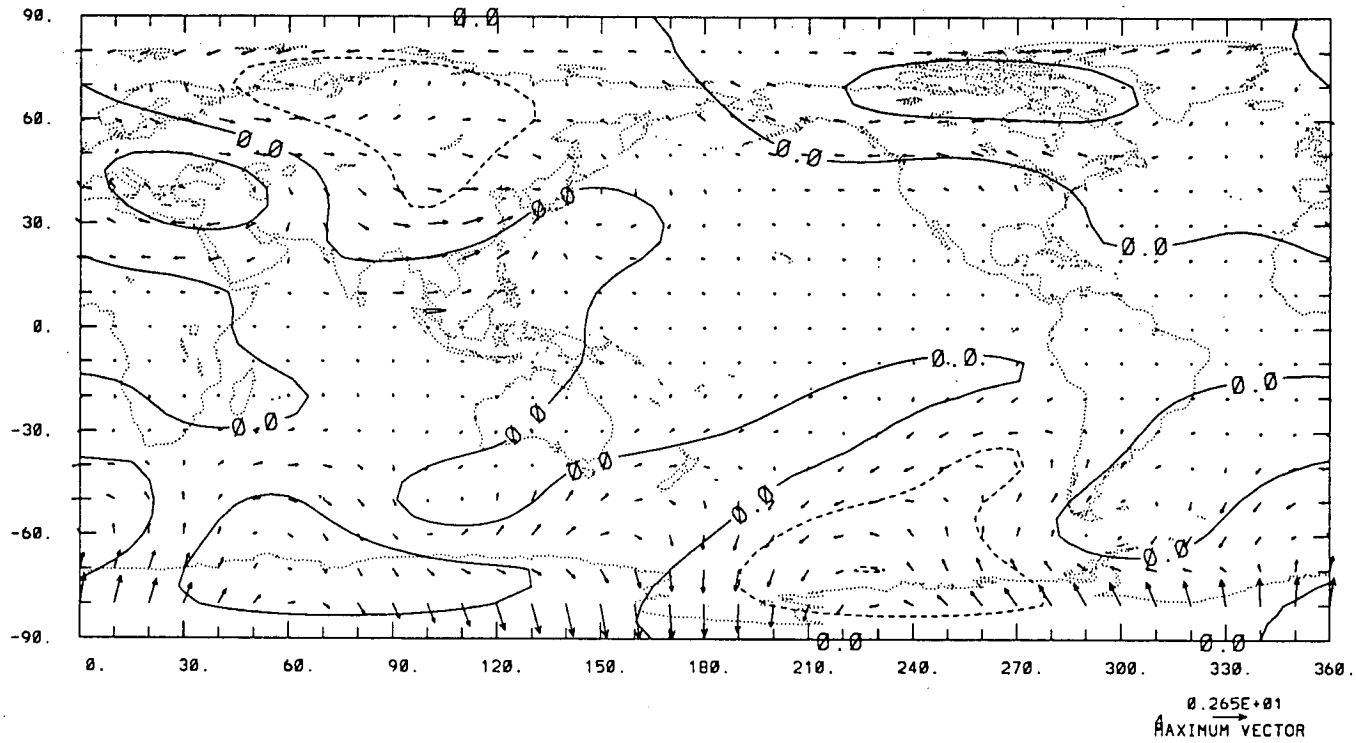

Figure 5.28: 700 mb as Figure 5.5, but for using zonal mean state interpolated into σ levels with insertion of global orography. The contour interval 10 units.

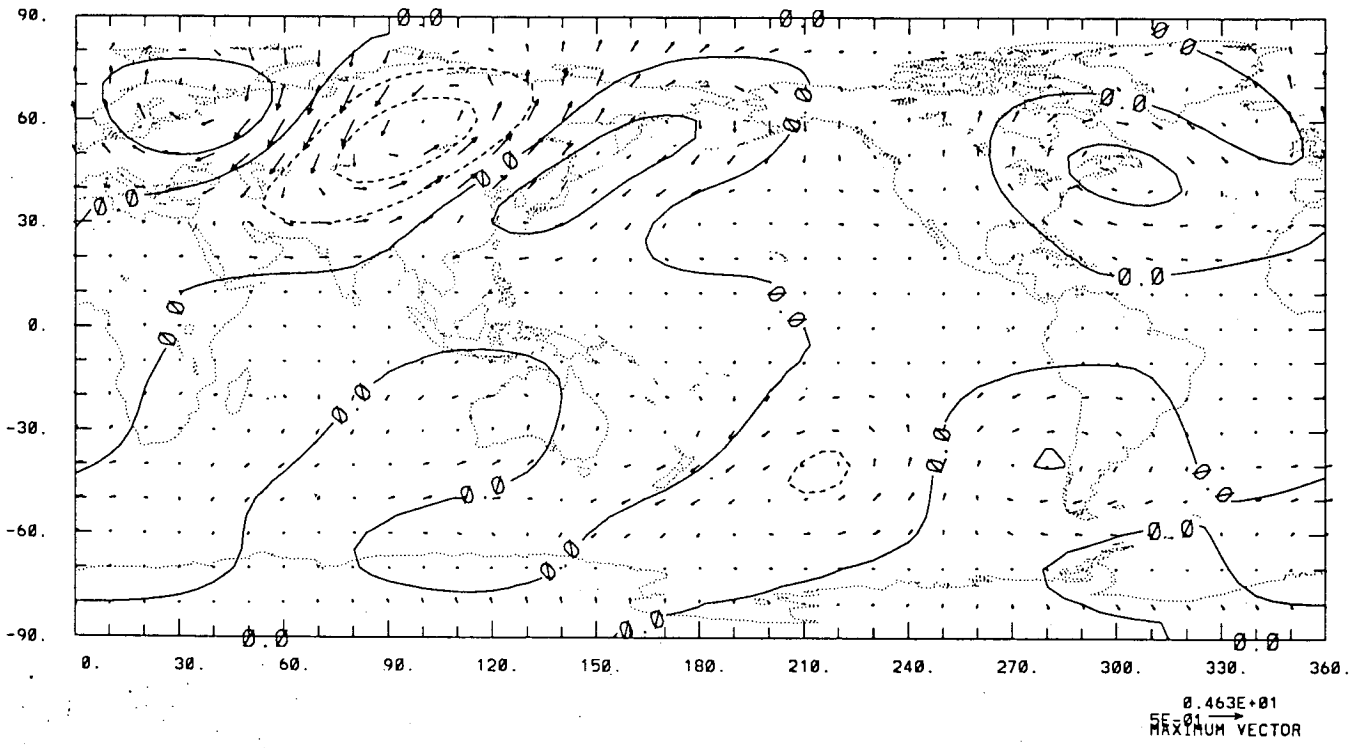

Figure 5.29: As Figure 5.28, but for 200 mb, with contour interval of 20 units.

§5.6.2 Sensitivity to the Dissipation Parameters

The damping rates are found to be very powerful and robust in tuning the model. A number of sensitivity experiments are performed. We here only choose to show the results for the case of response to tropical heating centred at 15^0N as in §5.4. The results in §5.4 are taken as a reference which is used to examine the sensitivity of the dissipative parameters. Three experiments are illustrated as follows.

Case A: change the enhancing factor of both frictional damping and Newtonian cooling in polar regions by $\left(\frac{\cos\varphi_0}{\cos\varphi}\right)^{3.0}$ rather than $\left(\frac{\cos\varphi_0}{\cos\varphi}\right)^{4.5}$;

Case B: as in case A, but decrease both of the biharmonic diffusion coefficients α and ν to one percent of their previous values;

Case C: as case B, but the horizontal distribution of the Newtonian cooling is set to be uniform, with increasing factor of Rayleigh friction in polar regions as $\left(\frac{\cos\varphi_0}{\cos\varphi}\right)^{4.0}$, and in critical layers by dividing factor ($[U]^2$) where ever $[U]$ falls below 1 $m\ s^{-1}$;

Case D: as in the reference case, but the coefficients of both Rayleigh friction and Newtonian cooling are relaxed to $(7\ days)^{-1}$ everywhere.

In comparing with the reference one, the results of Case A gives the impression that the slight modification of frictional damping and Newtonian cooling in polar regions could result in a noticable change in the model response over the globe. This can be illustrated from Figure 5.30 and 5.31. The response is generally amplified over the

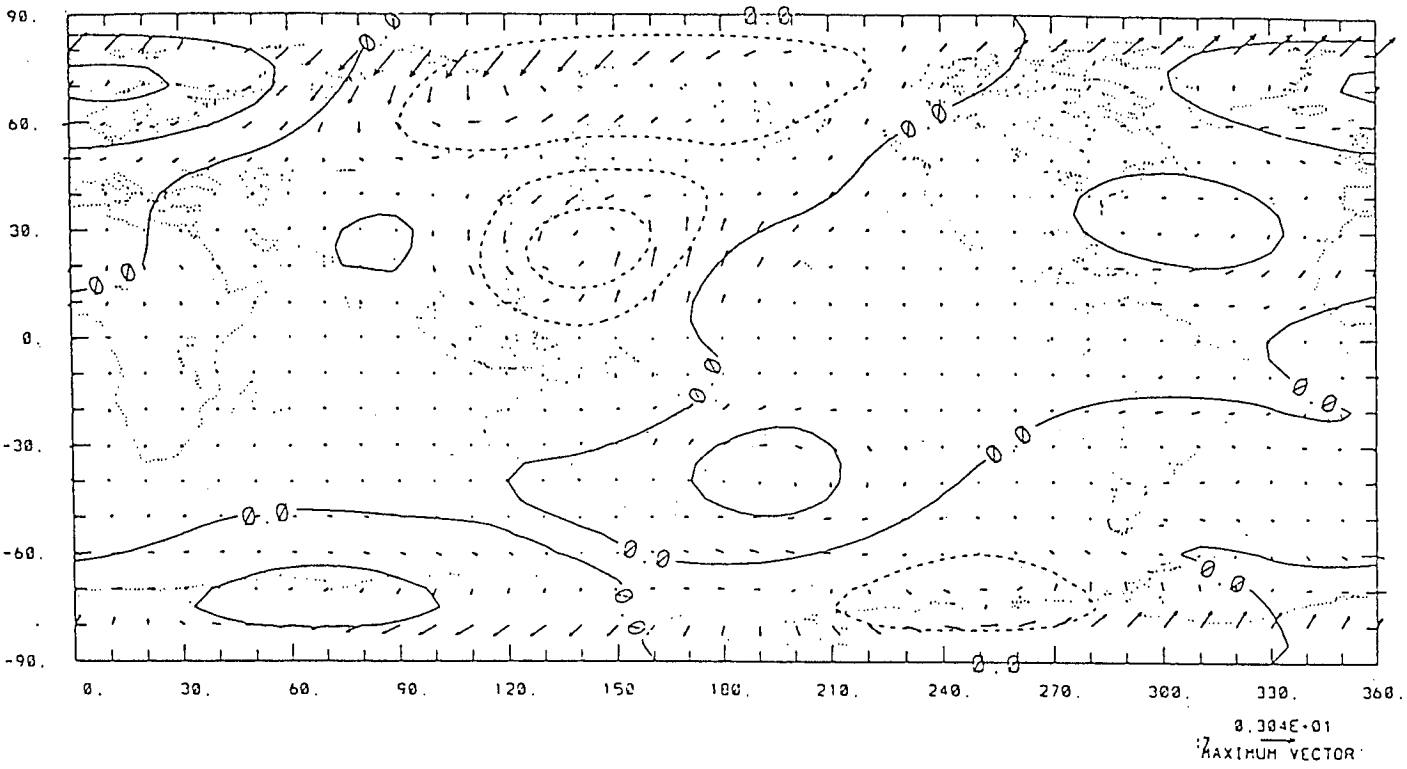

Figure 5.30: 700 mb as in Figure 5.16 but for sensitivity test in Case A. Contour interval is 10 units.

whole globe at both 700 mb and 200 mb levels. This is more obvious in northern polar regions at 200 mb and in both polar areas at 700 mb level. The main systems of the response visible in the reference case are not changed, and the significant remote response in the southern hemisphere can be more clearly identified. The Plumb flux is also sensitive, with downward propagation at 500 mb (Figure 5.33) as well as 800 mb (Figure 5.32) in the northern polar region. Moreover, the stronger horizontal propagation of wave activity in the southern Pacific can be seen at 500 mb. From the EP cross-section (Figure 5.34), the EP flux differs from the reference only in the lower troposphere of both polar regions.

For Case B, the results (not shown here) are almost identical to those of Case A, with the only visible difference that the marked value of the maximum arrow scale for horizontal velocity at 200 mb is slightly increased. It seems from this

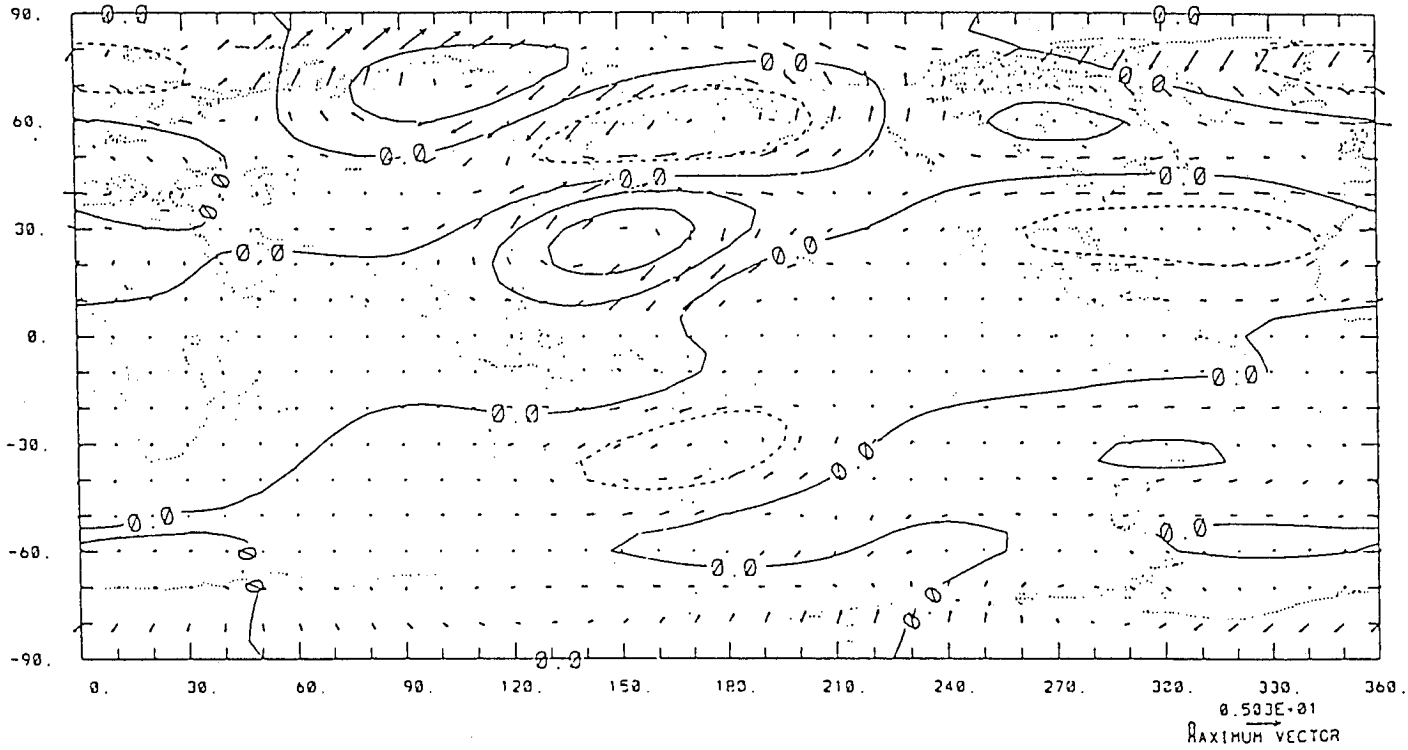

Figure 5.31: Same as Figure 5.30, but for 200 mb. Contour interval is 20 units.

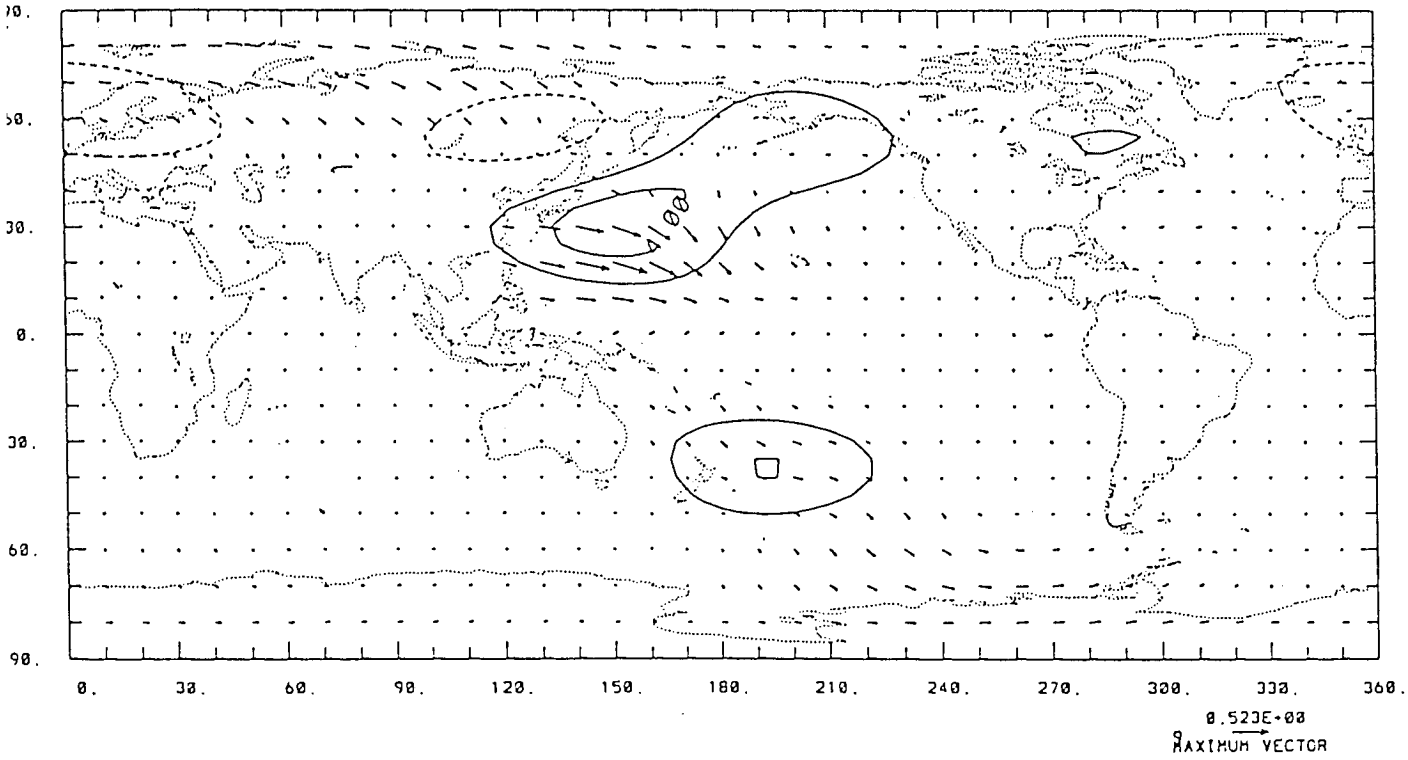

Figure 5.32: Plumb flux: As in Figure 5.18, but for sensitivity test in Case A. The contour interval is 2 units.

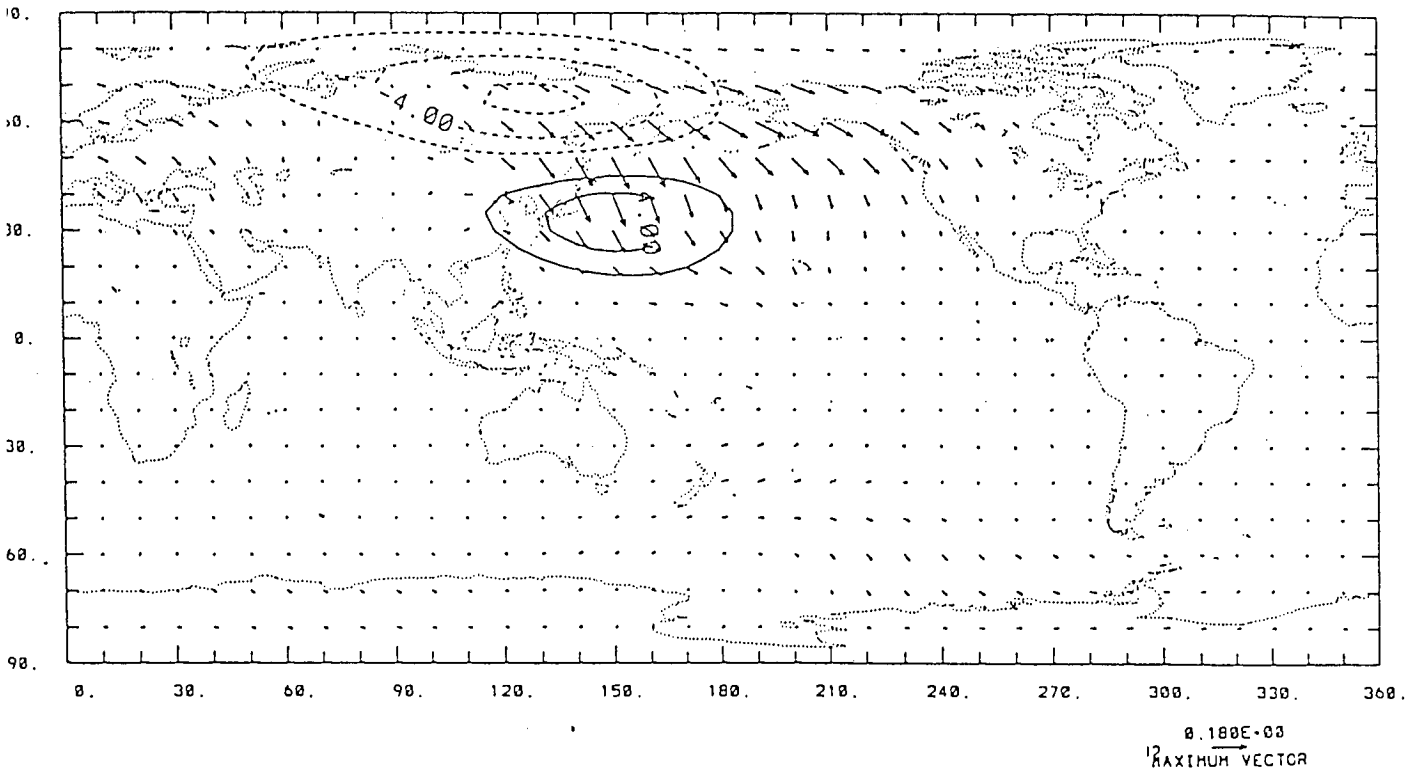

Figure 5.33: As in Figure 5.32, but for 500 mb. The contour interval is 2 unit.

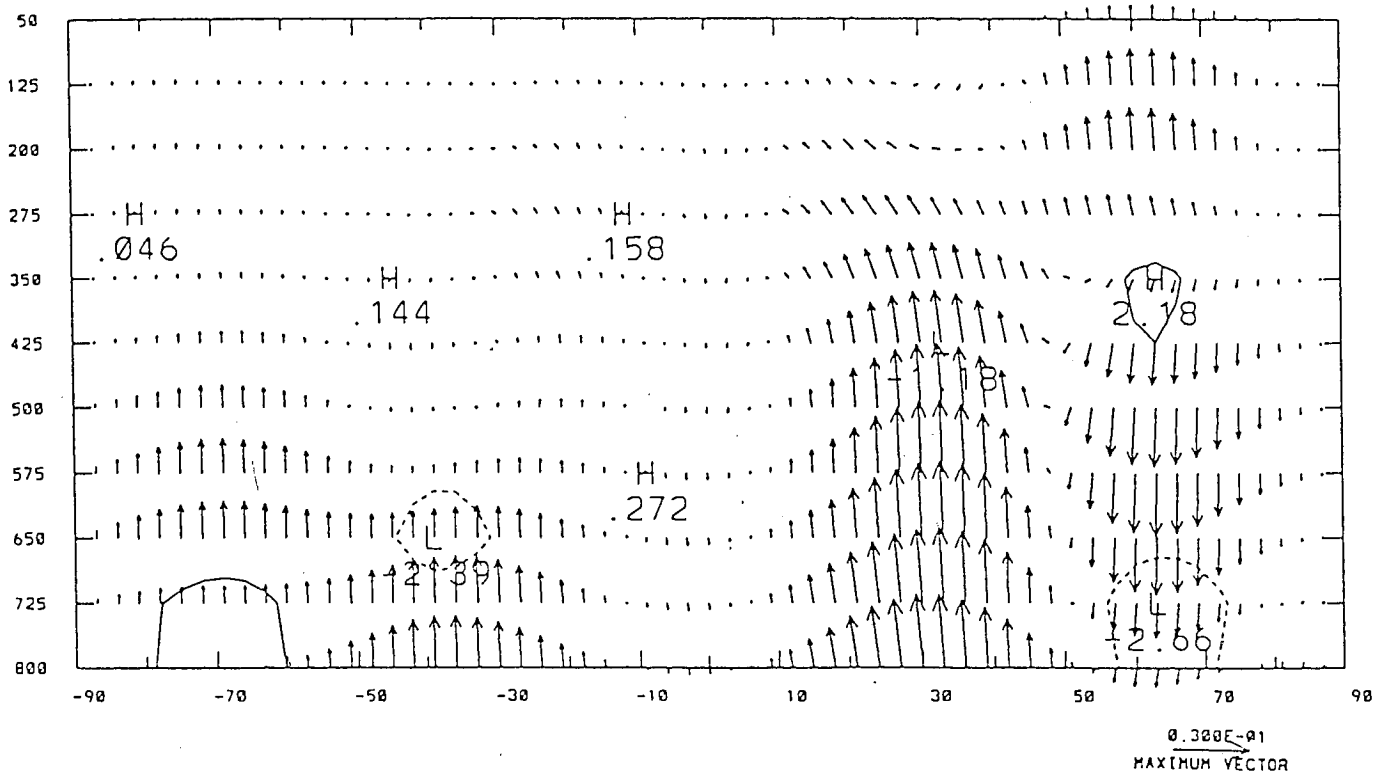

Figure 5.34: EP cross-section: As in Figure 5.20, but for sensitivity test of Case A. The contour interval is 1 units.

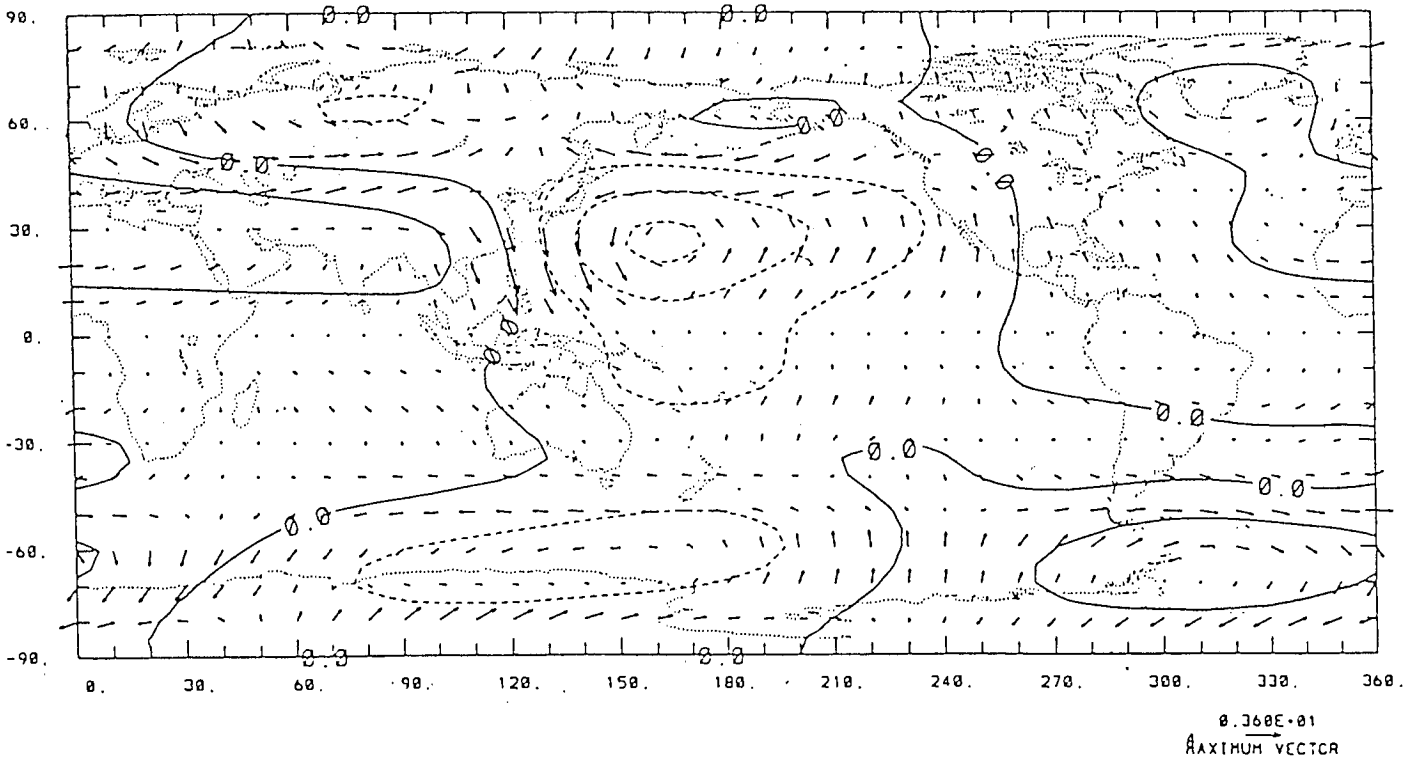

Figure 5.35: 700 mb as in Figure 5.30 but for sensitivity test in Case C. Contour interval is 20 units.

experiment that the diffusion coefficients do not have much influence on the quality of the model output although they have a small impact on the amplitude of the model response.

Comparing with Case B, the main circulation patterns of the model response in Case C is quite similar in most areas over the globe except southern polar region, but with very much increased amplitude (about double in low–latitudes and triple in high–latitudes) at both of the 700 mb and 200 mb levels. The results of this test can be viewed directly from Figure 5.35 and 5.36 for the streamfunction and velocity fields at those two levels respectively. This test shows that the model output is very sensitive to Newtonian cooling coefficients, and the appropriate treatment of them is of the essence in getting "correct" results of the model response both in quality and reasonable quantity.

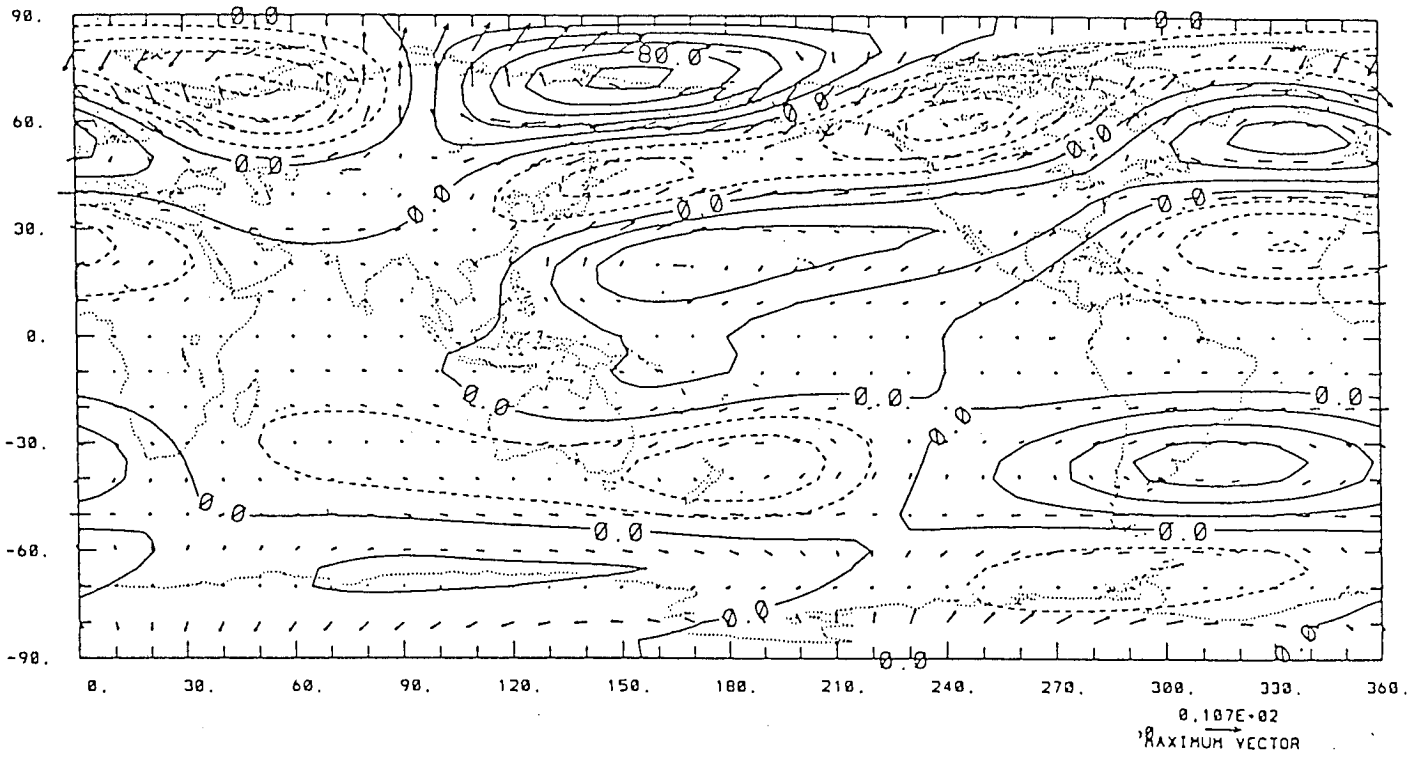

Figure 5.36: Same as Figure 5.35, but for 200 mb. Contour interval is 20 units.

One further test, Case D, is made by relaxing the frictional and Newtonian cooling coefficients to $(7days)^{-1}$ everywhere from the standard one. The corresponding results of response at 200 mb and 700 mb levels may be seen in Figure 5.37 and 5.38. This test also shows the characteristic linear features above the heating source with outflow at upper level, and two anti-cyclones in the west, two cyclones in the east of the heating centre at 200 mb straddling the equator, and reversed circulation at lower level. The results of the test are in good agreement with Gill (1980). Comparing to the standard one, the circulation of the model response in both location and amplitude is very sensitive in this Case.

Various experiments (not shown here) for the sensitivity test with different external forcing were also carried out. The experimental results provide the same general impression as the above four cases, i.e. the model is quite sensitive to the proper imposition of coefficients of Rayleigh friction R_f and Newtonian cooling, but less

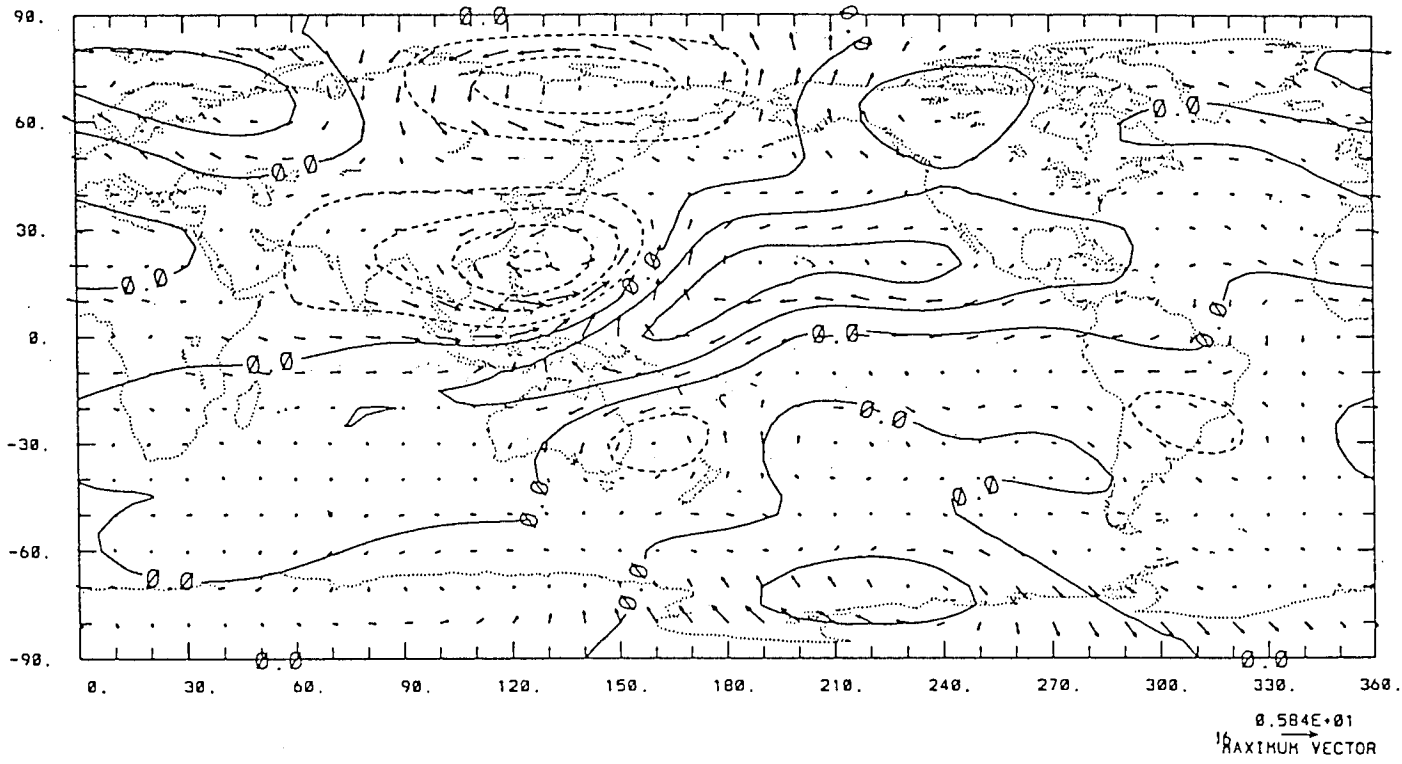

Figure 5.37: 700 mb as in Figure 5.30 but for sensitivity test in Case D. Contour interval is 20 units.

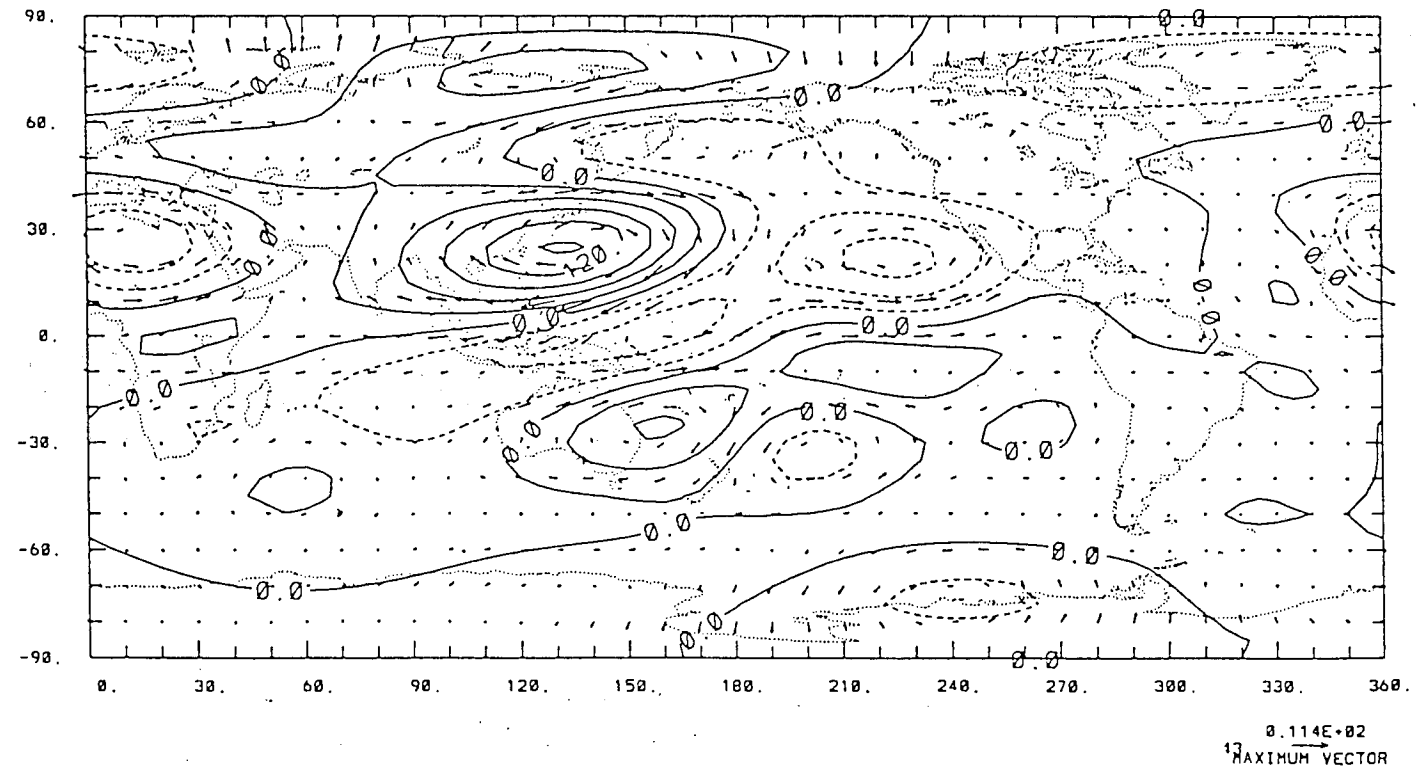

Figure 5.38: Same as Figure 5.37, but for 200 mb. Contour interval is 20 units.

sensitive to the bi-harmonic diffusion coefficients α and ν — increase (decrease) of the values will lead to little decrease (increase) amplitude of response. It is worth mentioning that the diffusion coefficients are usually very effective in tuning the output of numerical modelling. However, the model used here is a very simplified and highly truncated one and is insensitive to the value of the diffusion coefficients.

Chapter 6

Linear Response of Global Model Atmosphere to Orography and Diabatic Heating

§6.1 Introduction

The results of the numerical experiments for idealized forcing, displayed in the previous chapter, provide not only confidence of the model validity but also some essential features of the behaviour of stationary waves in the model atmosphere. Therefore, as indicated in Chapter 1, the model can now be used as a basic tool to carry out a number of experiments with actual global orography and climatological diabatic heating in the northern winter such that the contribution of large scale orography and diabatic heating in the formation of stationary waves can be studied. We start with experiments for the model atmospheric response to the actual global orography in §6.2. The stationary wave response to diabatic heating is described in §6.3. Finally, in §6.4, the response to the combination of the above two external forcings is discussed.

§6.2 Response to Global Orography

First, we consider the case where the only external forcing which drives the stationary waves is global orography. The horizontal distribution of the global surface orography in spectral form is obtained by spectral transformation with triangular truncation at zonal wave number 9, as shown in Figure 6.1. The predominant large scale mountains in Figure 6.1 are the Tibetan Plateau, the African Mountains, the Rocky Mountains, the Andes, the Antarctic and the Greenland Plateau. All the mountains are well represented at that degree of truncation except the Greenland Plateau which is not appropriately represented in both extent and the magnitude of height. This misrepresentation is due to the default deficiency of the numerical method used itself at the truncation limit. However, we simply consider the orography represented in Figure 6.1 as the realistic orography on global surface. These mountains may play different roles which will be discussed later in shaping the stationary waves.

Shown in Figure 6.2 and 6.3 are the perturbation streamfunction and horizontal velocity on 700 mb and 200 mb surfaces respectively, for the model response to the "realistic" orography as described in Figure 6.1. At 700 mb, there is a relatively strong cyclonic system situated in northern mid-latitudes, just east of the Tibetan Plateau. In contrast, an anti-cyclonic circulation exists roughly on the up-slope of the Tibetan mountains. Furthermore, a cyclonic circulation covers the east Pacific and west United States. Two more anti-cyclonic circulations are located over northeast Asia and north reaches of the Pacific, and most areas of the north Atlantic. It appears that there is a very weak or neglegible response in tropical areas of both hemispheres. This may be a result of the strong damping imposed in

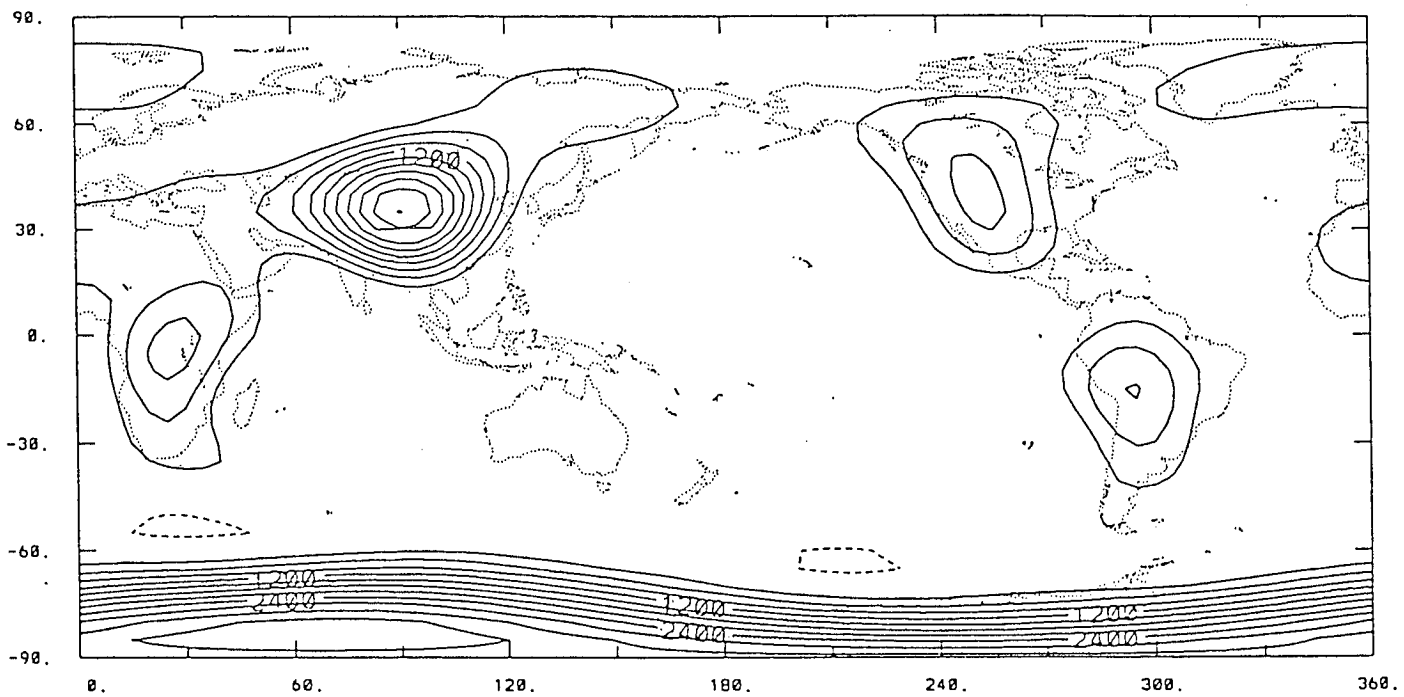

Figure 6.1: The horizontal distribution of surface geopotential height of the global orography. The original data is stored on a $1.875^0 \times 1.875^0$ grid mesh. It is plotted through spectral transformation with triangular truncation at zonal wave number $M = 9$. The contours represent the orography height with interval of 300m. The zero contour is excluded for clarity.

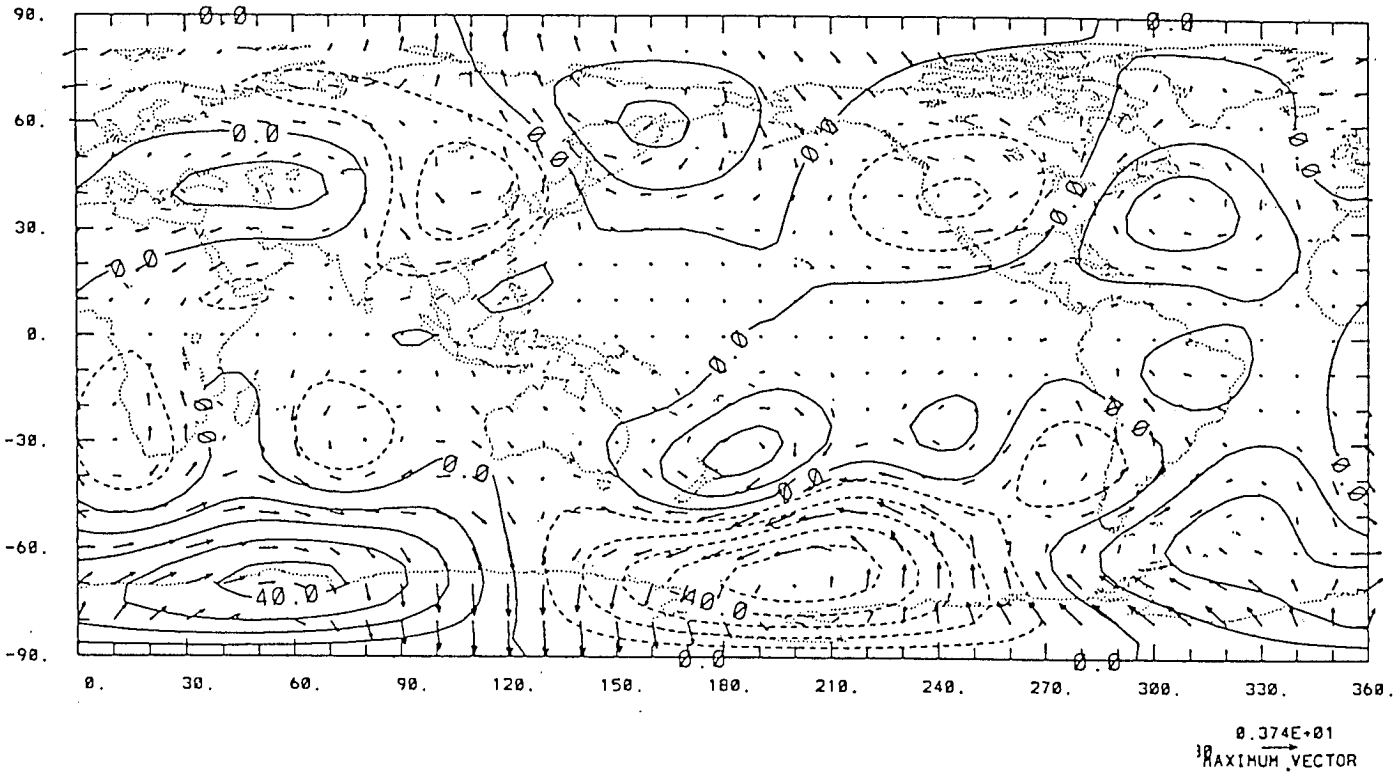

Figure 6.2: 700 mb perturbation stream field for the model response to the actual global orography. Contours represent the perturbation streamfunction ($\times 10^5\ m^2 s^{-1}$), with an interval of 10 units. The negative contours are dashed. Vectors denote the horizontal velocity on the isobaric surface, and an arrow scale in units of $m\ s^{-1}$ is indicated at bottom right of the picture.

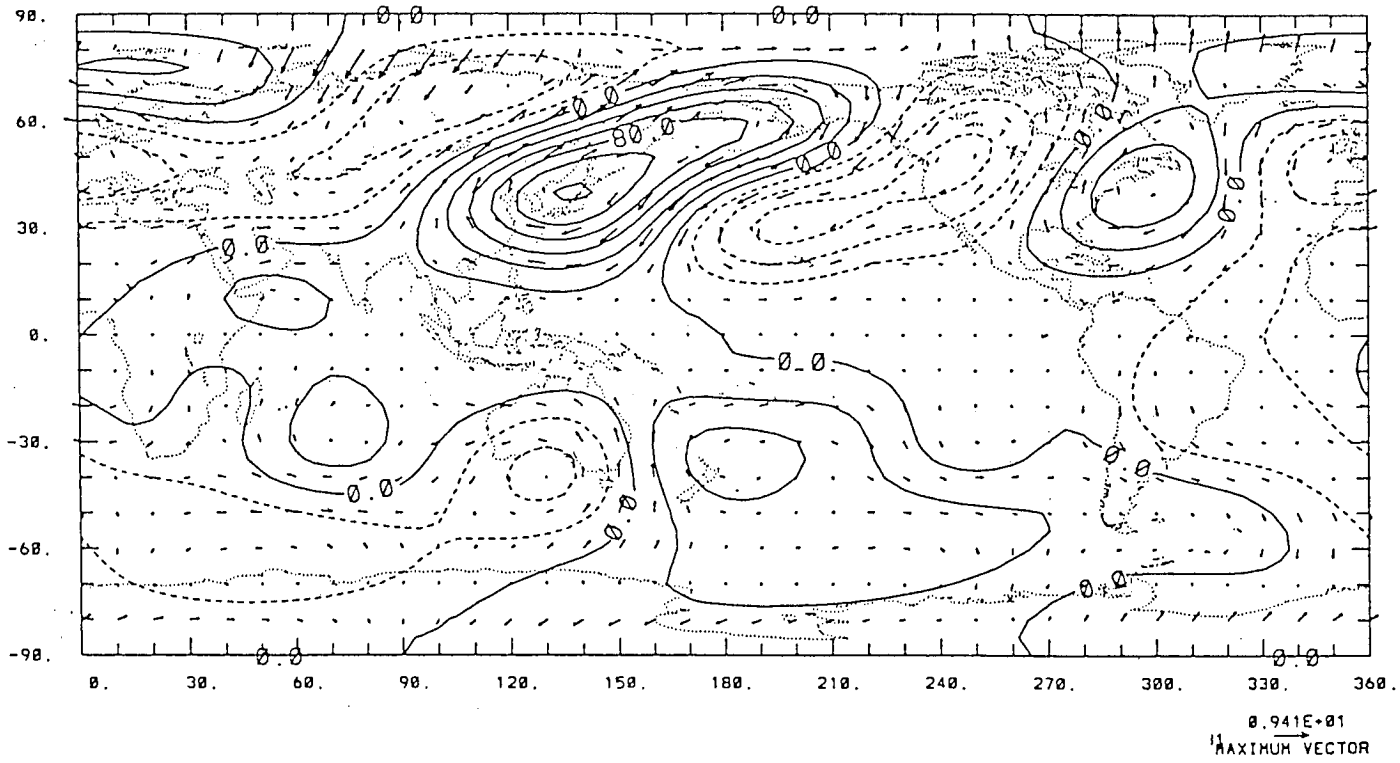

Figure 6.3: As in Figure 6.2, but for 200 mb, with contour interval of 20 units.

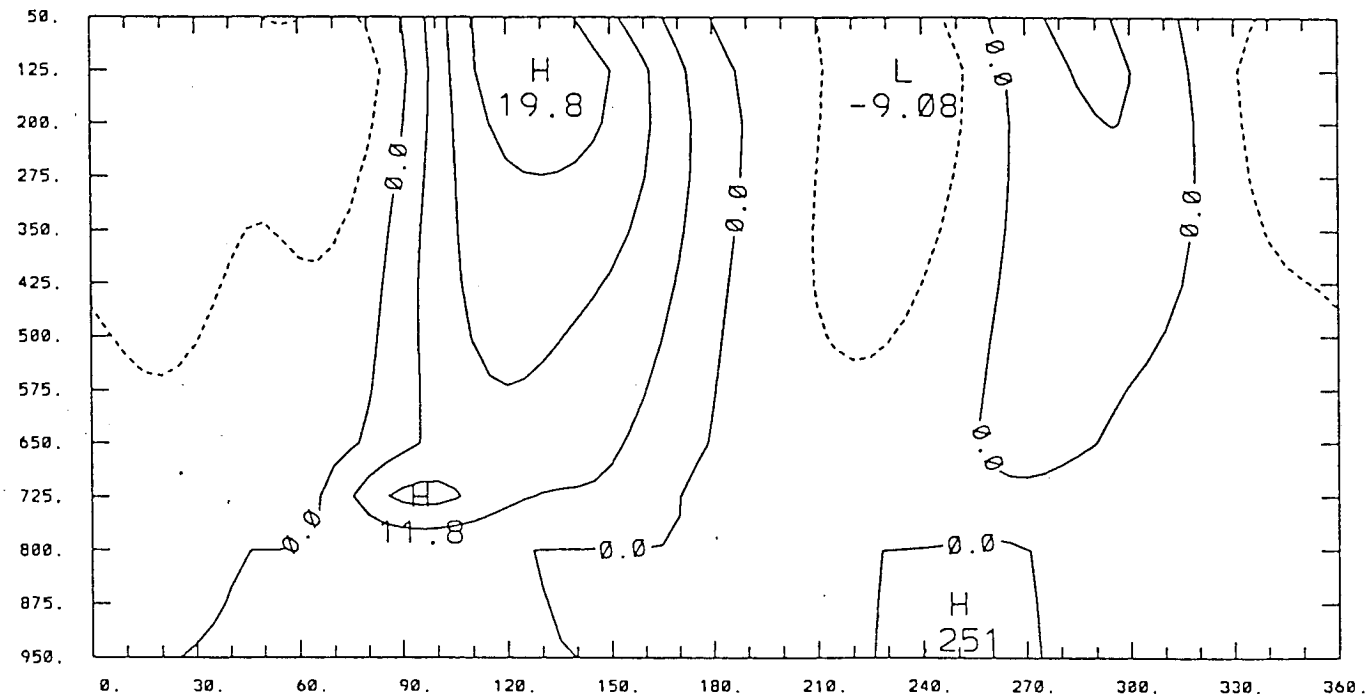

Figure 6.4: Longitude–pressure cross–section of the perturbation geopotential height at 45^0N for the model response to the realistic global orography. The contour interval is 5 dm.

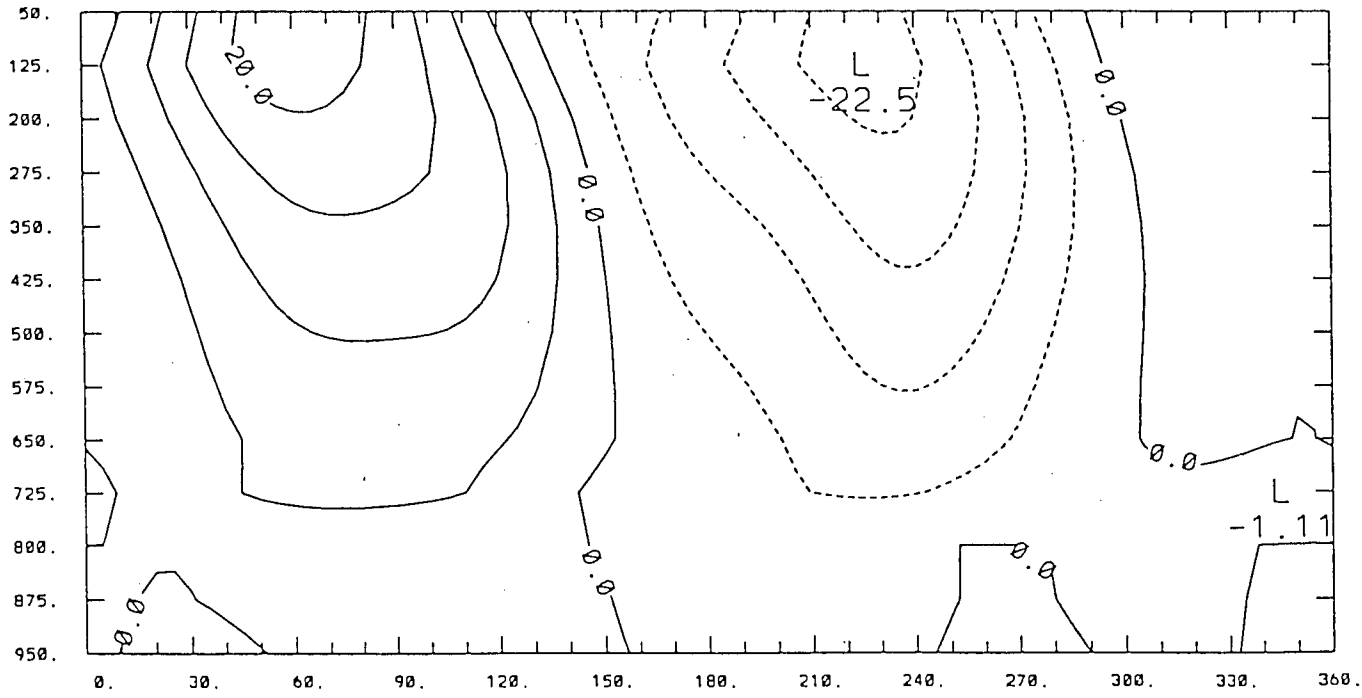

Figure 6.5: As in Figure 6.4, but at 60^0S with contour interval of 5 dm.

that area. In the southern hemisphere, however, the response pattern is relatively simple, and mainly in high latitudes, with an anti-cyclone, which is large in extent and strong in amplitude, in the southern Pacific near Antarctica and a cyclone in the same latitudes around Antarctica. The response in the southern hemisphere appears to be dominated by wave number one, which is in very good correspondence to the phase of the Antarctic Plateau, although other waves also have some effects on the response.

At the higher level, 200 mb, the features of stationary waves in the northern hemisphere are in general similar to those at 700 mb, but with much larger amplitude. In northern middle and low latitudes there are mainly two cyclonic systems over Euro-Asia and the western part of north America extending southwest-ward to subtropical areas of the eastern Pacific, with two anti-cyclonic circulations, one of them over the western Pacific covering east Asia and extending northeast-ward to

Canada in high latitudes, and the other over the eastern part of north America and the western Atlantic stretching across northern Europe. The vertical structure of the stationary wave response pattern in the northern hemisphere is almost independent of height, and exhibits barotropic characteristics. This can be seen clearly in Figure 6.4. In the southern hemisphere, however, the stationary wave response only exists in middle and high latitudes, and seems dominated by wave number one only, with an anti–cyclonic circulation from the southern Atlantic to Australia and a cyclonic circulation south of New Zealand. Moreover, it might be meaningful that the vertical structure of the response pattern in high latitudes of the southern hemisphere is also independent with respect to height, and displays barotropic property. This characteristic of barotropicity is shown in Figure 6.5.

Figures 6.6, 6.7 and 6.8 are the wave activity fluxes at 800 mb, 500 mb, and 200 mb respectively. At 800 mb, the wavetrains in the northern hemisphere propagates mainly upward, eastward and equatorward over Eurasia, originating from the Tibetan Plateau, and eastward and upward over north America, while in the southern hemisphere the significant wavetrains propagate mainly around the Antarctic, predominately eastward and horizontal. At 500 mb, the wave activity flux is much reduced in both horizontal and vertical in the southern hemisphere which is evidently associated with Antarctica. However the wave propagation in the northern hemisphere is still very vigorous and the strongest wave activity flux is situated over Eurasia. Furthermore, at 200 mb, the wavetrains propagate upward, eastward and equatorward over Eurasia, and the magnitude is comparable to that at 500 mb. This three–dimensional version of the wave activity flux may imply that the Tibetan Platean is the most important factor in the initiation of orographically forced stationary wave circulations, and could have a larger contribution to

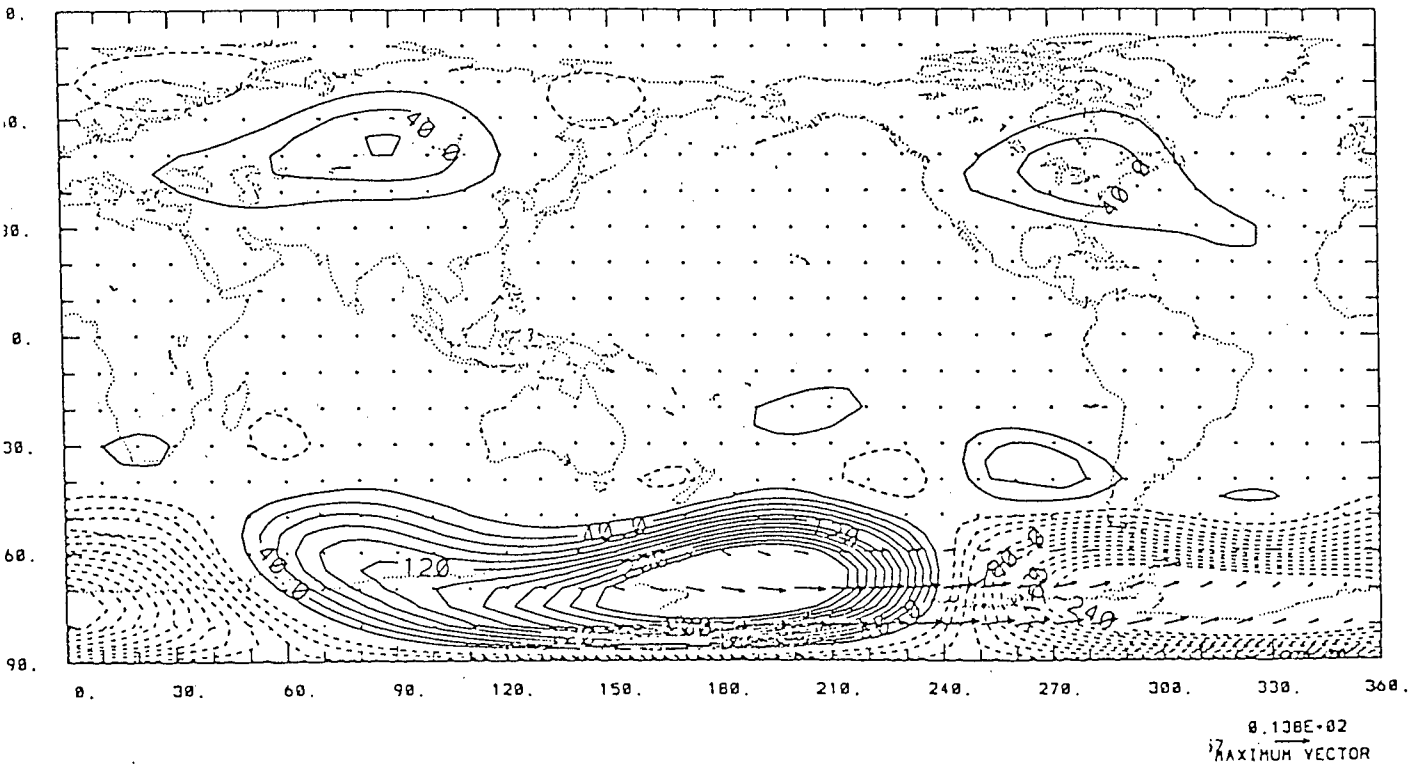

Figure 6.6: 800 mb wave activity flux as in Figure 5.7, but for the model response to realistic global orography. The contour interval is 20 units with the zero contour excluded.

the global circulation in both the troposphere and possibly the lower stratosphere than other large scale mountains, while Antarctica plays a significant part only in the lower troposphere. This is reinforced, although the remote response and the inter–hemisphere interaction have not been taken into consideration, by the associated EP cross-section (Figure 6.9) which shows that the convergence of the EP flux, which also means the generation of the wave activity, is in the shallow layers of the lower troposphere in southern high latitudes, and low levels of northern middle latitudes.

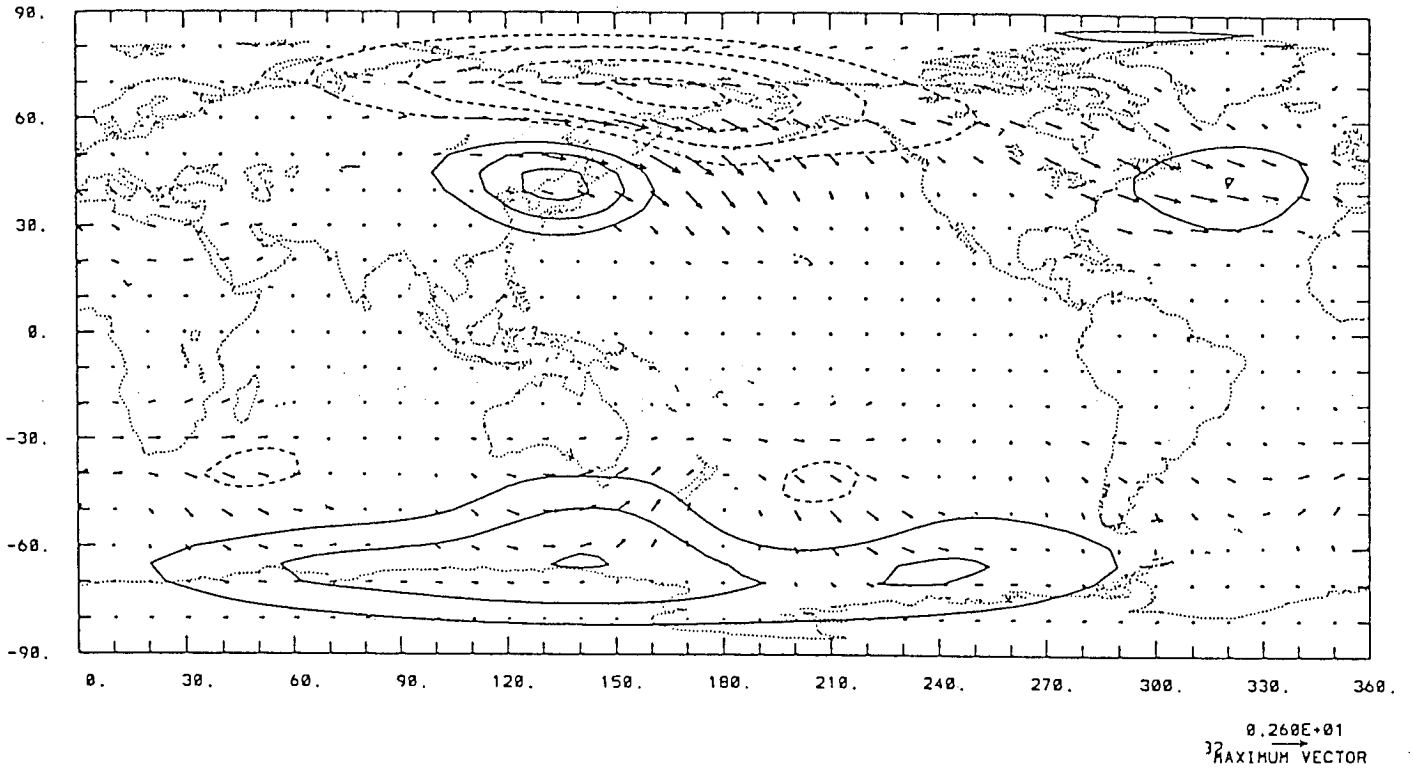

Figure 6.7: As Figure 6.6 but for 500 mb. The contour interval is 10 units.

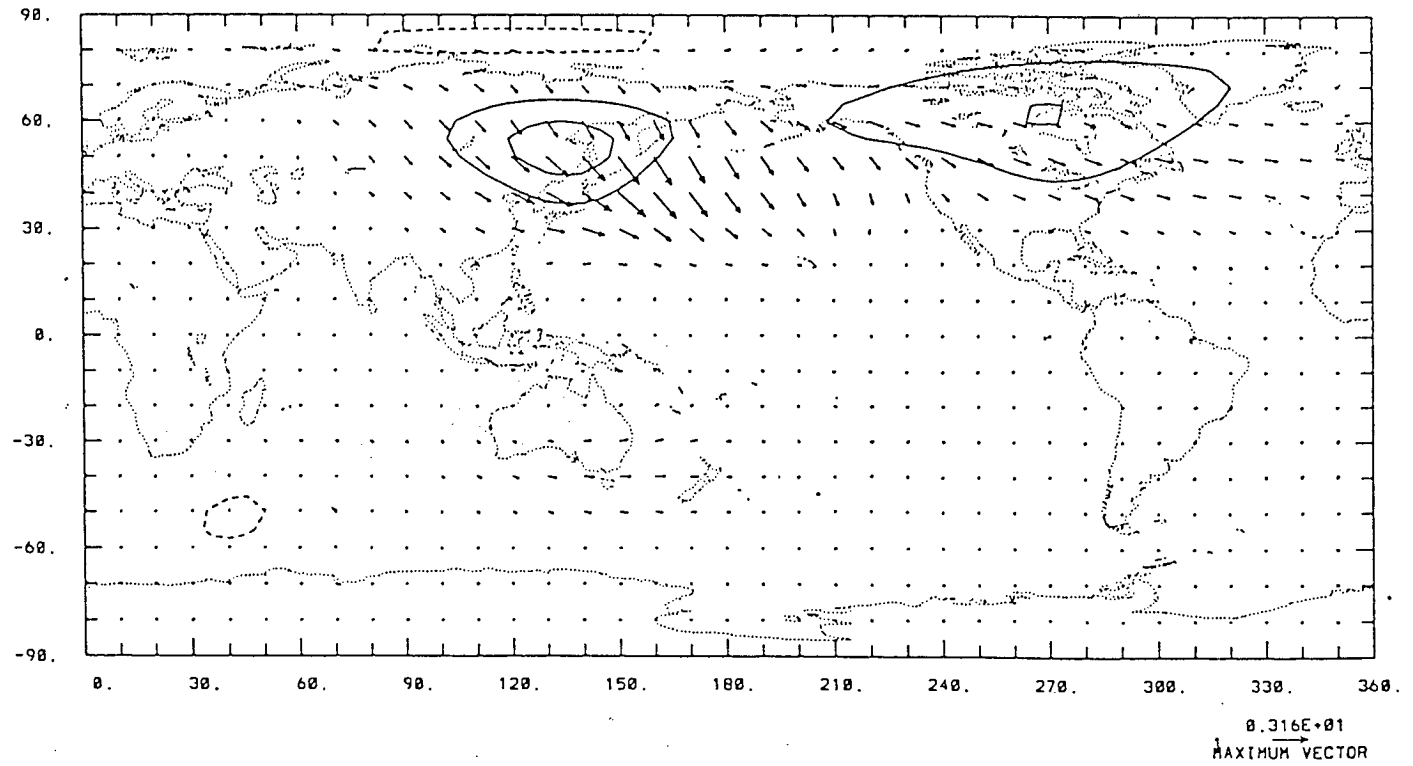

Figure 6.8: As Figure 6.6 but for 200 mb. The contour interval is 5 units.

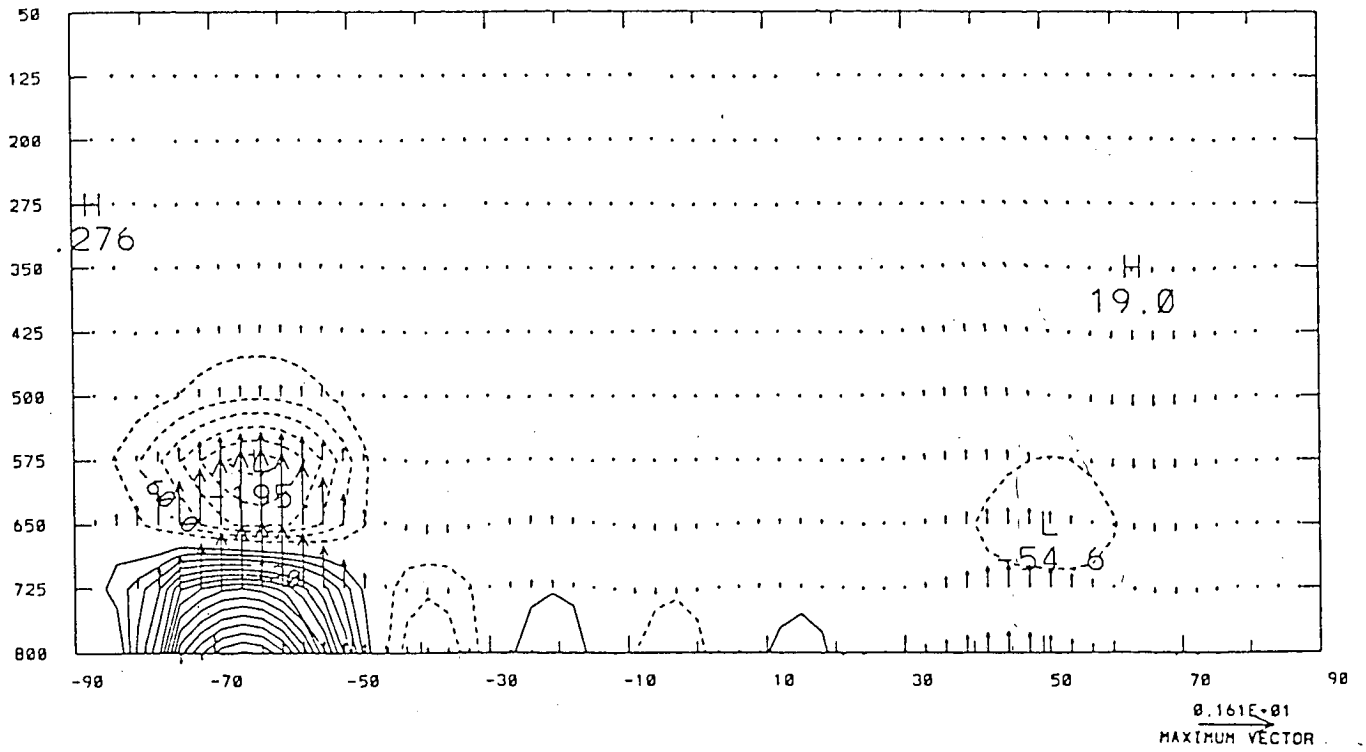

Figure 6.9: EP cross-section as Figure 5.9, but for the model response to the actual global orography. The contour interval is 30 units.

§6.3 Response to Diabatic Heating

In this section we will discuss the model response to the diabatic heating climatology in the northern winter. The calculation of the model response to diabatic heating is more complicated than that to orography, as discussed in the previous section, due to the involvement in the parameterization of the vertical distribution of the heating forcing (see, e.g. Schaack et al., 1990). The heating data used are available in three dimensions. They are incorporated into the model by spectral coefficients which are calculated by vertically integrating the data using the Gaussian quadrature method, then horizontally transforming it into spectral domain. The vertical distribution of the diabatic heating is parameterized by using an analytical expression (5.3). An alternative approach is also performed, i.e. the diabatic heating is incorporated into the model by three-dimensional directly transformed

spectral coefficients. The inter-comparison of the two approaches could also shed some lights on the adequateness and importance of the parameterization of the vertical distribution of the diabatic heating.

The horizontal distribution of the vertically integrated diabatic heating climatology in northern wintertime is illustrated in Figure 6.10. The Major features of the global distribution include the heating in regions of deep moist convection over Brazil, equatorial Africa, the ITCZ, the Asian monsoon circulation and the oceanic cyclone tracks over the western oceans of the norhth hemisphere. Net heating over the oceans and net cooling over the continents prevail in the northern hemisphere while the reverse is true in the southern hemisphere. Net cooling is predominant in polar regions and within anti-cyclonic circulations of the subtropics.

Figures 6.11 and 6.12 show the perturbation stream field for the model response to the above-described diabatic forcing at 700 mb and 200 mb respectively. At 700 mb, there are two main systems at high latitudes, and two small systems at middle latitudes in the northern hemisphere. There is a relatively large anti-cyclonic circulation over the Bering Sea connected to a relatively weak anti-cyclonic circulation over east Asia, a strong cyclonic circulation over northern America and the west Atlantic, and a small one over the north-east Pacific. Furthermore, another anti-cyclonic circulation is evident centred at the eastern subtropical Atlantic. In the southern hemisphere, however, the stationary wave circulation is more vigorous in intensity than in the northern. The systems are mainly present in middle latitudes, with anti-cyclonic circulations west of Australia and over the eastern Pacific, and cyclonic circulations over west to central southern Pacific and the southern Atlantic. The model response at 200 mb is much larger than

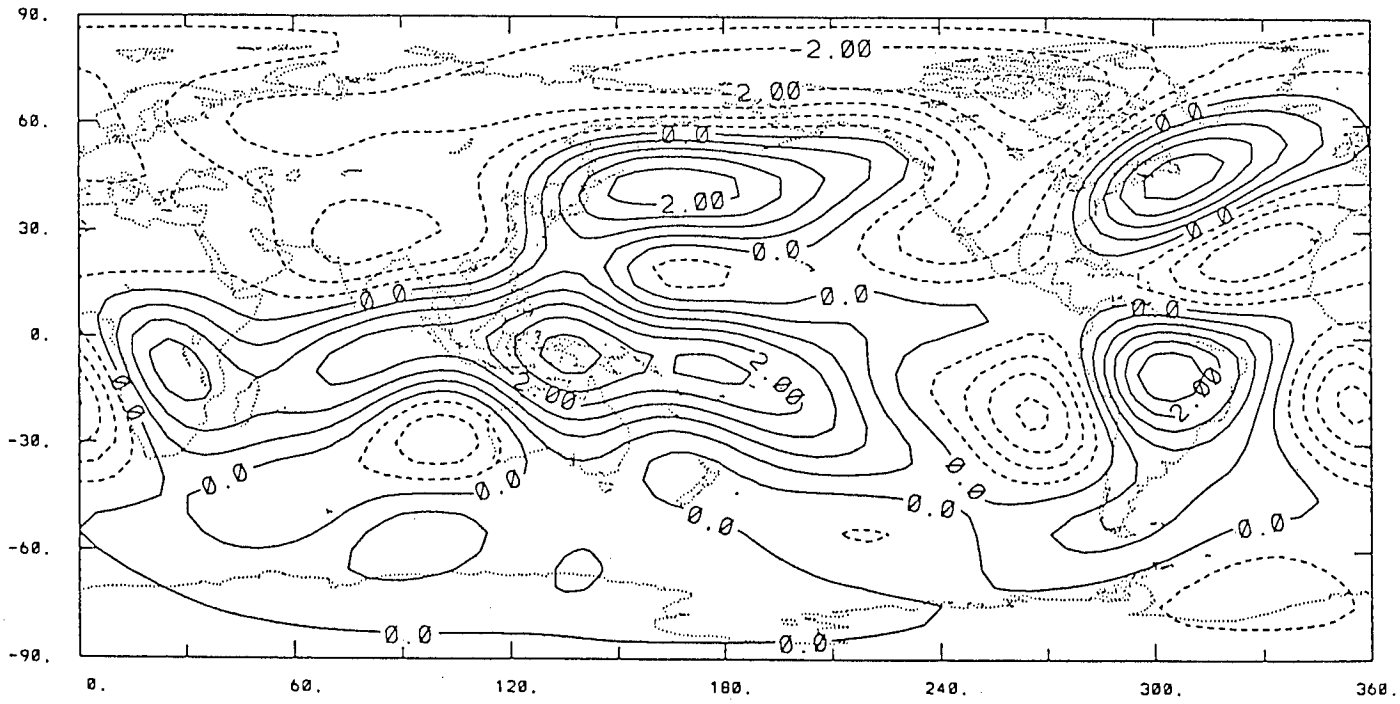

Figure 6.10: The horizontal distribution of the vertically integrated diabatic heating climatology for DJF (for more details see Hoskins et al (1989)). The original data are stored on $5^0 \times 5^0$ grid mesh. It is plotted through spectral transformation with triangular truncation at zonal wave number $MM = 9$. The contours represent the heating rate (K/DAY) with interval of 0.5 (K/DAY).

that at 700 mb, particularly in the tropical and subtropical areas of both hemispheres. There are four main systems in northern hemisphere. Two of them are cyclonic circulations, one of which is covering east Europe and Euro–Asia extending from the European Continent north–eastward to the Bering Sea, while the other is centred over north America. One of the two anti–cyclonic circulations is situated in the tropical and subtropical areas of the Pacific and extending northeastward to the north–west part of the United States and west part of Canada, while the other one is over the central and eastern Atlantic and crossing north–eastwardly over most of western Europe. In the southern hemisphere, the response features seem relatively weaker than those in northern hemisphere, and exist primarily in lower and middle latitudes. Notably there are an anti–cyclonic circulation in the west Pacific overlapping most of Australia, a cyclonic circulation in the central and eastern part of the southern Pacific, and one more cyclonic circulation in the central and eastern part of the southern Atlantic. There are no significant systems in high latitudes. Comparing Figure 6.10 with the features at 200 mb, it is of interest to note that the anti–cyclonic circulations are in a rough accordance with the net heating areas of the vertically integrated diabatic heating climatology, and it is also true for the cyclonic circulations with correspondance to the net cooling areas. It is further worth noting that the response patterns to diabatic heating are strongly height dependent in the northern hemisphere, but only weakly baroclinic in the southern hemisphere. This baroclinic characteristic is more evident from the longitude–pressure cross–sections of the perturbation geopotential height at 45^0N and 60^0S respectively in Figures 6.13 and 6.14.

The impact of the diabatic heating on the stationary waves can be elucidated by the wave activity flux from Figures 6.15, 6.16 and 6.17 for 800 mb, 500 mb, and

200 mb, respectively. At the lower level (800 mb), the propagation of wavetrains is complex. Around the Bering sea area, the wave activity propagates eastwards, polarwards and downwards, while downstream, it turns equatorwards and upwards, as well as eastwards. In the high latitudes of the southern Pacific, the vertical propagation of wave activity is stronger than in the northern hemisphere, and no equatorward propagation can be seen over the whole southern hemisphere. At 500 mb, around where the maximum value of the parameterization function is located, the wavetrains propagate predominantly downwards, equatorwards, and eastwards over most of the zone in middle and high latitudes of the northern hemisphere, whereas in the mid-latitudes of the southern hemisphere the propagation of wavetrains is mainly eastwards from the Greenwich Meridian, then turning equatorward around the dateline, but the vertical propagation seems less significant except in an area to the west of the southern Pacific. At higher level, 200 mb, the vertical propagation of the wavetrains is still very strong, in addition to the strong eastward and equatorward propagation, in the entire zone of the middle and high latitudes of the northern hemisphere. It is less pronounced elsewhere. From the above description of the three dimensional structure of the wave activity flux, the wavetrain propagation is more vigorous in the northern hemisphere than in the southern hemisphere. Moreover, the strong upward propagation of wave activity in the northern hemisphere could penetrate to the lower stratosphere. It seems however that there is no evidence of cross–equatorial wavetrain propagation, despite the fact that there is a strong tendency for equatorward wavetrain propagation from middle latitudes in the northern hemispheres. The vertical structure of the zonally–averaged wave activity flux can be seen from the EP cross–section (6.18). The EP cross–section makes more visible the fact that the wavetrains propagate up to the stratosphere in northern mid–latitudes, while there is not much influence

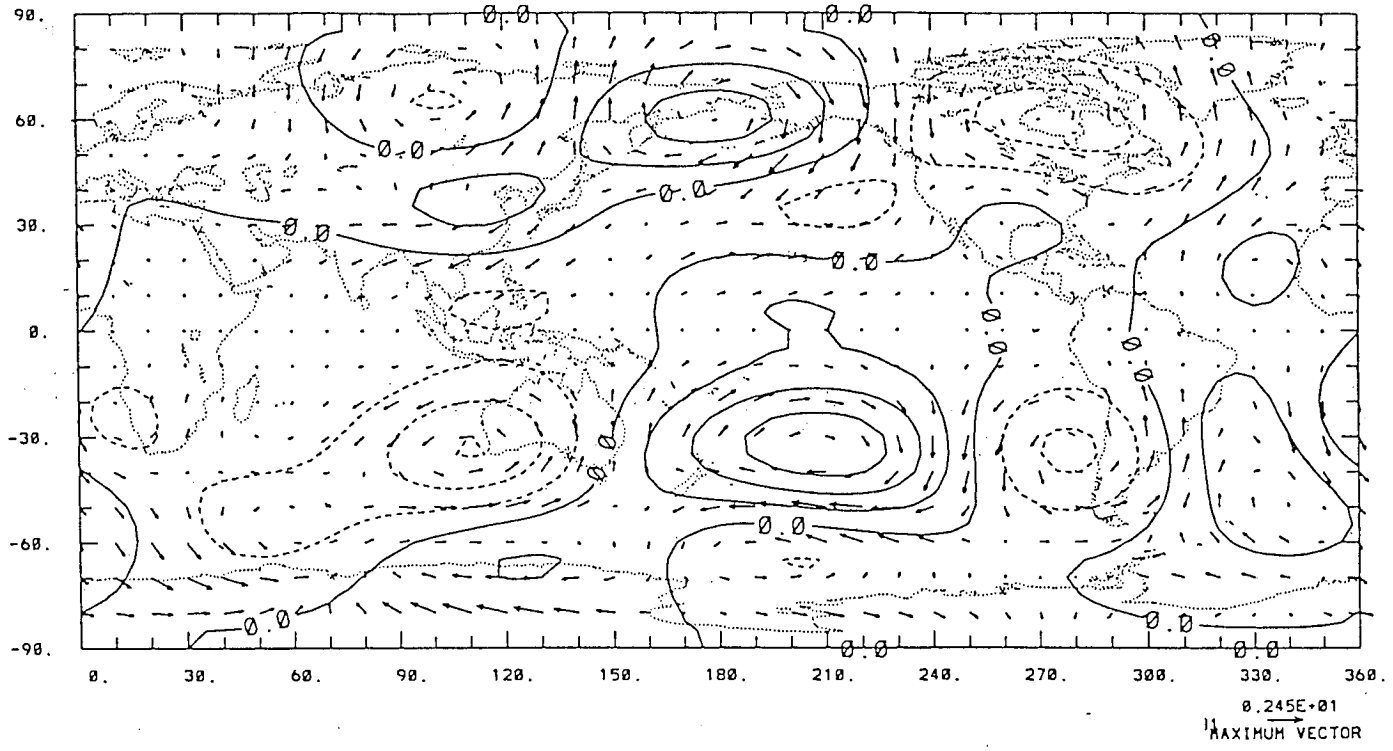

Figure 6.11: 700 mb perturbation stream field as Figure 6.2 but for the model response to the diabatic heating shown in Figure 6.10. The contour interval is 10 units.

from the diabatic heating on the upper troposphere in the southern hemisphere.

An alternative calculation was also made by incorporating the spectral coefficients which are directly transformed from the three dimensional data array, but with no change for other parameters. This calculation is physically more consistent than the foregoing case because the structure of the diabatic heating climatology is realistically represented. Comparing with the previous experiment, the model response pattern is in general agreement and is overall consistent, apart from the difference that the amplitude is comparable at 200 mb (6.20) and 500 mb (not shown) but smaller at 700 mb (6.19). The wave activity flux is similar at all levels in the northern hemisphere, but differs significantly at 800 mb (6.24) in polar region of the southern hemisphere. The result of this calculation also confirms

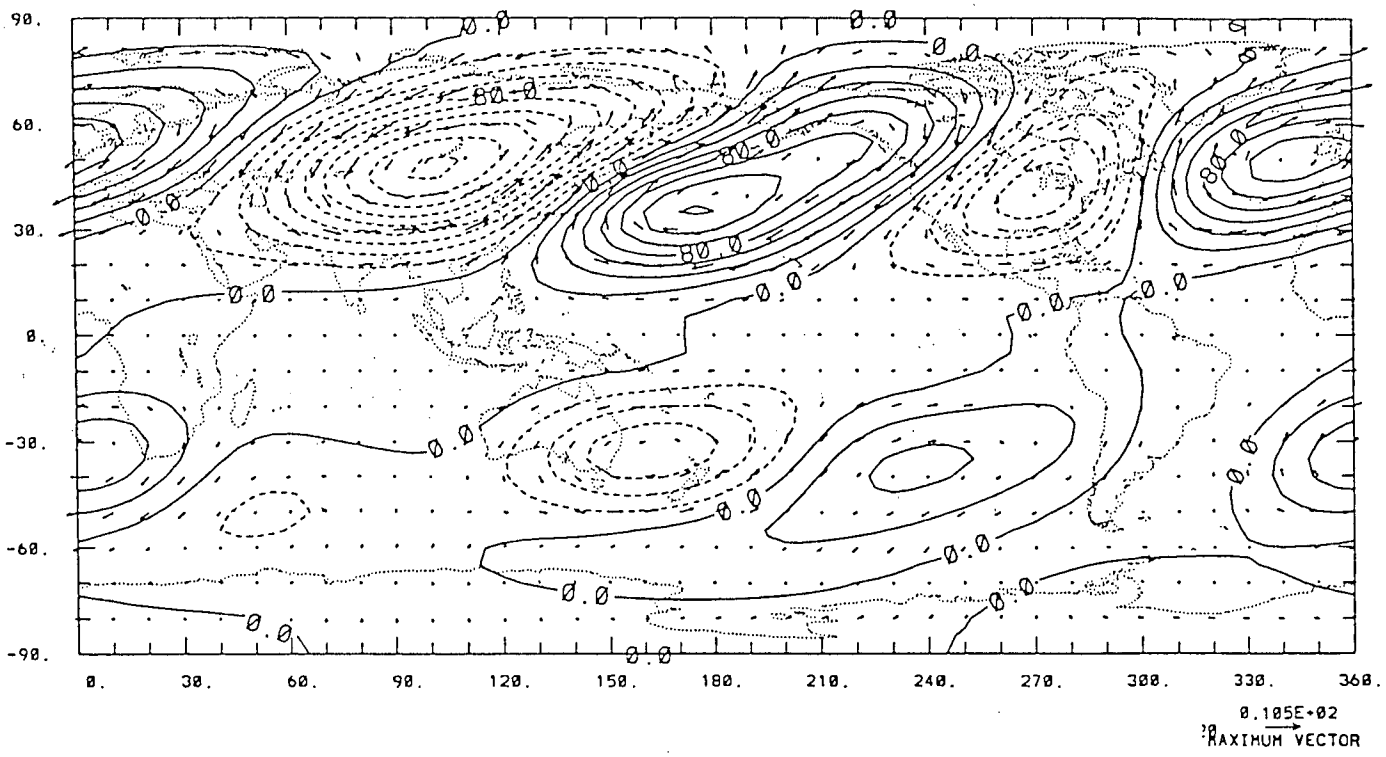

Figure 6.12: As in Figure 6.11, but for 200 mb, with contour interval of 20 units.

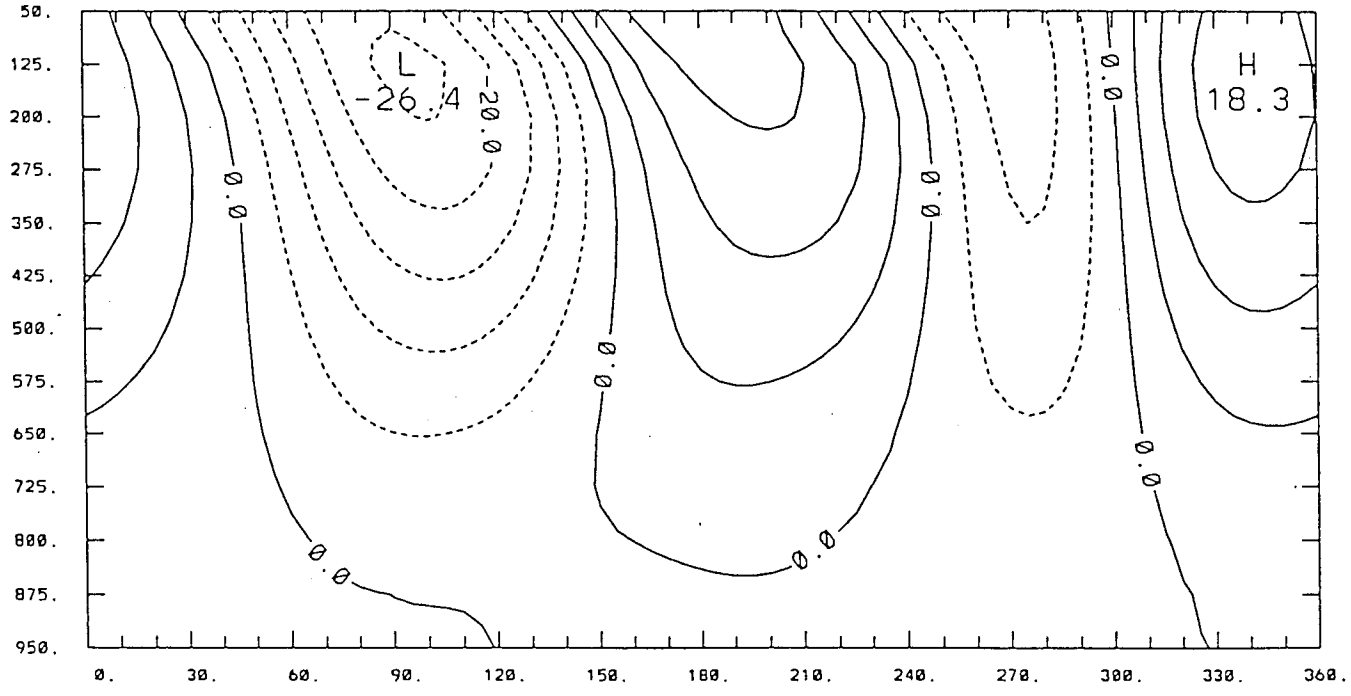

Figure 6.13: Longitude–pressure cross–section of the perturbation geopotential height at 45^0N for the model response to the winter diabatic heating climatology. The contour interval is 5 dm.

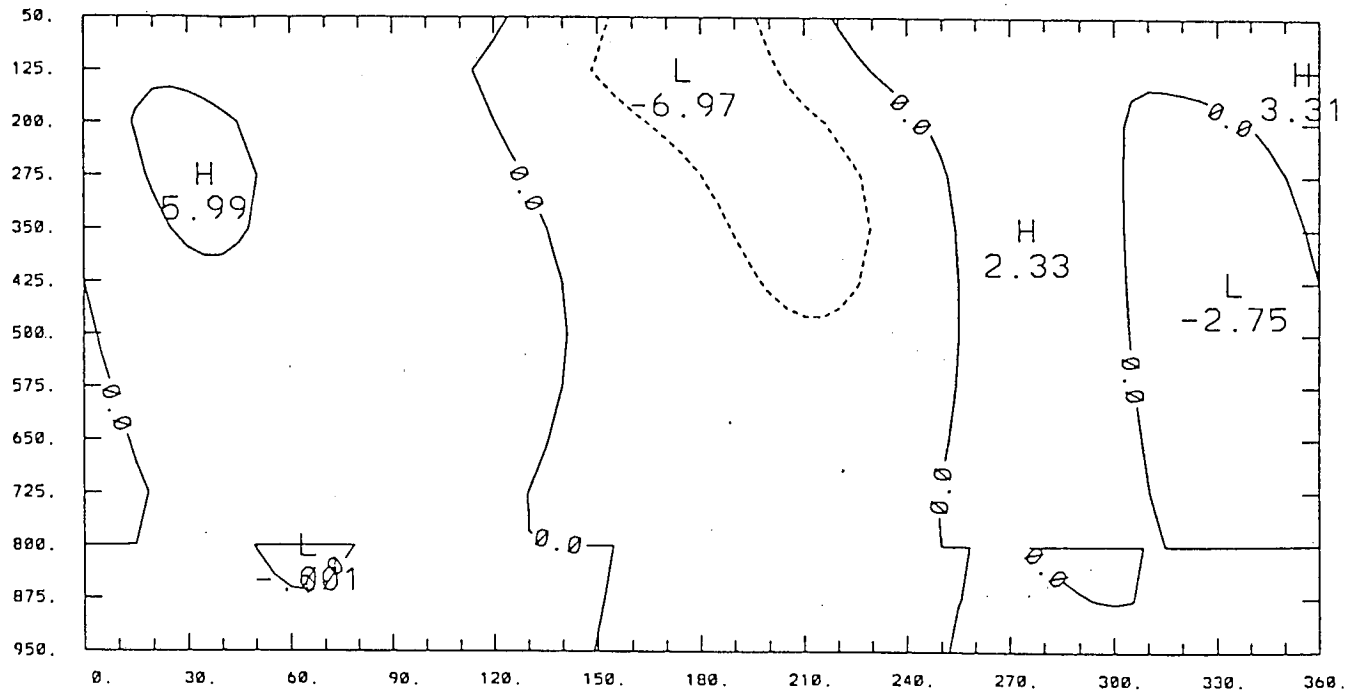

Figure 6.14: As in Figure 6.13, but at 60^0S with contour interval of 5 dm.

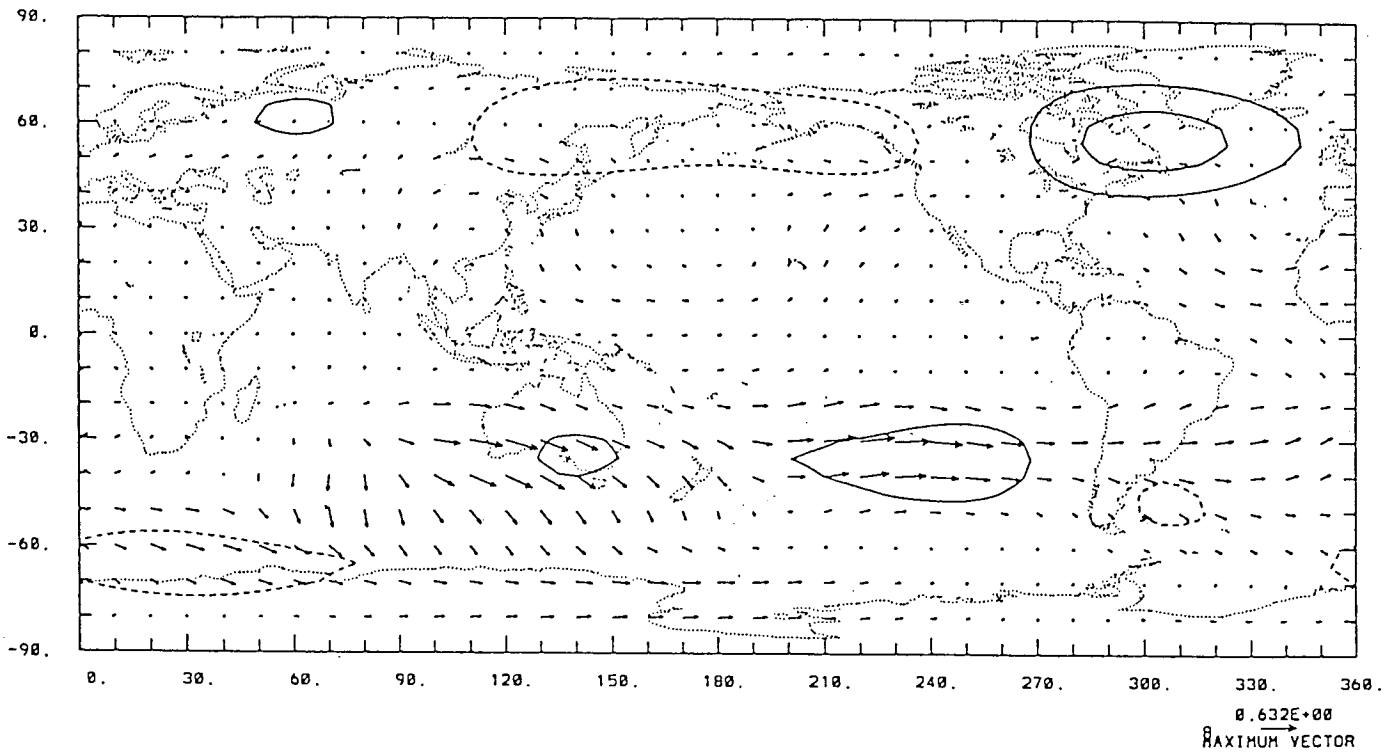

Figure 6.15: 800 mb wave activity flux as in Figure 6.6, but for the model response to the winter diabatic heating climatology. The contour interval is 10 units with the zero contour excluded.

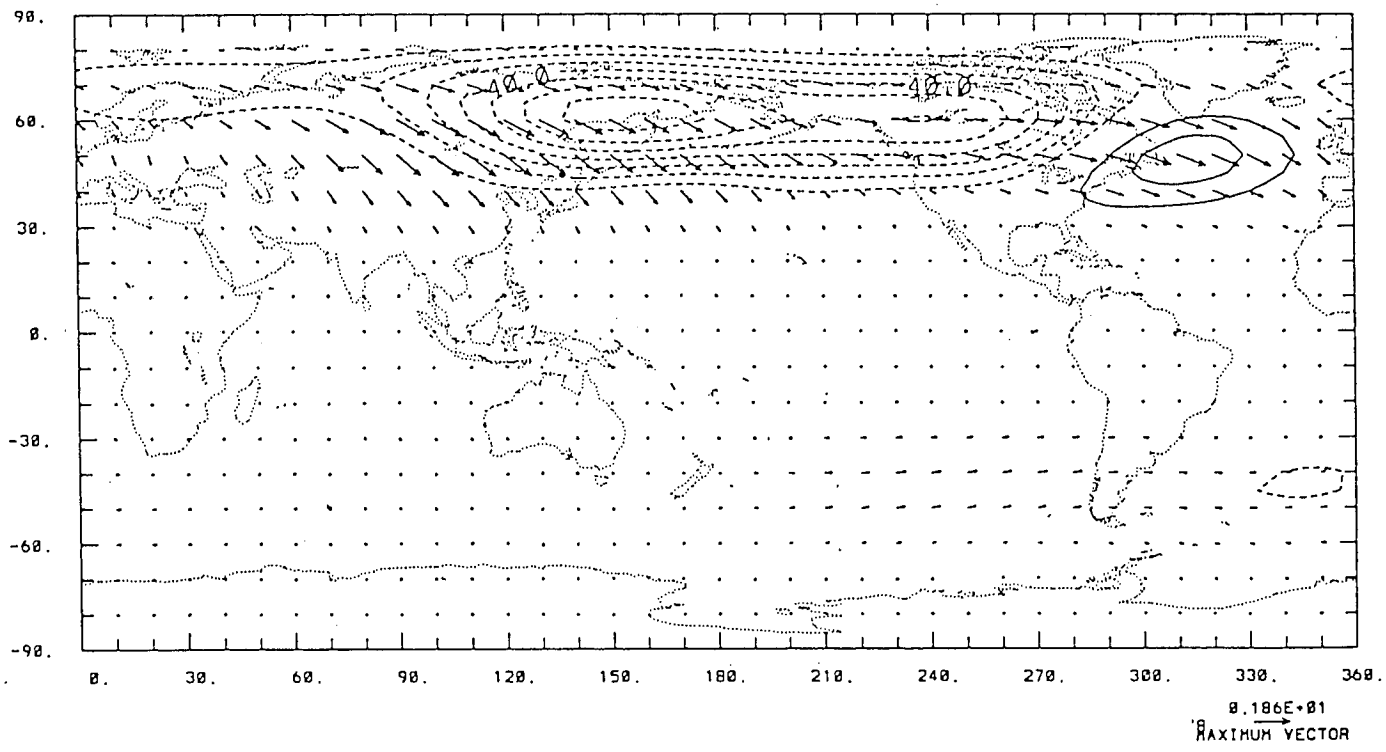

Figure 6.16: As Figure 6.15 but for 500 mb. The contour interval is 10 units.

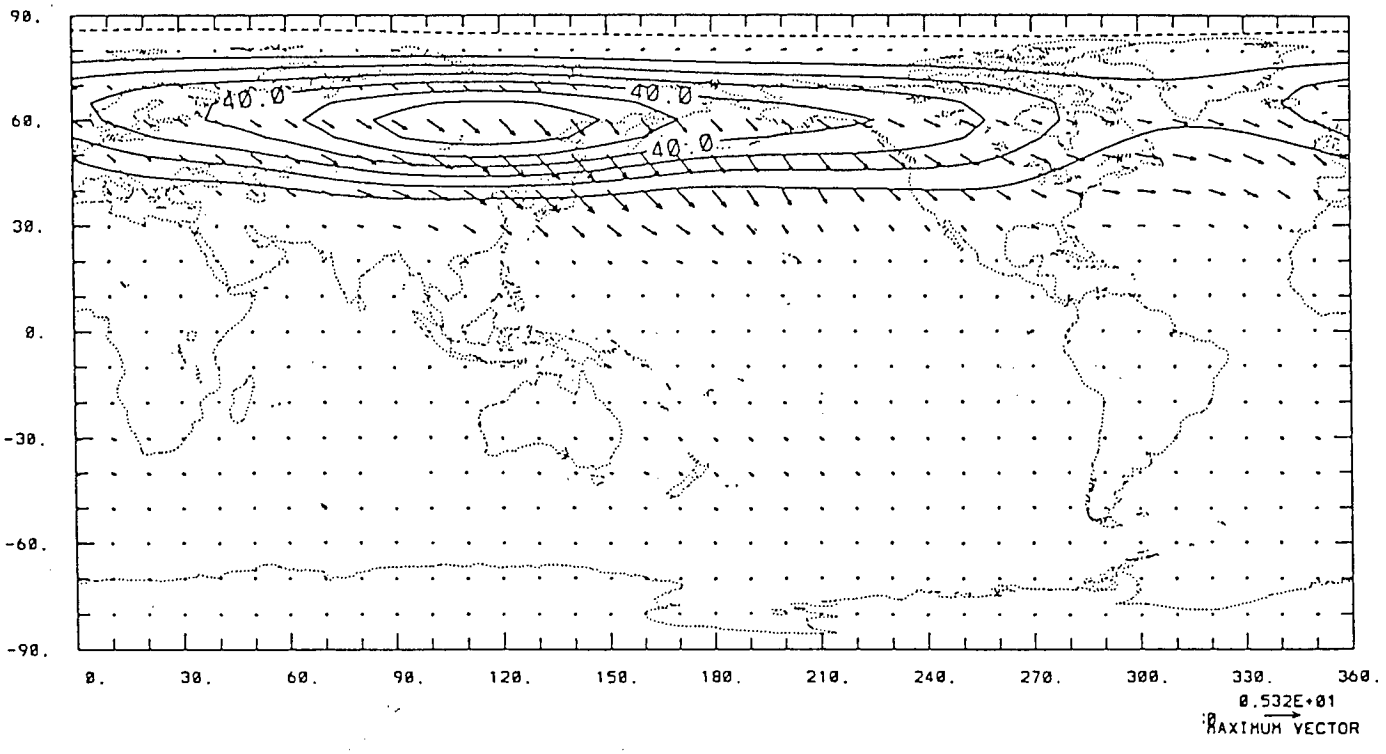

Figure 6.17: As Figure 6.15 but for 200 mb. The contour interval is 10 units.

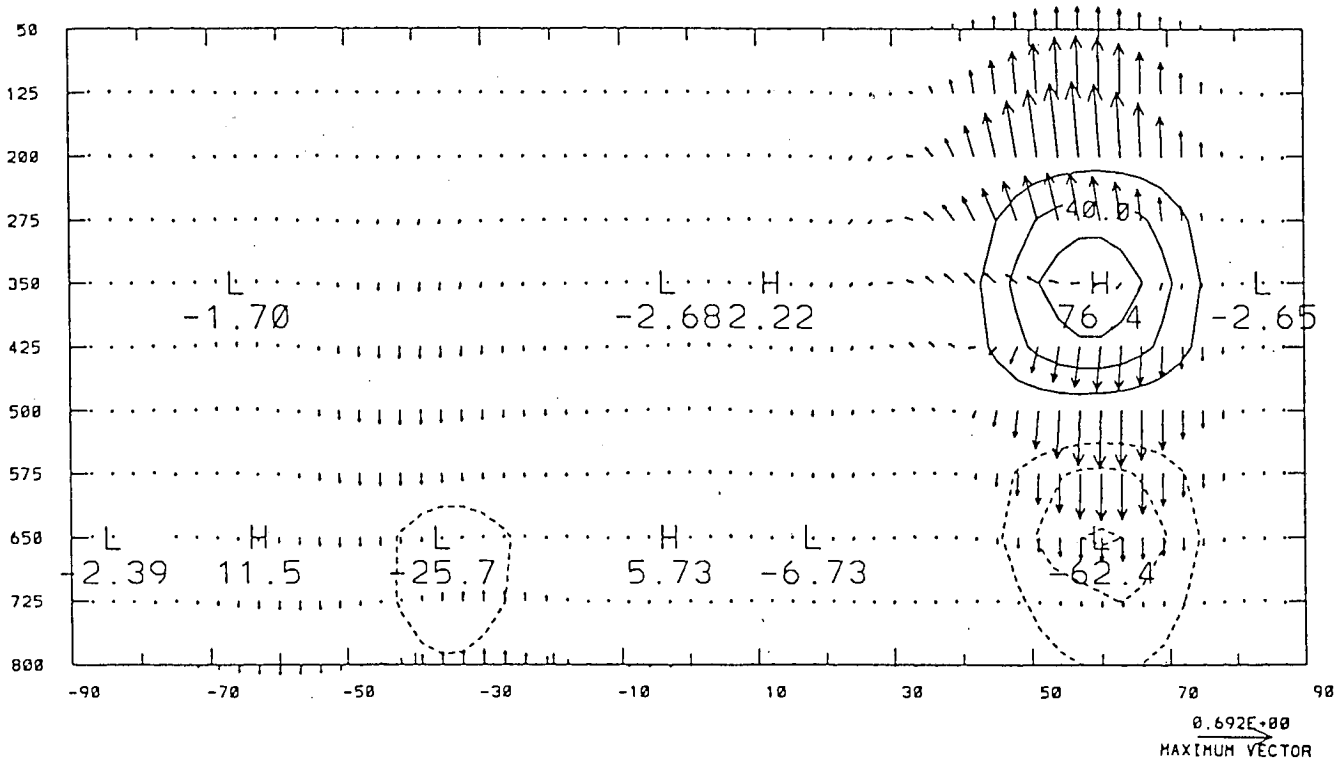

Figure 6.18: EP cross-section as Figure 5.9, but for the model response to the winter diabatic heating climatology. The contour interval is 20 units.

that the analytical expression (5.3), used previously in parameterising the vertical distribution of diabatic heating, is a very reasonable approximation to the true representation of the heating structure. However, it is also worth stating that the model result is sensitive to this sort of vertical parameterization for diabatic heating, as has already been percieved from this section for the response at 700 mb. Furthermore the amplitude of the geopotential perturbation in a longitudional cross-section is different between the two experiments (see Figs. 6.21 and 6.22). Therefore, from now on, we will carry on experiments with the true representation for diabatic heating climatology, not the analytical expression.

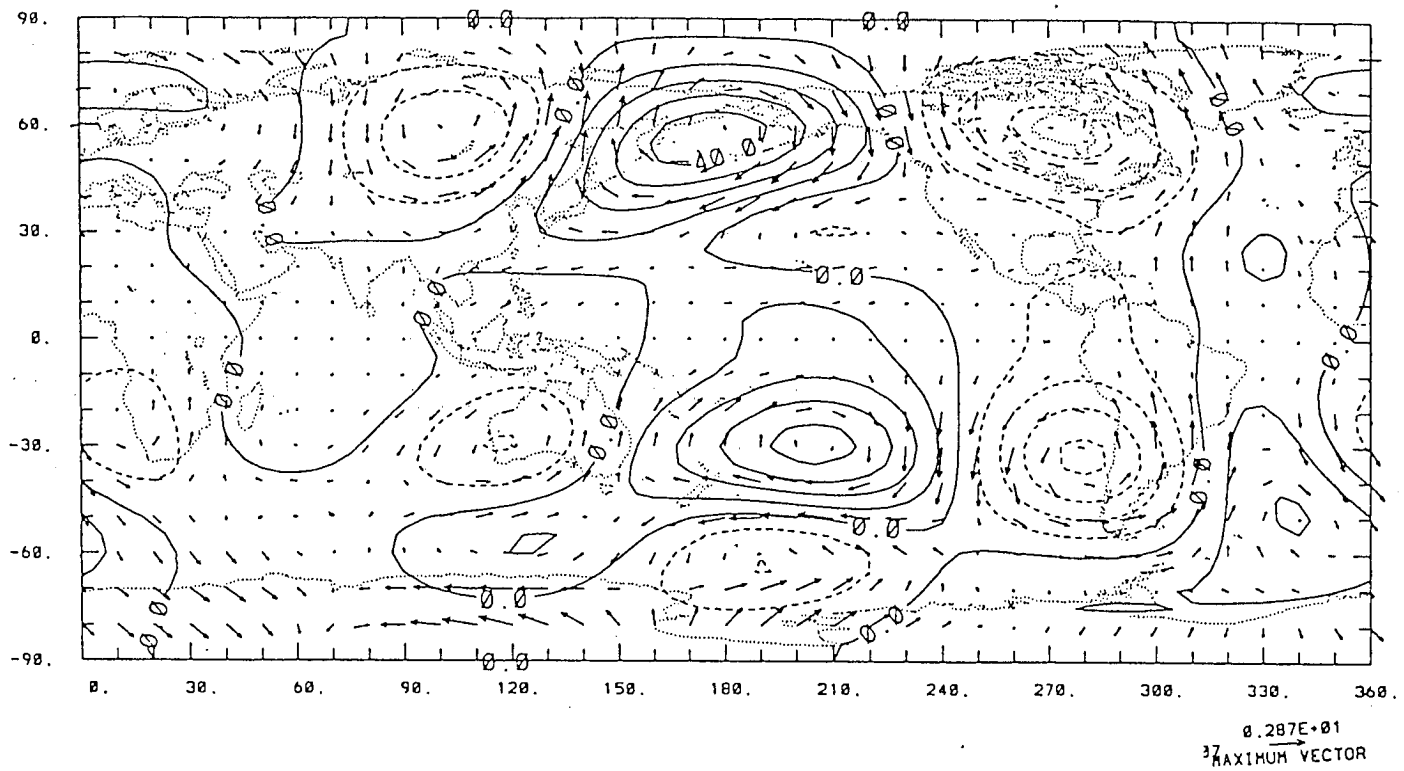

Figure 6.19: 700 mb perturbation stream field as Figure 6.11 but for the incorporation of the diabatic heating directly transformed from three dimensional data array. The contour interval is 10 units.

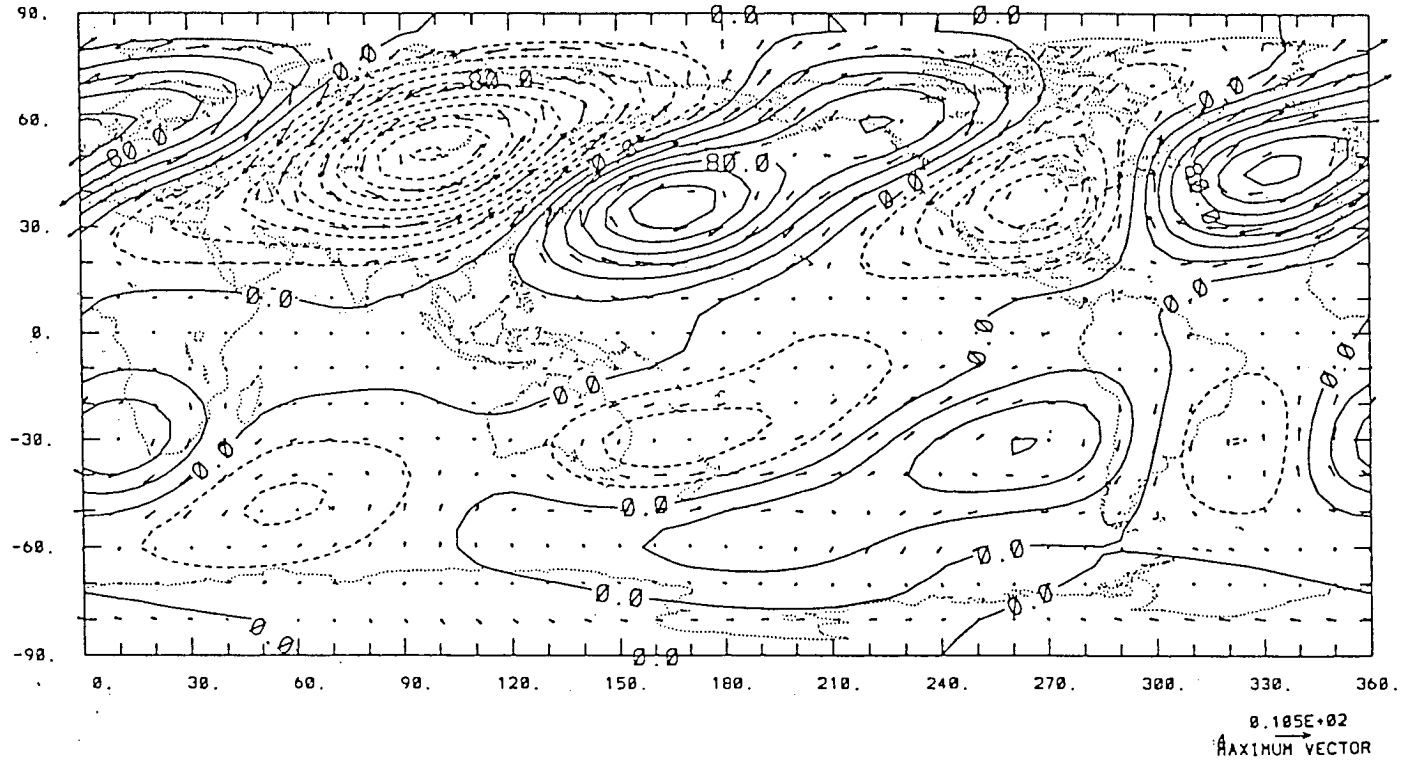

Figure 6.20: As in Figure 6.20, but for 200 mb, with contour interval of 20 units.

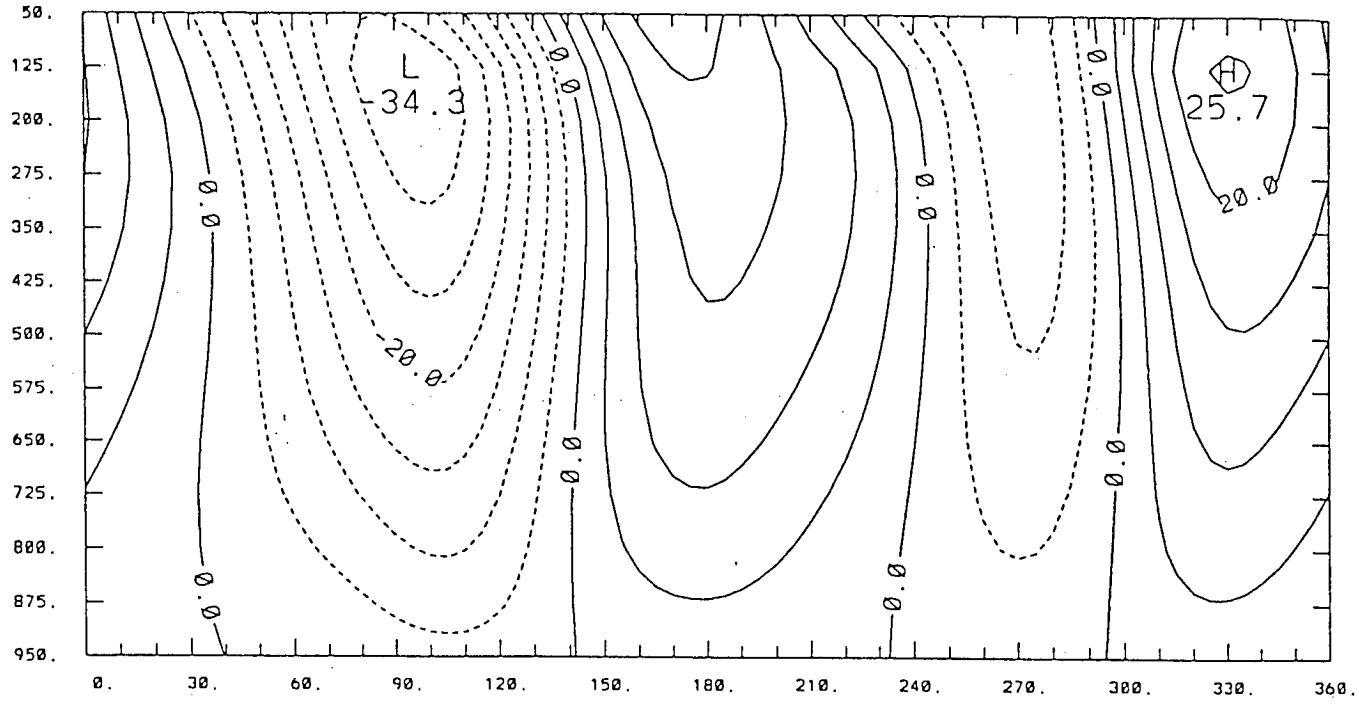

Figure 6.21: Longitude–pressure cross–section of the perturbation geopotential height at 45^0N for the model response to the winter diabatic heating climatology which is incorporated into the model by spectral coefficients directly transformed from three dimensional data array. The contour interval is 5 dm.

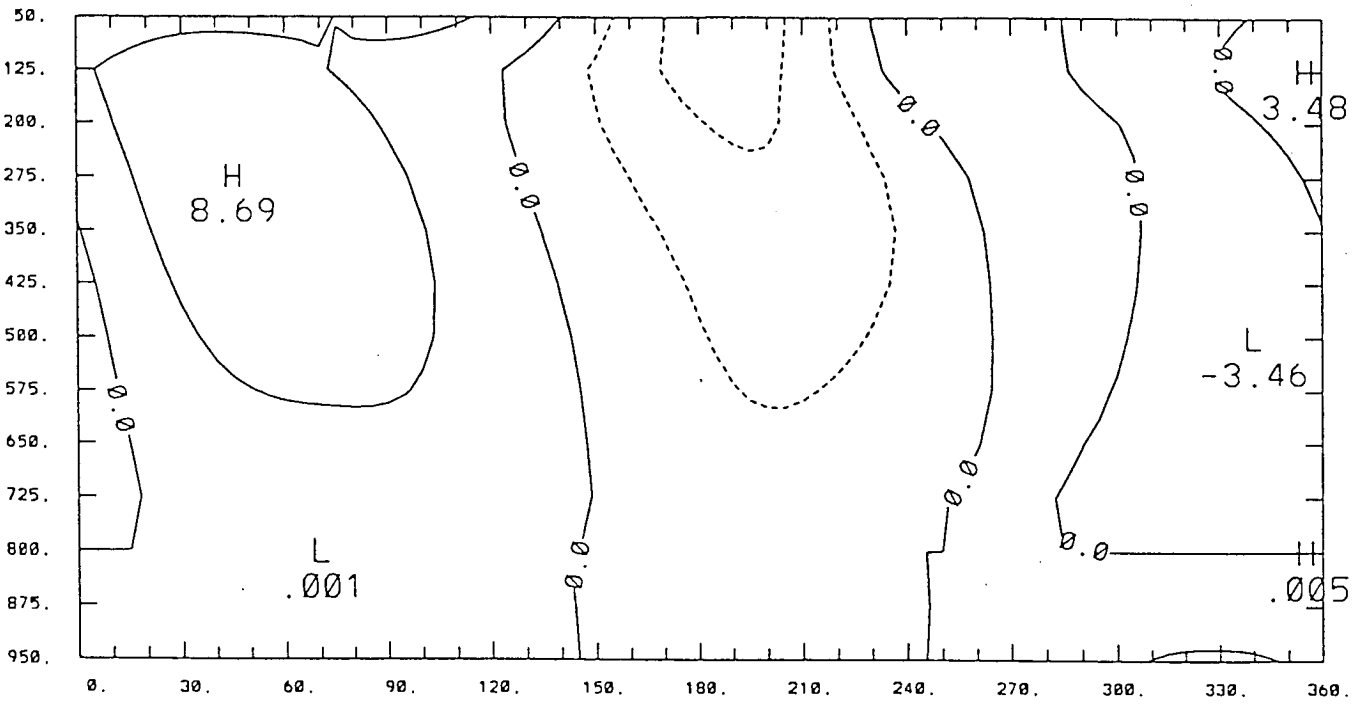

Figure 6.22: As in Figure 6.21, but at 60^0S with contour interval of 5 dm.

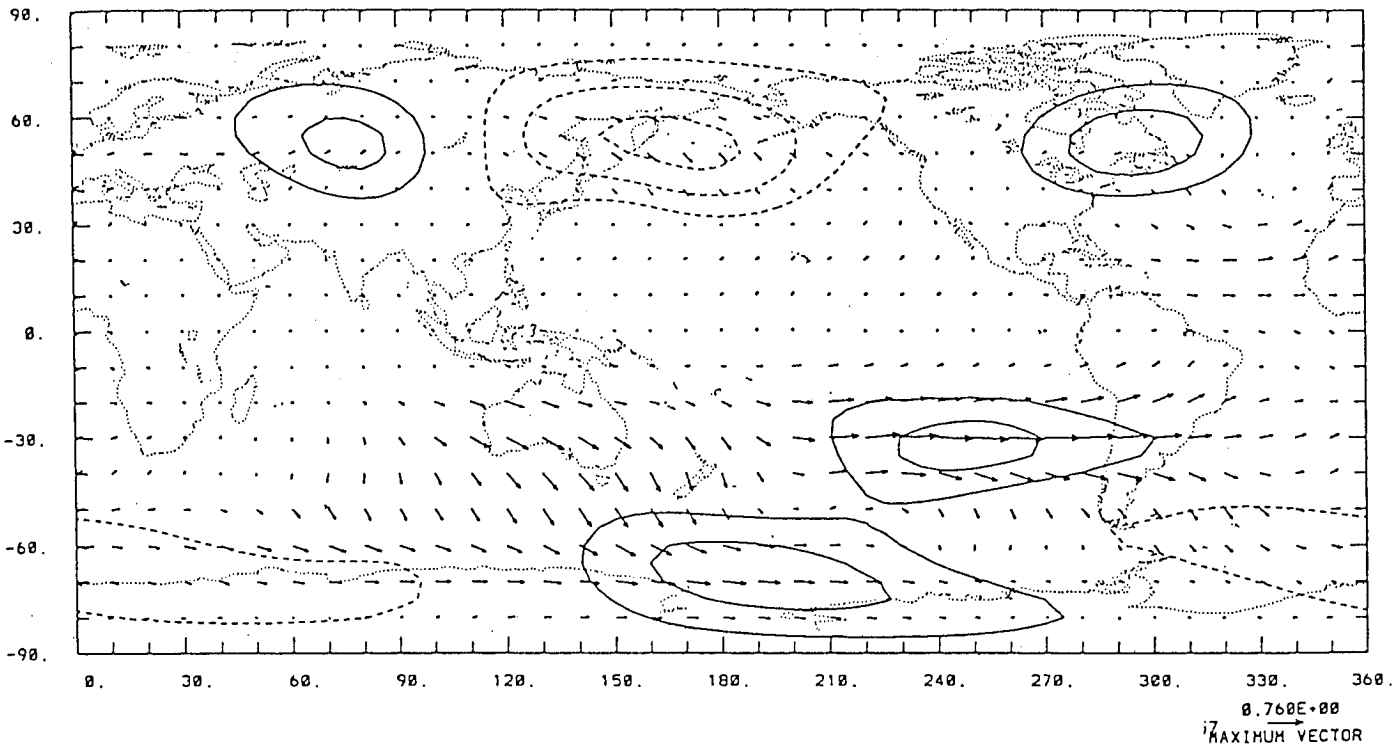

Figure 6.23: 800 mb wave activity flux as in Figure 6.15, but for the incorporation of the diabatic heating directly transformed from three dimensional data array. The contour interval is 10 units with the zero contour excluded.

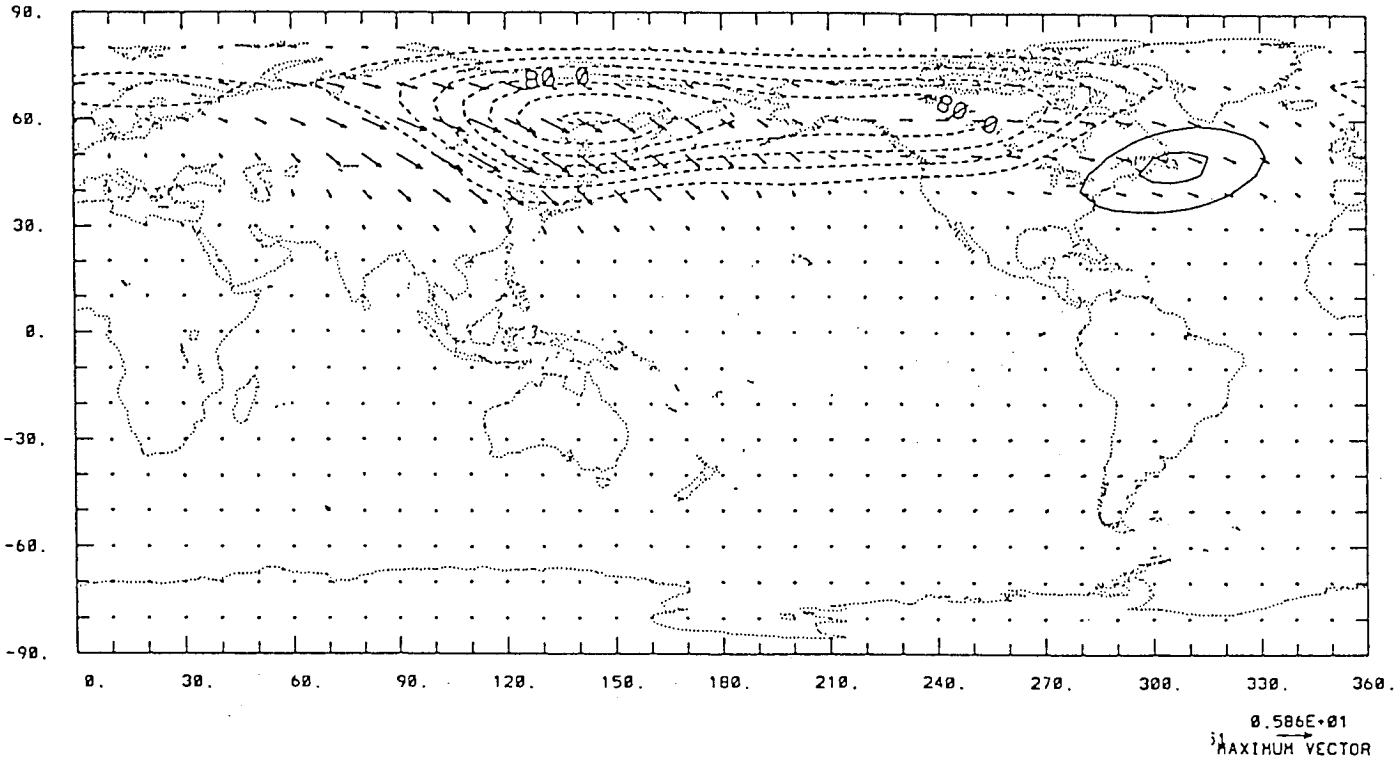

Figure 6.24: As Figure 6.23 but for 500 mb. The contour interval is 10 units.

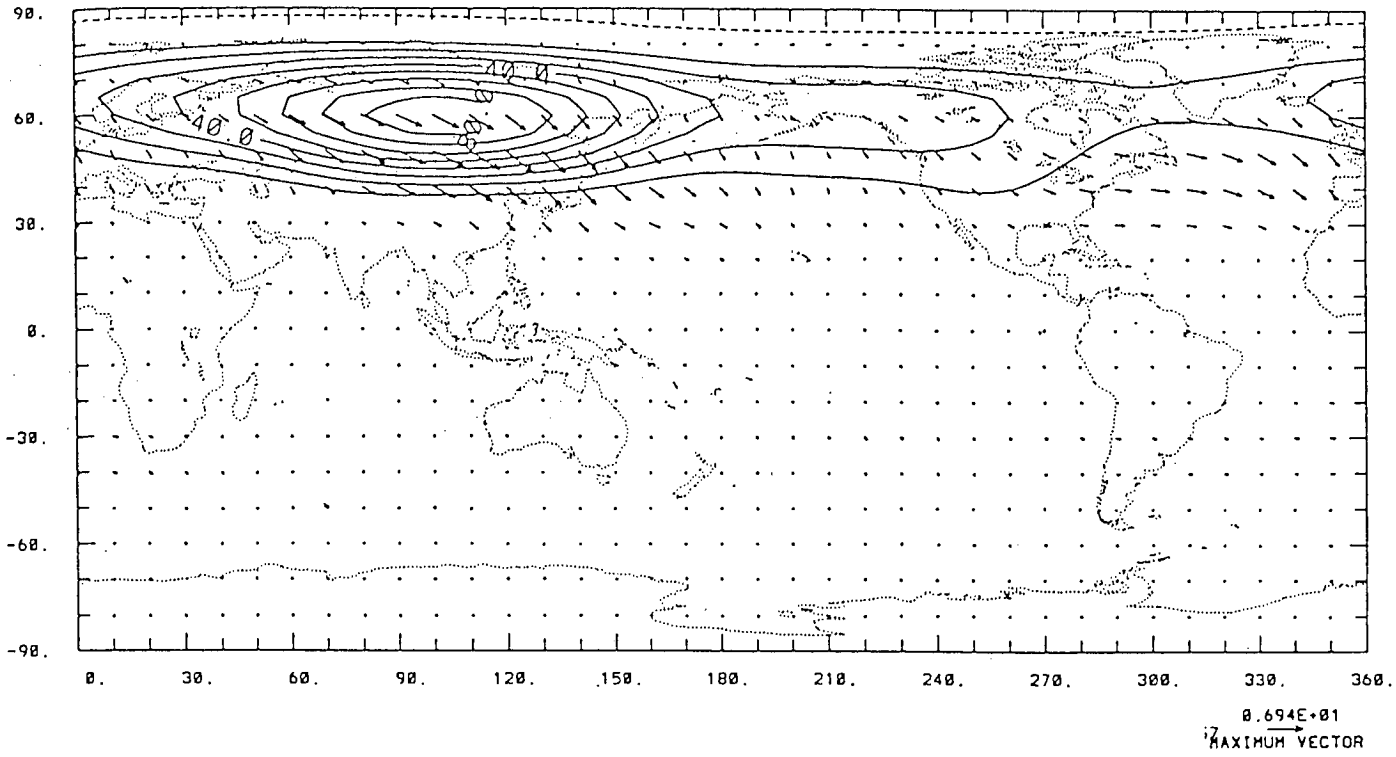

Figure 6.25: As Figure 6.23 but for 200 mb. The contour interval is 5 units.

§6.4 Response to Actual Orography and Diabatic Heating Climatology

The model atmospheric behaviour in response to the combined forcing of the global orography and diabatic heating climatology, which were used in the previous sections, signifies to a certain extent the stationary wave circulation climatology of the actual atmosphere, in the case of this study, in northern winter. According to linear theory, the solution of this calculation is simply a linear superimposition of the seperate linear calculations for the pure orographic and pure diabatic heating forcing. We will further discuss the effect and the contribution of the combined forcing to the stationary wave circulation where some comparison with the results in the previous sections for the separate forcing is made by visual perception to reveal the relative importance of the two categories of forcing.

Shown in Figures 6.26 and 6.27 are the perturbation streamfunction and horizontal velocity fields at 700 mb and 200 mb respectively, corresponding to the above-described combined forcing. At the 700 mb level, the stationary wave circulations have the main contribution from the orographic forcing over most of the globe, except for the circulations at northern high latitudes over the Bering Sea and northern America and middle latitudes of the southern Pacific, where the thermal forcing has a stronger effect on the intensity of the stationary wave circulation than the orographic forcing. The orographic contribution to the stationary wave circulation dominates at high latitudes in the southern hemisphere. At 200 mb, the contribution to the stationary waves from the orographic and thermal forcing is comparable. In some specific locations, however, the effect and impact of the two separate forcings are different, notably in the eastern Pacific in the northern hemisphere where the orographic forcing is stronger, and over the eastern Atlantic extending to Euro-Asia where the thermal forcing makes a greater contribution.

In spite of the fact that the model framework is very much simplified in comparison with the on-going processes of the actual atmosphere and cannot be expected to simulate the stationary wave climatology accurately, it is of great interest to see that the model results reproduce most features of the diagnostic results of a six-year climatology at 250 mb in winter (Hoskins, et al, 1989) (Figure 6.35), in both hemispheres, and the climatological results based on observation (Wallace, 1983) (see Figure 6.34), particularly in the middle latitudes of both hemispheres. This can further be shown from the longitude-pressure cross-section of perturbation geopotential height (Figs. 6.28), which is consistent with observational studies (see, e.g., Wallace, 1983).

Despite the model's ability to simulate some essential features of stationary waves, the deficiencies of the model are evident in comparison with the afore–mentioned diagnostic results at 250 mb. These can be outlined especially in the following aspects.

- The cyclonic circulation over Euro–Asia is too strong in the model
- The cyclonic circulation near the north–east Pacific is too weak in the model
- The anticyclonic circulation over the northern central Atlantic is too strong, whereas the cyclonic circulation to the south is too much damped in the model
- The circulations in tropical areas of both hemispheres and the southern subtropics are not significantly represented
- The phases of the circulation systems in high–latitudes of the southern hemisphere are almost reversed (e.g. 6.29).

These model deficiencies may be attributed to several factors, notably, low model resolution, inaccurate description of northern wintertime diabatic heating climatology, lack of transient effects explicitly included in the model, inappropriate imposition of damping coefficients, as well as prescription of zonal mean states derived from the monthly averaged climatology in January 1979. Furthermore, nonlinearity may be an important factor in modelling these circulation systems in the critical areas where the linear theory is violated. Also there is an evident difference between climatological statistics over a long period and the results of numerical simulation with climatological data as model input.

The wave activity fluxes shown in Figures 6.30 – 6.32 for 800 mb, 500 mb and 200 mb respectively illustrate that the wavetrains at 200 mb are propagating predominately eastward, equatorward and upward across Euro–asia and the northern Pacific, but weaker eastward and upward over the eastern, northern America and west and central Atlantic, whereas no significant wavetrain propagation can be identified in the whole southern hemisphere. Comparing this with Figures 6.8 and 6.25, it can be seen that the wavetrain propagation at 200 mb is mainly due to the diabatic heating rather than the orography which makes a relatively minor contribution to the wave activity at that level. At 500 mb, apart from the wave propagation directed eastward and equatorward over Euro–Asia and northern Pacific as well as eastern north America, and relatively weak eastward around southern central Atlantic, the vertical propagation of the wavetrain is jointly contributed from both the diabatic heating and orography. Apparently, in comparison of Figures 6.7 and 6.24, the upward component of the wave activity over Asia and northwest Pacific has originated from the orography, particularly the Tibetan Plateau, while that over the southern polar region results from the Antarctic continent. The influence of the Rocky Mountains is relatively small. The downward component of the wave activity fluxes is contributed mostly from diabatic heating. At the lower level of 800 mb, the pattern of wavetrain propagation is more like that for pure orography, particularly in the southern polar regions. Figure 6.33 shows the corresponding EP cross–section. It explains that the EP flux in the lower troposphere of the southern hemisphere is predominately determined by orographic forcing, and there is little influence on the upper troposphere and lower stratosphere from either orographic forcing or diabatic forcing. In the northern hemisphere, however, the EP flux in tropical and subtropical areas of the lower troposphere is derived mainly from the northern orographic forcing, while in middle and high latitudes

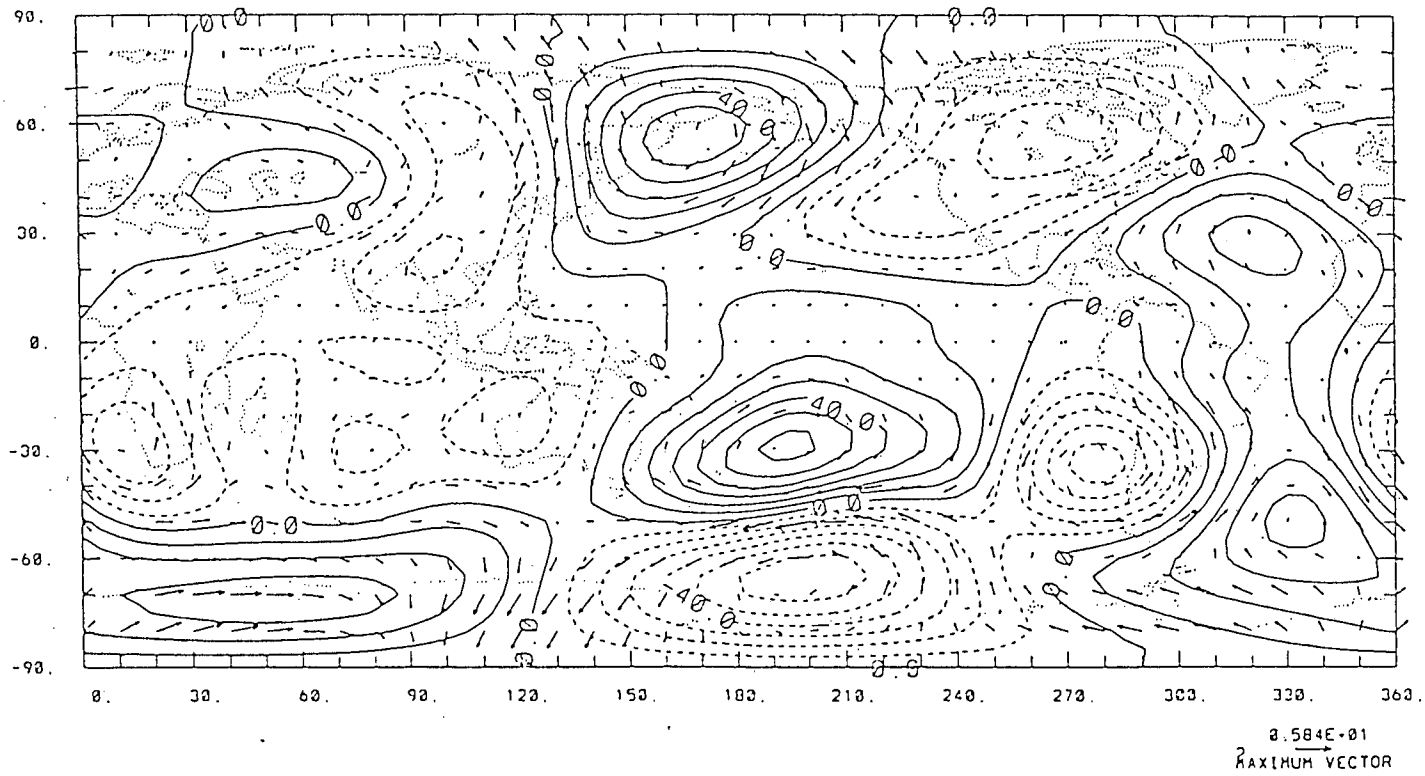

Figure 6.26: 700 mb perturbation stream fields as Figure 6.2 but for the model response to the combination of global orography and diabatic heating climatology which is directly transformed from three dimensional data array. The contour interval is 10 units.

at all levels of the atmosphere, diabatic heating forcing dominates. From the above description, it is clear that the stationary waves induced by the climatological thermal forcing had a comparable amplitude with those by the orographic forcing except in the lower troposphere of the Antarctic area. It might be considered that between these two categories of forcing, the orographic forcing was more important in the lower troposphere, particularly in high latitudes of the southern hemisphere, but having less role in the upper troposphere and lower stratosphere in the northern hemisphere, for the maintenance of the planetary stationary waves in northern wintertime.

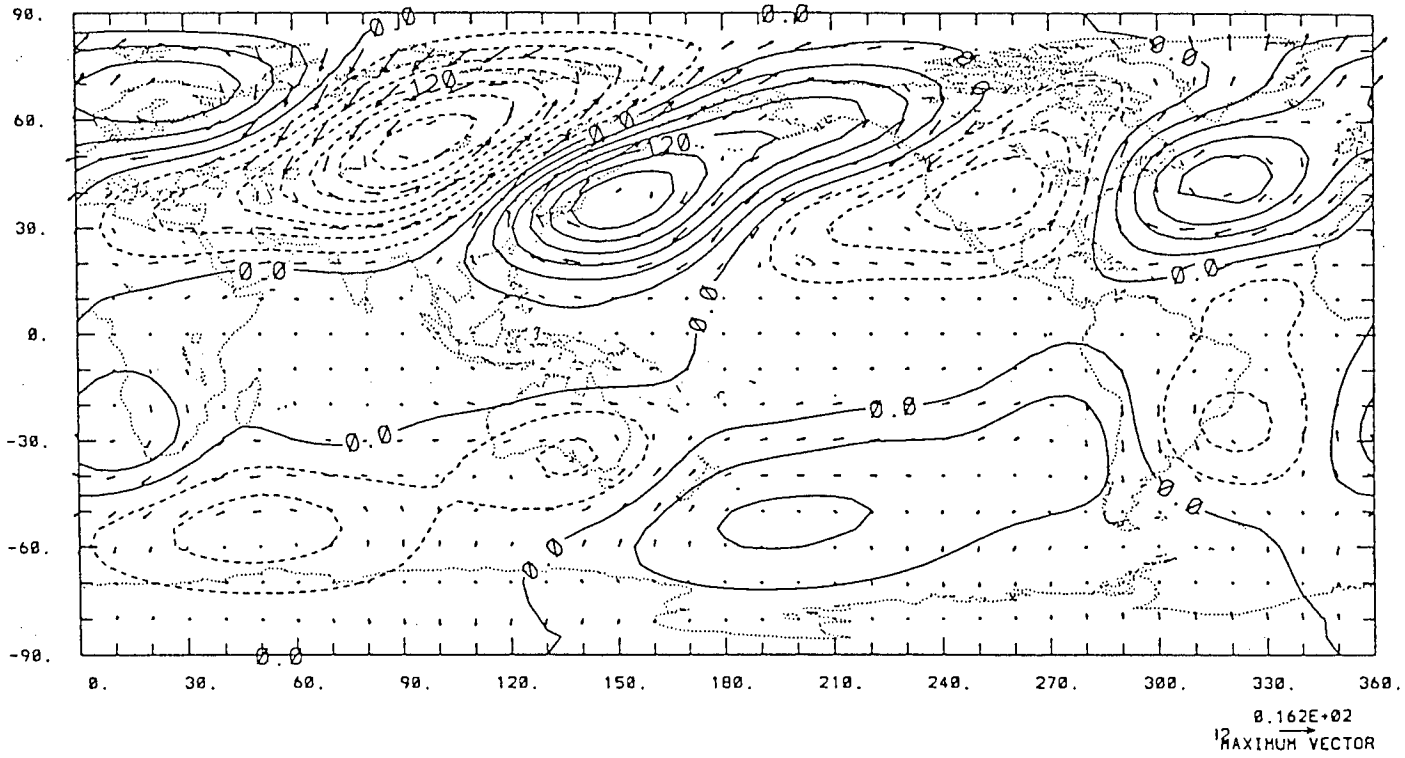

Figure 6.27: As in Figure 6.26, but for 200 mb, with contour interval of 20 units.

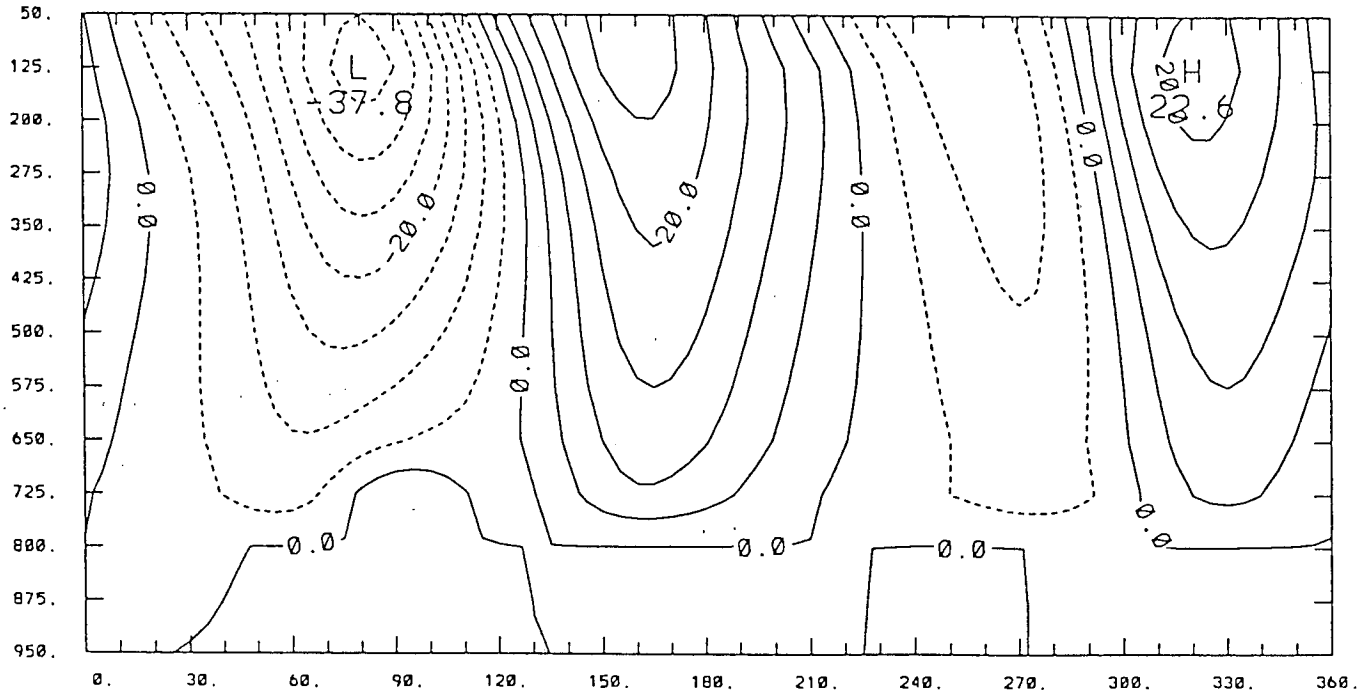

Figure 6.28: Longitude–pressure cross–section of the perturbation geopotential height at 45^0N for the model response to the combined forcing of orography and diabatic heating climatology. The contour interval is 5 dm.

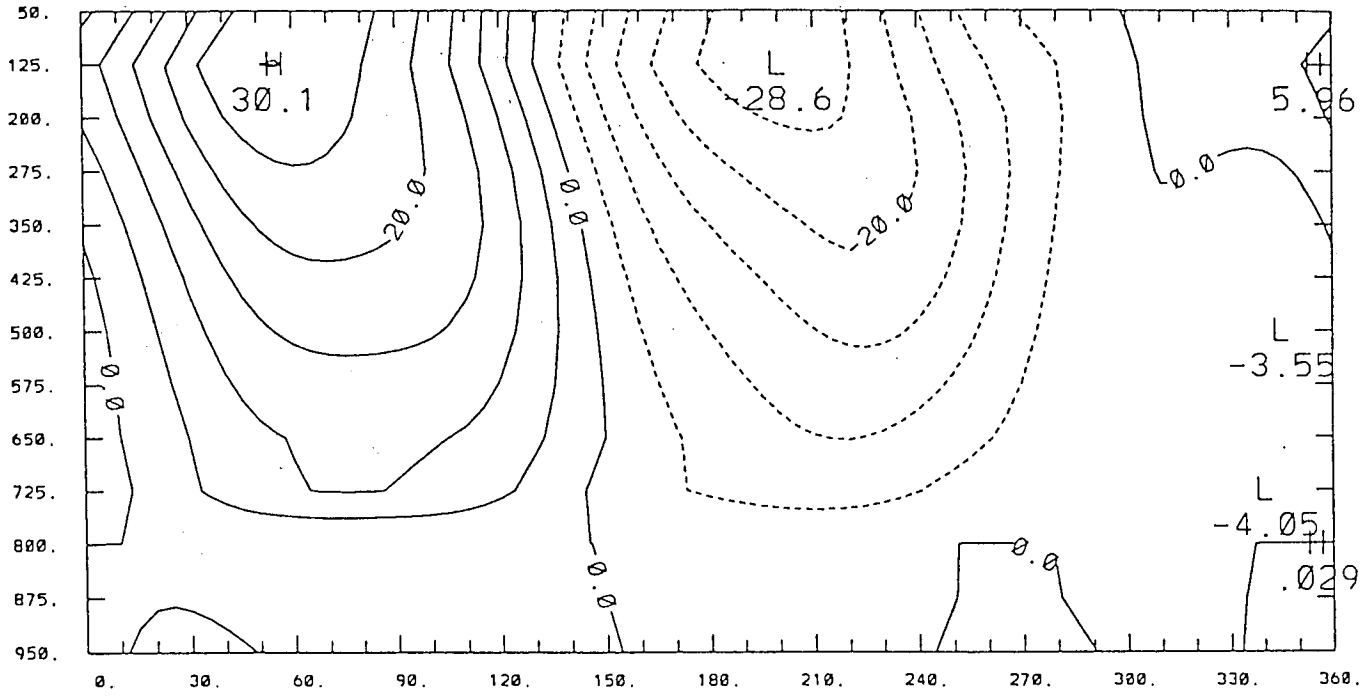

Figure 6.29: As in Figure 6.28, but at $60^0 S$ with contour interval of 5 dm.

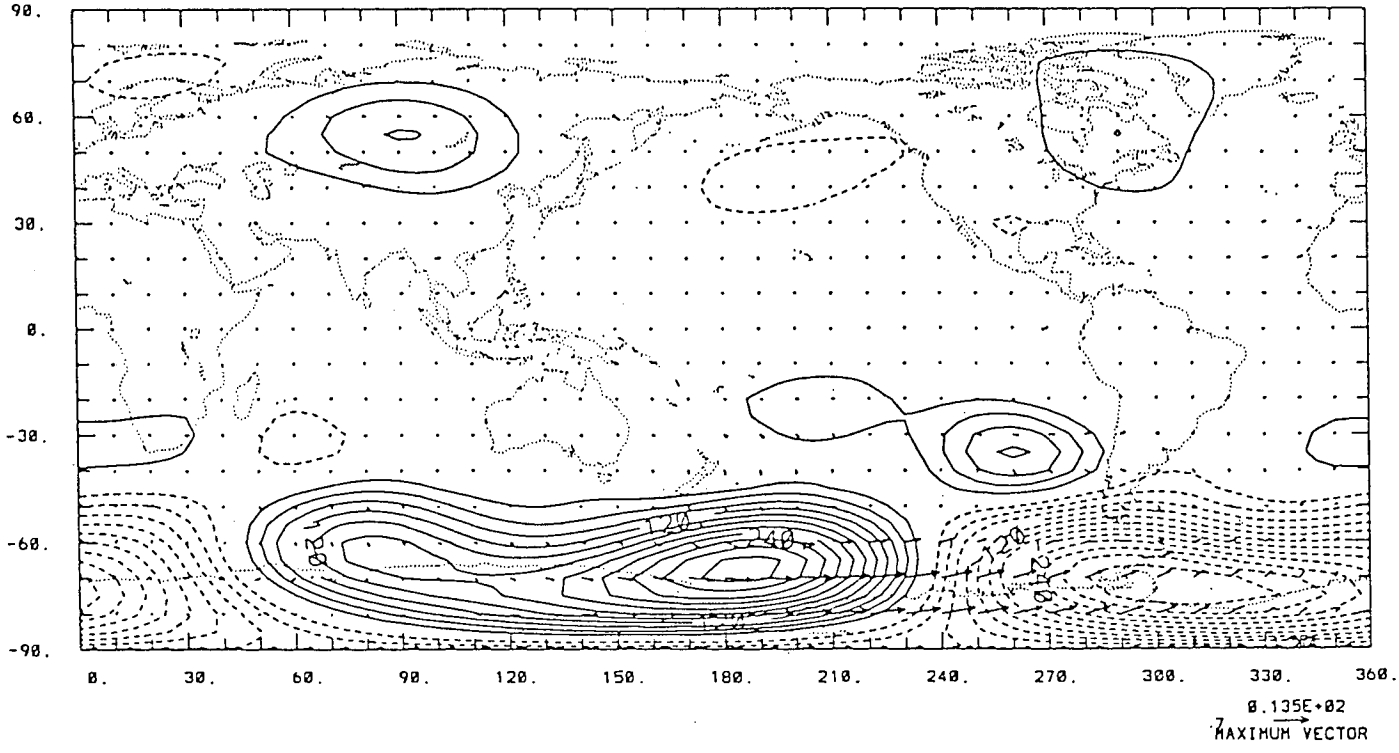

Figure 6.30: 800 mb wave activity flux as in Figure 6.6, but for the model response to the combination of the global orography and the diabatic heating climatology in northern winter which is directly transformed from three dimensional data array. The contour interval is 30 units with the zero contour excluded.

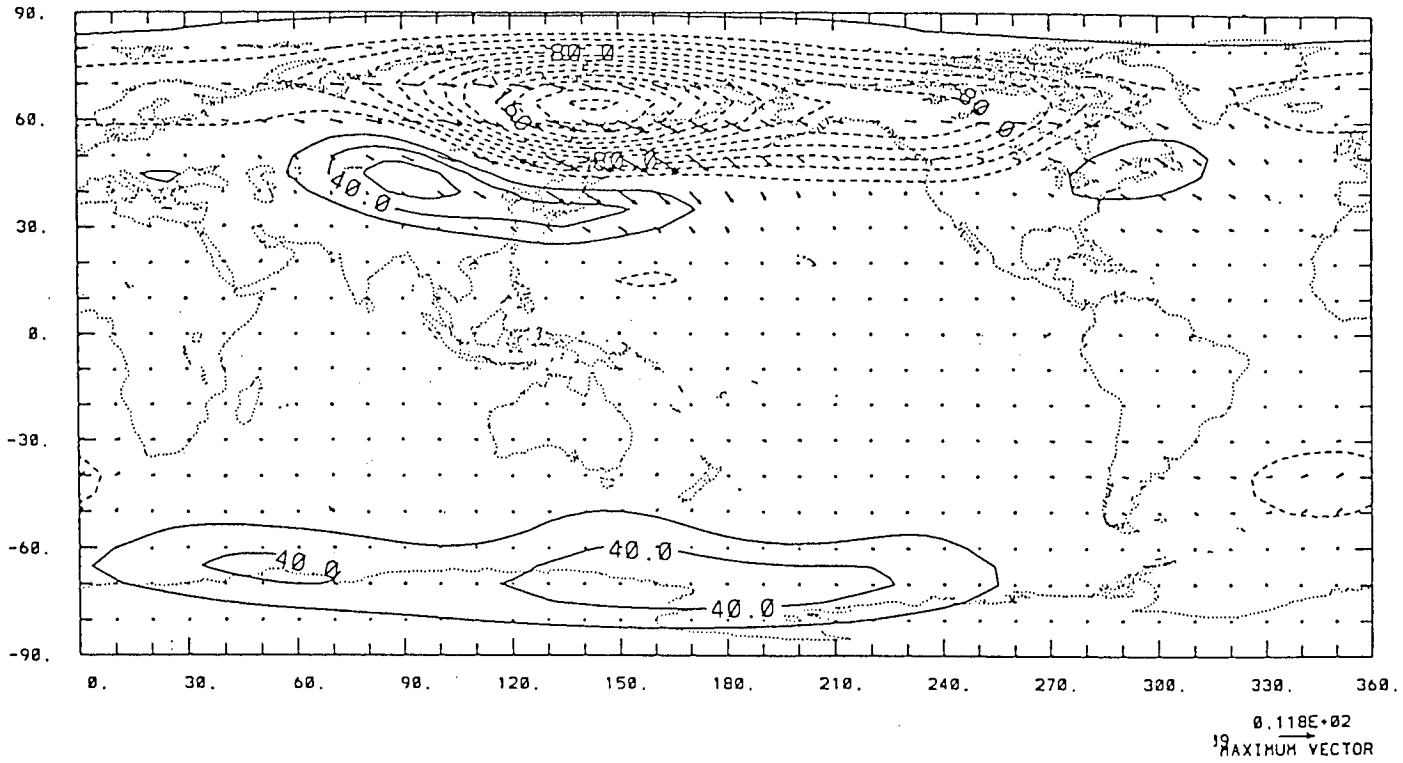

Figure 6.31: As Figure 6.30 but for 500 mb. The contour interval is 20 units.

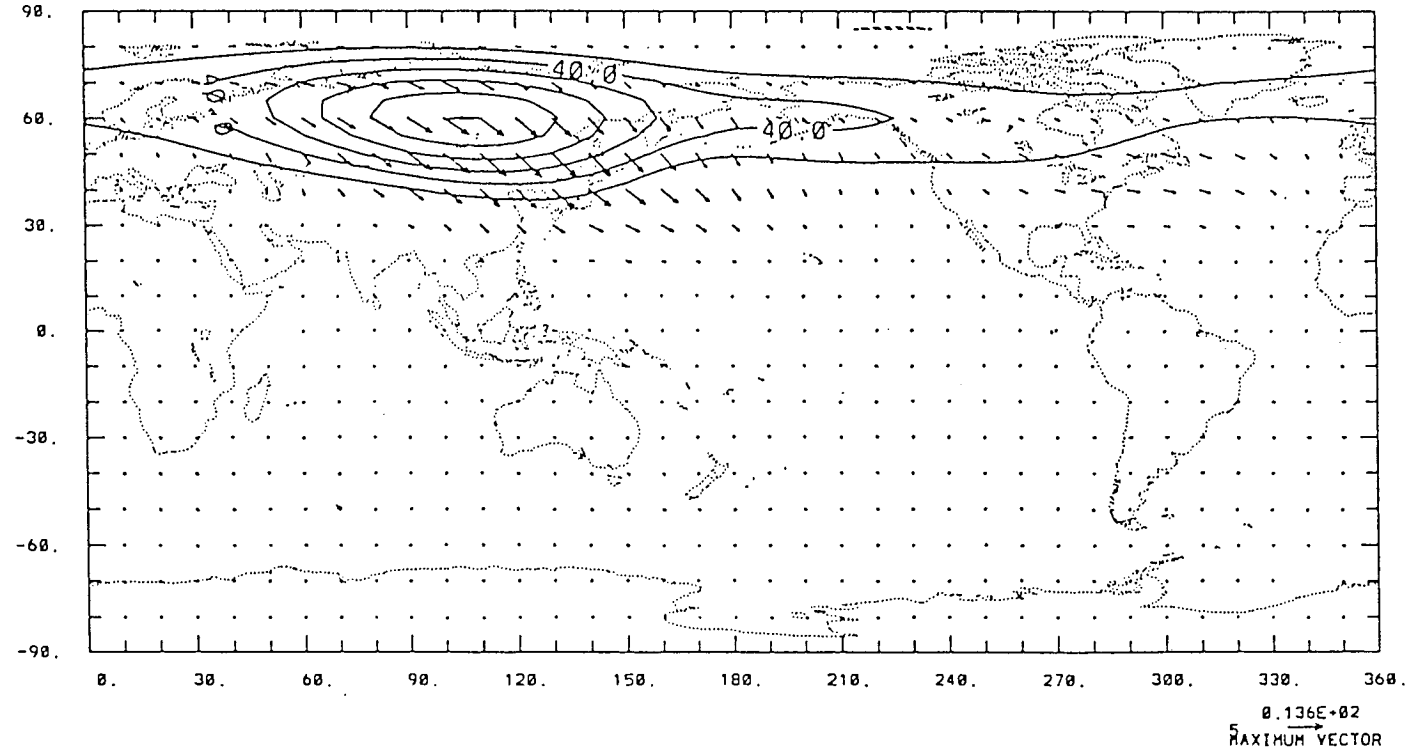

Figure 6.32: As Figure 6.30 but for 200 mb. The contour interval is 20 units.

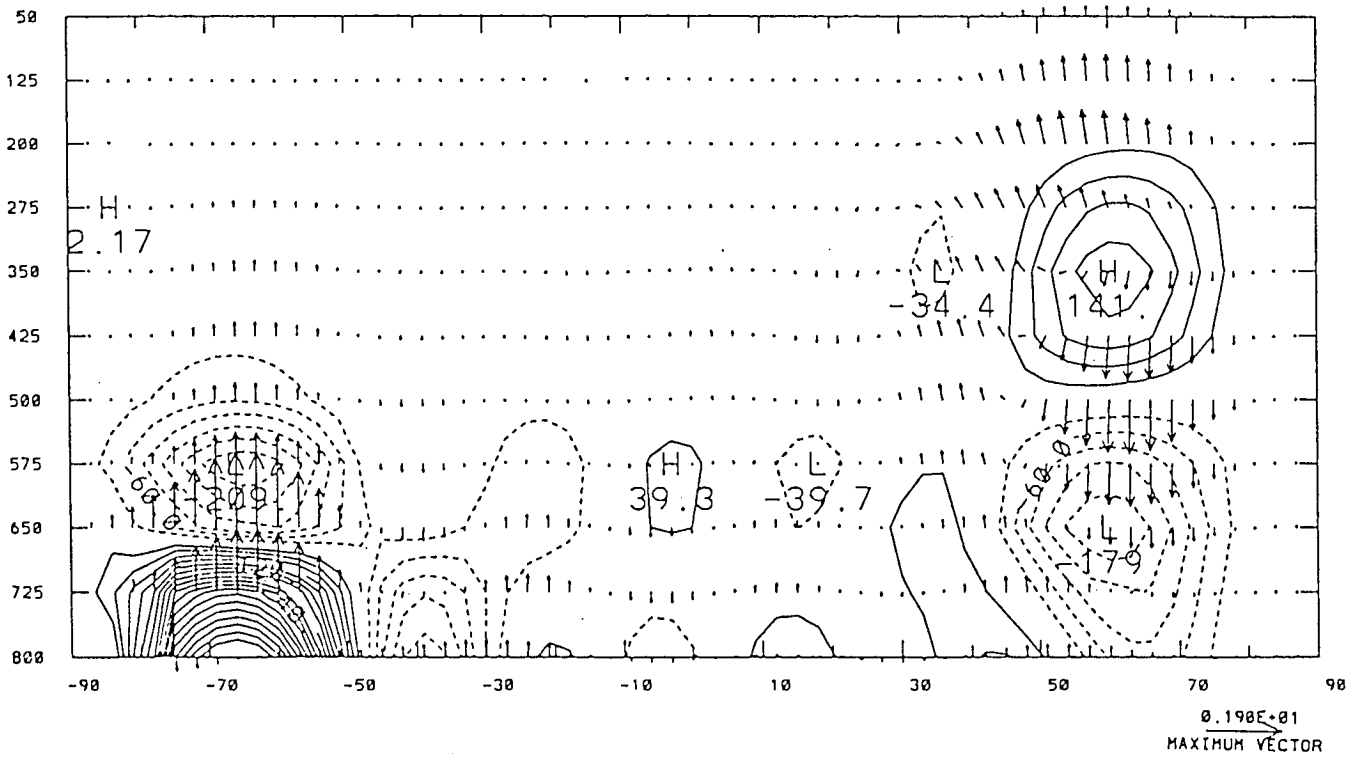

Figure 6.33: EP cross-section as Figure 5.9, but for the model response to the combined forcing of actual global orography and diabatic heating climatology in northern winter. The contour interval is 30 units.

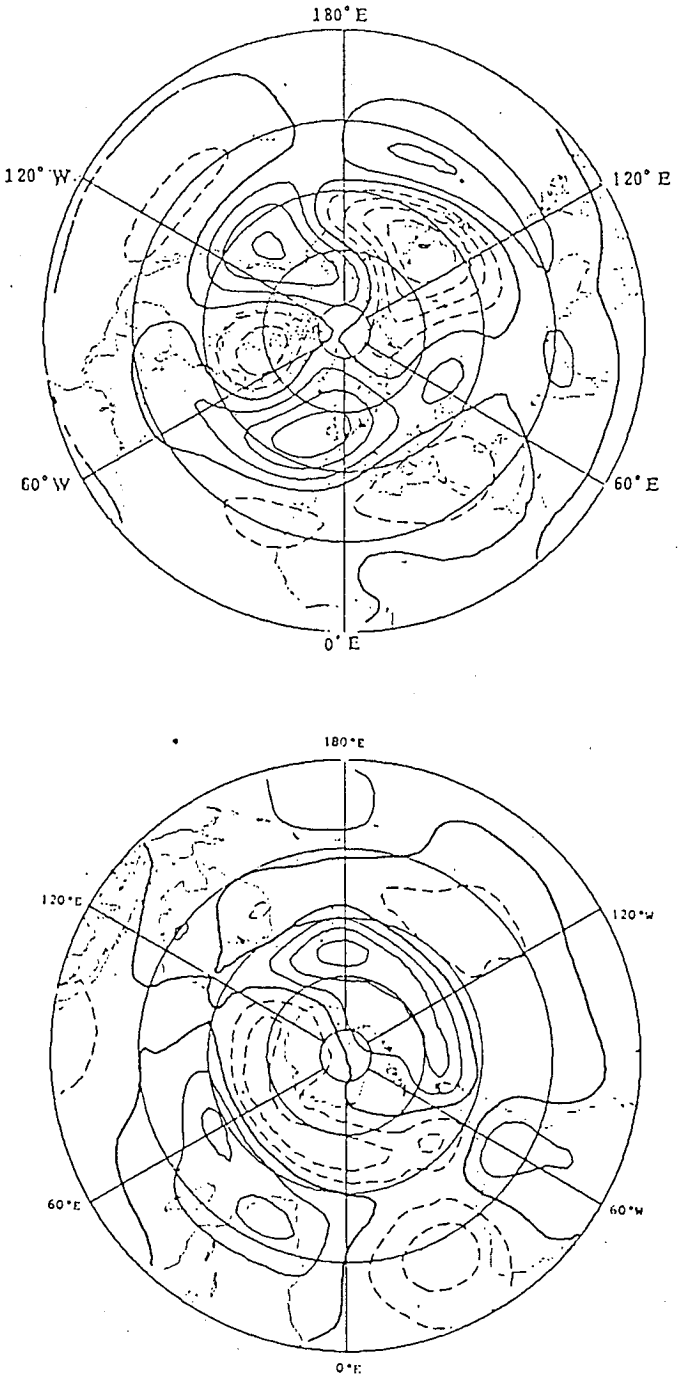

Figure 6.34: Climatological mean January distribution of stationary wave geopotential height at the 200 mb level in northern hemisphere (upper) and southern hemisphere (lower), photocopied from the paper of Wallace(1983). Contour interval is 6 dam (upper) and 3 dam (lower). The zero line is thicked, the positive contours are solid and the negative ones dashed. Lines of latitudes and longitudes are drawn every 20^0 and 60^0 respectively.

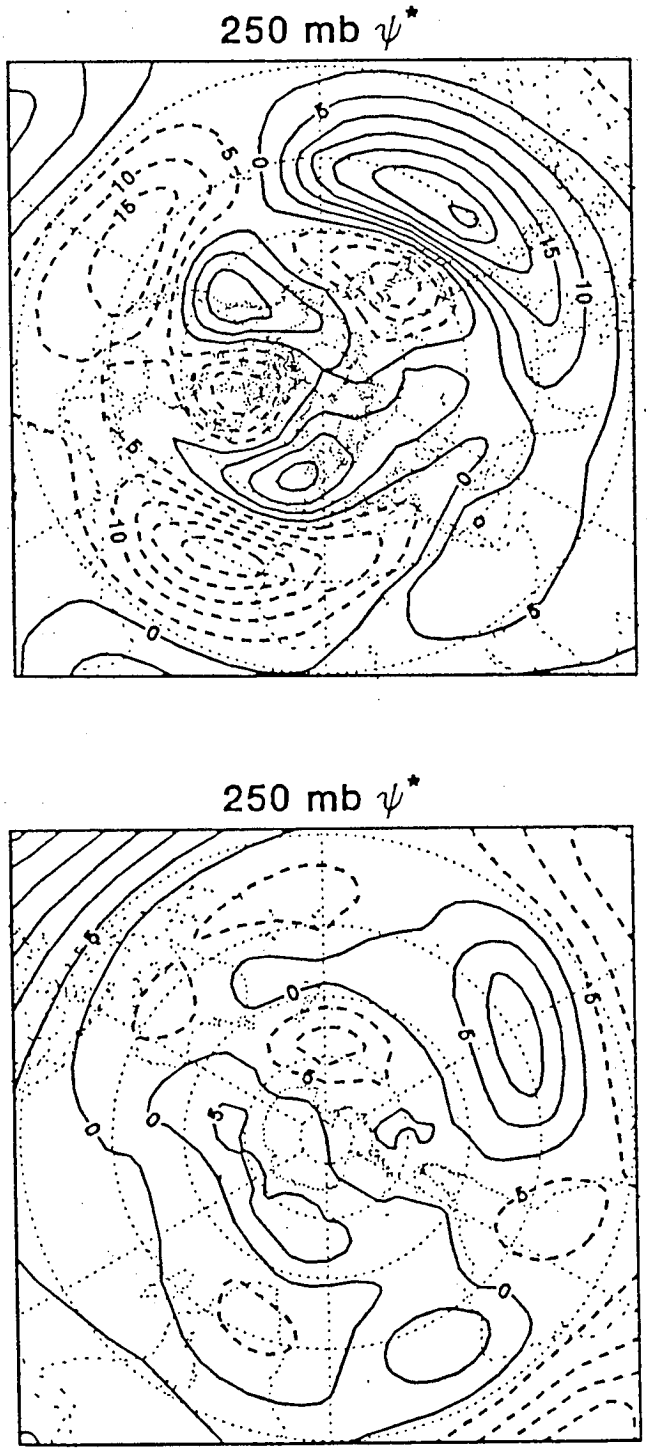

Figure 6.35: Six year climatological mean December–February distribution of stationary wave streamfunction at the 250 mb level in northern hemisphere (upper) and southern hemisphere (lower), photocopied from UGAMP report by Hoskins et al. (1989).

and Hoskins, 1983) have shown that vertical propagation of wave activity is important for stationary planetary waves with low zonal wave number. In order to investigate the three dimensional propagation of wave activity, the Plumb flux, which was also known as a generalized EP flux, and derived by Plumb (1985) for linear, quasi–geostrophic stationary waves on a zonal mean flow, was used as a diagnostic tool for the model solution. The Plumb flux is a conservable measure of the flux of wave activity, and is non–divergent for steady, conservative, linear waves. It is reduced to the EP flux if the Plumb flux is zonally averaged. By using the Plumb flux, together with EP cross–sections, the model atmospheric behaviour in response to the large scale orography and steady–state diabatic heating was investigated. It was identified that the relative importance of the two kinds of stationary forcing is dependent on geographic location and different levels of the model atmosphere. The main contributions from this study may be summarized as follows:

1. The linear model used in this study is developed on the basis of linear theory which linearizes the primitive equations using the perturbation method described in section §2.3. The inherent deficiency of the model itself is the neglect of stationary wave–wave interactions. However, the numerical solutions obtained show that this simplified model is suitable for qualitative analysis of the characteristics of stationary waves induced by large scale orography and steady–state diabatic heating in northern wintertime. The model is hence able to be used as a diagnostic tool for stationary waves.

2. The stationary wave pattern produced by the linear response to the realistic global orography and climatological diabatic heating in northern winter,

derived from the six year data archive of ECMWF (see Hoskins et al, 1989), was in general consistent with the observed climatological stationary waves in the northern hemisphere and southern mid–latitudes, but with reversed phase of the wave pattern in high latitudes of the southern hemisphere, and some apparent deficiencies which have already been described in section §6.4.

3. The diagnostic analysis in this study showed that the wave activity flux, which is based on the linearized quasi–geostrophic equations, is a useful diagnostic tool of the three–dimensional propagation of stationary wave activity, in spite of the fact that the evaluation of the wave activity flux involved a second order derivative of, and nonlinear calculation with respect to, the perturbation streamfunction, and thus the diagnostic result is quite sensitive to the streamfunction itself, which is in turn dependent on model parameters and external forcings. Regardless of this sensitivity, there were still grounds for believing that the diagnostic results for the model atmosphere framed in this study are meaningful and suggestive.

4. If a zonal average is taken, the wave activity flux is reduced to the EP flux, which is also indicative since it is a measure of net wave propagation in both the vertical and meridional directions, and its divergence is a direct measure of the total forcing of the zonal mean state by the stationary waves. It was shown that the wave activity flux for the idealized thermal forcing in northern middle latitudes propagates both upperward and downward from the wave activity source area situated in the middle troposphere where the maximum heating occurs. This result was also reinforced by the experiments for climatological thermal heating.

5. The numerical experiments for the response to the idealised orography in

northern middle latitudes and actual global orography showed that the Tibetan Plateau plays the most important role in the maintenance of the orographically forced stationary waves in the middle and upper troposphere as well as lower stratosphere of the northern hemisphere in the northern wintertime, while the forcing by the orographic effect of the Antarctic plateau is also very important, but restricted only to the lower troposphere of the southern high latitudes.

6. The middle latitude orographic forcing, in particular that by the Tibetan Plateau, makes a substantial contribution to the maintenance of the cyclonic circulation over the eastern tropical and subtropical Pacific as well as the reversed circulation over the western Pacific in the upper troposphere. These upper level systems are usually associated with some important phenomena such as the Walker circulation, Asian Monsoon etc. It is therefore suggested that the orographic forcing in mid-latitudes plays an important role in the maintenance of the planetary scale motion in the subtropics and tropics.

7. The stationary waves induced by the climatological thermal forcing had a comparable amplitude with those by the orographic forcing except in the lower troposphere of the Antarctic area. It might be considered that between these two categories of forcing, the orographic forcing was more important in the lower troposphere, particularly in high latitudes of the southern hemisphere, but having less role in the upper troposphere and lower stratosphere in the northern hemisphere, for the maintenance of the planetary stationary waves in northern winter. This was also supported by the longitude–presure cross–sections of geopotential height, from which it might be concluded that the thermal and orographic forcing were comparably important in the mid-

dle latitudes of the northern hemisphere, while the circulation in the high latitudes of the southern hemisphere is primarily orographic.

8. However, the vertical structure of the EP flux for the response to diabatic heating differred significantly from that to the actual global orography. The former had a smaller vertical component in the lower troposphere than the latter, especially around the Antarctic. However, the latter became dominant in the middle and upper troposphere of the northern hemisphere. Furthermore the thermal forcing made more contribution than the orographic forcing to the maintenance of the vertically propagating steady-state planetary waves in the stratosphere in the northern hemisphere. On the contrary, the EP flux from both the thermal and orographic forcing was negligible in the middle and upper troposphere of the southern hemisphere.

9. It was in a good agreement with others that the response to the diabatic heating had a more baroclinic nature than that to the realistic orographic forcing. The vertical structure of the perturbation geopotential height for the responses to the idealized and realistic orographic forcing showed the characteristic of this quasi-barotropic nature.

10. The three dimensional structure of the wave activity flux showed that the contribution to the maintenance of the stationary waves from the orographic forcing was very localized, while the thermal forcing contributed in larger areas.

11. The experiment for the response to an idealized diabatic heating in the tropical regions showed that an isolated tropical heating, under the condition that Newtonian cooling and Rayleigh friction were set to constant coeffi-

cients, produced not only a strong response in the tropical region itself, but also a strong extratropical response in both hemispheres, which appeared as a wavetrain propagating poleward as well as longitudinally, and suggested that the tropics may have a significant influence on the stationary waves in middle and high latitudes in the northern winter season. This speculation was also supported by the intercomparison with the response to diabatic heating. Even with the special conditions for this experiment, the EP flux was still very small around the equator. This may imply that the narrow band of the equatorial region has a natural ability to absorb wave activity flux.

12. From the sensitivity tests, it was found that the zonal mean state was sensitive to the model response to the idealized orography in northern midlatitudes, but less so to the idealized thermal forcing. Due to the simplicity of the model structure, this conclusion may only apply for this linear model.

13. The functional representation for the vertical distribution of diabatic heating used by (5.3) was shown to be a good approach for use with the linear model.

§7.2 Future Potential of the Study

Since the model used here is suitable for diagnostic analysis of the characteristics and behaviour of the stationary waves in response to large scale orography and steady–state thermal forcing, it has potential for use in future studies. A number of extensions can be made on the basis of this model.

- The influence of the zonal mean states can be further investigated. It seems that the model response to the orographic forcing is quite sensitive to the structure of zonal mean states as seen in the sensitivity test described in section §5.6.1. The zonal mean states used in this study are predefined and derived from monthly averaged climatology in January. An attempt to adjust $[U]$ and $[T]$ into a kind of balance state, e.g. linear balance, or geostrophic balance, will make the results more useful in understanding the true atmosphere.

- The appropriate introduction of damping coefficients considerably affects the model results which in turn affects the wave activity flux. The imposition of those coefficients in this linear model is physically understandable, but it is impossible to prevent some arbitrariness in their quantities. The simulated stationary wave behaviour will be altered if the structure of the damping coefficients is modified.

- It may be of interest to investigate the role of the orographic effects of particular large scale mountains by suppressing their geopotential height in the global orographic data, then comparing the resulting response with that to the actual global orography.

- The significance of the thermal forcing in tropical and subtropical areas needs to be investigated further. The difficulty lies in the introduction of the damping coefficients, while the orographic forcing exists.

- One of the defects of the model is the exclusion of the effects of the transient waves which are in fact very important in the atmosphere. The observed climatological stationary waves are the time–averaged features over a certain

period. Therefore the contribution of the transient forcing to the planetary stationary waves should not be ignored. The transient effects may be included into the model by collectively parameterizing the time–averaged transient eddy forcing as suggested by, e.g. Hoskins (1983).

- The model used in this study is very cheap to run, and can be easily implemented on mainframe computers or distributed systems which are commonly available in most academic institutions. However, due to the inherent nature of the linear theory, the quality of the simulated stationary waves in areas where the zonal symmetric component of velocity $[U]$ vanishes may not be good. Therefore one further step to develop a corresponding non–linear model must be of interest.

- In addition, it could be illuminating if the time derivatives of the dependent variables were to be represented by Fourier series. These could be included in the linear model to diagnose the time–evolving behaviour and characteristics of the stationary waves (Lin, personal communication).

Appendix A

Model Integrity

To test for possible errors in the coding of the linear model some simple experiments were conducted to compare the model output with some already known solutions. If a model is correctly configured, its results should be physically consistent and dynamically plausible. This is the criterion used to justify the appropriateness of the model for future use.

Two sets of experimental results are presented here: The first experiment is intended to reproduce features of Gill's (1980) analytical result in our model using one of his heating functions. The other test investigates the response of the isothermal atmosphere in super-rotation to a spherical harmonic boundary. The temperature of the isothermal atmosphere is predefined by $\frac{gH}{R}$, where g is the gravitational acceleration rate; H the scale height, taken to be 8000 metres; and R the gas constant for dry air. The details of the experimental results are described below.

§A.1 Model Features of Gill's Solutions

Gill (1980) presented analytical solutions of the response of the resting isothermal atmosphere to tropical heating on a β-plane. These results are in good agreement with the basic dynamics and physics of the atmosphere. The detailed interpretation of the solutions was given in Gill's paper.

Our purpose here is to make sure that the model is correctly coded before its use for further experimentation. The heating function used in this model is the same as Gill's which is symmetric with respect to equator. It is centred at 120^0E with coverage of 40 degree in longitude. The vertical distribution of the heating was parameterised by sinusoidal function with the maximum located at about 500 mb. The coefficients of Rayleigh friction and Newtonian cooling are set to be the same and spatially uniform with a damping time equal to 7 days. The model results are shown in Figures A.1 and A.2. It can be seen from Figure A.1 that the features of the flow pattern are almost identical between Gill's analytical solution and our model solution. The similarity of the features indicates that the linear model developed here observes well the physics and dynamics of the thermally maintained circulation mechanism, and is suitable for future use of studies of thermally driven circulations. In contrast to the flow at 700 mb, The model solution shows a reversed circulation at 200 mb, as shown in Figure A.2.

§A.2 Response to Spherical Harmonic Boundary

This experiment is intended to test the model response of an isothermal atmosphere in super-rotation to a simple spherical harmonic boundary. In this experiment, the zonal mean velocity $[u]$, where square brackets denote zonal mean, is set to be $10\,m\,s^{-1}$. The spherical harmonic boundary is prescribed as shown in Figure A.3

The solution at 700 mb is shown in Figure A.4. Since the model is linear, we expect that the model solution will have a similar feature to the boundary wave pattern, and observe the physics of the mechanically maintained circulations, i.e. anticyclonic

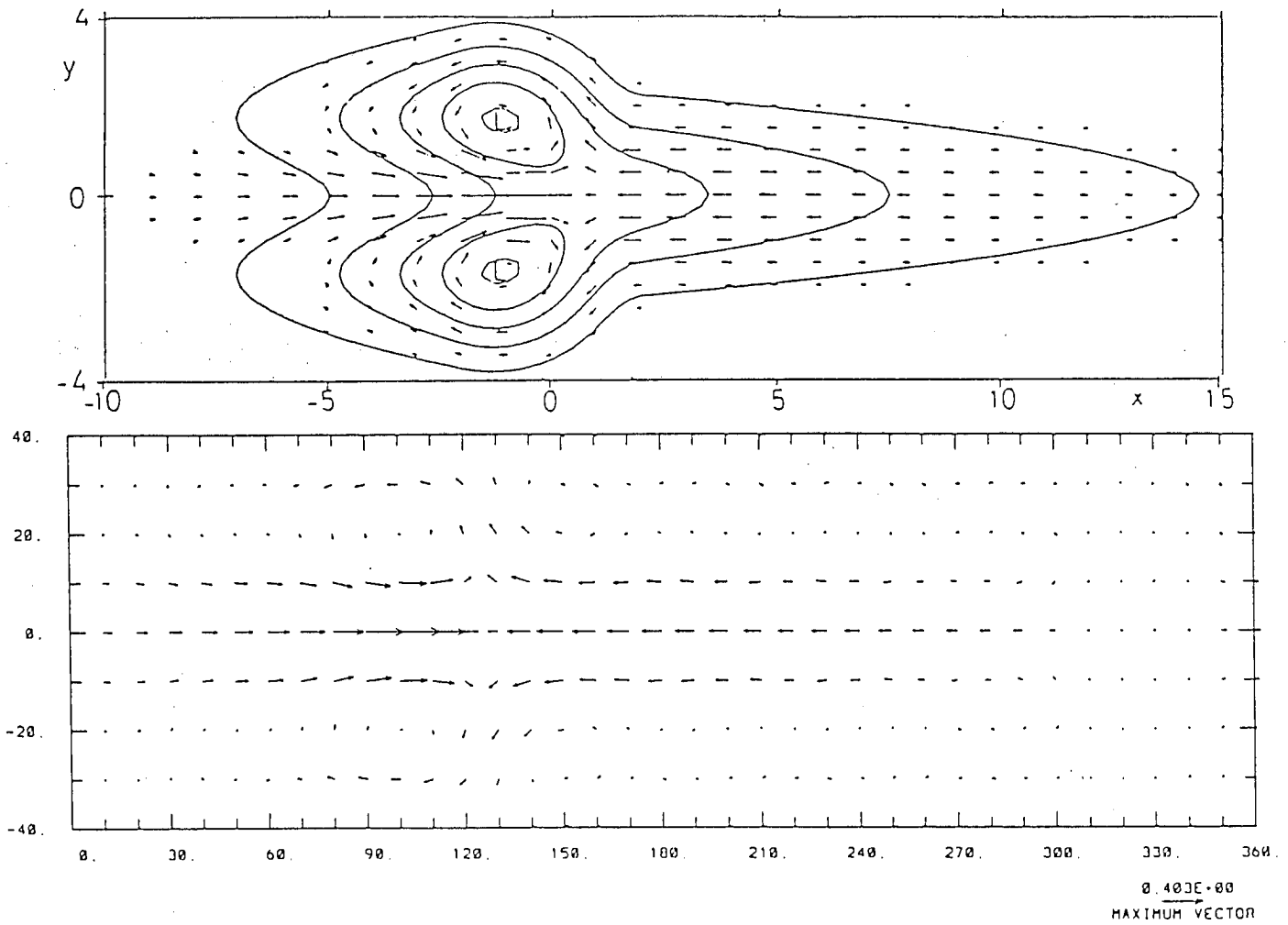

Figure A.1: Results of Gill's (1980) analytical solution (upper); and the model output at 700 mb (lower).

circulation ahead of the boundary ridge and cyclonic circulation behind the ridge. These circulation features are clearly shown in the Figure A.4.

The quasi-barotropic nature of the mechanically driven circulation can be visualised by comparing the Figures A.4 and A.5. It can be seen that this barotropicity preserves well away from the tropical area. The wave structure at 200 mb is still in good correspondence with the boundary.

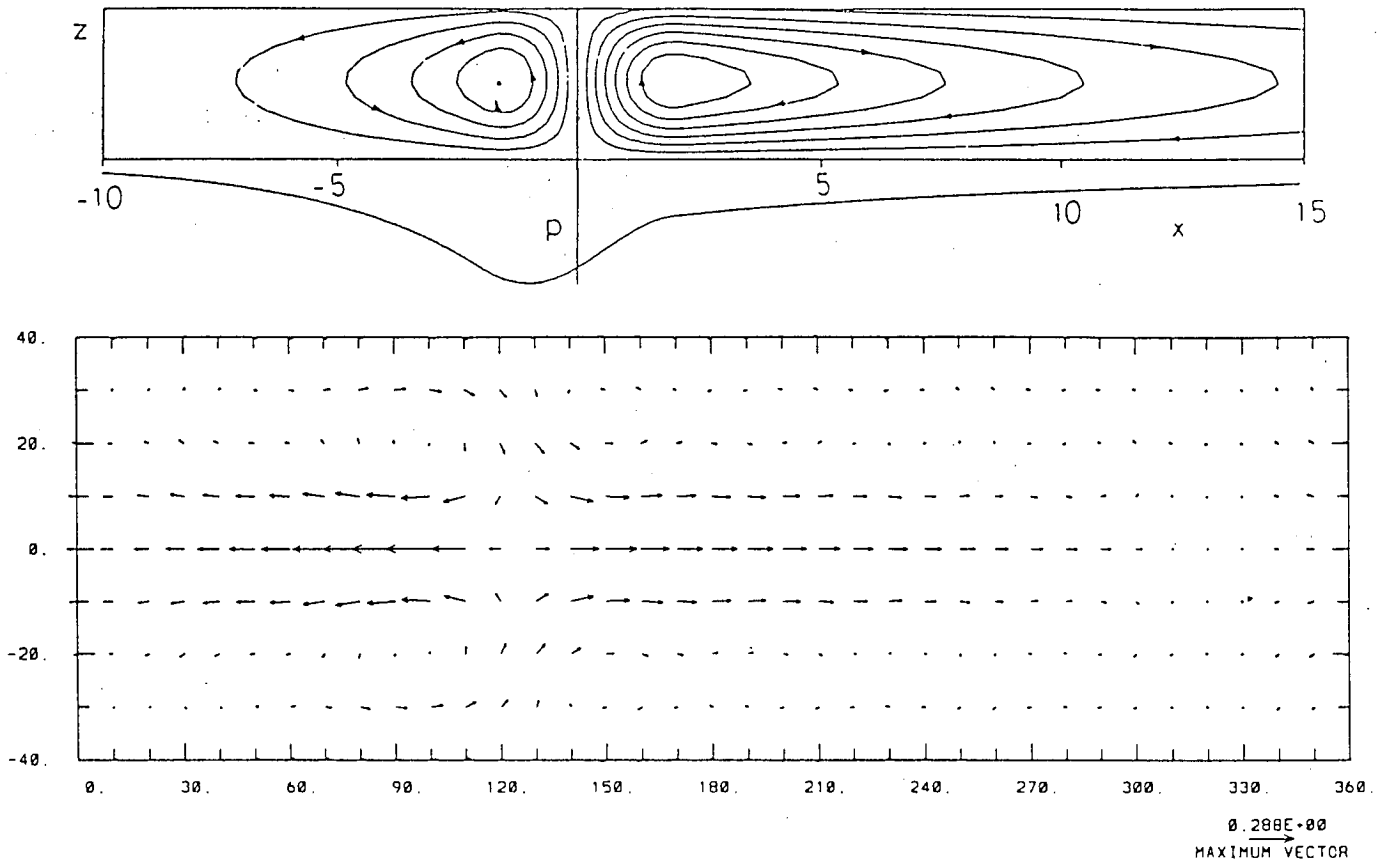

Figure A.2: Meridionally integrated vertical circulation of Gill's solution (upper); and the model output at 200 mb (lower).

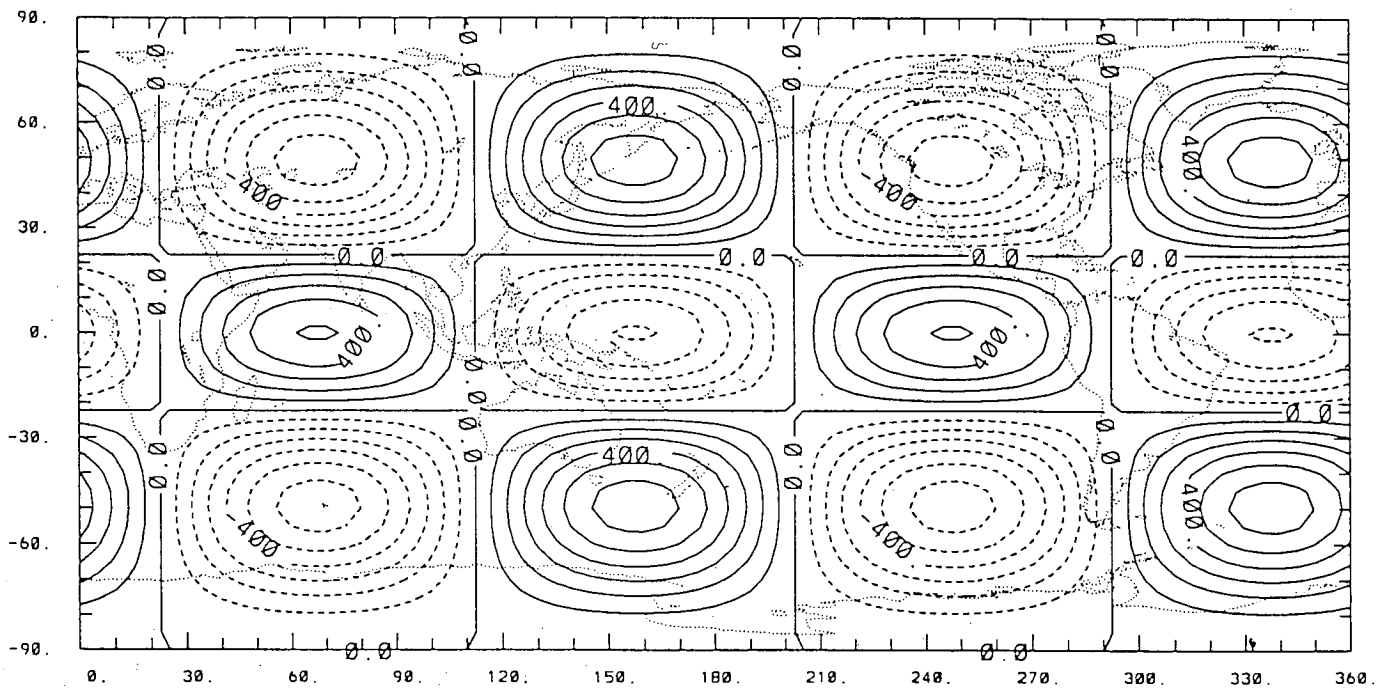

Figure A.3: The predefined spherical harmonic boundary over the globe. The contour interval is 100 m.

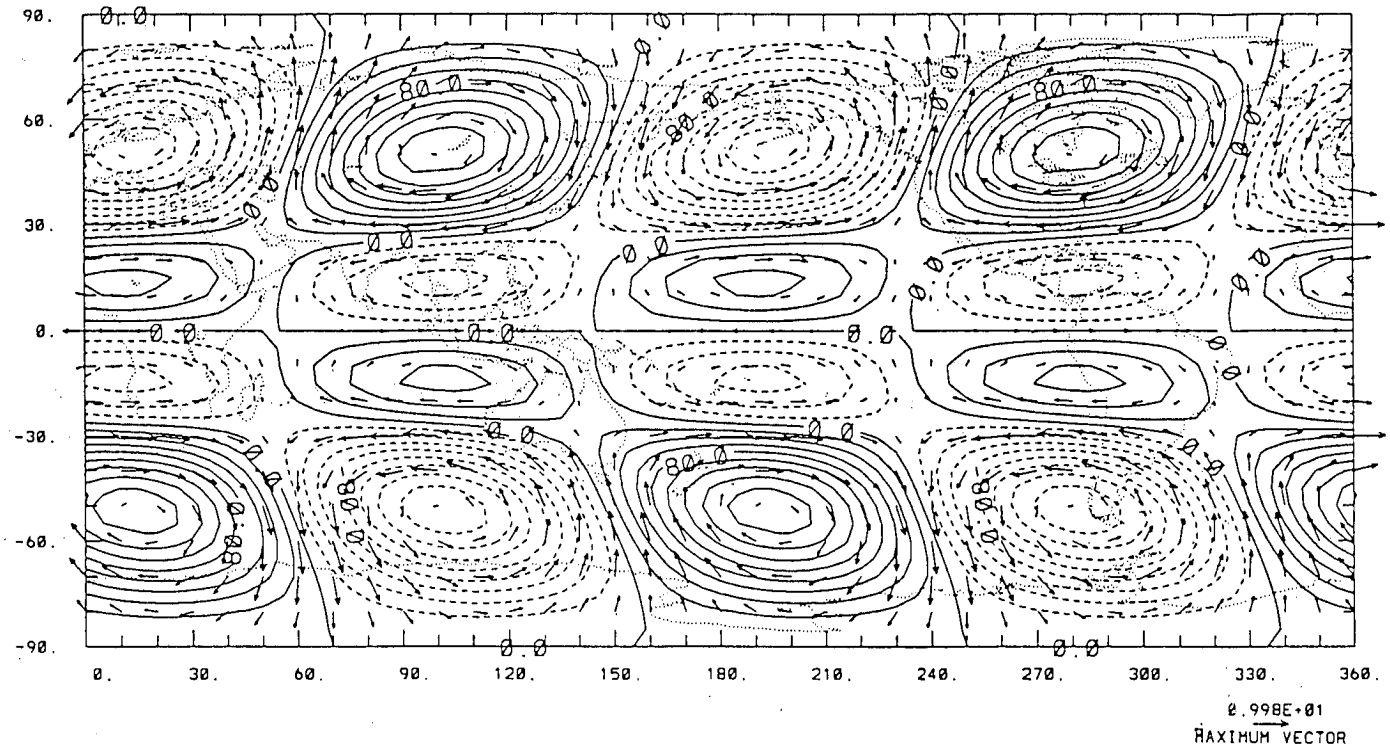

Figure A.4: Perturbation streamfunction and velocity fields at 700 mb for response of the superrotation isothermal atmosphere to the above specified spherical harmonic boundary. The contour interval is 20 units.

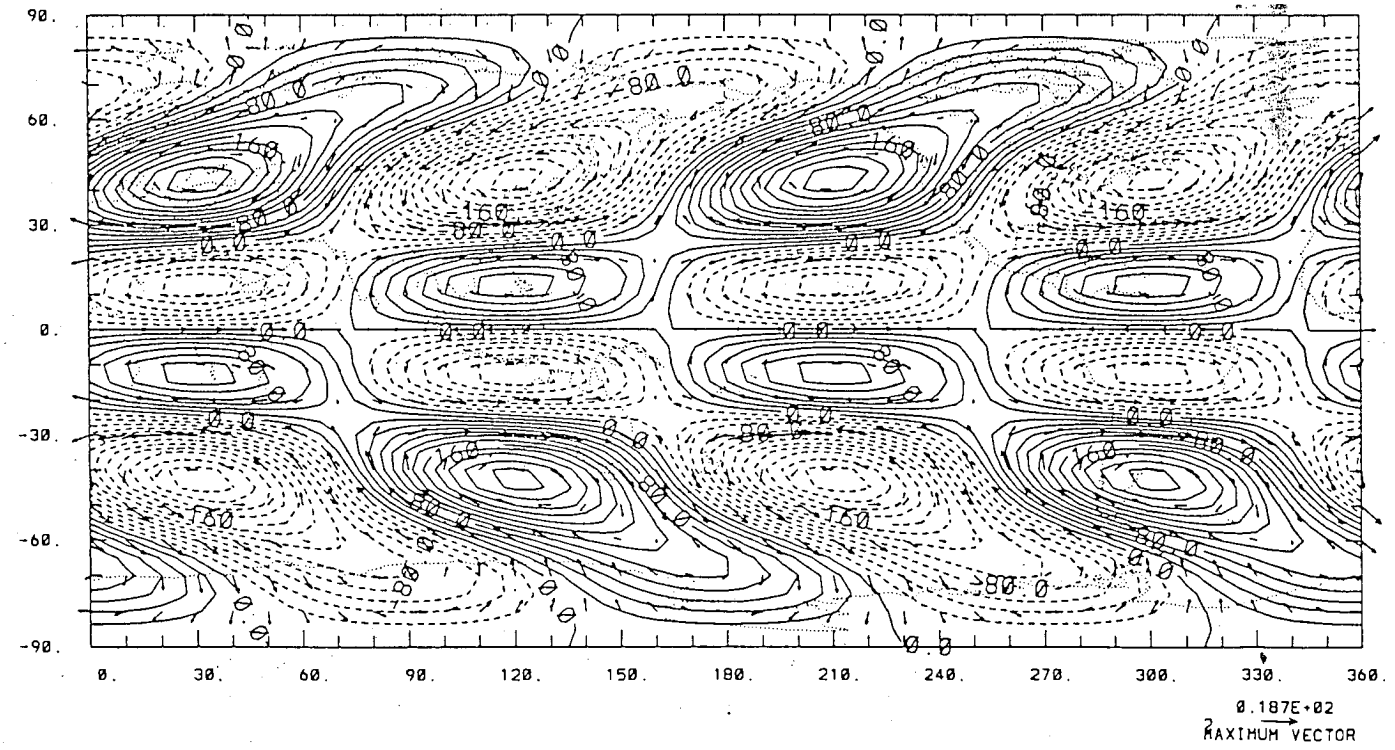

Figure A.5: Same as in Figure A.4 but for 200 mb. The contour interval is 20 units.

Bibliography

Andrews D. G. and McIntyre M. E. (1976): Planetary Waves in Horizontal and Vertical Shear: the Generalized Eliassen–Palm Relation and the Zonal Mean Acceleration. *J. Atmos. Sci.*, Vol. 33, pp: 2031–2048.

Andrews D. G. (1985): Wave–Mean–Flow Interaction in the Middle Atmosphere. *Adv. in Geophy.*, Vol. 28, pp: 249–275.

Andrews D. G. (1990): On the Forcing of Time-Mean Flows by Transient, Small Amplitude Eddies. *J. Atmos. Sci.*, Vol. 47, pp: 1837–1844.

Béland M. and Beaudoin C. (1985): A Global Spectral Model with a Finite Element Formulation for the Vertical Discretization: Adiabatic Formulation. *Mon. Wea. Rev.*, Vol. 113, pp: 1910–1919.

Bjerknes J. (1966): A Possible Response of the Atmospheric Hadley Circulation to Equatorial Anomalies of Ocean Temperature. *Tellus*, Vol. 18, pp: 820–929.

Bjerknes J. (1969): Atmospheric Teleconnections from the Equatorial Pacific. *Mon. Wea. Rev.*, Vol. 97, pp: 163–172.

Bourke W. (1972): An Efficient, One–Level, Primitive–Equation Spectral Model. *Mon. Wea. Rev.*, Vol. 100, pp: 683–689.

Bourke W. (1974): A Multi–Level Spectral Model. I. Formulation and Hemispheric Integrations. *Mon. Wea. Rev.*, Vol. 102, pp: 687–701.

Bourke W., McAvaney B, Puri K., and Thurling R. (1977): Global Modeling of Atmospheric Flow by Spectral Methods. *Methods in Computational Physics*, Vol. 17, Ed. J. Chang, Academic Press, New York,

pp: 267-324.

Boville B. A. (1991): Sensitivity of Simulated Climate to Model Resolution. *J. Climate*, Vol. 4, pp: 469–485.

Branstator G. (1990): Low–Frequency Patterns Induced by Stationary Waves. *J. Atmos. Sci.*, Vol. 47, pp: 629–648.

Browning G. L., Hack J. J. and Swarztrauber P. N. (1989): A Comparison of Three Numerical Methods for Solving Differential Equations on the Sphere. *Mon. Wea. Rev.*, Vol. 117, pp: 1058–1075.

Chang C.-P. and Lim H. (1982): On the effects of Viscous Damping on Equatorial Rossby Waves. *J. Atmos. Sci.*, Vol. 39, pp: 1726–1733.

Charney J. G. and Eliassen A. (1949): A numerical method for predicting the pertubation of the middle latitude westerlies. *Tellus*, Vol. 1, pp: 38–54.

Chervin R. M., Kutzbach J. E. et al (1980): Response of the NCAR General Circulation Model to Prescribed Changes in Ocean Surface Temperature. Part II: Midlatitude and Subtropical Changes. *J. Atmos. Sci.*, Vol. 37, pp: 308–332.

Da Silva A. M. and Lindzen R. S. (1987): A Mechanism for Excitation of Ultralong Rossby Waves. *J. Atmos. Sci.*, Vol. 44, pp: 3625–3639.

Daley R. and Bourassa Y. (1978): Rhomboidal versus Triangular Spherical Harmonic Truncation: Some Verification Statistics. *Atmosphere–Ocean*, Vol. 16, pp: 187–196.

Dunkerton T. J., C.–P. F. Hsu and McIntyre (1981): Some Eulerian and Lagrangian Diagnostics for a Model Stratospheric Warming. *J. Atmos. Sci.*, Vol. 38,, pp: 819–843.

Edmon H. J., Hoskins B. J., McIntyre M. E. (1980): Eliassen–Palm Cross Section for the Troposphere. *J. Atmos. Sci.*, Vol. 37, pp: 2600–2615.

Eliasen E., Machenhauer B., Rasmussen E. (1970): On A Numerical Method For Integration Of The Hydrodynamical Equations With A Spectral Representation Of The Horizontal Fields. *Report No. 2*, Institut for Teoretisk Meteorologi, University of Copenhagen. 37pp.

Eliasen E. (1990): On the Effects of Horizontal Resolution and Diffusion in a Two-Layer General Circulation Model with a Zonally Symmetric Forcing. *Tellus* Vol. 42A, pp: 520–530.

Frederiksen J. S. and Sawford B. L. (1981): Topographic Waves in Nonlinear and Linear Spherical Barotropic Models. *J. Atmos. Sci.*, Vol. 38, pp:69–86.

Frederiksen J. S. (1981): Disturbances and Eddy Fluxes in Southern Hemisphere Flows: Linear Theory. *J. Atmos. Sci.*, Vol. 38, pp: 673–689.

Gate W. L., Schlesinger M. E. (1977): Numerical Simulation of the January and July Global Climate with a Two–Level Atmospheric Model. *J. Atmos. Sci.*, Vol. 34, pp: 36–76.

Gill A. E. (1980): Some Simple Solutions for Heat–Induced Tropical Circulation. *Quart. J. R. Meteor. Soc.*, Vol. 106, pp:447–462.

Hartmann D. L. (1985): Some Aspects of Stratospheric Dynamics. *Adv. in Geophy.*, Vol. 28, pp: 219–247.

Hartmann D. L., Hendon H. H. and Houze R. A. (1984): Some Implication of Mesoscale Circulations in Tropical Cloud Clusters for Large Scale Dynamics and Climate. *J. Atmos. Sci.*, Vol. 41, pp: 113–121.

Held I. M. (1983): Stationary and Quasi–Stationary Eddies in the Extratropical Troposphere: Theory. *Large–Scale Dynamical Processes in the Atmosphere.* Ed. Hoskins, B. J. and Pearce R. P., 397pp.

Held I. M. and Hoskins B. J. (1985): Large–Scale Eddies and the General Circulation of the Troposphere. *Adv. in Geophy.*, Vol. 28, pp: 3–31.

Held I. M., Lyons S. W. and Nigam S. (1989): Transients and the Extratropical Response to El Niño. *J. Atmos. Sci.*, Vol. 46, pp: 163–174.

Hendon H. H. and Hartmann D. L. (1982): Stationary Waves on a Sphere: Sensitivity to Thermal Feedback. *J. Atmos. Sci.*, Vol. 39, pp: 1906–1920.

Holopainen E. O. (1983): Transient Eddies in Mid–Latitudes: Observations and Interpretation. *Large–Scale Dynamical Processes in the Atmosphere.* Ed. Hoskins, B. J. and Pearce R. P., 397pp.

Holton J. R. (1979): An Introduction to Dynamic Meteorology. 2nd Edition, Academic Press, New York, 391pp.

Horel, J. D. and Wallace, J. M. (1981): Planetary Scale Atmospheric Phenomena Associated with the Southern Oscilation. *Mon. Wea. Rev.*, Vol. 109, pp: 813–829.

Hoskins B. J. (1980): Representation of the Earth Topography Using Spherical Harmonics. *Mon. Wea. Rev.*, Vol. 108, pp: 111–115.

Hoskins B. J. (1983): Modelling of the Transient Eddies and Their Feedback on the Mean Flow. *Large–Scale Dynamical Processes in the Atmosphere.* Ed. Hoskins, B. J. and Pearce R. P., 397pp.

Hoskins B. J. and Karoly D. J. (1981): The Steady Linear Response of a Spherical Atmosphere to Thermal and Orographic Forcing. *J. Atmos. Sci.*,

Vol. 38, pp: 1179–1196.

Hoskins B. J., Hsu H. H., James I. N., Masutani M., Sardeshmukh P. D. and White G. H. (1989): Diagnostics of the Global Atmospheric Circulation, Based on **ECMWF** Analyses 1979–1989. **UGAMP** *Technical Report, No. 7.* Dept. of Meteorology, University of Reading. 217pp.

Hurrell J. W. and Vincent D. G. (1990): Relationship Between Tropical Heating and Suntropical Westerly Maxima in the Southern Hemisphere During **SOP-1, FGGE**. *J. Climate*, Vol. 3, pp: 751–768.

Kang In-Sik (1990): Influence of Zonal Mean Flow Change on Stationary Wave Fluctuations. *J. Atmos. Sci.*, Vol. 47, pp: 141–147.

Karoly D. J. (1982): Eliassen–Palm Cross Section for the Northern and Southern Hemisphere. *J. Atmos. Sci.*, Vol. 39, pp: 178–192.

Karoly D. J. and Hoskins B. J (1982): Three–Dimensional Propagation of Planetary Waves. *J. Meteoro. Soc. Jpn.*, Vol. 60, pp:

Karoly D. J. and Hoskins B. J (1983): The Steady, Linear Response of the Stratosphere to Tropospheric Forcing. *Quart. J. R. Meteor. Soc.*, Vol. 109, pp: 455–478.

Krylov V. I. (1962): Approximate Calculation of Integrals. The Macmillan Company, New York, 375pp.

Keyser D., Schmidt B. D. and Duffy D. G. (1989): A Technique for Representing Three–Dimensional Vertical Circulations in Baroclinic Disturbances. *Mon. Wea. Rev.*, Vol. 117, pp: 2463–2494.

Laprise R., and Girard C. (1990): A Spectral General Circulation Model Using a Piecewise-Constant Finite-Element Representation on a Hybrid

Vertical Coordinate System. *J. Climate*, Vol. 3, pp: 32–52.

Lau N.-C. (1984): Transient Eddy Forcing of the Time-Mean Flow as Identified by Geopotential Tendencies. *J. Atmos. Sci.*, Vol. 41, pp: 313–328.

Laursen L. and Eliasen E. (1989): On the Effects of the Damping Mechanisms in an Atmospheric General Circulation Model. Forcing. *Tellus*, Vol. 41A, pp: 385–400.

Lei Z. C. (1986): Linear and Nonlinear Response of a Model Atmosphere to Large Scale Topography and Diabatic Heating. *Ph.D Thesis*, 246pp.

Lim H. and Chang C.-P. (1981): A theory for Midlatitude Forcing of Tropical Motions During Winter Monsoons. *J. Atmos. Sci.*, Vol. 38, pp: 2377–2392.

Lindzen R. S. (1986): Stationary Planetary Waves, Blocking, and Interannual Variability. *Adv. in Geophy.*, Vol. 29, pp: 251–273.

Lindzen R. S. and Fox–Rabinovitz M. (1989): Consistent Vertical and Horizontal Resolution. *Mon. Wea. Rev.*, Vol. 117, pp:2575–2583.

Machenhauer B. and Rasmussen E. (1972): On the integration of the spectral hydrodynamical equations by a transform method. *Report No. 3*, Institut for Teoretisk Meteorologi, University of Copenhagen. 44pp.

Machenhauer B. and Daley R. (1972): A Baroclinic Primitive Equation Model with a Spectral Representation in Three Dimensions. *Report No. 4*, Institut for Teoretisk Meteorologi, University of Copenhagen. 62pp.

Machenhauer B. (1979): The Spectral Method. **GARP** *Publication Series 17*, Vol.2, Chapter 3.

McIntyre M. E. (1982): How Well Do We Understand the Dynamics of Sudden Warmings? *J. Meteoro. Soc. Jpn.*, Vol. 60, pp: 37–65.

Mellor G. L., Blumberg A. F. (1985): Modeling Vertical and Horizontal Diffusivities with the Sigma Coordinate System. *Mon. Wea. Rev.*, Vol. 113, pp: 1379–1383.

Namias J. (1976): Some Statistical and Synoptic Relationships Associated with El Niño. *J. Phys. Oceanogr.*, Vol. 6, pp: 130–138.

Navarra A. (1990): Steady Linear Response to Thermal Forcing of an Anomaly Model with an Asymmetric Climatology. *J. Atmos. Sci.*, Vol. 47, pp: 148–168.

Nigam S., Held I. M. and Lynos S. W. (1986): Linear Simulation of the Stationary Eddies in a General Circulation Model. Part I: The No–Mountain Model. *J. Atmos. Sci.*, Vol. 43, pp: 2944–2961.

Nigam S., Held I. M. and Lynos S. W. (1988): Linear Simulation of the Stationary Eddies in a General Circulation Model. Part II: The Mountain Model. *J. Atmos. Sci.*, Vol. 45, pp: 1433–1452.

Nigam S. and Lindzen R. S. (1989): The Sensitivity of Stationary Waves to Variations in the Basic State Zonal Flow. *J. Atmos. Sci.*, Vol. 46, pp: 1746–1768.

O'Brien E. (1989): Minimal Modeling of the Extratropical General Circulation. *Tellus*, Vol. 41A, pp: 292–307.

O'Brien and Branscome (1989): Minimal Modelling of the Extratropical General Circulation. *Tellus*, Vol. 41A, pp: 292–307.

Opsteegh J. D. and Van den Dool H. M. (1980): Seasonal Differences in the Stationary Response of a Linearized Primitive Equation Model: Prospects for Long–Range Weather Forecasting? *J. Atmos. Sci.*, Vol. 37, pp: 2169–2185.

Otto–Bliesner B. L., Branstator G. W. and Houghton D. D. (1982): A Global Low–Order Spectral General Circulation Model. Part I: Formulation and Seasonal Climatology. *J. Atmos. Sci.*, Vol. 39, pp: 929–948.

Palmer, T. N. (1981): Diagnostic Study of a Wavenumber–2 Stratospheric Sudden Warming in a Transformed Eulerian–Mean Formalism. *J. Atmos. Sci.*, Vol. 38, pp: 844–855.

Plumb R. A. (1985): On the Three-Dimensional Propagation of Stationary Waves. *J. Atmos. Sci.*, Vol. 42, pp: 217–229.

Puri K. and Bourke W. (1974): Implications of Horizontal Resolution in Spectral Model Integrations. *Mon. Wea. Rev.*, Vol. 102, pp: 333–347.

Robertson A. W. and Frankignoul C. (1990): The Tropical Circulation: Simple Model versus General Circulation Model. *Quart. J. R. Meteor. Soc.*, Vol. 116, pp: 69–87.

Rowntree P. R. (1972): The Influence of Tropical East Pacific Ocean Temperature on the Atmosphere. *Quart. J. R. Meteor. Soc.*, Vol. 98, pp: 290–321.

Rowntree P. R. (1976): Response of the Atmosphere to a Tropical Atlantic Ocean Temperature Anamoly. *Quart. J. R. Meteor. Soc.*, Vol. 102, pp: 607–626.

Ruosteenoja K. (1991): Simulation of the Partial Reflection by the Critical Latitude with a Linear Model. Part II: Stationary Wave Response to Total Forcing. *J. Atmos. Sci.*, Vol. 48, pp: 1529–1534.

Sardeshmukh P. D. and Hoskins B. J. (1984): Spatial Smoothing on the Sphere. *Mon. Wea. Rev.*, Vol. 112, pp: 2524–2529.

Schaack T. K., Johnson D. R., and Wei Ming-Ying (1990): The Three-Dimensional Distributation of Atmospheric Heating During the **GWE**. *Tellus*, Vol. 42A, pp: 305–327.

Schneider E. K. (1989): A Method for Direct Solution of a Steady Linearized Spectral General Circulation Model. *Mon. Wea. Rev.*, Vol.117, pp: 2137–2141.

Schneider E. K. (1990): Linear Diagnosis of Stationary Waves in a Genaral Circulation Model. *J. Atmos. Sci.*, Vol. 47, pp: 2925–2952.

Shukla S. (1986): **SST** Anomalies and Blocking. *Adv. in Geophy.*, Vol. 29, pp: 443–452.

Simmons A. J. (1982): The Forcing of Stationary Wave Motion by Tropical Diabatic Heating. *Quart. J. R. Meteor. Soc.*, Vol. 108, pp: 503–534.

Simmons A. J. (1987): Some Aspects of the Design and Performance of the Global ECMWF Spectral Model. pp: 249–304, **ECMWF** *Workshop Proceeding*, Techniques for Horizontal Discretization in Numerical Weather Prediction Models, 377pp.

Smagorinsky J. (1963): General Circulation Experiments with the Primitive Equations. I: The Basic Experiments. *Mon. Wea. Rev.*, Vol. 91, pp:99-164.

Stone P. H. and Yao M.-S. (1990): Development of a Two-Dimensional Zonally Averaged Statistical-Dynamical Model. Part III: The parameterization of the Eddy Fluxes of Heat and Moisture. *J. Climate*, Vol. 3, pp: 726–740.

Ting M.–F., Held I. M. (1990): The Stationary Wave Response to a Tropical SST Anomaly in an Idealized GCM. *J. Atmos. Sci.*, Vol. 47, pp: 2546–2566.

Ting M.–F. (1991): The Stationary Wave Response to a Midlatitude SST Anomaly in an Idealized GCM. *J. Atmos. Sci.*, Vol. 48, pp: 1249–1275.

Vernekar A. D. (1981): Response of a Steady–State Model for Quasi-Stationary Pertubations to Simulated Anomalies at the Earth's Surface. *J. Atmos. Sci.*, Vol. 38, pp: 531–543.

Wallace J. M. (1983): The Climatological Mean Stationary Waves: Observational Evidence. Large–Scale Dynamical Processes in the Atmosphere. Ed. Hoskins, B. J. and Pearce R. P., 397pp.

Wallace J. M. and Hobbs P. V. (1977): Atmospheric Science: An Introductory Survey. Academic Press, 467pp.

Wallace J. M. and Gutzler D. S. (1981): Teleconnections in the geopotential height field during the northern hemisphere winter. *Mon. Wea. Rev.*, Vol. 109, pp: 785–812.

Watterson I. G. and Schneider E. K. (1987): The Effect of the Hadley Circulation on the Meridional Propagation of Stationary Waves. *Quart. J. R. Meteor. Soc.*, Vol. 113, pp: 779–813.

Weber G.-R (1990): North Pacific Circulation Anomalies, EL Niño and Anomalous Warmth over the North American Continent in 1986–1988: Possible Cause of the 1988 North American Drought. *International Journal of Climatology*, Vol. 10, pp: 279–289.

Webster P. J. (1981): Mechanisms Determining the Atmospheric Response to Sea Surface Temperature Anomalies. *J. Atmo. Sci.*, Vol. 38, pp: 554–571.

Webster P. J. (1982): Seasonality in the Local and Remote Atmospheric Response to Sea Surface Temperature Anomalies. *J. Atmo. Sci.*, Vol. 39, pp: 41–52.

White A. A. (1990): Steady State in a Turbulent Atmosphere. *Meteorological Magazine*, Vol. 119, No. 1410, pp: 1–9.

Williamson D. L. (1983): Description of **NCAR** Community Climate Model (CCM0B). **NCAR** *Technical Note*, NCAR/TN–210 + STR. 88pp.

Williamson D. L., Kiehl J. T., Ramanathan V., Dickinson R. T., and Hack J. J. (1987): Description of **NCAR** Community Climate (CCM1). **NCAR** *Technical Note*, NCAR/TN–285 + STR. 112pp.

Xu Jin-Song, von Storch H. and van Loon H. (1990):The Performance of Four Spectral GCMs in the Southern Hemisphere: The January and July Climatology and the Semiannual Wave. *J. Climate*, Vol. 3, pp: 53–70.

Zimmerman J. E., Smith P. J. and Smith D. R. (1990): The Role of Latent Heat Release in the Evolution of a Weak Extratropical Cyclone. *Mon. Wea. Rev.*, Vol. 117, pp: 1039–1057.